CALIBRATION AND EVALUATION OF THE 3RD GENERATION WAVE MODELS UNDER EXTREME CONDITIONS IN BLACK SEA BASIN

A THESIS SUBMITTED TO
THE GRADUATE SCHOOL OF NATURAL AND APPLIED SCIENCES
OF
MIDDLE EAST TECHNICAL UNIVERSITY

BY

ÇAĞIL KİREZCİ

IN PARTIAL FULFILLMENT OF THE REQUIREMENTS
FOR
THE DEGREE OF MASTER OF SCIENCE
IN
CIVIL ENGIREERING

SEPTEMBER 2016

Approval of the thesis:

CALIBRATION AND EVALUATION OF THE 3RD GENERATION WAVE MODELS UNDER EXTREME CONDITIONS IN BLACK SEA BASIN

submitted by **ÇAĞIL KİREZCİ** in partial fulfillment of the requirements for the degree of **Master of Science in Civil Engineering Department, Middle East Technical University** by,

Prof. Dr. Gülbin Dural Ünver _____
Dean, Graduate School of **Natural and Applied Sciences**

Prof. Dr. İsmail Özgür Yaman _____
Head of Department, **Civil Engineering**

Asst.Prof. Gülizar Özyurt Tarakcıoğlu _____
Supervisor, **Civil Engineering Department, METU**

Examining Committee Members:

Prof. Dr. Ahmet Cevdet Yalçıner _____
Civil Engineering Department, METU

Asst.Prof. Gülizar Özyurt Tarakcıoğlu _____
Civil Engineering Department, METU

Prof. Dr. Ayşe Burcu Altan Sakarya _____
Civil Engineering Department, METU

Asst. Prof. Dr. Cüneyt Baykal _____
Civil Engineering Department, METU

Asst. Prof. Dr. Melih Çalamak _____
Civil Engineering Department, TED University

Date: 05.09.2016

I hereby declare that all information in this document has been obtained and presented in accordance with academic rules and ethical conduct. I also declare that, as required by these rules and conduct, I have fully cited and referenced all material and results that are not original to this work.

Name, Last Name: Çağıl Kirezci

Signature:

ABSTRACT

CALIBRATION AND EVALUATION OF THE 3RD GENERATION WAVE MODELS UNDER EXTREME CONDITIONS IN BLACK SEA BASIN

Kirezci, Çağıl

M.S., Department of Civil Engineering

Supervisor: Asst. Prof. Gülizar Özyurt Tarakcıoğlu

September 2016, 233 pages

In this study, performances of 3rd generation wave models, SWAN and WAVEWATCH III, under storm conditions in Black Sea are compared considering two different wind source (CFSR and ECMWF operational) data. Basic wave parameters (outputs of the spectral wave models) demonstrate that the governing physical processes in deep water consist of three terms; wind-wave interaction, dissipation of energy due to whitecapping and swell, and nonlinear wave-wave interactions. Effects of different methodologies for the solutions of these physical processes over the frequency and directional space are discussed. Best representation of extreme events in Black Sea was obtained by using WAVEWATCH III model

coupled with CFSR wind data. All parametric and solution methodology variations modelled with different wind source data generated results in good agreement with the observations from buoy data in Sinop, Hopa and Gelendzhik. Although, wind wave interaction and dissipation terms defined in Ardhuin et al., 2010 also performed significantly better than the other available methods with its higher correlation to buoy data. Finally, most appropriate boundary conditions and parametrizations for Black Sea basin is introduced for both SWAN and WAVEWATCH III, as a result of calibration and sensitivity analysis study using the observations.

Keywords: Wind wave modeling, Extreme Events, 3rd Generation Wave Models, Black Sea, Wave Hindcasting

ÖZ

KARADENİZ BASENİNDE FIRTINA KOŞULLARI İÇİN
3. NESİL DALGA MODELLERİNİN KALİBRASYONU VE
DEĞERLENDİRMESİ

Kirezci, Çağıl

Yüksek Lisans, İnşaat Mühendisliği Bölümü

Tez Yöneticisi: Yrd.Doç.Dr. Gülizar Özyurt Tarakcıoğlu

Eylül 2016, 233 sayfa

Bu çalışmada, 3. Nesil dalga modelleri olan SWAN ve WAVEWATCH III sayısal modelleri Karadeniz'de gözlenen ekstrem fırtına koşulları için kalibre edilmiş ve performans değerlendirmeleri yapılmıştır. Oluşan fırtınalardaki etkin fiziksel olaylar incelenmiş ve tartışılmıştır. Çalışma sırasında iki farklı rüzgar kaynağı (CFSR ve ECMWF operasyonel) kullanılmıştır. Model sonucunda elde edilen temel dalga parametreleri derin deniz koşullarında etkili olan fiziksel olaylar, rüzgar dalga etkileşimi, derin deniz dalga kırılmasına ve soğulan dalgalara bağlı enerji yitimi ve

linear olmayan dalga-dalga etkileşimleri olduğunu göstermektedir. Bu fiziksel olayları açıklamak için modellerdeki mevcut methodlar frekans ve yönsel uzayda uygulanmış ve karşılaştırmalı olarak tartışılmıştır. Tüm metotların sonuçları kabul edilebilir sınırlar içinde kalmasına rağmen Karadeniz baseninde, gerçek dalga ölçümleri ile en yüksek uyumu gösteren model CFSR rüzgar verileri ile çalıştırılan WAVEWATCH III modeli olmuştur. Ayrıca diğer yöntemlere kıyasla, Ardhuin et al., 2010 tarafından önerilen rüzgar dalga etkileşimi ve derin deniz dalga kırılmasına bağlı enerji yitimi yöntemi gerçek veri ile en yüksek korelasyon değerlerini vermiştir. Son olarak hem SWAN hem de WAVEWATCH III modeli için kalibrasyon çalışması ve hassasiyet analizleri yapılmış ve Karadeniz baseni için en uygun sınır koşulları ve değişken değerleri, ortaya çıkarılmıştır.

Anahtar Kelimeler: Rüzgar Dalga Modeli , Ekstrem Olaylar, 3. Nesil Dalga Modeli, Karadeniz, Dalga Tahmini.

to my family,

ACKNOWLEDGEMENTS

First of all, I would like to thank Dr. Ayşen Ergin who has given me chance to become part of this amazing laboratory and supported me throughout my graduate studies. She had a great influence on me with her amazing perspective on life and never ending energy. She was the main reason for me to choose field of coastal engineering.

My deepest gratitude are for my supervisor Dr. Gülizar Özyurt Tarakcıoğlu who has spent many hours with me to make this thesis possible. She has been a great supervisor, mentor, supporter and I feel lucky to have the chance to work with her.

My special thanks are for Dr. Ahmet Cevdet Yalçıner who has supported me throughout my graduate studies. He has enlighten my way with his guidance and experience. He inspired me in many things in life. He had a great role on my great experience in coastal engineering laboratory.

I would like to thank Dr. Işıkhan Güler, who has always supported and believed in me. His ideas and comments on my research and on any other topic have always been inspiring and valuable for me.

I would like to thank Dr. Cüneyt Baykal who has been very helpful with his precious comments and suggestions throughout my study. He has been a great mentor for my academic perspective. I am glad I have the chance to both work with him and be his student.

I would like to express my gratitude to Ebru Demirci. She is my life, my greatest chance, my inspiration, my source of joy and everything that completes me. Knowing that she will always walk along with me, makes me stronger and delighted

in life. Many crucial things that I have achieved in my life and this thesis would not be possible if she was not part of my life.

Another special thanks are for Cem Özcan, who had a valuable contribution in finalizing this thesis. His precious help has saved my days. I know that he is there for me whenever I need.

I would like to thank Onur Can Erdil for his many late night psychological supports to me which was significant for this thesis.

I also would like to thank my friends Bora Pulatsü, Burak Can Kaplan, Erkin Güngör, Oğuz Polat, Ahmet Koçak, Denizhan Yıldız, Burak Birlik, Kubilay Kahveci, Arın Öztürk, Yasemin Kapucu, Ceren Emre and all members of the group "roses of the uncle" (Aydın Okul, Burak Üçok, Cihan Yiğitbaşı, Eren Mete, and Mehmet Pektaş). Their presence in my life and all the memories we share are really valuable and essential for me.

I would like to thank Gökhan Güler, probably the best roommate I will ever have for his valuable support and help. I also would like to thank my old neighbor in lab and part of "last-minute" team, Güney Doğan for her support.

I would like to thank my dearest friends and work partners in coastal engineering family and K5 building, Duha Metin, Nilay Doğulu, Bora Yalçıner (as the late night guardians of K5), Deniz Can Aydın, Naeimeh Sharghivand, Hazal Ak for all the support and great moments we have shared together. I would like to thank to our lab staff Arif Kayışlı, Yusuf Korkut and Nuray Sefa for their support as well. I would like to thank the apple tree in front of laboratory for appeasing my hunger during the long nights in K5 laboratory.

Finally, I would like to thank my beloved mother Fergin Kirezci and my father Levent Kirezci for everything they have done for me so far. No word is enough to express my gratefulness to them. They have always been great role model, supporter and inspiration for all my life decisions. I owe almost everything to them.

TABLE OF CONTENTS

LIST OF TABLES

TABLES

LIST OF FIGURES

FIGURES

LIST OF ABBREVIATIONS

H	Wave height
H_s	Significant wave height
H_{max}	Maximumu wave height
T	Wave period
$T_{m0}1$	Spectral Mean Wave period
$T_{m0}1$	Spectral Mean Wave period
$E(\sigma,\theta)$	Energy Density Function
$N(k,\theta)$	Action Density Function
σ	Frequency
$\tilde{\sigma}$	Mean frequency
k	Wave number
$\tilde{k}$	Mean wave number
θ	Direction
C_g	Group Velocity
S_{in}	Wind-Wave interaction input source term
U_*	Friction Velocity
U_{10}	Wind Speed at 10m elevation
σ_{PM}^*	Peak frequency of the fully developed sea ,in Pierson and Moskowitz (1964)

ρ_a	Density of air
ρ_w	Density of waater
β	Miles constant (Miles ,1957)
β_{max}	Non-dimensional growth parameter (Jansen, 2004)
z_e	Effective roughness length
κ	Von Karman constant
$S_{ds,w}$	Whitecapping dissipation source term
Γ	Steepness dependent coefficient
C_{ds}	Proportionality coefficient of rate of whitecapping dissipation
δ	Wave number dependency coefficient
$\tilde{s}$	Overall wave steepness
$\tilde{s}_{PM}$	Overall wave steepness of the Pierson-Moskowitz spectrum
p	Power of steepness term in Komen et al (1984)
λ	Dimensionless coefficient in DIA
$C, Cnl\mathrm{i}\ Cnl4$	Proportionality constant in DIA
E	Energy Density
$S_{ds,b}$	Bottom friction source term
C_b	JONSWAP Bottom friction coefficient
C_D	Drag coefficient in Wu(1982)
α_{BJ}	Proportionality coefficient of the rate of dissipation in Battjes and Janssen (1978)
γ	Breaker index
z_α	Coefficient that controls wave age shift

z_1	Roughness length
τ_w	Wave-supported stress
α	Charnock coefficient
τ_{hf}	Stress supported by shorter waves
S_U	Shletering coefficient
$\emptyset$	Empirical function accounting for the development stage of wave field
b_0, b_1, b_2, b_3	Dimensionless coefficients in ST2 dissipation term
α_n	Phillips' non-dimensional high-frequency energy level
a_0, a_1, a_2	Empirical constants in ST2
$s_1, s_2, s_3, s_4, s_5, s_6, s_7$	Swell dissipation terms in ST4
Re	Reynold number
Re_c	Critical Reynold Number
$u_{orb,s}$	Surface orbital velocity
ν_α	Air viscosity
$S_{out,tur}$	Turbulent boundary layer value
$S_{out,vis}$	Viscous boundary layer value
r_{tur}	Weight of turbulent boundary layer value
r_{vis}	Weight of viscous boundary layer value
f_e	Friction factor
B_r	Constant saturation threshold
$B(k)$	Direction-integrated spectral saturation
C_{turb}	Coefficient adjust ocean stratification

σ_r	Reference frequency
θ_{12}	Angular gap between the wavenumbers $k_1$and k_2
C_{deep}	Proportionally constants for deep water
C_{shal}	Proportionally constants for shallow water
B_{deep}	Deep water scaling function
B_{shal}	Shallow water scaling function
S_{nl}	Nonlinear interactions source term
$\Phi(f)$	Nonlinear filter in NLS
C_{nlf}	Proportionality constant of the DIA in filter
c_1, c_2, c_3	Nondimensional parameters in nonlinear filter
S_a, S_b	Mirror image quadruplets
S_{max}	Limitation parameter in nonlinear filter
α_{34}	Relative offset of quadruplets 3 and 4
$\Delta \boldsymbol{t_g}$	Global time step in WW3
Δt_{xy}	Spatial propagation time step in WW3
Δt_k	Spectral propagation time step in WW3
Δt_s	Source time step in WW3

CHAPTER 1

INTRODUCTION

"In the coastal area, the main masses of our planet air, water, and land meet. Each has a dynamic nature to certain extend. They intersect with each other to create a complicated environment for engineering activities" (Ergin, 2009).

"Waves are the most important phenomenon to be considered among the environmental conditions affecting maritime structures, because they exercise the greatest influence" (Goda, 2000). Design of a coastal structure starts with consideration of basic wave parameters such as wave height and wave period parameters, therefore reliability of those parameters have significant importance.

The utilization of the coastal areas of the Black Sea basin has increased in the recent years with the projects such as large commercial ports, international transportation hubs, gas and petrol pipelines, tourism and recreational infrastructures along surrounding shoreline as well as in deep waters. Therefore, careful monitoring of the storms and verification of numerical tools with reliable data has become important in order to maintain the safety of the coastal zone.

The design wave parameter is in general decided considering the critical wave heights and wave periods which usually occur under extreme storm conditions. Many active physical processes existing in wave generation and wave transformation are

shown in the Figure 1.1. Different methods have been used for forecast of random sea waves throughout the history. Since 1970s most convenient methods are based on spectral calculation methods.

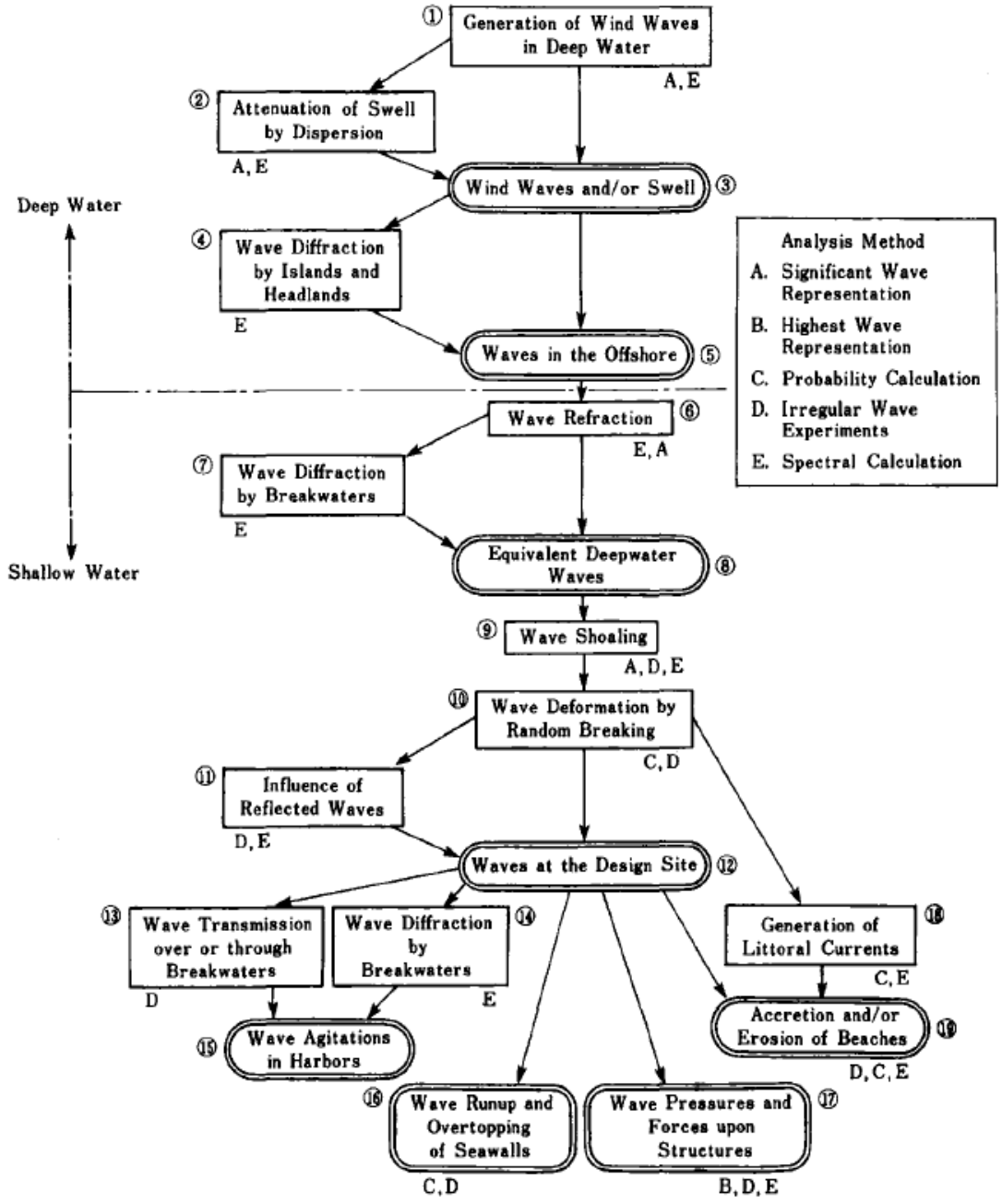

Figure 1.1 Flow of the generation, transformations and actions of sea waves with suggested methods for their calculation (Goda, 2000)

Today, spectrum averaged numerical models which are called wave generation models are commonly used for solving the complex physics of wind-wave interaction. The main processes in generation of wind waves in deep water can be stated as wave growth by wind, deep water dissipation of wave energy (whitecapping) and deep water non-linear wave-wave interactions (Tolman, 2014).

The main objective of this study is to investigate the storm nature of Black Sea and evaluate the capabilities of 3rd generation wave models, SWAN (Simulating Waves Nearshore) and WAVEWATCH III, under extreme conditions. Model results were compared and analyzed using the data of three buoys (Sinop, Hopa, and Gelendzhik) in Black Sea considering the extreme wave conditions occurred in years between 1994-2004. In this study effects of different physical phenomena such as energy dissipation, wind-wave interaction and nonlinear wave-wave interactions were investigated under extreme conditions in Black Sea. In numerical models, different source terms formulations of above phenomena were applied for 54 selected events. In SWAN and WAVEWATCH III models, 4 and 12 source combinations were performed, respectively. Most of these combinations were also carried out for 2 different wind sources (CFSR and ECMWF Operational). Moreover, calibration of these wave models for Black Sea were also done in order to obtain more accurate results. Sensitivity of the model results with respect to different physical resolutions (time, direction, frequency, geographical) were also investigated.

In chapter two, historical developments of wave modelling are explained considering the definitions of 1st, 2nd and 3rd generation models. Also a literature survey for the application of third generation wave models in Black Sea basin is presented.

In chapter three, detailed information of the models, SWAN and WAVEWATCH III, used in the study are introduced considering the governing equations, propagations schemes, and deep water source term physics. A brief comparison of the selected models is also present in this chapter. Finally, statistical methods used in the calibration and the sensitivity analysis of the model results are introduced.

In chapter four, data used in the study are introduced which consist of wind forcing fields, bathymetry, and the buoy data which is used for calibration. Moreover, selected storm events modelled in the study are also described in details.

In chapter five, implementation of SWAN model to Black Sea basin considering available source term options are introduced. Calibration and sensitivity analysis of SWAN model are also presented. Discussion of the performance of the SWAN model is also given in this chapter.

In chapter six, implementation of WAVEWATCH III model to Black Sea basin considering available source term options are introduced. Calibration and sensitivity analysis of WAVEWATCH III model are also presented. The performance of WAVEWATCH III model is also discussed in this chapter.

In chapter seven, the study is summarized, and final discussions on the models are presented. Future recommendations in light of the obtained results are given for the continuum of the study.

CHAPTER 2

LITERATURE REVIEW

Throughout the history, wind generated waves are observed although the mathematical formulation of the motion of water waves was introduced in 19th century (Goda, 2010).

In this chapter, developments of wave generation models, and the previous studies of wave model implementations in Black Sea are presented.

2.1 Wave Generation Models

Wind generated waves have irregular wave heights and periods, caused by the irregular nature of wind. Due to this irregular nature, the sea surface is continually varying, which means that a deterministic approach to describe the sea surface is not feasible (SWAN Team, 2015). Waves or spectral wave components in water with limited depth and non-zero mean currents are generally described using several phase and amplitude parameters (Tolman, 2014)

“For monochromatic waves, the amplitude is described as the amplitude, the wave height, or the wave energy. For irregular wind waves, the (random) variance of the sea surface is described using variance density spectra” (Tolman, 2014).

The desire and the first attempts for the forecasting of wave heights have started during the Second World War for the Normandy invasion in 1945 (Kanbua, n.d).

"In 1947, Sverdrup and Munk have developed a forecast method that relates the wind speed to sea surface oscillations which to be used during landings." (Schwartz, 2006) "As early as in 1952, a group of American oceanographers, headed by Pierson 5 took the first step in recognizing the irregularity of ocean waves as a fundamental property and incorporating this fact in the design process. The so called P-N-J method of wave forecasting, often compared with the S-M-B method, introduced the concept of wave spectrum as the basic tool for describing wave irregularity. The generation and development of wind waves, the propagation of swell and wave transformation near the shore were all explained in detail via the concept of wave spectrum" (Goda, 2010). In 1953, Nuemann derived wave spectral relations relating significant wave height and periods (Schwartz, 2006). Then it is followed by the work of Pierson et al. (1955) that derived graphical methods for engineering application using spectra (Schwartz, 2006). It is accepted that wave energy spectrum was introduced by Pierson in 1957 which was based on the assumption that the sea surface may be represented as a Fourier series of superimposed waves with different wave lengths and with statistically random phases (Kanbua, n.d).

First generation models were started to be implemented in 1960s using two dimensional spectrum which are frequency and direction. In 1st generation models, nonlinear energy transfer was implicitly expressed through wind and energy input. Those models assumed that the wave components suddenly stopped growing as soon as they reached a universal saturation level (Phillips, 1958). The saturation spectrum, represented by the one-dimensional f^{-5} frequency spectrum of Phillips and an empirical equilibrium directional distribution, was prescribed. Nowadays it is generally recognized that a universal high-frequency spectrum (in the region between 1.5 and 3 times the peak frequency) does not exist because the high-frequency region of the spectrum not only depends on whitecapping but also on wind input and on the

low-frequency regions of the spectrum through nonlinear transfer (Janssen and Bidlot, 2003).

Before the early 1970's, attention was focused on the physical models, trying to track the development of each single wave component, and those proposed by Barnett (1968) and Ewing (1971) attained a remarkable degree of success. At this time the role that nonlinear wave-wave interactions play in the development of a wind wave spectrum was becoming increasingly clear. Through the end of 1960s and the first half of the 1970s, investigation of nonlinear interactions and the wind input details were expanded with the wave growth experiments (Mitsuyasu, 1968, 1969; Hasselmann et al., 1973) Direct measurements of the wind input to the waves (Snyder et al., 1981; Hasselmann et al., 1986) were considered and helped a breakthrough invention of JONSWAP spectrum by Hasselmann et al., 1973. Because of the practical possibility of correctly including nonlinear interactions into the physical approach, in which they were implicitly taken into account through the assumed shape of the spectrum represented by a limited number of parameters (Cavaleri and Rizzoli, 1981), JONSWAP spectrum and the better understanding of the physical processes of wind waves led to the development of the parametric models (Hasselmann et al., 1976).

The second generation models used spectral shape of JONSWAP spectrum. (Hasselmann et al., 1973). Non-linear interactions were parameterized by applying a reference spectrum to reorganize the energy over frequencies (Kanbua, n.d). These models are called as parametrical models (Hasselmann el al., 1976).

The main problem of the second generation wave models is the inconsistency between numbers of degrees of freedom of spectrum and nonlinear parameterizations caused by the restrictions in the spectral shape. Moreover, source functions in the first two generations have needed to be improved for better representation of the sea states. The shortcomings of first and second generation models have been documented and discussed in the SWAMP wave-model intercomparison study (SWAMP Group, 1985).

The development of 3rd generation wave models have started with WAM model by the WAMDI group in 1986. The group aimed that by presenting a third generation wave model, future model improvements can be introduced at appropriate level, namely in the source functions presenting the physics rather than by modifying the form of the wave spectrum (WAMDI group). Thus, the main difference of the third generation wave models is that parameterizations of physical processes are solved explicitly without imposing spectral shapes or energy levels. (Tolman,2010) WAM model can be accepted as the predecessor of the 3rd generation wave models which is followed by WAM Cycle 4 in 1992, WAVEWATCH III in 1996 and SWAN in 1999.

Compared to first two generations, 3rd generation wave models are more versatile since the need for site-specific tuning is less and the new research is directly applicable. However, 3rd generation models are more expensive in matter of computational cost which is a general problem with the developed numerical models in many aspects. Until today, improvement of the wave models continue especially with the help of developed computational powers, quality observations, application of models to different case studies. Even though the model structure frames of the models are similar, there are differences in propagation schemes, source and sinks approaches between the 3rd generation wave models. These differences are explained in
Chapter 3.

2.2 Previous Studies of Wave Model Implementations in Black Sea

Despite having a history over 40 years considering second and third generation wave models, implementation of these wave generations models in Black Sea has started quite short time ago.

The first wave model implementation which was research oriented in Black Sea was the "Turkish Coast Wind and Deep Water Wave Atlas", (Özhan and Abdalla,1999) in which wind and wave climate of Turkish coast were investigated. In Özhan and Abdalla (1999) WAM model was implemented with ECMWF wind fields. Model calibrations were carried out using continuous wave data from 3 buoys in Black Sea (Hopa, Sinop and Gelendzhik). The study was a long term oriented research and the main output of the study was the wave atlas which was consisted of yearly and seasonal wind and wave roses, extreme value analyses and significant wave height vs. mean wave period relations at the each ECMWF grid near Turkish coasts with a resolution of 0.25° x 0.25°.

At the same year, basin-scale level the WAM model had also been applied by Cavaleri et al. (1999) using again ECMWF winds fields and results were calibrated using TOPEX satellite altimeter data (Cavaleri et al., 1999;Cherneva et al,2008)

Kortcheva et al. (2000) have represented the discrete spectral shallow water wave model named VAGBUHL1. This model is used for real-time Black Sea state forecasting. The model was verified against the second European Remote Sensing Satellite (ERS-2) of the European Space Agency altimeter wave height data. The results of statistical analysis of comparing the model significant wave height with altimeter data from ERS-2 were summarized and the comparison with the ERS-2 significant wave height values indicated a 0.63 m standard deviation of the error in case of ARPEGE wind input.

Cherneva et al. (2008) implemented WAM Cycle 4 model Black Sea basin for 41 year wave hindcast study. Cherneva used a regional atmosphere model called (REMO), which was driven with the conditions from the global NCEP re-analysis project. Finally the WAM Cycle 4 model was calibrated using again the NATO-TU Waves buoys as in Özhan and Abdalla(1999). Cherneva et al. (2008) have found that, WAM model showed poor performance when low wind energy fields were

supplied to system and also model was not compatible with the rapid and frequent change in wind directions.

Rusu (2009) has studied the wave energy assessments for Black Sea focusing on the western part. Wave climate was determined with a medium term wave analysis using in situ data in order to gain a first sight, and then, wave generation and nearshore transformation were estimated with SWAN numerical model. Various tests were performed considering data measured at three different locations along the Black Sea coast. Comparisons with the measured data revealed well agreement with the predicted values, especially in terms of significant wave heights and mean periods. Wave energy field distributions were analyzed by increasing the resolution in geographical space.

Kortcheva et al. (2009) described the wind wave forecasting operational system that is coupled atmospheric and wave numerical models aiming at a detailed and accurate sea state forecast on an operational level. The numerical wave models VAG, WAVEWATCH III and WAM, developed by the research groups of MeteoFrance, NCEP and WAMDI, have been adopted for the Black Sea area and implemented at the National Institute of Meteorology and Hydrology Bulgarian Academy of Sciences (NIMH-BAS) to allow real-time forecasts and hindcasts of the waves in the Black Sea. The coupling of two atmospherics models ARPEGE and ALADIN has been used to force the wave models. In this study 10 different severe storms were modelled in the period of 2003-2007. The operational use had indicated that the system is suitable for general purposes and the results are generally satisfactory. A comparison between the model results and the altimeter data from the satellites ERS1/2 and ENVISAT demonstrated that the models fairly reproduced the observed characteristics of waves.

Bernardino et al. (2012) conducted high resolution wind and wave simulation using satellite information. The wave model implemented was SWAN model which was forced by the 10 meter wind field simulated by the WRF using ERA-INTERIM reanalysis.

Akpınar and Kömürcü (2013) have studied the variability of wave energy resource potential of the Black Sea based on 15-year hindcast data. Wave parameters were obtained using SWAN forcing the ECMWF ERA interim wind field data into the model with 0.0167° × 0.0167° spatial resolution and 6 hour time intervals. Wave height and wave power charts were presented in the form of charts on monthly, seasonal and annual basis. The areas with the highest wave energy resource were determined and the south west coasts of the Black Sea are suggested as the best site for the installation of a wave farm.

Aydoğan et al. (2013) evaluated the wave energy potential at Black Sea where the wave properties were calculated with MIKE 21 SW (Spectral Wave Model) using ECMWF wind data. The wave model was calibrated using the wave measurements conducted at five different stations. Wave energy found to be decreasing along the coast from west to east. It was found that the most energetic region is the South Western part and it was concluded that the most promising location is the Thracian shores of Turkey, especially west side of Istanbul. Also authors presented annual wave energies (kWh/m) for different regions.

Galabov (2013) compared the modeled mean wave power flux output from the SWAN wave model with the only available long term measurements from the buoy of Gelendzhik for the period 1997-2003 using ERA Interim reanalysis of ECMWF. Also, the estimated wave power was compared with the modeled data by SWAN, using ALADIN regional atmospheric model winds for the year 2003. The purpose of the study was to determine the limitations of the numerical modeling approach to the evaluation of the wave energy potential in Black Sea.

Arkhipkin et al. (2014) estimated the statistical wave parameters and assessed interannual and seasonal wave parameter variability for Black Sea using SWAN wave model. Initial conditions (wind speed and direction) for the period between 1949 and 2010 were derived from the NCEP/NCAR reanalysis. According to the results of the study, the average significant wave height on the Black Sea does not exceed 0.7 m. The spatial distributions of significant wave heights, wave lengths and

periods show that the heavy sea is mostly observed in southwestern and the northeastern parts of the sea. Also, long-term annual variations of wave parameters were estimated in the study.

Majority of the wave model implementations in Black Sea usually concentrated on the long term wave hindcast and the general wave climate of Black Sea. However, in 2015, Akpinar and Leon have carried out a study which has been consisted of assessment of wind reanalysis for the modelling of an extreme event. Akpinar and Leon (2015) has shown that recommended parametrization of the wave models were not able to represent the extreme events in Black Sea, so that new set of parameterization which was based on the dissipation source was developed. Throughout the study SWAN wave model has been used with several wind re-analysis data. According to Akpinar and Leon (2015) CFSR wind fields has shown the best configuration with SWAN model in an extreme case.

Moreover, Van Vledder and Akpınar (2015) evaluated the performance of different wind field data on the third generation wave model, SWAN, in the Black Sea and the capability of the model to predict both normal and extreme wave conditions during 1996. Wind data were obtained from NCEP CFSR, NASA MERRA, JRA-25, ECMWF Operational, ECMWF ERA40, and ECMWF ERA-Interim. Wave data of 1996 were obtained at three locations in the Black Sea within the NATO TU-WAVES project. Main purpose of the study was to investigate the impact of different wind field data on wave hindcast performance by analyzing the sensitivity of wave model forecasts due to variations in spatial and temporal resolutions of the wind field products and the impact of using various wind field products on predicting extreme wave events by focusing on storm peaks and on an individual storm event in October 1996. It was found that the CFSR winds are more suitable in comparison with the others for modelling both normal and extreme events in the Black Sea. Also, it is indicated that the quality and spatial resolution of the wind data affects the wave model predictions where the temporal resolution does not have significant effect.

CHAPTER 3

DESCRIPTION of 3RD GENERATION WAVE MODELS

In this chapter, the general descriptions of wave generation models are introduced. Governing equations, numerical approaches of the chosen wave models, SWAN and WAVEWATCH III model, are explained in detail. A comparison of the two wave models within the scope of this study regarding the numerical approaches and methodology is also given. Finally, the statistical methods and the ranking system used in the evaluation of the model performance are given.

3.1 SWAN Model

Simulating Wave Nearshore (SWAN) is a third generation wave model developed by Delft University of Technology. SWAN solves spectral action balance equation in order to explain the sea state and wave growth. Action balance equation considers the effects of spatial propagation, refraction, shoaling, generation, dissipation, and non-linear wave-wave interactions (SWAN Team, 2015). SWAN model uses source and sinks terms that add or extract energy from the system during the simulation of evolution of wind waves.

3.1.1 Propagation of SWAN Model

Spectral energy density function E(σ,θ) where σ and θ represents frequencies and propagation direction respectively are used in SWAN to explain the sea surface elevation. Action density is defined as N=E/σ.

SWAN model is an fully discrete spectral model based on the action balance equation (Booij,1996;SWAN Team, 2015) which is given below:

$$\frac{\partial N}{\partial t} + \nabla_{\vec{x}} . \left[\left(\overrightarrow{C_g} + \overrightarrow{U}\right) N\right] + \frac{\partial c_\sigma A}{\partial \sigma} + \frac{\partial c_\theta A}{\partial \theta} = \frac{S_{tot}}{\sigma} \quad (3.\ 1)$$

Left hand of the equation is the kinematic part, where the first term represents the effect of time on action density, the second term represents propagation of wave energy in two dimensional space ($\vec{x}$) with group velocity (C_g). The third term represents the effect of shifting of the radian frequency due to variations in depth and mean currents. The fourth term represents depth-induced and current-induced refraction (SWAN Team, 2015). Right hand of the Eq. 3.1 represents the sink and source terms.

3.1.2 Source and Sink Terms of SWAN Model

All the physical processes that effect the energy of total system such as dissipation, wind-wave interaction, bottom friction etc. are explained with the source and sink parameters (Figure 3.1) in SWAN.

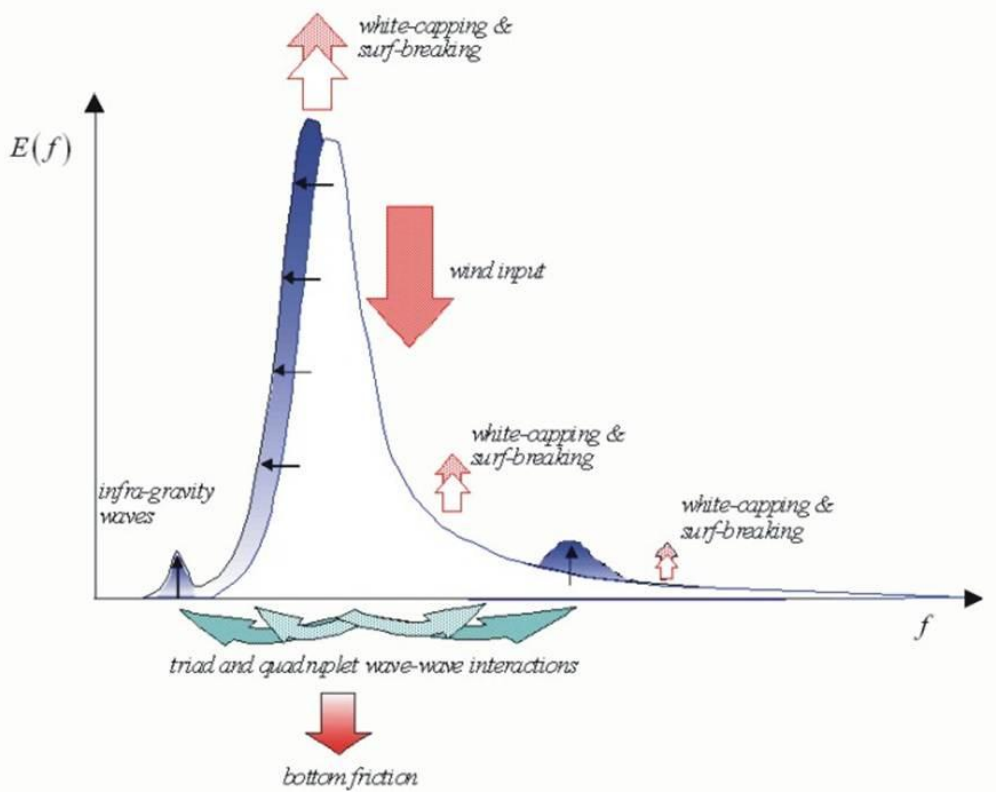

Figure 3.1 Source and Sink Terms in Wave Models (Ardhuin, 2014)

Deep water source terms (wind-wave interaction, whitecapping dissipation, nonlinear wave-wave interaction) are the main source terms considered in this study. Some if the shallow water approaches are also included in the simulations such as bottom friction and depth induced breaking. Although there are many different source and sink terms, only the dominant and the applied terms will be discussed in the following sections. The detailed explanation can be found in SWAN technical documentation (SWAN Team, 2015).

3.1.2.1 Wind-Wave Interaction Term

Wind-wave formation starts with small random pressure fluctuations which are caused by the constant blowing wind over a water surface (Phillips, 1957). This process creates waves in the order of few centimeters. If wind continues to blow over already disturbed water surface, up and down movement of sea surface increases and pressure differences between the through and crest points of wave gets larger. So that energy transfer from wind to wave occurs. According to Miles (1957), this process is found to be increasing exponentially in time caused by the shear instabilities occurring at the water surface.

The main source of the wave generation models is the wind input. In SWAN model wave growth by wind is described as in Eq. 3.2:

$$S_{in}(\sigma,\theta) = A + BE(\sigma,\theta) \tag{3. 2}$$

Where A and B represents the linear and exponential growth respectively.

Linear part of the equation (A), based on the Cavaleri and Malanotte-Rizzoli (1981) study (SWAN Team, 2015), is given as follows:

$$A = \frac{1.5x10^{-3}}{2\pi g^2}(U_* \max[\,0, \cos(\theta - \theta_w)])^4 H \tag{3. 3}$$

$$H = \exp\left\{-\left(\frac{\sigma}{\sigma^*_{PM}}\right)^{-4}\right\} \tag{3. 4}$$

$$\sigma^*_{PM} = \frac{0.13g}{2U_*}2\pi \tag{3. 5}$$

Where U_* is the friction velocity which is dependent on the wind speed at 10m elevationU_{10}, θ_w is the wind direction, H is the filter to eliminate wave growth at frequencies lower than Pierson-Moskowitz frequency which is introduced by Tolman,1992 and σ_{PM}^* is the peak frequency of the fully developed sea state according to Pierson and Moskowitz (1964) as formulated in terms of friction velocity.

For the exponential part of the wind input, SWAN model has two options. First option is the Komen (1984) methodology which is also used in WAM Cycle 3. Komen (1984) approach is as follows:

$$B = \max[\,0, 0.25 \frac{\rho_a}{\rho_w} (28 \frac{U_*}{c_{ph}} cos(\theta - \theta_w) - 1] \sigma \qquad (3.6)$$

Where c_{ph} is the phase speed, ρ_a and ρ_w are the density of air and water, respectively.

The second option is based on the Miles (1957) and Janssen (1991) methodology and parameterization which will be called as Janssen method here after. The formulations given below are also used in WAM Cycle 4.

$$B = \beta \frac{\rho_a}{\rho_w} (\frac{U_*}{c_{ph}})^2 \ \max[0, cos(\theta - \theta_w)]^2 \, \sigma \qquad (3.7)$$

Where β is the miles constant which is defined as;

$$\beta = \frac{1.2}{\kappa^2} \lambda ln^4 \lambda, \ \lambda \leq 1 \qquad (3.8)$$

$$\lambda = \frac{gz_e}{C_{ph}^2} e^r, \quad r = \kappa c / |U_* \cos(\theta - \theta_\omega)| \tag{3. 9}$$

In above equations, λ is the non-dimensional critical height, κ is the Von Karman constant which is equal to 0.41. z_e is the effective roughness length which is depends on the roughness length, the wave induced stress and the total surface stress. In Eq. 3.9 if $\lambda > 1$, β is equal to 0.

3.1.2.2 Whitecapping Dissipation Term

Whitecapping can be also called as deep water wave breaking which is the top breaking of the waves in deep water. This phenomenon is directly related with the steepness of waves. When a wave becomes too steep so that it cannot maintain its forms and breaks. This process causes certain loss of wave energy in deep water and considered as sink term in wave generation models.

There exist 3 different options for calculation of whitecapping dissipation of energy in SWAN model, however only 2 of them, Komen (1984) and Janssen (1992), are used within this scope of study. The main formulation for the whitecapping dissipation depends on the Komen (1984) study which can be seen as follows in Eq. 3.10.

$$S_{ds,w}(\sigma, \theta) = -\Gamma \tilde{\sigma} \frac{k}{\tilde{k}} E(\sigma, \theta) \tag{3. 10}$$

Where $\tilde{\sigma}$ stands for mean frequency, $\tilde{k}$ stands for mean wave number, Γ is a steepness dependent coefficient which is defined as follows;

$$\Gamma = \Gamma_{KJ} = C_{ds}(1-\delta) + \delta\frac{k}{\tilde{k}})\left(\frac{\tilde{s}}{\tilde{s}_{PM}}\right)^{p} \quad (3.\ 11)$$

Where C_{ds} is the coefficient for determining the rate of whitecapping dissipation, δ is the coefficient which determines the dependency of the whitecapping on wave number, p is power of steepness normalized with the wave steepness of a Pierson-Moskowitz spectrum. $\tilde{s}$ stands for overall wave steepness and calculated as:

$$\tilde{s} = \tilde{k}\sqrt{E_{tot}} \quad (3.\ 12)$$

Lastly, $\tilde{s}_{PM}$ is the overall wave steepness of the Pierson-Moskowitz spectrum (1964) which has default value of $\tilde{s}_{PM} = \sqrt{3.02x10^{-3}}$.

The above coefficients are tuned according to wind input of Komen (1984) both for developing and fully developed sea conditions and used in WAM Cycle 3. Tuning of whitecapping coefficients are also done by Janssen (1992) considering the use of Janssen (1991) WAM Cycle 4 wind input formulations. The coefficient of C_{ds}, $\tilde{s}_{PM}$, δ , p are tunable in SWAN model, and default parameterization of those parameters for the Komen and Janssen approaches are given in Table 3.1

Table 3.1 Whitecapping dissipation default parameterizations for Komen (1984) and Janssen(1992) approaches

	C_{ds}	δ	ρ
Komen(1984)	$2.36x10^{-5}$	1	4
Janssen(1992)	$4.10\ x10^{-5}$	0.5	4

3.1.2.3 Nonlinear Wave- Wave Interaction Term

Nonlinear wave-wave interactions are the energy exchange between wave components and redistribution of energy over spectrum. In deep water, four wave components with wavenumber vectors named as k1, k2, k3, k4 are active which are called quadruplets. Quadruplets causes energy transfer from the spectral peak to lower frequencies and to higher freqeuncies where the energy is dissipated by whitecapping (SWAN Team, 2015). Nonlinear wave-wave interactions in deep water causes peak frequency to shift towards low end of spectrum (SWAN Team, 2015).

Quadruplets are considered as another deep water sink term in wave models. In SWAN model there are 3 different approaches for the solution of the quadruplets, however only two of them was considered in this study. Since XNL method requires 10^3 to 10^4 times more computational effort and it is only appropriate for highly idealized cases(SWAN Team, 2015)

First method is the Discrete Interaction Approximation (DIA) which is proposed by Hasselmann et. al. (1985). Even though DIA is an approximation, it is accepted as a quite good representation of the nonlinear wave-wave interactions of a developing wave spectrum. (SWAN Team, 2015).

In DIA application, it is assumed that two wave numbers are equal:

$$\overrightarrow{k_1} = \overrightarrow{k_2} \tag{3. 13}$$

Other wave numbers $\overrightarrow{k_3}$ and $\overrightarrow{k_4}$ have different magnitude and angles (Vledder,2000).

Frequencies of wavenumber in DIA method take the following form

$$\sigma_1 = \sigma_2$$

$$\sigma_3 = (1+\lambda)\sigma_1$$

$$\sigma_4 = (1-\lambda)\sigma_1 \qquad (3.\ 14)$$

Where λ is the coefficient for quadruplet configurations which ranges between 0 and 0.45 (Vledder, 2000). Recommended value of λ is 0.25 in SWAN model.

With DIA method, the rates of change in energy densities, $S_{nl1}, \delta S_{nl3}$ and δS_{nl4} within one wave number quadruplets are given by:

$$\begin{pmatrix} \delta S_{nl1} \\ \delta S_{nl3} \\ \delta S_{nl4} \end{pmatrix} = \begin{pmatrix} 2 \\ -1 \\ -1 \end{pmatrix} C g^{-4} f^{11} \left[{E_1}^2 \left(\frac{E_3}{(1+\lambda)^4} + \frac{E_4}{(1-\lambda)^4} \right) - \frac{2E_1E_3E_4}{(1-\lambda^2)^4} \right] \qquad (3.\ 15)$$

Where the recommended value for $C = 3x10^7$, E_1 is the energy density of wave number k1.

In DIA, Eq. 3.13 is evaluated for all values of the $\overrightarrow{k_1} = \overrightarrow{k_2}$, that correspond to the wave numbers of the discretized spectrum (Vledder,2000; SWAN Team, 2015).

Since DIA model is sensitive to the frequency resolution, originally DIA approach is tuned in WAM model with frequency resolution of 10% which stands for:

$$f_{i+1} = f_i * 1.1 \qquad (3.\ 16)$$

Since, DIA methodology is an approximation; it might not always satisfy the adequate accuracy. Therefore, the second method available in SWAN model is a developed version of DIA. It has revealed by Hashimoto et al. (2002) that, increasing the accuracy of DIA is possible when the number of quadruplet configuration are increased. Therefore, DIA methodology with 6 wave number configuration applied

in SWAN model as a new way of solution for nonlinear wave-wave interaction which is called multiple DIA or MDIA.

3.1.2.4 Bottom Friction Term

Empirical formulation of JONSWAP is used for bottom friction term in SWAN. given as the following:

$$S_{ds,b} = -C_b \frac{\sigma^2}{g^2 sinh^2 kd} E(k,\theta) \quad (3.\ 17)$$

Where, C_b is the JONSWAP bottom friction coefficient that depends on the bottom orbital motion. Hasselmann(1973) suggested that $C_b = 0.038 m^2 s^{-3}$ for swell dissipation and $C_b = 0.067 m^2 s^{-3}$for depth limited wind-sea conditions. (Bouws and Komen, 1983; SWAN Team, 2015)

It is recently found by Zijlema et al. (2012) that, if a second order polynomial fit for wind drag is employed, default value of $C_b = 0.038 m^2 s^{-3}$ can be used for all conditions. The second order polynomial fit for wind drag is defined as follows (Eq. 3.18) in SWAN model.

$$C_D(U_{10}) = \left(0.55 + 2.97\widetilde{U} - 1.49\widetilde{U}^2\right) x 10^{-3} \quad (3.\ 18)$$

Where C_D is the drag coefficient by Wu (1982) and $\widetilde{U}$ is defined as;

$$\widetilde{U} = \frac{U_{10}}{U_{ref}} \quad (3.\ 19)$$

U_{ref} is the reference wind speed which is set equal to 31.5 m/s where drag attains its maximum value in above expression.

3.1.2.5 Depth Induced Wave Breaking Term

In SWAN model, Battjes and Janssen (1978) approach is used to describe the depth induced wave breaking. According to Battjes and Janssen (1978), all waves in a random field will break after they reach their maximum wave height which is controlled by the depth parameters. The mean rate of energy dissipation per unit horizontal area due to wave breaking is expressed as

$$D_{tot} = -\frac{1}{4}\alpha_{BJ} Q_b \left(\frac{\tilde{\sigma}}{2\pi}\right) H_{max}^2 \quad (3.\ 20)$$

in which $\alpha_{BJ} = 1$ in SWAN, Q_b is the fraction of breaking waves determined by:

$$\frac{1-Q_b}{lnQ_b} = -8\frac{E_{tot}}{H_{max}^2} \quad (3.\ 21)$$

The maximum wave height is determined from:

$$H_{max} = \gamma d \quad (3.\ 22)$$

Where, γ is the breaker parameter chosen as 0.73 and d is the local depth.

3.1.3 Numerical Approaches of SWAN Model

Because of the physical nature of the wind waves, third generation models need to use multiple time scales which causes a numerical difficulty. Third generation wave model solutions both need to be economic and numerically stable during the run of the model. "The steady-state solution in the SWAN model is obtained in an iterative manner, which can be regarded as a time marching method with a pseudo time step. This pseudo time step generally does not match the relatively small time scale in frequency space and consequently, divergence will occur." (Booij et al.,1999). In order to ensure the numerical stability in wave models, limiters are introduced. Limiter restricts the rate of chance of the energy spectrum which has a higher effect on the high frequency end of spectrum where for high frequency waves using an equilibrium level is sufficient (SWAN Team, 2014). Since more energy is present on the low end of spectrum, this part of spectrum should be solved accurately without intervention of limiter. SWAN model converges in a fast manner while minimizing the role of limiter (SWAN Team, 2014). In SWAN model, discretization is needed for the action balance equation (Eq.3.1) on both geographical space and spectral space. The finite difference method is used for discretization. Rectangular grids are chosen on the geographical space with constant mesh sizes (Δ_x and Δ_y). The direction and frequency is also divided into equally sized bins in spectral space (Δ_θ and Δ_σ/σ). The grid counters defined as $1 \leq i \leq N_x$, $1 \leq j \leq N_y$, $1 \leq l \leq N_\sigma$, $1 \leq m \leq N_\theta$ in x,y,σ,θ spaces respectively (SWAN Team, 2015).

3.1.3.1 Discretization in geographical space

A first order upwind scheme is used for the geographical space discretization. The fluxes of $c_x N$ and $c_y N$ at (i+1/2,j,l,m) and (i,j+1/2,l,m) are defined as follows (SWAN Team, 2015)

$$c_x N|_{\mathrm{i+1/2,j,l,m}} = \begin{cases} c_x N|_{\mathrm{i,j,l,m}}\,, & c_x|_{\mathrm{i,j,l,m}} > 0 \\ c_x N|_{\mathrm{i+1,j,l,m}}\,, & c_x|_{\mathrm{i+1,j,l,m}} < 0 \end{cases} \tag{3. 23}$$

$$c_y N|_{\mathrm{i,j+1/2,l,m}} = \begin{cases} c_y N|_{\mathrm{i,j,l,m}}\,, & c_y|_{\mathrm{i,j,l,m}} > 0 \\ c_y N|_{\mathrm{i,j+1,l,m}}\,, & c_y|_{\mathrm{i+1,j,l,m}} < 0 \end{cases} \tag{3. 24}$$

When above terms are combined with the time discretization, this scheme known as first order, backward space, backward time (BSBT) scheme (SWAN Team, 2015) This propagation scheme have some drawback such as accuracy of the model is not always satisfied since scheme is numerically diffusive . In SWAN model alternative second order Stelling/Leendertse scheme for non-stationary runs is available which is better in terms of numerical diffusive problems (SWAN Team, 2015).

In Stelling/Leendertse scheme, x and y derivatives are replaced with,

$$\left(\frac{\frac{5}{6}(c_x N)_{i_x} - \frac{5}{4}(c_x N)_{i_x-1} + \frac{1}{2}(c_x N)_{i_x-2} \frac{1}{12}(c_x N)_{i_x-3}}{\Delta x}\right)_{i_y, i_\sigma, i_\theta}^{i_t, n} + \left(\frac{(c_x N)_{i_x+1} - (c_x N)_{i_x-1}}{4\Delta x}\right)_{i_y, i_\sigma, i_\theta}^{i_t-1} \tag{3. 25}$$

$$\left(\frac{\frac{5}{6}(c_y N)_{i_y} - \frac{5}{4}(c_y N)_{i_y-1} + \frac{1}{2}(c_y N)_{i_y-2} \frac{1}{12}(c_y N)_{i_y-3}}{\Delta y}\right)_{i_x, i_\sigma, i_\theta}^{i_t, n} + \left(\frac{(c_y N)_{i_y+1} - (c_y N)_{i_y-1}}{4\Delta y}\right)_{i_x, i_\sigma, i_\theta}^{i_t-1} \tag{3. 26}$$

3.1.3.2 Discretization in spectral space

It is not possible to use first order upwind scheme since it is very diffusive for some frequencies. So that, hybrid central /upwind scheme is employed (Eq. 3.27 and Eq. 3.28) (SWAN Team, 2015).

$$c_\sigma N|_{\mathrm{i,j,l+1/2,m}} = \begin{cases} (1-0.5\mu)c_\sigma N|_{\mathrm{i,j,l,m}} + 0.5\mu c_\sigma N|_{\mathrm{i,j,l+1,m}},\ c_\sigma|_{\mathrm{i,j,l,m}} > 0 \\ (1-0.5\mu)c_\sigma N|_{\mathrm{i,j,l+1,m}} + 0.5\mu c_\sigma N|_{\mathrm{i,j,l,m}},\ c_\sigma|_{\mathrm{i,j,l+1,m}} < 0 \end{cases} \quad (3.\ 27)$$

$$c_\theta N|_{\mathrm{i,j,l,m+1/2}} = \begin{cases} (1-0.5\mu)c_\theta N|_{\mathrm{i,j,l,m}} + 0.5\mu c_\theta N|_{\mathrm{i,j,l,m+1}},\ c_\theta|_{\mathrm{i,j,l,m}} > 0 \\ (1-0.5\mu)c_\theta N|_{\mathrm{i,j,l,m+1}} + 0.5\mu c_\theta N|_{\mathrm{i,j,l,m}},\ c_\theta|_{\mathrm{i,j,l,m+1}} < 0 \end{cases} \quad (3.\ 28)$$

3.1.3.3 Solution Algorithm

In SWAN model, system of linear equations, which are obtained after discretization process, are solved using Gauss-Seidel technique in one step (SWAN Team, 2015; Wesseling, 1992). In solution algorithm, sweeping through the geographical domain is completed for four corners of grids for each iteration, then energy propagated after sweeps.

3.2 WAVEWATCH III Model

WAVEWATCH III (WW3) is a third generation wave model which has been developed by Marine Modeling and Analysis Branch (MMAB) of the Environmental Modeling Center (EMC) of the National Centers for Environmental Prediction (NCEP). Previous versions, Wavewatch I and Wavewatch II are developed by University of Technology and NASA Goddard Space Flight Center, respectively. WAVEWATCH III is distinguished from earlier versions with its numerical and physical approaches, to governing equations.

WAVEWATCH III is a phase averaged wave hindcast, forecast and transformation model which solves spectral action/energy balance equation. In WW3, the variance of the sea surface is described using the energy density spectra (Tolman et. al.,

2014). In order to explain the physical processes, WW3 uses source and sink terms just like SWAN model.

3.2.1 Propagation of WAVEWATCH III Model

In WW3 model, wave propagation is described as:

$$\frac{DN}{Dt} = \frac{S}{\sigma} \tag{3. 29}$$

Where; $\frac{DN}{Dt}$ represents the total derivative of action density spectrum and S represents the net effect of sources and sinks. If the balance Eq. 3.1 is written in Eulerian form for the spectrum $N(k, \theta; x, t)$ Eq. 30 is obtained which is the applied version of equation to WW3 model as in SWAN model.

$$\frac{\partial N}{\partial t} + \nabla_{\vec{x}} . \dot{x}N + \frac{\partial \dot{k}N}{\partial k} + \frac{\partial \dot{\theta}N}{\partial \theta} = \frac{S_{tot}}{\sigma} \tag{3. 30}$$

Where in kinematic part (left-hand terms), first time represent change in time, second term represents advection in geographical space, third and fourth terms represent the advection in spectral space.

3.2.2 Source and Sink Terms in WAVEWATCH III Model

WW3 model considers the sources and sinks in order to explain the physical processes similar to SWAN model. In WW3, different options of the physical processes are named as switches, and this term will be used hereinafter.

In deep water, three processes define the total source term which are, wind-wave interaction, whitecapping dissipation and nonlinear wave-wave interaction. Even though wind-wave interaction and whitecapping dissipation are different processes, since they are interrelated and define the integral growth characteristics of the wave model together, they are considered together and controlled by the same switch in WW3 model. This approach is slightly different than the previously defined approach of SWAN. Comparison of the two models are explained in detail in Section 3.3.

In shallow water, the dominant source and sinks terms considered are the wave-bottom interaction (bottom friction) and depth induced wave breaking.

Some of the other available sink terms of WAVEWATCH III model such as wave-ice interactions are not considered in this study since they are not applicable to Black Sea.

3.2.2.1 Wind-Wave Interaction Term

The main source of the wind input of WWIII is defined same as in SWAN model which is described in Eq. 3.2.

The linear part of the equation (A) is based on the Cavaleri and Malanotte-Rizzoli (1981) study.

Low frequency energy filter, H, introduced by Tolman (1992) is also applied in WW3. (Eq. 3.4 and Eq. 3.5). However, for the filter frequency in Eq. 3.4, WW3 model has more options and parameters that can be set by users.

For the exponential part of the wind-wave interaction (S_{in}), five different approaches are available. All of the exponential approaches are tried and compared in the preliminary runs. The four approaches used in the bulk runs for the final comparison of this study are described below.

1st approach which is referred as ST1 is based on the WAM Cycle 3, Snyder et. al. (1981) and Komen(1984). ST1 is also referred as Komen(1984) approach in the SWAN part of this chapter.

Wind input source term of the 2nd approach (ST2) is based on the studies of Chalikov and Belevich (1993) and Chalikov (1995). The source term is defined as;

$$S_{in}(k,\theta) = \sigma\beta N(k,\theta) \tag{3. 31}$$

Where β is the non-dimensional wind-wave interaction parameter which depends on non-dimensional frequency of a spectral component, wind direction, wind velocity at a height equal to the 'apparent' wave length and the drag coefficient. Only input for the model is the wind speed and a reference height of wind. Others parameters are defined using those two parameters. In addition, filtered input source term is defined in order to solve the overestimation of the swell dissipation caused by opposing and weak winds. (Tolman, 2014) Details can be found in WW3 manual (Tolman, 2014).

3rd approach which is referred as ST3 is based on the WAM Cycle 4. ST3 is source term based on Miles(1957) and Janssen (1982) which is referred as the Janssen method in SWAN part of this chapter. However, some small modifications were done by Jannsen (2004) and final input source term becomes Eq. 3.32 as follows:

$$S_{in}(k,\theta) = \frac{\rho_a}{\rho_w}\frac{\beta_{max}}{\kappa^2}e^Z Z^4 \left(\frac{U_*}{C} + z_\alpha\right)^2 cos^{p_{in}}(\theta - \theta_w)\sigma N(k,\theta) + S_{out}(k,\theta) \tag{3. 32}$$

Where p_{in} is constant that controls the directional distribution of $S_{in}(k,\theta)$. Above equation is slightly different than previously defined equations Eq. 3.7, 3.8 and 3.9 in SWAN part of this chapter. z_α is a tuning parameter that controls wave age shift to account for gustiness which has an important effect on wave growth. Essentially it shifts the wave age of the long waves, which typically increases the growth, and even

generates waves that travel faster than the wind. This accounts for some gustiness in the wind and should possibly be resolution-dependent. (Tolman, 2014) Z in Eq. 3.32 stands for logarithm of dimensionless critical wave heights which is defined as follows (Eq.3.33):

$$Z = \log(kz_1) + \kappa/[\cos(\theta - \theta_u)(\frac{U_*}{C} + z_\alpha) \quad (3.33)$$

Where z_1 is the roughness length which is defined as:

$$z_1 = \alpha_0 \frac{\tau}{\sqrt{1-\tau_w/\tau}} \quad (3.34)$$

Where, τ_w is the wave-supported stress which is calculated using below equation;

$$\tau_w = \left|\int_0^{k_{max}} \int_0^{2\pi} \frac{S_{in}(k',\theta)}{C}(cos\theta, sin\theta)dk'd\theta + \tau_{hf}(U_*, \alpha)(cos\theta_u, sin\theta_u)\right| \quad (3.35)$$

Where α is the Charnock coefficient and τ_{hf} is the stress supported by shorter waves, and τ is defined as;

$$\tau = {U_*}^2 \quad (3.36)$$

Above equations are slightly different than the previously defined equations Eq. 3.7, 3.8 and 3.9 in SWAN part of this chapter.

This parameterization is sensitive to the spectral level atk_{max}. A higher spectral level will lead to a larger value of U_* and thus positive feedback on the wind input viaz_1.

The final approach (ST4) is based on the study of Ardhuin et Al. (2010) which uses the positive part of the wind input as in WAM Cycle 4, with a reduction of U_* implemented in order to allow a balance with a saturation-based dissipation (Tolman, 2014). This correction also reduces the drag coefficient at high winds. This is done by reducing the wind input for high frequencies and high winds. So that U_* in WAM Cycle 4, Janssen formulation is replaced by $U'_*(k)$ defined as:

$$U'_*(k) = \left| U_*^2(cos\theta_U, sin\theta_U) - |S_U| \int_0^k \int_0^{2\pi} \frac{S_{in}(k',\theta)}{C} (cos\theta, sin\theta) dk' d\theta \right| \quad (3.37)$$

Where S_U is the sheltering coefficient which is used to tune the stresses at high winds.

3.2.2.2 Whitecapping and Swell Dissipation Term

Since the source input,S_{in}, and dissipation terms are defined together in WW3 model. Whitecapping dissipation approaches are also called as ST1, ST2, ST3 and ST4.

ST1 approach is based on WAMDI Group (1988), WAM Cycle 3 which is the main methodology used in SWAN model.

The equation of the dissipation term is similar in Eq. 3.11 for SWAN model. However, in WW3 model, equivalent parameterizations of δ and p values in Eq.3.11 are set to 0 and 4 respectively in ST1 approach. C_{ds} is the coefficient for determining the rate of whitecapping dissipation and $\tilde{s}_{PM}$ is the overall wave steepness of the Pierson-Moskowitz spectrum values are tunable in ST1 dissipation term.

In ST2 approach dissipation term is examined under two parts based on frequency; the dominant part of low frequency ($S_{ds,l}(k,\theta)$) (turbulent like dissipation) and the recessive empirical high frequency dissipation($S_{ds,h}(k,\theta)$).

Most general term is given as in Eq. 3.38:

$$S_{ds}(k,\theta) = AS_{ds,l}(k,\theta) + (1-A)S_{ds,h}(k,\theta) \quad (3.38)$$

Where A is the coefficient which is defined as in Eq. 3.39:

$$A = \begin{cases} 1 \; for \; f < f_1 \\ \frac{f-f_2}{f_1-f_2} \; for \; f_1 \leq f \leq f_2 \\ 0 \; for \; f > f_2 \end{cases} \quad (3.39)$$

In Eq. 3.39 f_1 and f_2 are based on peak frequency of the positive part of the input source term, $f_{p,i}$ which is given as in Eq. 3.40:

$$f_{p,i} = \frac{\int\int f^{-2} c_g^{-1} \max[0, S_{wind}(k,\theta)] df d\theta}{\int\int f^{-3} c_g^{-1} \max[0, S_{wind}(k,\theta)] df d\theta} \quad (3.40)$$

In ST2 approach, f_1 is set to $f_1 = 1.75 f_{p,i}$ and f_2 is set to $f_2 = 2.50 f_{p,i}$ while minimum value of $f_{p,i}$ is specified as 0.009.

The low frequency part of the dissipation term is formulated based on the analogy with dissipation due to turbulence (Eq. 3.41).

$$S_{ds,l}(k,\theta) = -2U_* h k^2 \emptyset \, N(k,\theta) \quad (3.41)$$

In above equation h is a mixing scale determined from the high-frequency energy content of the wave field (Eq. 3.42).

$$h = 4\left(\int_0^{2\pi}\int_{f_h}^{\infty} F(f,\theta)dfd\theta\right)^{0.5} \quad (3.42)$$

In Eq. 3.40, $\emptyset$ represents the empirical function accounting for the development stage of the wave field which consist of linear and nonlinear parts (Eq 3.43).

$$\emptyset = b_0 + b_1\widetilde{f_{p,i}} + b_2\tilde{f}_{p,i}^{-b_3} \quad (3.43)$$

Linear part of Eq. 3.43 explains the dissipation for growing waves while nonlinear part of the equation is used in order to allow control on over fully grown conditions by defining minimum value of $\emptyset$ for the minimum value of $f_{p,i}$.

In Eq. 3.43, the tunable coefficients b_0 and b_1 are set to $0.3\text{x}10^{-3}$ and 0.47 respectively for the effects of stability on the growth rate of waves based on Kahma and Calkoen, 1992, (KC stable) are included in the source term. For KC unstable version b_0 and b_1 values are calibrated as $-5.8\text{x}10^{-3}$ and 0.60 respectively.

b_2 and b_3 are coefficients dependent on $\emptyset_{min}$, b_0 ,b_1 and frequency. Formulations of the coefficients b_2 and b_3 are change depending on whether $\emptyset_{min}$ is below the or above the linear curve.

High frequency dissipation part of Eq. 3.38 ($S_{ds,h}(k,\theta)$) is represented by the equations below.

$$S_{ds,h}(k,\theta) = -a_0\left(\frac{U_*}{g}\right)^2 f^3\, \alpha_n^B N(k,\theta) \quad (3.44)$$

$$B = a_1 \left(\frac{fU_*}{g}\right)^{-a_2} \tag{3. 45}$$

$$\alpha_n = \frac{\sigma^6}{c_g g^2 \alpha_r} \int_0^{2\pi} N(k,\theta) d\theta \tag{3. 46}$$

In above equations, α_n is Phillips' non-dimensional high-frequency energy level normalized with α_r. a_0, a_2, α_r are empirical constants. Values of a_0, a_1, a_2 are 4.8, 1.7x10^{-4}, 2.0 respectively in KC stable version, and 4.5, 2.3x10^{-4}, 1.5 respectively in KC unstable version parameterizations (Tolman, 2014).

Dissipation term of ST3 approach is explained in two parts. First one is the $S_{out}(k,\theta)$ term in Eq. 3.32 which represents the linear damping of swells (Eq. 3.47) and the dissipation term.

$$S_{out}(k,\theta) = 2 s_1 \kappa \frac{\rho_a}{\rho_w} \left(\frac{U_*}{C}\right)^2 \left[\cos(\theta - \theta_u) - \frac{\kappa C}{U_* \log(k z_0)}\right] \tag{3. 47}$$

Where s_1 is the swell parameter when $s_1 = 1$ linear damping of swell is activated. In WAM Cycle 4 $s_1$is taken as 0.

The second part is the $S_{ds}(k,\theta)$ which is based on the WAM Cycle 4 formulations (Eq. 3.48).

$$S_{ds}(k,\theta) = C_{ds}\, \bar{\alpha}^2 \bar{\sigma} \left[\delta_1 \frac{k}{\bar{k}} + \delta_2 \left(\frac{k}{\bar{k}}\right)^2\right] N(k,\theta) \tag{3. 48}$$

Where C_{ds} is the non-dimensional coefficient, δ_1 and δ_2 are weight parameters,

$$\bar{k} = \left[\frac{\int k^p N(k,\theta)d\theta}{\int N(k,\theta)d\theta}\right]^{1/p} \quad (3.\ 49)$$

$$\bar{\sigma} = \left[\frac{\int \sigma^p N(k,\theta)d\theta}{\int N(k,\theta)d\theta}\right]^{1/p} \quad (3.\ 50)$$

$$\bar{\alpha} = E\bar{k}^2 \quad (3.\ 51)$$

Where $\bar{k}$, $\bar{\sigma}$and $\bar{\alpha}$ are mean wave number, mean frequency and mean steepness respectively in WAM Cycle 4 formulations.

ST4 approach of dissipation term is an improved version of the ST3 parameterization especially in terms of swell dissipation. First of all, s_1 value is different than 0 in order to activate swell dissipation terms. Moreover, viscous boundary layer value is added to the $S_{out}(k,\theta)$ term beside turbulent boundary layer value and total $S_{out}(k,\theta)$ term becomes:

$$S_{out}(k,\theta) = r_{vis}S_{out,vis}(k,\theta) + r_{tur}S_{out,tur}(k,\theta) \quad (3.\ 52)$$

Where r_{vis} and r_{tur} coefficient are defined from a modified air-sea boundary layer significant Reynolds number (Eq. 3.53), critical Reynolds number (Re_c) and swell coefficient (s_7) as in Eq. 3.53 and Eq.3.54.

$$r_{vis} = 0.5(1 - \tanh((Re - Re_c)/s_7 \quad (3.\ 53)$$

$$r_{tur} = 0.5(1 + \tanh((Re - Re_c)/s_7 \quad (3.\ 54)$$

$$Re = 2u_{orb,s}H_s/\nu_\alpha \quad (3.\ 55)$$

Where, $u_{orb,s}$ is the significant surface orbital velocity defined in Eq.3.56, H_s is significant wave height and ν_α is the air viscosity

$$u_{orb,s} = 2[\iint \sigma^3 N(k,\theta) dk d\,\theta]^{0.5} \quad (3.56)$$

Formulation of viscous boundary values are as follows in Eq. 3.57 is the linear viscous decay by Dore (1978) (Tolman,.,2014):

$$S_{out,vis}(k,\theta) = -s_5 \frac{\rho_a}{\rho_w}\{2k\sqrt{2\nu\sigma}\}N(k,\theta) \quad (3.57)$$

Where s_5 is a swell tuning parameter, ν is the kinematic viscosity of water.

Turbulent boundary value is defined as in Eq. 3.58.

$$S_{out,tur}(k,\theta) = -\frac{\rho_a}{\rho_w}\left\{16 f_e \sigma^2 \frac{u_{orb,s}}{g}\right\} N(k,\theta) \quad (3.58)$$

In above equation f_e represents the friction factor which is a function of wind speed and direction. f_e (Eq. 3.59) is adjusted to overcome the problem of underestimation large swells and overestimation small swells.

$$f_e = s_1 f_{e,GM} + [|s_3| + s_2 \cos(\theta - \theta_u)] \frac{U_*}{u_{orb}} \quad (3.59)$$

Where $f_{e,GM}$ is the friction factor given by Grant and Madsen's (1979) theory for rough oscillatory boundary layers, s_2 and s_3 are swell attenuation factors.

It is suggested by Philips (1984) that, dissipation rate is proportional to the nondimensional spectrum which is called saturation spectrum (Ardhuin et al, 2010). Moreover, Alves and Banner (2003) suggested that wave breaking is the dominant dissipative process contributing to total dissipation term for wind driven seas which is also affected by the wave-turbulence interaction and have found a correlation between the probability of breaking of dominant waves and direction integrated spectrum saturation (B) (Ardhuin,2010). In the ST4 method which is based on Ardhuin et al.(2010), breaking of waves are considered and controlled by a threshold value that, when a nondimensional spectrum exceeds the threshold, waves start breaking. Such consideration was not available in dissipation terms of WAM Cycle 3 or 4. Eq. 3.57 given in chapter 3 consists of this approach.

The dissipation term of ST4 ($S_{ds}(k,\theta)$) is parameterized using the wave spectrum saturation since directional wave spectra are narrow (Tolman, 2014). Total dissipation term (Eq. 3.60) consists of saturation-based term and cumulative breaking term ($S_{bk,cu}(k,\theta)$) .

$$S_{ds}(k,\theta) = \sigma \frac{C_{ds}^{sat}}{B_r^2} [\delta_d \max\{B(k) - B_r, 0\}^2 + (1-\delta_d) \max\{B'(k,\theta) - B_r, 0\}^2] N(k,\theta) + S_{bk,cu}(k,\theta) + S_{turb}(k,\theta) \quad (3.60)$$

Where $B(k)$ represents direction-integrated spectral saturation (Eq. 3.61) and B_r is defined as the constant saturation threshold (Ardhuin et. al.,2010).

$$B(k) = \max\{B'(k,\theta), \theta \in [0,2\pi]\} \quad (3.61)$$

Source term of the breaking terms is defined as follows in ST4 model by Ardhuin et. al., 2010 in Eq. 3.62.

$$S_{bk,cu}(k,\theta) = \frac{-14.2C_{cu}}{\pi^2} N(k,\theta) \int_0^{r_{cu}^2 k} \int_0^{2\pi} \max\left\{\sqrt{B(f',\theta')} - \sqrt{B_r}, 0\right\}^2 d\theta' dk' \quad (3.62)$$

Where r_{cu} is the maximum ratio of the frequencies of long waves that will wipe out the short waves, and C_{cu} is a tuning coefficient (Ardhuin et. al., 2010).

Final part of dissipation term in ST4, total dissipation source term is the wave-turbulence interaction term which is based on Teixeira and Belcher (2002) and Ardhuin and Jenkins (2006). It is defined in Eq.3.63:

$$S_{turb}(k,\theta) = -2C_{turb}\sigma \cos(\theta_u - \theta)\, k \frac{\rho_a U_*^2}{g\rho_w} N(k,\theta) \quad (3.63)$$

Where C_{turb} is the coefficient that adjust ocean stratification and wave groupiness.

3.2.2.3 Nonlinear Wave- Wave Interaction Term

In this study, three different methods are used for the solution of nonlinear wave-wave interaction source.

The first method is called NL1 in WW3 model which is the DIA approach of Hasselmann et al. (1985). NL1 methodology is same with the mentioned DIA approach in SWAN model except for the recommended value of C coefficient in Eq. 3.15. In SWAN model C coefficient is set to $3x10^{7,}$ however in WW3 model different value of C is recommended depending on the chosen dissipation term (Table 3.2).

Table 3.2 Recommended λ_{nl} and C values for different dissipation terms (Tolman, 2014)

	λ_{nl}	C
ST1	0.25	2.78×10^7
ST2	0.25	1.00×10^7
ST4	0.25	2.50×10^7

In WW3 model source terms are usually solved on action-density spectrum ($N(k,\theta)$). However DIA is solved on the variance density (energy density) spectrum ($E(\sigma,\theta)$ since it is originally developed for variance density spectrum by Hasselmann et al. (1985).

NL3 method is called Generalized Multiple DIA (GMD) which is developed version of DIA aprroach by Tolman (2003,2004, 2005, 2008, 2010, 2013). Improvement of DIA consist of 3 parts. "First the definition of the representative quadruplets is expanded. Second, the equations are developed for arbitrary depths. Third, multiple representative quadruplets are used." (Tolman, 2014).

Basic GMD formulations are given below:

$$\sigma_1 = a_1 \sigma_r$$

$$\sigma_2 = a_2 \sigma_r$$

$$\sigma_3 = a_3 \sigma_r$$

$$\sigma_4 = a_4 \sigma_r$$

$$\theta_{12} = \theta_1 \pm \theta_{12}$$

$$a_1 + a_2 = a_3 + a_4 \tag{3. 64}$$

Where the final term satifies the general resonance condition in Eq.3.14, σ_r is reference frequecny and θ_{12} is the angular gap between the wavenumbers $k_1$and k_2 (Tolman, 2014).

A scaling function is defined in GMD, as deep water and shallow water. The deep scaling function represents the weak interactions in deep water while shallow scaling represents strong interaction in shallow water. The proportionally constants for deep water (C_{deep}) and shallow water (C_{shal}) corresponds the proportionality constant in DIA in Eq.3.15(can be represented as C or Cnl or Cnl4 in different sources)(Tolman, 2014 2010). The difference between DIA and GMD is that, in GMD method all quadruplets are solved for actual water depth which enhances the representation of the nonlinear interaction especially in shallow water.

The final discrete interaction in Eq. 3.15 becomes as in Eq. 3.65 below in GMD.

$$\begin{pmatrix} \delta S_{nl1} \\ S_{nl2} \\ \delta S_{nl3} \\ \delta S_{nl4} \end{pmatrix} = \begin{pmatrix} -1 \\ -1 \\ 1 \\ 1 \end{pmatrix} \left(\frac{1}{n_{q,d}} C_{deep} B_{deep} + \frac{1}{n_{q,s}} C_{shal} B_{shal} \right) x$$

$$\left[\frac{c_{g,1}E_1}{k_1\sigma_1} \frac{c_{g,2}E_2}{k_2\sigma_2} \left(\frac{c_{g,3}E_3}{k_3\sigma_3} + \frac{c_{g,4}E_4}{k_4\sigma_4} \right) - \frac{c_{g,3}E_3}{k_3\sigma_3} \frac{c_{g,4}E_4}{k_4\sigma_4} \left(\frac{c_{g,1}E_1}{k_1\sigma_1} + \frac{c_{g,2}E_2}{k_2\sigma_2} \right) \right] \tag{3. 65}$$

Where B_{deep} and B_{shal} are deep water and shallow water scaling functions define in following equations (Eq. 3.66 & Eq. 3.67):

$$B_{deep} = \frac{k^{4+m}\sigma^{13-2m}}{(2\pi)^{11} g^{4-m} c_g^2} \tag{3. 66}$$

$$B_{shal} = \frac{g^2 k^{11}}{(2\pi)^{11} c_g} (kd)^n \tag{3. 67}$$

Further detail can be found on Tolman et al.(2010).

Final method used for nonlinear wave-wave interactions is a nonlinear filter applied to DIA method. Quadruplets cannot be solved by discrete spectral grid, if λ_{nl} is so small. In such case numerical for of DIA changes to simple diffusion tensor. "If this tensor is filtered so that it is applied to the high-frequency tail of the spectrum only, then a conservative filter results, which retains all conservation properties of the nonlinear interactions."(Tolman, 2008b, 2011a).

Formulations for the NLS is given in Eq. 3.68 to Eq.3.72 for the change in spectral density (δN_i) at quadruplet i.

$$\begin{pmatrix} \delta N_3 \\ \delta N_1 \\ \delta N_4 \end{pmatrix} = N_1 \begin{pmatrix} 0 \\ 1 \\ 0 \end{pmatrix} + N_1 \frac{S\Delta t}{N_1} \begin{pmatrix} 1 \\ -2 \\ 1 \end{pmatrix} \tag{3. 68}$$

$$S = \frac{C_{nlf}\, k^4 \sigma^{12}}{(2\pi)^9 g^4 c_g} \left[\frac{N_1^2}{k_1^2} \left(\frac{N_3}{k_3} + \frac{N_4}{k_4} \right) - 2 \frac{N_1}{k_1} \frac{N_3}{k_3} \frac{N_4}{k_4} \right] \tag{3. 69}$$

$$\Phi(f) = \exp\left[-c_1 \left(\frac{f}{c_2 f_p} \right)^{-c_3} \right] \tag{3. 70}$$

Where C_{nlf} is the proportionality constant of the DIA used in the filter, Φ is the filter applied to localize the smoother at higher frequencies, c_1, c_2, c_3 are the tunable parameters.

Two mirror image quadruplets occurs as a result of DIA approach which is named as S_a and S_b. After the filter is applied the effective nondimensional strengths of S_a and S_b takes it form in Eq. 3.71.

$$\widetilde{S_a} = \Phi(f) M_1 S_a \Delta_t / N_1 \;\; \& \; \widetilde{S_b} = \Phi(f) M_1 S_b \Delta_t / N_1 \tag{3. 71}$$

In above equation, N_1 is the action density at the center component of the quadruplet, M_1 is a factor accounting for the redistribution of the contribution over the discrete spectral grids. In order to convert these terms into stable diffusive factor, a limitation parameter $\widetilde{S_{max}}$ is applied which can be defined by user.

Also, the relative offset of quadruplets 3 and 4 (α_{34}) in frequency grid is defined as free parameter of the filter, from which λ_{nl} is denifed as in Eq. 3.72 (For details, Tolman, H., 2011)

$$\lambda_{nl} = \alpha_{34}(X_\sigma - 1) \tag{3. 72}$$

Where X_σ stands for the frequency grid.

3.2.2.4 Bottom Friction Term

Out of different bottom friction methods available in WW3, empirical JONSWAP parameterization of Hasselmann et al. (1973) is used for the bottom friction term in WW3 runs similar to SWAN model. C_b ,the JONSWAP bottom friction coefficient is chosen as $C_b = 0.038 m^2 s^{-3}$ for swell dissipation and $C_b = 0.067 m^2 s^{-3}$ for depth limited wind-sea conditions. (Bouws and Komen,1983)

3.2.2.5 Depth Induced Wave Breaking Term

Battjes and Janssen (1978) methodology is used for the depth induced wave breaking term as in SWAN model with gamma value γ=0.73.

3.2.3 Numeric Approaches of WAVEWATCH III Model

Classical action balance equation (Eq.3.1) cannot be solved with only one time step as it is explained in above sections. In WW3 model, terms in action- balance equation is split off in a way that allows the use of separate and dynamically adjusted time steps for each term. 4 different time step is available in WW3 model.

$\Delta \boldsymbol{t_g}$ Global time step which is used for the propagation of the entire solution in time.

$\Delta \mathbf{t_{xy}}$ Time step only for spatial propagation.

$\Delta \mathbf{t_k}$ Time step only for intra-spectral propagation.

$\Delta \mathbf{t}_{\boldsymbol{s}}$ Time step for the integration of the source term

3.2.3.1 Spatial Propagation

The parts of action balance equation corresponding to spatial propagation for spherical coordinates become as follows:

$$\frac{\partial \mathcal{N}}{\partial \mathrm{t}} + \frac{\partial}{\partial \phi}\dot{\phi}\mathcal{N} + \frac{\partial}{\partial \lambda}\dot{\lambda}\mathcal{N} = 0 \qquad (3.\ 73)$$

Where $\mathcal{N}$ is the propagated quality, can be defined as in Eq. 3.74:

$$\mathcal{N} = \mathrm{N}c_g^{-1}cos\phi \tag{3. 74}$$

There are 3 spatial propagation schemes available in WW3 model.

First one is the first order unwind scheme. Action density at time n+1 can be written as the following:

$$\mathcal{N}_{i,j,l,m}^{n+1} = \mathcal{N}_{i,j,l,m}^{n} + \frac{\Delta t}{\Delta\phi}\left[F_{i,-} - F_{i,+}\right] + \frac{\Delta t}{\Delta\lambda}\left[F_{j,-} - F_{j,+}\right] \tag{3. 75}$$

Where $\mathcal{N}$ is the action density, F is the flux, Δt is the propagation time step, $\Delta\phi$ and $\Delta\lambda$ are latitude and longitude increments, respectively.

Second one is the second order upstream non-oscillatory 2nd order (UNO2) advection scheme (Tolman, 2014; Li, 2008). The final second order propagation can be denoted as in Eq. 3.76:

$$F_{i,-} = \phi_b N_{i-}^{*}; \quad N_i^{n+1} = N_i^{n} + \frac{\Delta t}{\Delta\phi}\left[F_{i,-} - F_{i,+}\right] \tag{3. 76}$$

Third scheme is the third order "QUICKEST scheme (Leonard, 1979; Davis and More, 1982) combined with the ULTIMATE TVD (total variance diminishing) limiter (Leonard, 1991)." (Tolman, 2014) This is the recommended scheme for spatial propagation scheme for WW3 because it is accurate in both space and time. The final third order propagation can be denoted as in Eq.3.77:

$$\mathcal{N}_{i,j,l,m}^{n+1} = \mathcal{N}_{i,j,l,m}^{n} + \frac{\Delta t}{\Delta\phi}\left[F_{i,-} - F_{i,+}\right] \tag{3. 77}$$

3.2.3.2 Spectral Propagation

Part of the action balance equation which corresponds the spectral propagation can be written as follows;

$$\frac{\partial N}{\partial t} + \frac{\partial}{\partial k}\dot{k_g}N + \frac{\partial}{\partial \theta}\dot{\theta_g}N = 0 \quad (3.\ 78)$$

Where $\dot{k_g}$ and $\dot{\theta_g}$ are the wave number velocity and wave direction velocity with relative to grid. There are 3 spectral propagation schemes available in WW3 model.

First one is the first order scheme which can be written as in Eq. 3.79:

$$\mathrm{N}_{i,j,l,m}^{n+1} = \mathrm{N}_{i,j,l,m}^{n} + \frac{\Delta t}{\Delta\theta}\left[F_{l,-} - F_{l,+}\right] + \frac{\Delta t}{\Delta \mathrm{k}_m}\left[F_{m,-} - F_{m,+}\right] \quad (3.\ 79)$$

Where $\Delta\theta$ is the directional increment, $\Delta \mathrm{k}_m$ is the local wave increment.

The UNO2 scheme is also applicable on the spectral space assuming directional bins are regularly spaced:

$$\mathrm{N}_{i-}^{*} = \mathrm{N}_c + sign(\mathrm{N}_d - \mathrm{N}_c)\frac{(\Delta k_c - |\dot{k_{i-}}|\Delta t)}{2}\min\left(\left|\frac{N_u - N_c}{k_u - k_c}\right|, \left|\frac{N_c - N_d}{k_c - k_d}\right|\right) \quad (3.\ 80)$$

Where $i-$ is the wave number k bin index, $\dot{k_{i-}}$ is the face velocity of $i-$ face and u, c, d stand for upstream, central and downstream respectively.

Third order scheme is selected as ULTIMATE QUICKEST scheme which is applied to spectral space in a similar manner for physical space. Final scheme for the wavenumber space becomes as follows.

$$\mathcal{N}_{i,j,l,m}^{n+1} = \mathcal{N}_{i,j,l,m}^{n} + \frac{\Delta t}{\Delta \mathrm{k}_m}\left[F_{i,-} - F_{i,+}\right] \quad (3.\ 81)$$

3.3 Comparison of SWAN and WWIII

In this section, differences in the source and propagation of the models are introduced only by definition. Even though, most of the approaches and formulations of the these two models are based on WAM model, slight modifications and improvements in the models, formulations or propagation schemes create significant differences between the outputs of the two models.

The main difference between SWAN and WW3 model is the discrepancy between the numerical methods chosen in order to solve the same action balance equation.

However, the differences in the outputs are not only caused by the numerical methods but also caused by the source term calculations. Variable implementations such as filter extensions of the same source formulations are another reason of the output differences.

3.3.1 Propagation Scheme

Numerical diffusion which is called "Garden Sprinkler Effect" (GSE) is a common problem for the first order propagation schemes used in wave modeling. Therefore, higher order schemes are usually chosen because they are free of such effect. WW3 has the high order (third order) propagation schemes while SWAN model only uses second order Stelling and Leendertse scheme. SWAN has a default GSE correction for the scheme which is based on Booij and Holthuijsen (1987). In WW3, same GSE alleviation is active for second order scheme. Moreover, WW3 is using spatial averaging technique as GSE alleviation method for the third order scheme.

Another crucial difference between models is the general approach to the solution of action balance equation. SWAN model solves the full equation after discretization of the formulations. SWAN model uses iterative approach with pseudo time step and

active limiter to stabilize the iteration process. This is a fast converging method however, the application of DIA to sweeping method requires memory since spectral source term for every grid is stored in memory which can be a drawback. SWAN only uses one general time step, while using false time step for parameters with high sensitivity such as nonlinear wave-wave interactions. In WW3 model approach, action balance equation terms are split and solved individually with their corresponding time step. Therefore 4 different time step are used in WW3 model. Although this situation gives more control to user on time stepping effects and sensitivity on parameters regarding time steps, it requires more effort for calibration of the model. The differences on the propagation schemes also reflect on computational cost. It has been observed that, when the resolutions are same in all spaces for SWAN and WW3 and WW3's global time step is to set equal to regular time step in SWAN, WW3 model requires longer time for the solution in a single core.

3.3.2 Source-Sink Differences

In order to solve the physical processes of the nature, many different solutions are available in wave models.WW3 model has more option compared to SWAN model for the calculations of source and sink terms especially for swell dissipation terms. This is because the main purposes of the models are not exactly the same. SWAN model focuses more on near shore processes while WW3 model is more concerned on ocean modeling. Many source and sink terms of both models depends on the WAM Cycle 3 and WAM Cycle 4 methods. Nevertheless, during implementation of terms some adjustments are made regarding consistency of the source terms with the corresponding model. Because of those adjustments such as filters or limiters, comparing the results of the two models with each other is not directly possible to understand the sources of the differences in the results. All the considered options for the physical processes and related methods are given in the Table 3.3.

Table 3.3 Considered options for the physical processes and related methods for SWAN and WW3

Physical Process	Methods in SWAN	Method in WW3
Linear Wind Growth	Cavaleri and Malanotte-Rizzoli (1981)	Cavaleri and Malanotte-Rizzoli (1981)
Exponential wind growth	Snyder et al. (1981)	Snyder et al. (1981)
	Janssen (1989)	Chalikov and Belevich(1993) and Chalikov(1995)
		Janssen (1989)
		WAM Cycle 4 modified by Ardhuin(2010)
White Capping and Swell Dissipation	Komen et al. (1984)	Komen et al. (1984)
	Janssen(1991)	Tolman and Chalikov(1996)
		Janssen(1991)
		Ardhuin(2009) (Swell dissipation)
		Ardhuin(2010)
Nonlinear Wave Wave Interactions	Hasselmann et al. (1985) (DIA)	Hasselmann et al. (1985) DIA
	MDIA (modified DIA)	Tolman (2010) , Tolman (2014) (GMD)
		Tolman (2011) Nonlinear filter app. To DIA
Depth-induced breaking	Battjes and Janssen (1978)	Battjes and Janssen (1978)
Bottom Friction	JONSWAP(1973)	JONSWAP(1973)

3.4 Statistical Analysis Methods used in Study

In order to evaluate the performance of the models, different statistical analysis methods were considered. Those methods were selected according to their different approaches to the error calculation and their different expressions for the correspondence between predictions (outputs of the wave generation models, shown with P hereafter) and the observed values (buoy data, shown with O hereafter).

The methods were chosen considering the statistical concepts such as precision, accuracy and bias so that the evaluation process of the model could be more coherent. Precision means the absence of random error and random error can be defined as error that is independent of the observed (true) value (Walter and Moore, 2005). Bias on the other hand represents the error caused by the difference between prediction and observation. Finally accuracy is defined as the overall distance between estimated (or observed) values and the true value (Bainbridge 1985; Walter and Moore, 2005). Bias and precision combine to define the accuracy of the model.

3.4.1 Root Mean Squared Error (RMSE) and Normalized Root Mean Squared Error (NRMSE)

The root mean square error (RMSE) is one of the widely used, standard statistical metric to measure model performance in meteorology, air quality, and climate research studies (Chai and Draxler, 2014). RMSE and NRMSE are used in order to define accuracy of the predictions with respect to observations. The formulations are given below in Eq.3.82 and 3.83. Lower the RMSE values correspond to better the accuracy of model.

$$RMSE = \sqrt{[N^{-1} \sum_{i=1}^{N} (P_i - O_i)^2]} \tag{3. 82}$$

$$NRMSE = \sqrt{\frac{\sum_{i=1}^{N} (P_i - O_i)^2}{\sum_{i=1}^{N} {O_i}^2}} \tag{3. 83}$$

The normalized version of RMSE was also included in this study, in order to make comparisons between the outputs of different events which were produced using same model configuration. Also the normalization of the error allows a quantitative comparison between widely different sea state regimes (Ardhuin et al., 2010).

3.4.2 Systematic RMSE (RMSEs) and Unsystematic RMSE (RMSEu)

RMSE represents the accuracy which include both systematic (dependent on observation) and unsystematic (independent of observation) errors. RMSEs and RMSEu are used in order to define these errors which are already present in RMSE (Eq. 3.84).

$$RMSE^2 = {RMSE_U}^2 + {RMSE_S}^2 \quad (3.84)$$

Since there are many reasons that cause error in applications such as wave modeling, quantifying this error in terms of basic systematic and unsystematic approaches is highly beneficial for the calibration of models and reaching higher accuracies.

RMSEs indicated the bias while RMSEu represents the random variation. According to Willmott(1982), a good model's RMSEs should approach to zero while RMSEu approaches RMSE. The formulations of RMSEs and RMSEu are given below in Eq. 3.85 and Eq.3.86

$$RMSE_S = \sqrt{\left[\frac{1}{N}\sum_{i=1}^{N}\left(\widehat{P_i} - O_i\right)^2\right]} \quad (3.85)$$

$$RMSE_U = \sqrt{\left[\frac{1}{N}\sum_{i=1}^{N}\left(P_i - \widehat{P_i}\right)^2\right]} \quad (3.86)$$

Where $\widehat{P_i}$ is defined as in Eq.3.86:

$$\widehat{P_i} = a + bO_i \quad (3.87)$$

Where a and b coefficients were estimated using least squares analysis.

The graphical representations of RMSE, RMSEs and RMSEu are given below in Figure 3.2

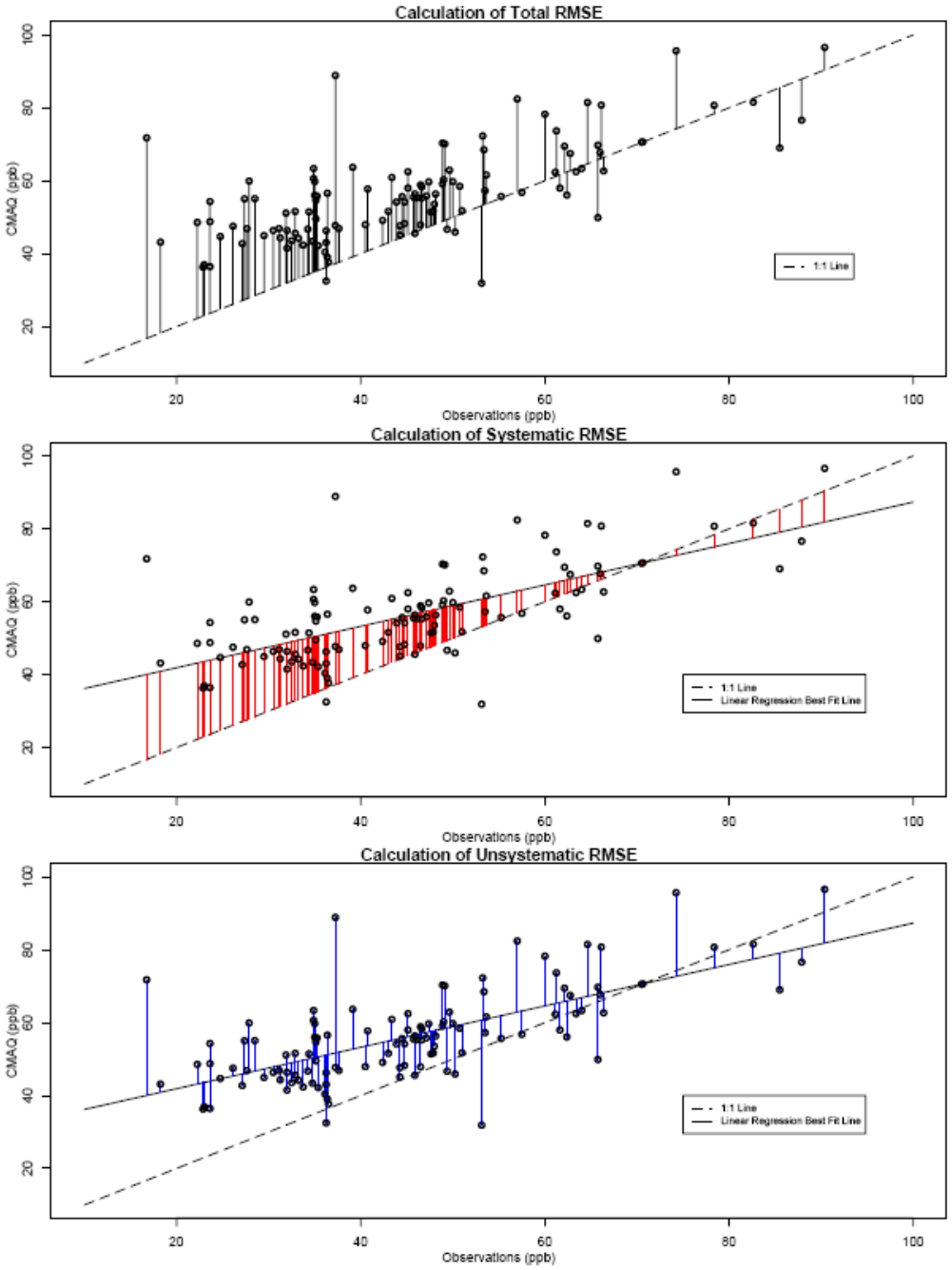

Figure 3.2 RMSE, RMSEs and RMSEu (Hogrefe et al., 2006)

3.4.3 Mean Absolute Error (MAE) and Normalized Mean Absolute Error (NMAE)

MAE is also one of the most basic and effective statistical methods that shows accuracy. It is the absolute average of the differences of predictions and observations. Formulations of MAE and NMAE are given below (Eq.3.88 to Eq.3.90). Lower the MAE values correspond to better the accuracy of model.

$$MAE = N^{-1} \sum_{i=1}^{N} |P_i - O_i| \quad (3.88)$$

$$NMAE = \frac{MAE}{S} \quad (3.89)$$

Where S is the standard deviation of the observed data which is calculated as follows;

$$S = \sqrt{\frac{1}{N-1} \sum_{i=1}^{N} \left|O_i - \tilde{O}\right|^2} \quad (3.90)$$

Where $\tilde{O}$ is the mean of the observed values which is calculated as in Eq.3.90

$$\tilde{O} = \frac{1}{N} \sum_{i=1}^{N} O_i \quad (3.91)$$

There are many discussions on which method, MAE or RMSE is more advantageous in defining accuracy for the numerical models. The main reason of this discussion is caused by the different approaches of methods. While MAE gives the same weight to all errors; the RMSE penalizes variance as it gives errors with larger absolute values more weight than errors with smaller absolute values. (Chai and Draxler, 2014) Both

statistical terms are included in this study in order to consider different behaviors of methods.

3.4.4 BIAS and NBIAS

In measurement or sampling situations, bias is "the difference between a population mean of the measurements or test results and an accepted reference or true value" (Kowalewski, 1994). Bias shows the under or overestimation of prediction data compared to observation data. Positive bias means underestimation while negative bias means overestimation. Formulations of BIAS and NBIAS given in Eq. 3.92 and Eq. 3.93

$$BIAS = N^{-1} \sum_{i=1}^{N} O_i - P_i \quad (3.92)$$

$$NBIAS = \frac{\sum_{i=1}^{N} O_i - P_i}{\sum_{i=1}^{N} O_i} \quad (3.93)$$

3.4.5 Scatter Index (SI)

Scatter index represent variability so that precision of the model is described. SI is used to define random, unsystematic error. Lower the SI values correspond to better the accuracy of model. Formulation of SI is given in Eq. 3.94:

$$SI = \sqrt{\frac{\sum_{i=1}^{N} [(O_i - \widetilde{O}) - (P_i - \widetilde{P})]}{\sum_{i=1}^{N} {O_i}^2}} \quad (3.94)$$

3.4.6 Pearson's Linear Correlation Coefficient (R)

Pearson's Linear Correlation Coefficient (R) (Pierson, 1895) measures the linear correlation between prediction and observation. The correlation coefficient changes in the range of 1 to -1 where 1 represent the full correlation, 0 represents no correlation and -1 represents full negative correlation. Negative correlations mean that, if one variable shows tendency to increase, other variable shows tendency to decrease. The formulation of Pearson's linear correlation coefficient is given in Eq. 3.95

$$r = \frac{\sum_{i=1}^{N}[(O_i - \widetilde{O})(P_i - \widetilde{P})]}{\sqrt{\sum_{i=1}^{N}[(O_i - \widetilde{O})^2 (P_i - \widetilde{P})^2]}} \quad (3.95)$$

3.4.7 Ranking System Used in the Evaluation

A ranking system was formed to compare both the parametrization methods of the models and the individual storms. The ranking system for model comparison was based on NRMSE, NMAE, NBIAS, SI and R.

In ranking system, all runs with same specifications (same source term, wind data and parameterizations) were grouped and named with short abbreviations, such as "SCKD" which stands for "S"wan model has run using "C"FSR winds with "K"omen formulations for whitecapping dissipation and "D"IA method for nonlinear wave wave interaction (abbreviation list is given below in section 5.2). Then statistical analysis methods were applied to results of all groups with respect to observed data and obtained values were sorted under each statistical method. For NRMSE, NMAE, NBIAS, and SI the lowest value were given the highest point(total number of groups in ranking system (n)) and second lowest value were given n-1

points. With this approach, worst group was only given 1 point from the considered analysis methods. For ranking of R, group with highest R was given highest point n. An illustration of ranking system is given below in Table 3.4 where the best performance belongs to SCKD with a total of 15 points.

Table 3.4 Example Ranking System

Groups	NRMSE	NMAE	NBIAS	SI	R
A	0.50	0.54	0.28	0.30	0.93
B	0.40	0.30	0.19	0.20	0.92
C	0.30	0.21	0.32	0.40	0.95
SCKD	0.20	0.20	0.10	0.35	0.90

Groups	NRMSE	NMAE	NBIAS	SI	R	Total Points
A	1	1	2	3	3	10
B	2	2	3	4	2	13
C	3	3	1	1	4	12
SCKD	4	4	4	2	1	15

CHAPTER 4

INPUT DATASETS OF THE STUDY

In order to obtain realistic wave condition for the study area, SWAN and WW3 models require well prepared input data. In this chapter, main input of wind re-analysis data, wave buoy data used for validation of the third generation wave models and bathymetry data are introduced. Moreover, the extreme wind and wave climate of Black Sea basin is discussed and the selected extreme events are explained.

4.1 Sea Bottom Topography (Bathymetry)

For this study, Black Sea Basin is selected as domain between the latitudes 40.5˚ N - 47.5˚N and longitudes 27.0˚E – 42.0˚E (Figure 4.1). The bathymetric data is retrieved from 1 minute grid dataset of "Global Bathymetric Prediction for Ocean Modeling and Marine Geophysics" by Sandwell and Smith (2001) which was partly funded by Marine Geology and Geophysics Division Program at NSF and the NASA Global Geodynamics Program. This dataset was prepared using all available ship soundings that are collected over 30 years and altimeter data (high-resolution marine

gravity information) from the Geosat, ERS-1/2, and Topex/Poseidon satellites (Sandwell and Smith,1996).

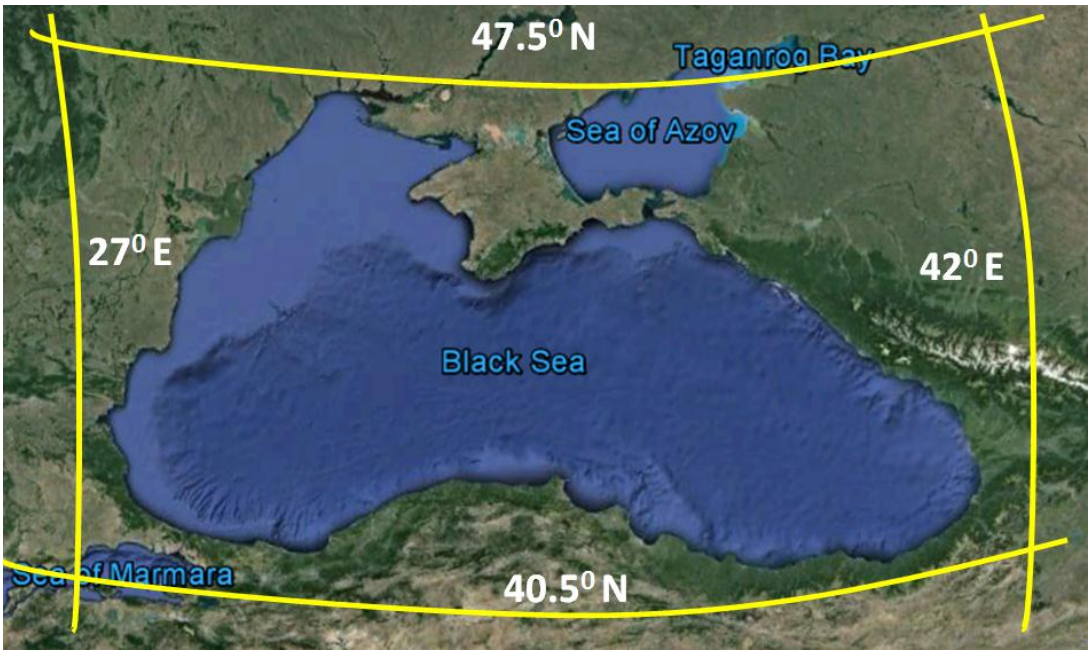

Figure 4.1 Study Basin

A coarser grid resolution is adequate for this study since the main concern of the study focuses on deep water source and sink terms which are not affected by bottom topography. The buoys were also located in deep water. Nevertheless, during the propagation of waves toward the coastline, near shore processes are affected by the change in resolution. Therefore, an optimum grid resolution was needed to be obtained for the study considering the buoy locations, resolution of the wind models and the computational cost of the model runs. In order to reduce the computational cost, 1 minute gridded bathymetry was re-gridded using Surfer11 software using "krigging" methodology, one of the available interpolation built-in options. The new coarser bathymetry had a resolution of 3 minutes. Additionally, 6 minutes and 1.5 minutes gridded bathymetries were prepared to test the sensitivity of the models to bathymetry resolution.

4.2 Wave Data Records of the NATO-TU WAVES project

The wave parameter recordings that are required during validation and calibration of the wave hindcasting models, are obtained from the buoys of NATO-TU WAVES project. "NATO TU-WAVES Project, which aimed to find out the wave climate affecting the Turkish coast as well as the whole Black Sea region, was carried out during the period of 1994-2000 with generous financial support provided by the Science for Stability (SfS) Programme (Phase III) of NATO (Özhan and Abdalla,1999)." In addition, one of the main objectives of the program was to implement a third generation wave model for Turkish coast (Özhan and Abdalla,1999).

In Black Sea, records of 3 wave buoys are available which were located in Sinop, Hopa, Gelendzhik (Figure 4.2) with observation dates between 1994 to 2003 . The buoys used during the project were the Datawell directional waverider buoys which measured the displacements, filters and perform FFT every 30 minutes. (Özhan and Abdalla) Buoys had a cut-off frequency of 0.6 Hz. Available parameters were significant wave height (H_s) , mean wave period (T_m) and mean wave direction (Dir). The exact locations of the buoys and related information can be found in Table 4.1

Figure 4.2 Buoy Locations

Table 4.1 NATO-TU Waves Project Buoy information

Station	Latitude	Longitude	Water Depth(m)	Distance From Shore(km)
Gelendzhik	44.5075	37.9783	85	7.00
Sinop	42.1233	35.0867	100	11.60
Hopa	41.4233	41.3833	100	4.60

4.2.1 Storm Selection

In order to investigate the storm nature and extreme events of Black Sea, storms were selected from the continuous wave data. Events were determined depending on their observed wave heights. During selection process peak over threshold method was considered. Peak wave heights over 2 meters were selected whereas wave heights lower than 0.5 meter were considered as calm sea state. Duration between the end of calm sea state and start of new calm state which includes the selected peaks was defined as a storm. These individual selected events will be called storm hereafter,

not to be mistaken with the common definition of the word storm. In other words, a storm is the duration which significant wave heights are greater than 0.5 meter and peak wave observations over 2 meters exist. Durations of the selected events varies because of the selection process which depends on the sea state.

It has been observed that model results are more accurate when 2 consecutive storms for which duration between is less than 2 days, are combined as one event rather than running model for each individual storms. An example situation for combining the storms is illustrated with Hopa 22 storm which occurred between dates 02.02.1999 and 12.02.1999. Hopa 22 was consisted of four successive peaks which were over 2 m. After each peak, significant wave heights have dropped under 0.5 meter which means that if only the threshold criteria was used, Hopa 22 storm would be divided into four discrete storms as Hopa 22-01, Hopa 22-02 Hopa22-03, Hopa22-04 (Table 4.2)

Table 4.2 Hopa 22 Storm and Sub Storms

Storm #	Start Date	End Date	Duration(days)
Hopa_22	2.2.1999 06:00	12.2.1999 00:00	9.5
Hopa_22-01	2.2.1999 00:00	5.2.1999 00:00	3
Hopa_22-02	6.2.1999 00:00	8.2.1999 00:00	1.5
Hopa_22-03	8.2.1999 00:00	9.2.1999 12:00	1.5
Hopa_22-04	9.2.1999 12:00	12.2.1999 00:00	2.5

As it can be seen from Figure 4.3, the obtained results were more accurate when combined storm was modeled rather than the solutions of the separate shorter storms. The differences occurred possibly due to the different energy levels before individual storms, as shorter storms had no energy when the model was started.

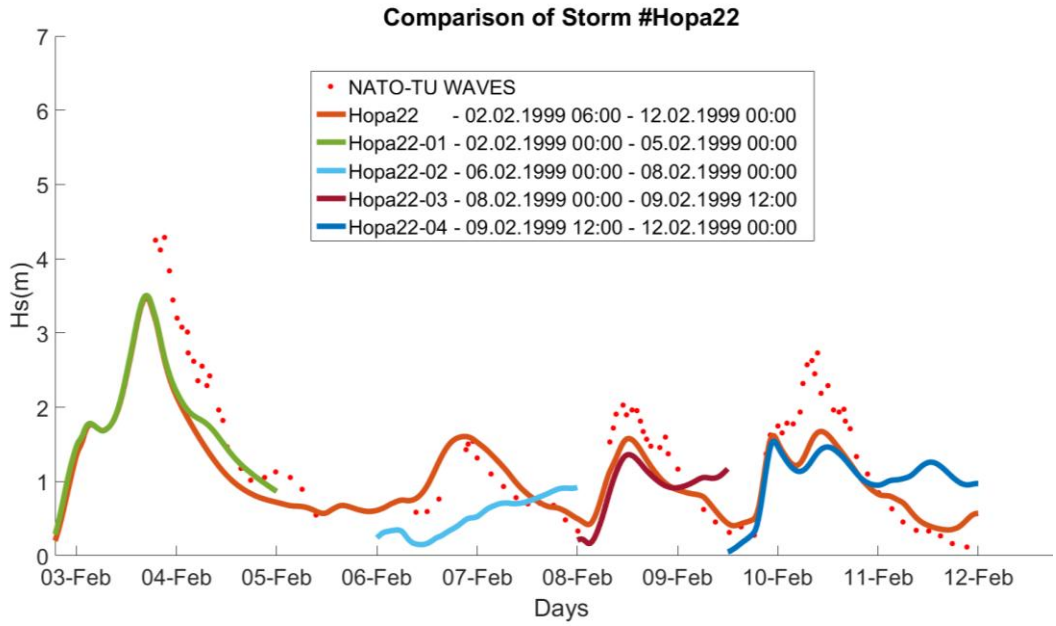

Figure 4.3 Hopa 22 and Hopa 22 sub storms

The energy transfer from the previous sea states were explained better when these storms were combined. Therefore, for this study, longest duration among selected events is as high as 39 days while shortest duration is 3.5 days. Peak and mean wind speeds of the selected storms were analyzed using Climate Forecast System Reanalysis (CFSR) of National Center for Environmental Predictions (NCEP) and European Centre for Medium Range Weather Forecast (ECMWF) operational datasets which is discussed in Section 4.3.

In the end, 54 events were defined as storms from 3 different locations in Black sea between years 1995-2003 to be modeled in this study.

4.2.2 Gelendzhik Buoy and Selected Storms

Gelendzhik wave buoy is named after its location near the Russian city Gelendzhik in the northeastern coast of Black Sea . Wave buoy was located 7 km offshore in 85 meters of water depth (Table 4.1). Wave buoy records start in July, 1996 and end in December 2003 which is the longest duration among all three buoys. However, during some periods the buoy data is not available; between April, 1998 and May, 2000, between February and May of 2001, and between December, 2001 and April,2002.

24 storms selected from the wave data in Gelendzhik are given in Table 4.3. Gelendzhik has the maximum number storms studied in this study. Moreover, the highest observed peak wave height (7.50 m) of the study was observed here in February 2002. The longest storm duration (39 days) of the study also took place in Mart-April 1997.

Table 4.3 Gelendzhik Storms

Storm #	Start Date	End Date	Duration(days)
Gelendzhik_1	1996.09.02	1996.10.02	30
Gelendzhik_2	1996.10.20	1996.11.06	17
Gelendzhik_3	1996.11.20	1996.12.01	11
Gelendzhik_4	1996.12.13	1997.01.12	30
Gelendzhik_5	1997.01.18	1997.02.20	33
Gelendzhik_6	1997.03.14	1997.04.22	39
Gelendzhik_7	1997.10.01	1997.10.10	9
Gelendzhik_8	1997.11.17	1997.11.24	7
Gelendzhik_9	1997.11.30	1997.12.23	23
Gelendzhik_10	1998.01.04	1998.01.18	14
Gelendzhik_11	1998.01.28	1998.02.09	12
Gelendzhik_12	1998.02.10	1998.02.22	12
Gelendzhik_13	1998.03.01	1998.03.28	27
Gelendzhik_14	2000.06.17	2000.06.24	7
Gelendzhik_15	2000.09.05	2000.09.11	6
Gelendzhik_16	2000.12.11	2001.01.02	22
Gelendzhik_17	2001.01.08	2001.01.16	8
Gelendzhik_18	2001.06.03	2001.06.11	8
Gelendzhik_19	2001.10.19	2001.10.27	8
Gelendzhik_20	2001.11.11	2001.12.06	25
Gelendzhik_21	2002.12.19	2003.01.20	32
Gelendzhik_22	2003.01.26	2003.02.15	21
Gelendzhik_23	2003.03.30	2003.04.11	12
Gelendzhik_24	2003.10.03	2003.10.15	12

4.2.3 Sinop Buoy and Selected Storms

Sinop wave buoy is named after its location near the Turkish city Sinop in the central south coast of Black Sea. Wave buoy was located 11.6 km offshore which is the farthest buoy to shore for this study. The buoy was in 100 meters of water depth

(Table 4.1). Sinop buoy was only active for a short period of time therefore, obtained wave records only cover a total of 9 months, the duration between November – December 1994 and December 1995 to June 1996. Since available data is less, 7 storms were selected from the wave data. Maximum observed significant wave height was around 4.5 meters and longest selected storm was 33 days long (one of the highest). List of storms observed in Sinop are available in Table 4.4

Table 4.4 Sinop Storms

Storm #	Start Date	End Date	Duration(days)
Sinop_1	1994.11.03	1994.11.17	14
Sinop_2	1994.11.19	1994.12.22	33
Sinop_3	1995.12.14	1996.01.01	18
Sinop_4	1996.01.27	1996.02.05	9
Sinop_5	1996.03.16	1996.03.20	4
Sinop_6	1996.03.31	1996.04.15	15
Sinop_7	1996.05.28	1996.06.09	12

4.2.4 Hopa Buoy and Selected Storms

Hopa buoy is named after its location near the Turkish town Hopa which is located near the border of Georgia in the south east coast of Black Sea. Wave buoy was located 4.6 km offshore which is the closest buoy to shore for this study. The bottom slopes in Hopa region is very steep, thus deep water limit even for extreme cases is very close to the shore. Hopa buoy was in 100 meters of water depth (Table 4.1). Hopa buoy was active from the start of 1995 until April, 1999. During that period of time, the buoy was offline only for four months between February 1997 and May 1997. 23 storms were selected from the Hopa dataset. Even though maximum observed significant wave height was around 4.8 meters, most of the storms observed in Hopa had low peak wave heights around 2.20 to 2.5 meters and usually storm

duration were less compared to other buoys. List of storms observed in Hopa are available in Table 4.5

Table 4.5 Hopa Storms

Storm #	Start Date	End Date	Duration(days)
Hopa_1	1995.01.13	1995.02.01	19
Hopa_2	1995.03.11	1995.03.20	9
Hopa_3	1995.10.27	1995.11.02	6
Hopa_4	1995.11.05	1995.11.15	10
Hopa_5	1995.11.17	1995.11.28	11
Hopa_6	1995.12.15	1995.12.24	9
Hopa_7	1996.04.12	1996.04.15	3
Hopa_8	1996.06.15	1996.06.21	6
Hopa_9	1996.09.15	1996.09.23	7
Hopa_10	1996.10.12	1996.10.17	5
Hopa_11	1996.10.20	1996.11.01	12
Hopa_12	1996.12.22	1997.01.01	10
Hopa_13	1997.08.11	1997.08.21	10
Hopa_14	1997.08.31	1997.09.07	7
Hopa_15	1997.11.02	1997.11.08	6
Hopa_16	1997.12.04	1997.12.15	11
Hopa_17	1998.02.05	1998.02.11	6
Hopa_18	1998.02.25	1998.03.16	19
Hopa_19	1998.05.27	1998.06.01	5
Hopa_20	1998.06.20	1998.06.25	5
Hopa_21	1998.07.09	1998.07.14	5
Hopa_22	1999.02.02	1999.02.12	10
Hopa_23	1999.03.14	1999.03.18	4

4.3 Wind Input Data Information

The main input term for the 3rd generation wave models is the wind input. It is a well-known fact that, performance of a numerical wind-wave forecasting model depends on the quality and accuracy of the wind fields (Akpinar and Leon, 2015).

Models work best with the wind input as wind fields over the study basin. The best option to obtain such wave fields is to use the re-analysis atmospheric datasets that are available globally with different temporal and spatial resolutions. Those re-analysis datasets usually cover long period of times (15 to 50 years) and consist of many different atmospheric parameters including u and v components of wind velocity.

In this study, re-analysis data sets of two atmospheric models are chosen to see the differences caused by the wind-forcing for both wave models. First one is the Climate Forecast System Reanalysis model (CFSR) of National Center for Environmental Prediction (NCEP) and the second one is the operational re-analysis model of European Centre for Medium-Range Weather Forecasts (ECMWF). Both re-analysis models are commonly used datasets for many applications around the globe and the producing organizations are well known and respected globally. Details of wind inputs are given in the following section.

4.3.1 Climate Forecast System Reanalysis (CFSR) data of NCEP

CFSR model has been created in 2010 for climate studies by NCEP which is a sub organization of National Oceanic and Atmospheric Administration (NOAA) of U.S Department of Commerce. CFSR datasets covers the years between 1979 and 2009. "The CFSR was designed and executed as a global, high-resolution coupled atmosphere–ocean–land surface–sea ice system to provide the best estimate of the state of these coupled domains over this period" (Saha et al.,2010). One of the main

innovations of CFSR model compared to other re-analysis models is that CFSR includes coupling of the atmosphere and ocean.

CFSR reanalysis dataset is prepared using many different sources including meteorological stations, observation platforms, and satellite altimeter data (Topex/Jason1). CFSR has a temporal resolution of 1 hour and global spatial resolution of 0.312˚ x 0.312˚. The spatial resolution corresponds to 1323 grid points in Black Sea. U and V components of wind velocities 10 meters above the sea surface are obtained from the system in order to prepare the wind field inputs for the wave models.

4.3.2 ECWMF Operational dataset

ECMWF is an independent organization that produces global numerical weather forecasts. ECMWF organization supported by 34 countries, is one of the six members of co-ordinated organization which includes the North Atlantic Treaty Organization (NATO) (ECMWF Annual Report,2015).

ECMWF has many different reanalysis atmospheric data sets. All of ECMWF's forecasts and reanalysis use a numerical model called Integrated Forecasting System (IFS) developed by ECMWF. In this scope of study, only ECMWF operational dataset is chosen to be used considering its spatial resolution of 0.1˚ x 0.1˚. Also, ECMWF Operational dataset is available to METU-OERC by courtesy of the agreement between the Turkish State of Meteorological Service and ECMWF.

ECMWF Operational dataset contains data from many meteorological stations, observatories, and satellite data. Available data start from the year 1982 and the database is monthly updated. U and V components of wind velocities 10 meters above the sea surface are obtained from the archive with a temporal resolution of 6 hours. In ECMWF operational data set, 10721 grid points exist in the study basin with the 0.1˚ x 0.1˚ spatial resolution.

4.3.3 Comparison of Wind Data for Extreme Cases in Black Sea Basin

Both of the atmospheric models are calibrated considering many parameters and accepted as good quality data worldwide. However, it is known that significant differences exist between the outputs of the models. According to global wave hind cast study of Rascle and Ardhuin (2012) "CFSR and NCEP analyses have systematically higher values than ECMWF analyses of the wind speed, and this is even truer for the highest speed range". Also according to Cavaleri and Sclavo (2006), it has been noted that ECMWF underestimates wind fields in closed basins, so such underestimation can be expected in Black Sea as well. Since wind fields are the main input for wave generation models, such error in wind field input will be carried to wave fields, as well. Moreover, in this study, extreme events are determined by the peak wind speeds, reflection of such systematic error is expected to be more profound in the wave model results.

In order to analyze the difference between the two wind datasets for extreme events, a basic comparison study is carried out. Two of the available grid points closest to each buoy locations are selected from ECWMF operational and CFSR datasets. The location and the exact coordinates are given in Figures 4.4, 4.6, and 4.8. Moreover, wind roses of closest grids (ECMWF and CFSR) are also given for each location in order to see the dominant wind direction and the percentage distribution of wind speeds close to buoy points. (Figure 4.5 , 4.7 , 4.9).

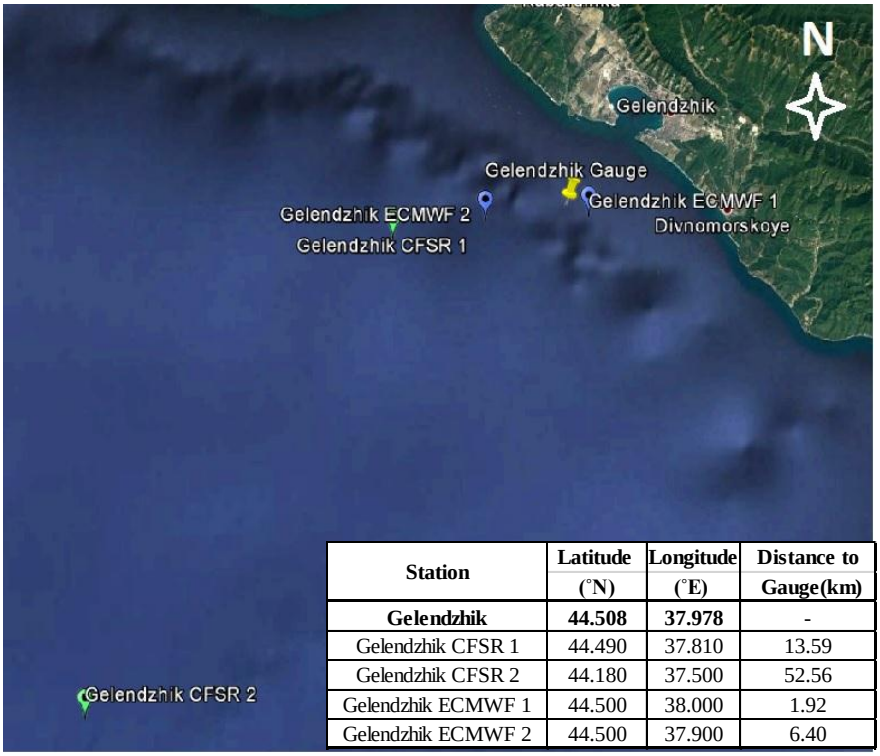

Station	Latitude (°N)	Longitude (°E)	Distance to Gauge(km)
Gelendzhik	**44.508**	**37.978**	-
Gelendzhik CFSR 1	44.490	37.810	13.59
Gelendzhik CFSR 2	44.180	37.500	52.56
Gelendzhik ECMWF 1	44.500	38.000	1.92
Gelendzhik ECMWF 2	44.500	37.900	6.40

Figure 4.4 Gelendzhik CFSR and ECMWF Points

The dominant wind direction in Gelendzhik is from North East direction. The annual wind roses obtained from different wind sources near Gelendzhik buoy can be seen in Figures 4.5

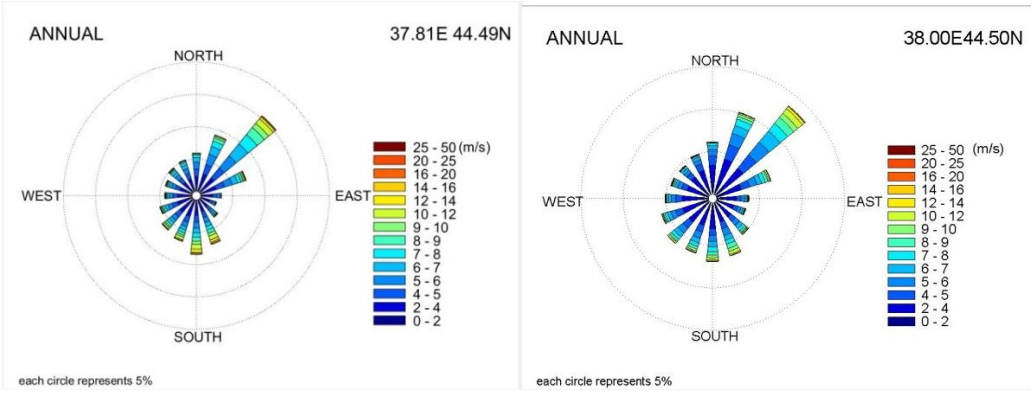

Figure 4.5 Wind Rose near Gelendzhik from CFSR (left) and ECMWF Opr.(right)

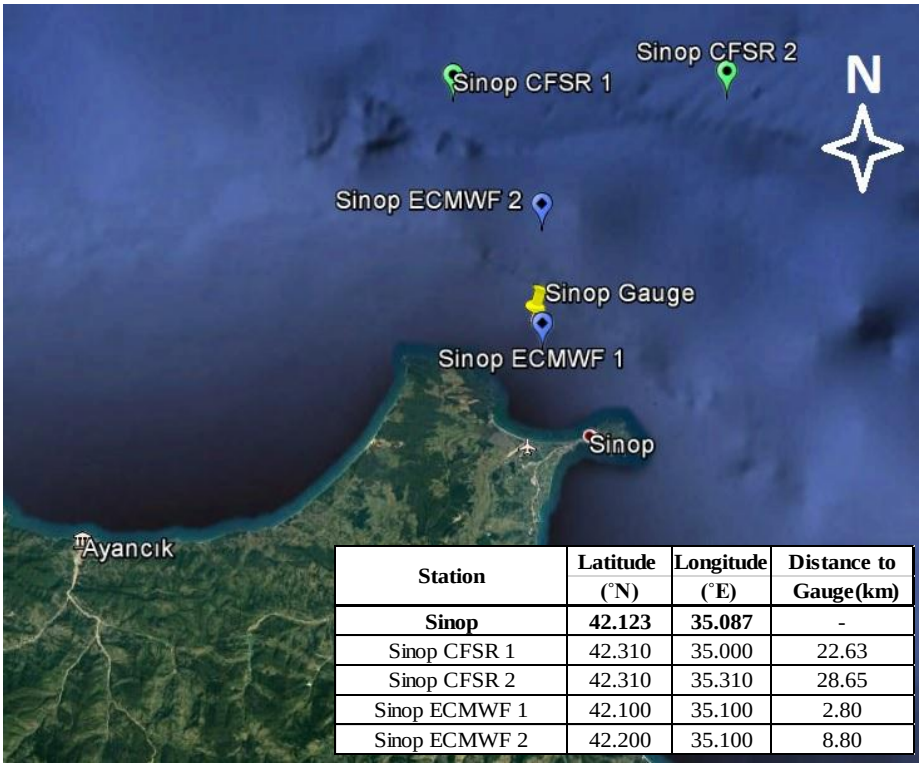

Station	Latitude (˚N)	Longitude (˚E)	Distance to Gauge(km)
Sinop	**42.123**	**35.087**	-
Sinop CFSR 1	42.310	35.000	22.63
Sinop CFSR 2	42.310	35.310	28.65
Sinop ECMWF 1	42.100	35.100	2.80
Sinop ECMWF 2	42.200	35.100	8.80

Figure 4.6 Sinop CFSR and ECMWF Points

The dominant wind direction in Sinop is from North East direction. The annual wind roses obtained from different wind sources near Sinop buoy can be seen in Figures 4.7

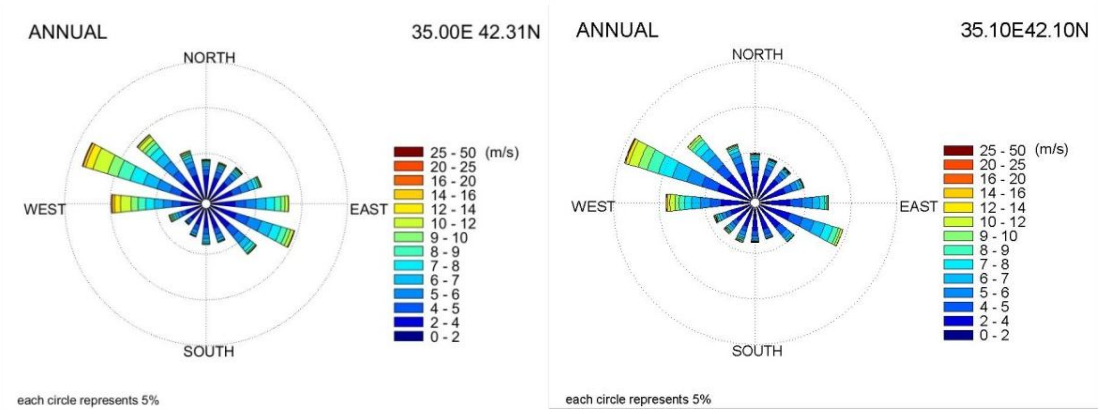

Figure 4.7 Wind Rose near Sinop from CFSR (left) and ECMWF Opr.(right)

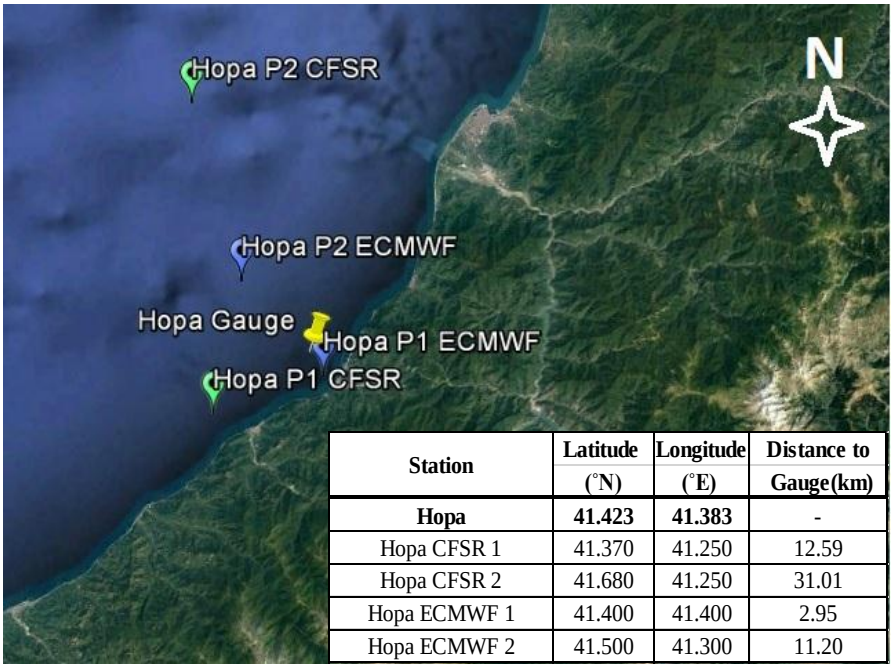

Station	Latitude (°N)	Longitude (°E)	Distance to Gauge(km)
Hopa	**41.423**	**41.383**	-
Hopa CFSR 1	41.370	41.250	12.59
Hopa CFSR 2	41.680	41.250	31.01
Hopa ECMWF 1	41.400	41.400	2.95
Hopa ECMWF 2	41.500	41.300	11.20

Figure 4.8 Hopa CFSR and ECMWF Points

The dominant wind direction in Hopa blows from SSE (South South East). On the other hand, winds towards West direction cannot be ignored. The annual wind roses obtained from different wind sources near Hopa buoy can be seen in Figure 4.9

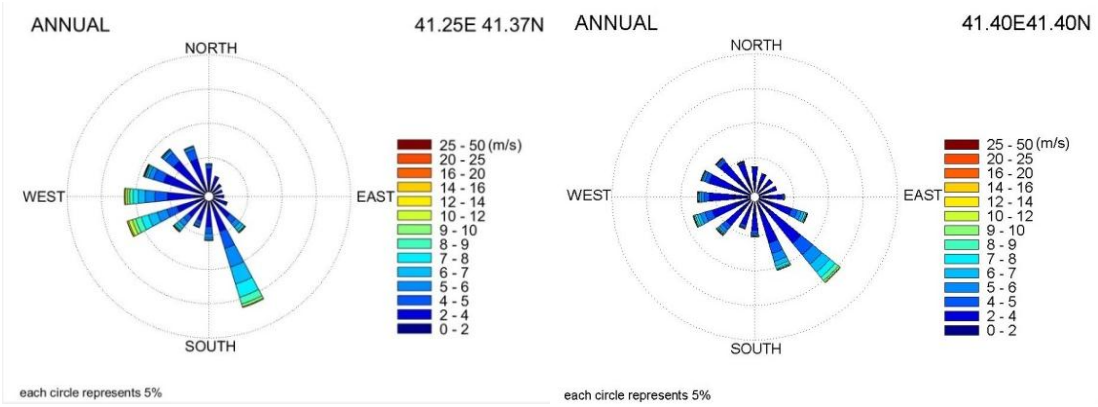

Figure 4.9 Wind Rose near Hopa from CFSR (left) and ECMWF Opr.(right)

The wind model grid points were selected considering the wind direction, wave direction, and fetch distances. Also, the course spatial resolution of the CFSR dataset hinders the selection of a point that is less than 10 km distance from the wave buoy. For the selected points, mean and peak wind speeds of all the storms were calculated. The average of peak and mean wind velocities of all storms for each grid point are given in Table 4.6 below.

Table 4.6 Average of Peak and Mean Wind Velocities of Each Location

Location	**Peak Wind Sp. (m/s)**	**Mean Wind Sp. (m/s)**
Gelendzhik		
Gelendzhik CFSR 1	15.63	6.38
Gelendzhik CFSR 2	16.63	7.36
Gelendzhik ECMWF 1	10.75	4.93
Gelendzhik ECMWF 2	11.04	5.09
Sinop		
Sinop CFSR 1	13.45	5.91
Sinop CFSR 2	13.60	6.07
Sinop ECMWF 1	10.09	4.48
Sinop ECMWF 2	10.62	4.75
Hopa		
Hopa CFSR 1	11.26	4.81
Hopa CFSR 2	14.58	5.84
Hopa ECMWF 1	6.83	3.02
Hopa ECMWF 2	7.53	3.34

Grid points distant from the shoreline are expected to have greater peak and mean wind speeds. This expectation holds true for every location which can be easily seen for CFSR1and CFSR2 points in Hopa. However, 45.4 % difference in peak wind speeds between the closest points of different models (ECMWF 2 and CFSR1) in Gelendzhik cannot be only explained with the location of the grid points. This discrepancy highlights the high error margin between the models. This idea is also supported in Hopa, since ECMWF 2 grid point that is more distant to shore than

CFSR 1 grid point, still has a 49.5 % lower value for the peak wind velocities on average. It is true that precise judgments cannot be made on peak and mean wind speed differences between CFSR and ECMWF points as the selected grid points of the models do not coincide. Nevertheless, such comparison provides preliminary information on the differences between the wind input dataset used in the wave models.

Figure 4.10 presents a scatter diagram consist of every storms peak wind velocity comparing CSFR wind data to ECMWF operational data for all the locations. The figure clearly indicates that wind speeds of ECWMF operational wind fields are less than CFSR's for the study locations in Black Sea.

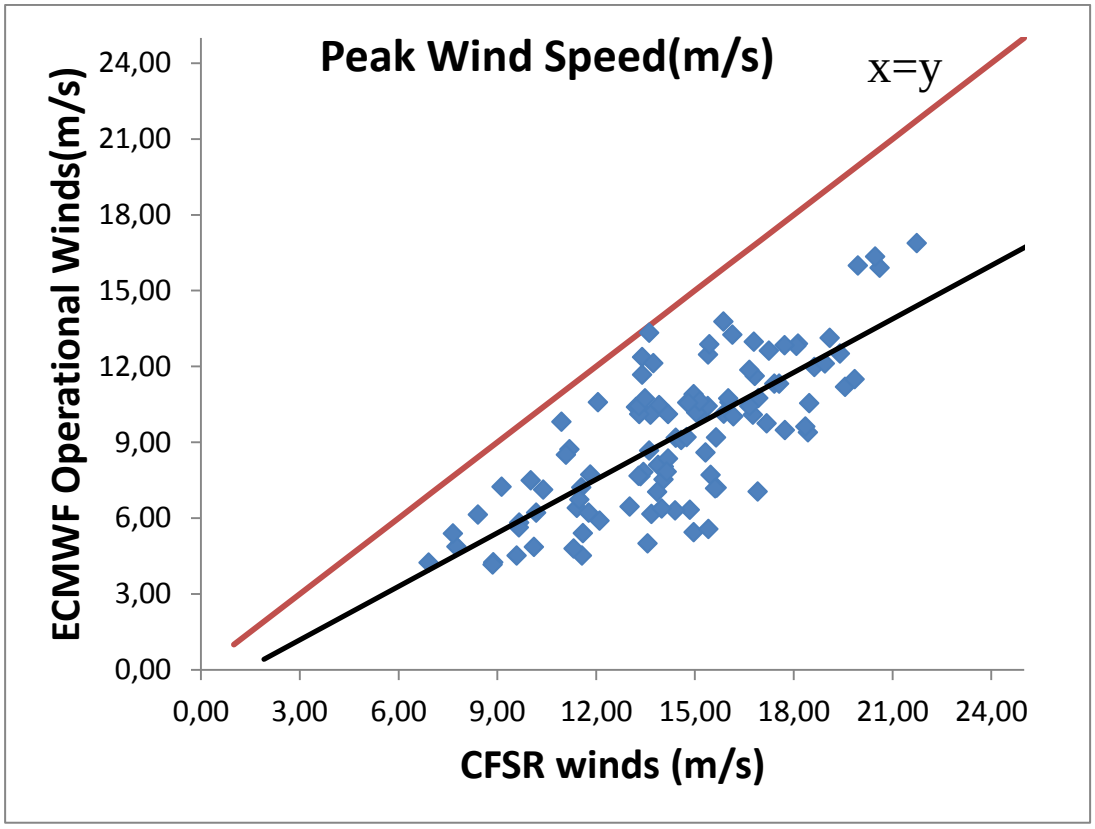

Figure 4.10 Peak Wind Speeds Scatter Diagram

In another study, Vledder and Akpinar (2015) presented that for the year of 1996, ECMWF dataset underestimated the mean wind speeds compared to NCEP dataset for all Black Sea Region (Figure 4.11).

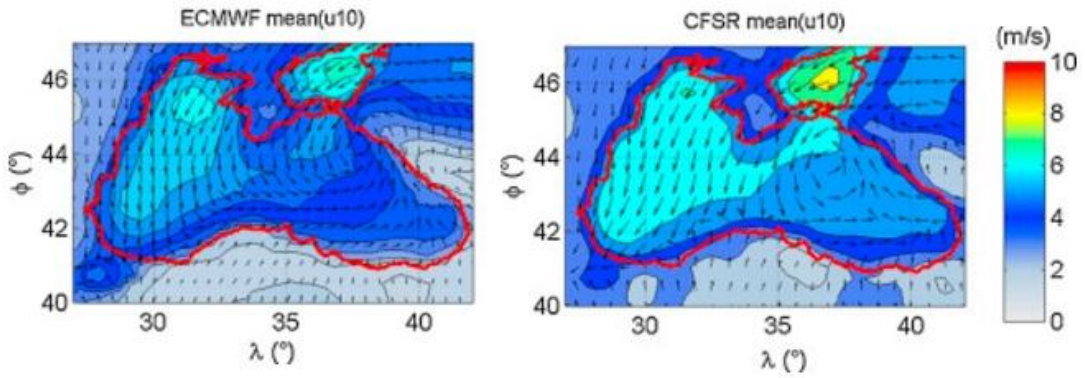

Figure 4.11 Spatial variation of mean wind speed in the Black Sea area for 1996 as obtained from ECMWF Operational and CFSR datasets (Vledder and Akpinar, 2015)

Table 4.6 shows that the result of the wind models are comparably closer in Sinop which is the farthest west location of the study whereas the differences increase towards the east of the basin. A similar discussion was presented by Vledder and Akpinar (2015) that, the spatial distributions of wind speed errors are found to be largest along the south-eastern boundary of the Black Sea and in the Sea of Azov.

CHAPTER 5

IMPLEMENTATION OF SWAN MODELS TO BLACK SEA BASIN

In this chapter, implementation of 3rd generation wave model, SWAN, for Black Sea basin is illustrated in detail. Several combinations of numerical approaches of SWAN applied in the study are introduced. Calibration and validation of the model were performed separately. Improvements of the model are explained using different statistical methods. Effects of parameterization in the model are discussed for all buoy locations and for overall study area.

5.1 SWAN Model General Description

In this study, SWAN version 41.01 was used to model the wave generation in Black Sea in deep water. Therefore, the governing processes are whitecapping and nonlinear wave-wave interactions which are the deep water source terms of SWAN.

Flow chart of model implementation is explained below. Moreover, mesh size, resolutions in frequency, directional and geological space, input and output details of the SWAN runs which were kept constant except for the sensitivity analysis are given in section 5.1.2.

5.1.1 Flow Chart of the Implementation and Evaluation of SWAN Model

SWAN was used to model 54 storms with 2 wind sources using different combinations of available methods for whitecapping and nonlinear wave-wave interactions. These initial runs were modeled with the recommended values of SWAN as given in SWAN technical documentation. Then, the results were compared to buoy data and the best combination was chosen to calibrate the model in terms of deep water sources and wind field considerations.

A selection criterion of the best combination was based on a basic ranking system of the results of statistical analysis. Statistical analysis methods explained in section 3.4 were considered with the ranking system (section 3.4.6) in the selection procedure.

RMSE, RMSEs, and RMSEu, BIAS results were used for tuning of parameters in calibration part of study for each storms, individually. Additionally, if the same storm is used for all combinations, these statistics were also included in the overall comparison of the model performance.

One representative storm from each location (three storms in total) was chosen to calibrate different parameters of the model. The selected calibrated model was applied to all 54 storms and the results were compared using different statistical techniques. Additionally, SWAN model was tested for its sensitivity against spatial, temporal resolution and different propagation schemes. The analysis of the results followed the same approach explained above.

5.1.2 General Model Parameters Used in All SWAN Runs

SWAN model uses two dimensional spectrum in order to specify the incoming wave components at the wave boundaries (SWANTeam,2015). Boundaries of geographical space are considered either as land or water. Computational grid which is defined as

land is an absorbent boundary that absorbs all wave energy and does not generate waves. On the other hand, water points are active boundary where action balance equation is applied (SWAN Team, 2015).

Some parameters and physical properties were kept constant for all SWAN runs. First off all, computational mesh for model was set to 301x141 squared meshes with 0.05˚ x 0.05˚ spatial resolution. Spectral direction was chosen to cover all directions, and 360˚ is divided into 36 which corresponds the mesh size 10˚ on direction space. Lowest and the highest frequencies were chosen as 1 and 0.05, respectively. Frequency distribution and resolution in SWAN model is defined as in Eq.5.1 and Eq.5.2

$$f_{i+1} = (\gamma + 1) f_i \tag{5.1}$$

$$\Delta f = (-1 + \left(\frac{f_{High}}{f_{Low}}\right)^{1/m}) \tag{5.2}$$

Where f_i stands for frequency and γ is the resolution constant. Δf is frequency resolution and m as the one less number of frequencies.

Frequency interval was divided into 40 (m=40) using the above logarithmic distribution, so that γ =0.0778. SWAN runs were carried out in spherical coordinates with nonstationary formation which means time was also considered in action balance equation. Computational time step and output time step were chosen as 15 min and 30 min, respectively. BSBT (backward space backward time) scheme was selected as propagation scheme (details in section 3.2.3.1). Threshold value for the fraction of breaking waves (qb) was set to 1.0.

Field and point outputs were provided at the end of the model runs. Parameters obtained in field outputs were;

- Significant wave height (Hs) (m)
- Wind speed (m/s)
- Wave direction (degrees)

Parameters obtained in point outputs were;

- Significant wave height (H_s) (m),
- Mean wave periods ($T_{m0}1$ and T_{m02}) (s)

$T_{m0}1$ and T_{m02} are both spectral mean wave periods which are derived from the energy density spectrum. The formulations are given below in Eq. 5.3 and Eq.5.4

$$T_{m01} = \frac{m_0}{m_1} \tag{5.3}$$

$$T_{m02} = \sqrt{\frac{m_0}{m_2}} \tag{5.4}$$

Where m_n stands for the n-th moment of the energy density spectrum (Eq. 5.5)

$$m_n = \int_0^\infty f^n E(f)\, df \tag{5.5}$$

The zeroth moment is the area under spectral curve. The first moment gives a weight to higher frequencies and second moment even to higher frequencies.

- Wave direction (degrees)
- Wind speed, (m/s)

- Coordinates and depth information

Outputs were drawn, compared and evaluated using a graphical user interface which was prepared on MATLAB software specifically for this thesis (Appendix B). A sample swan input file can also be found in Appendix A1.

5.2 SWAN Runs with Recommended Values

In this section, the effect of selected methodology that defines different deep water source terms in SWAN model are discussed. Available methods for whitecapping are Komen and Janssen methods, and for nonlinear wave-wave interactions, DIA and MDIA approaches can be used. XNL approach was not applied to all storms. To describe different combinations used in the model runs, a set of abbreviations was used (Table 5.1).

Table 5.1 Abbreviations for model runs in SWAN

Used Method, Model & Data	Abbreviation
SWAN	S
CFSR	C
ECMWF Opr.	E
Komen	K
Janssen	J
DIA	D
MDIA	M

5.2.1 Komen and DIA (SCKD or SEKD)

Komen and DIA formulations were applied for whitecapping dissipation and quadruplets, respectively. Table 5.2 presents the coefficients used in these runs.

Iquad=2 stands for fully explicit computation of the nonlinear transfer with DIA per sweep.

Table 5.2 Komen & DIA Parameters

White Capping - Komen		
C_{ds}	δ	ρ
2.36x10-5	1	2
Quadruplets- DIA		
Iquad	λ	C_{nl}
2	0.25	3x107

Performance of the Komen and DIA combination with default coefficient values for Black Sea Basin is presented in statistical terms using data of all buoy locations in Table 5.3.

Table 5.3 Komen & DIA Statistical Analysis Results for all storms

	CKD	EKD
R	0.88	0.75
NBIAS	0.16	0.43
SI	0.31	0.44

In general, KD combination showed a good agreement for the Black Sea when CFSR winds were used. In addition, stronger systematic error (higher nbias) was observed for ECMWF operational winds compared to CFSR winds (Figure 5.1).

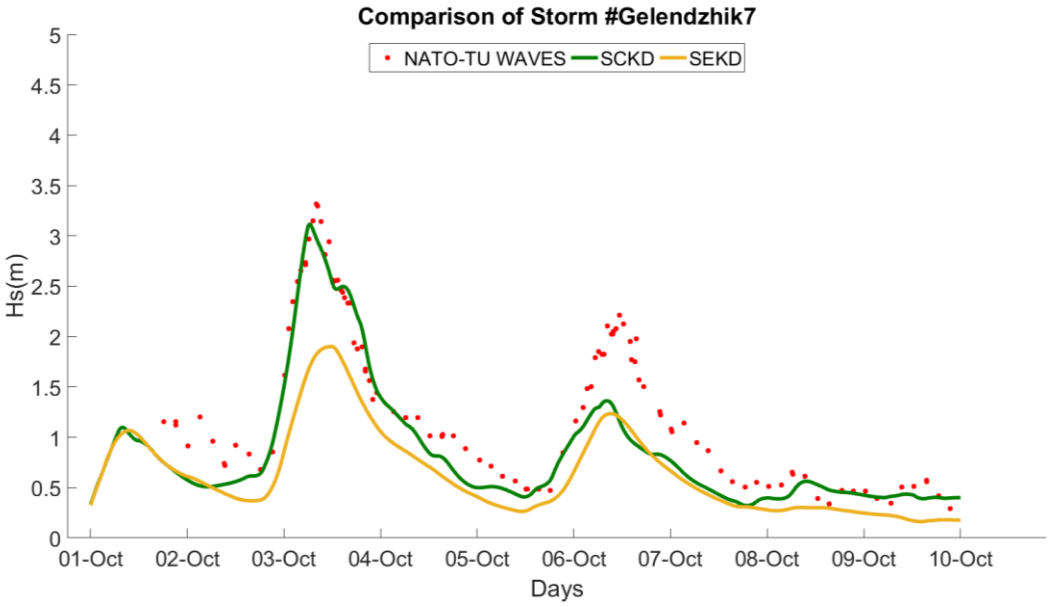

Figure 5.1 ECMWF CFSR comparisons for storm of Gelendzhik 7

However, both wind fields data presented similar problems in the model run results. First problem was the systematic underestimation of the wave heights. The second problem was the low accuracy on modeling the peak wave heights especially if peaks were over 4 meters and occurred in a short period (steeper climbs and falls in time series). This problem was also related with the underestimation problem, since it was observed less for CFSR winds for which NBIAS values were low. As this problem was seen for all the combination, a general discussion is included in Section 5.2.5.

Table 5.4 Komen & DIA Statistical Analysis Results for Buoys

		RMSE	RMSEs	RMSEu	NBIAS	R
CKD	Gelendzhik	0.47	0.26	0.38	0.09	0.88
	Sinop	0.45	0.39	0.22	0.26	0.87
	Hopa	0.43	0.33	0.24	0.19	0.89

The correlation coefficients and RMSE values of buoys were quite close to each other as seen in Table 5.4. However, this does not mean that, KD method had the similar performance for all buoys. Differences in systematic and unsystematic parts of RMSE showed that, the reasons behind the error were variable depending on the buoy. In Hopa and Sinop, significant part of RMSE was the systematic error (RMSEs), which was reflected in the stronger systematic underestimation of the wave heights compared to Gelendzhik. The higher NBIAS values for Sinop and Hopa supported this conclusion as well. According to Table 5.4, strongest systematic underestimation occurred in Sinop buoy. An illustration of this situation can be seen in Figure 5.2 for Sinop2 storm.

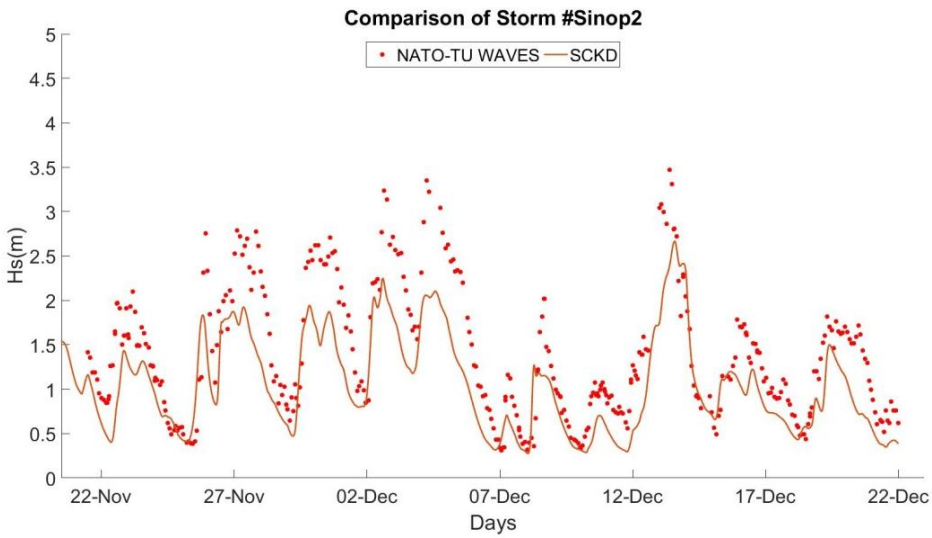

Figure 5.2 SCKD Graph for Sinop 2 Storm

5.2.2 Janssen and DIA (SCJD or SEJD)

Janssen and DIA formulations were applied for whitecapping dissipation and quadruplets, respectively. Table 5.5 presents the coefficients used in these runs.

Iquad=2 stands for fully explicit computation of the nonlinear transfer with DIA per sweep.

Table 5.5 Janssen and DIA Parameters

White Capping - Janssen		
C_{ds}	δ	ρ
4.5	0.5	2
Quadruplets- DIA		
Iquad	λ	C_{nl}
2	0.25	3x107

Performance of the JD combination in Black Sea is presented below in Table 5.6

Table 5.6 JD Statistical Analysis Results for CJD and EJD

	NRMSE	RMSE	RMSEs	RMSEu	NBIAS	SI	R
CJD	0.34	0.50	0.28	0.39	0.15	0.36	0.86
EJD	0.51	0.70	0.65	0.22	0.39	0.44	0.76

In JD combination, strong underestimation was seen for ECMWF winds. The dominant part of RMSE error was because of this systematic error which was also reflected as lower correlation coefficients compared to CFSR winds. On the contrary, main component of error in CFSR winds was RMSEu.

In Gelendzhik, effect of Janssen methods was strongly observed for CFSR winds. Even though lower bias values were obtained compared to all Black Sea, unsystematic RMSE has reached 25% more than the overall average of Black Sea (Table 5.7).

Table 5.7 CJD Statistical Analysis Results for Gelendzhik

	RMSE	RMSEs	RMSEu	NBIAS	SI	R
CJD	0.56	0.22	0.50	-0.03	0.35	0.85

Coupling JD with CFSR also caused overestimation for many storms which resulted in small negative NBIAS value. In case of low systematic error (low RMSEs and low bias), some events have shown high correlation with the observed data despite high unsystematic error. An example of this situation is presented in Figure 5.3 for Gelendzhik storm 5, which has a bias, RMSEs and RMSEu values of -7.3 cm, 0.09 and 0.53 respectively and correlation coefficient of 0.91.

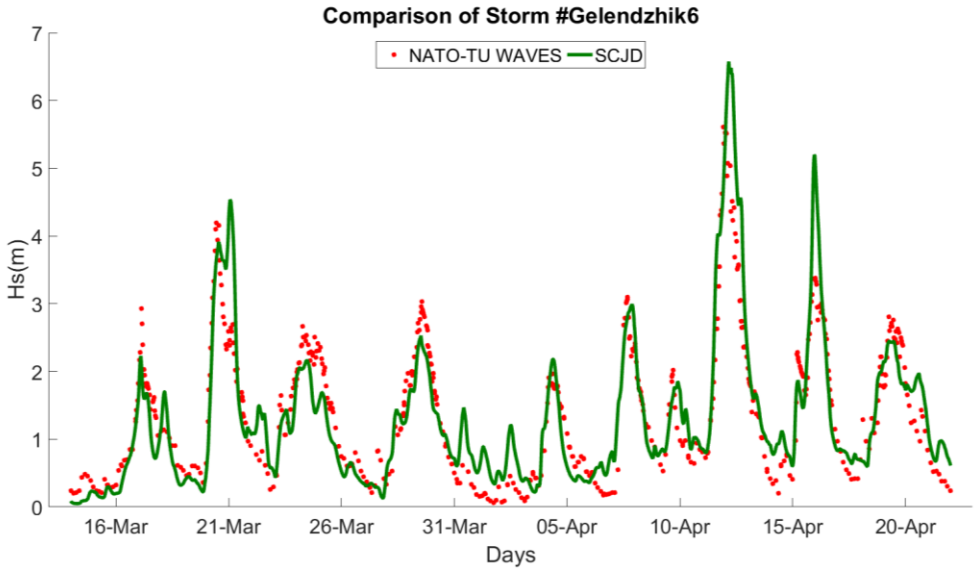

Figure 5.3 SCJD configurations for Gelendzhik storm 6

In general, CFSR winds were in better agreement with KD combination than JD combination. However in Sinop buoy, statistical analysis of JD has demonstrated better results (Table 5.8). One possible reason behind this changed behavior of SWAN according to location could be due to the fact that JD combination models

higher wave heights and KD combination significantly underestimated the wave heights in Sinop. This result could conclude that in cases with large positive biases of KD combination, SWAN model shows better agreement using JD instead KD. Moreover, such condition is not related to the source of wind field (It may occur for CFSR and ECMWF winds as well).

Table 5.8 Comparison of CKD & CJD in Sinop

	RMSE	RMSEs	RMSEu	NBIAS	SI	R
CKD	0.45	0.39	0.22	0.26	0.30	0.87
CJD	0.42	0.33	0.24	0.24	0.29	0.88

5.2.3 Komen and MDIA (SCKM or SEKM)

Komen and MDIA formulations were applied for whitecapping dissipation and quadruplets respectively. Table 5.8 presents the coefficients used in these runs. Iquad=4 stands for Multiple DIA. When MDIA is chosen, SWAN model disables the tuning of the nonlinear wave-wave action parameters.

Table 5.9 Komen & MDIA Parameters

White Capping - Komen		
C_{ds}	δ	ρ
2.36x10-5	1	2
Quadruplets- MDIA		
Iquad	λ	C_{nl}
4	-	-

Performance of the Komen and MDIA combination with default coefficient values for Black Sea Basin is presented in statistical terms using data of all buoy locations in Table 5.10.

Table 5.10 Statistical Analysis for CKM and EKM

	NRMSE	MAE	NBIAS	SI	R
CKM	0.29	0.41	0.15	0.30	0.89
EKM	0.52	0.76	0.39	0.44	0.76

It has been observed that, when CKM combination was used, R and SI values of all buoys were closer to each other than any other combination. Usually those values were ranged in a large interval (Table 5.11).

Table 5.11 SI and R values for CKM

	SI	R
Gelendzhik	0.29	0.89
Sinop	0.28	0.89
Hopa	0.32	0.90
Black Sea	0.30	0.89

The underestimation of values continues for ECMWF winds for all buoy locations. On the other hand, strong correlation was observed for CFSR winds and KM combination.

The selection of MDIA instead of DIA had shown almost no change in Gelendzhik buoy, where the statistical analysis can be seen from Table 5.12

Table 5.12 Statistical Analysis for Gelendzhik Buoy considering KD and KM

	RMSE	RMSEs	RMSEu	NMAE	NBIAS	SI	R
KD	0.59	0.47	0.31	0.56	0.23	0.36	0.81
KM	0.58	0.45	0.31	0.55	0.22	0.35	0.82

The MDIA affected the wave height with slightly greater values in other locations. Rarely up to 15% changes in NRMSE was observed on the basis of individual storms. Also, at some of the peak points the difference between KD and KM was increased, such a situation can be seen from Figure 5.4.

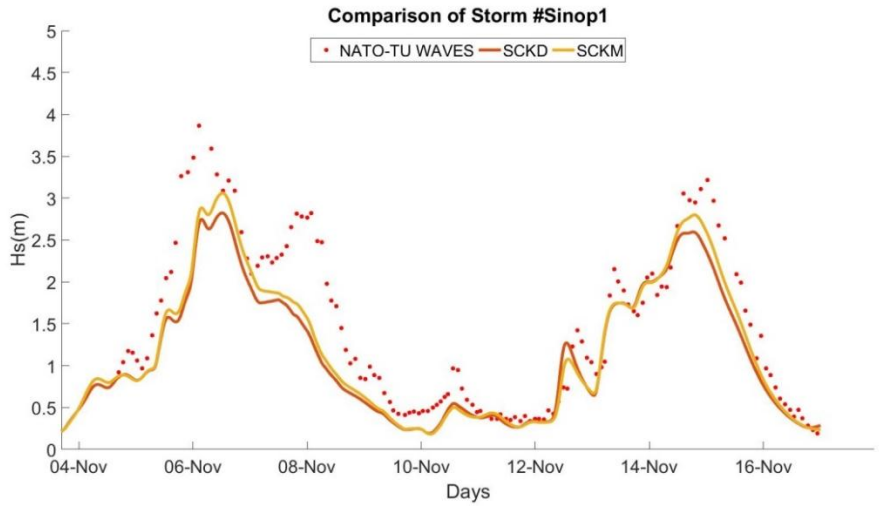

Figure 5.4 Comparison of Significant Wave Heights according to KD & KM for Sinop1 Storm

5.2.4 Janssen and MDIA (SCJM or SEJM)

Janssen and MDIA formulations were applied for whitecapping dissipation and quadruplets respectively. Table 5.13 presents the coefficients used in these runs.

Table 5.13 Janssen & MDIA Parameters

White Capping - Janssen		
C_{ds}	δ	ρ
4.5	0.5	2
Quadruplets- MDIA		
Iquad	λ	C_{nl}
4	-	-

Performance of JM combinations using statistical analysis is available in Table 5.14

Table 5.14 Statistical Analysis Results for JM

	NRMSE	MAE	NBIAS	SI	R
CJM	0.47	0.64	-0.32	0.45	0.87
EJM	0.42	0.58	0.14	0.44	0.76

When Janssen wind wave interaction and dissipation method is coupled with multiple DIA quadruplet configurations, fundamental changes were observed in statistical analysis. The main effect of this situation was the significantly high wave height values that were obtained from JM combination. Since CFSR wind fields have greater wind speed values (chapter 4.3.3) compared to ECMWF winds speeds, this combination had different effects on statistical analysis for different wind field data. JM caused systematic overestimation of wave heights with CFSR data (Figure 5.5) which can be observed from the high negative bias obtained for CJM.

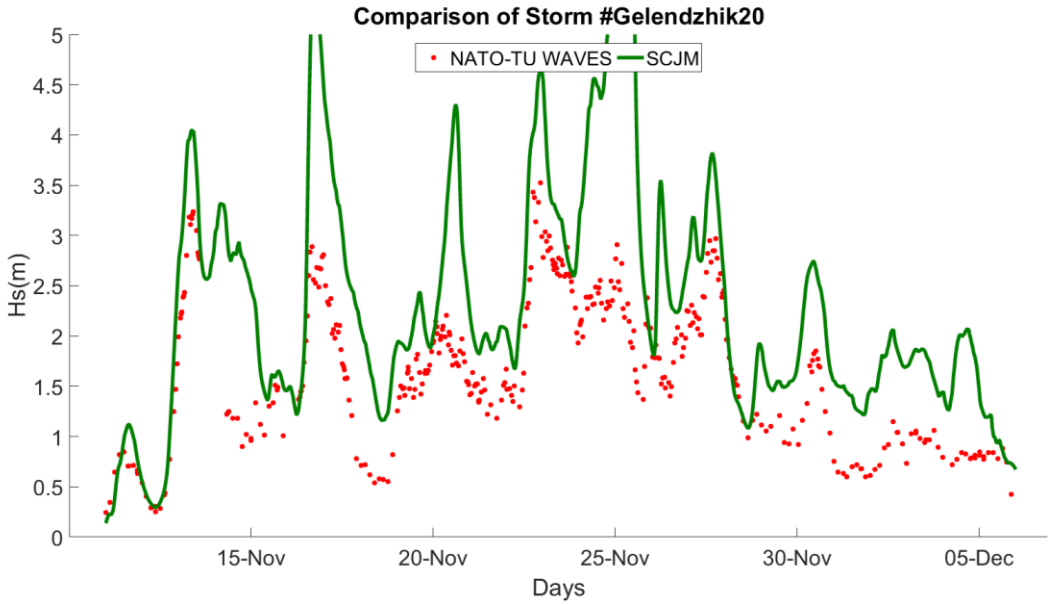

Figure 5.5 SCJM combinations for storm Gelendzhik 20

On the other hand, lower NBIAS values are observed for ECMWF dataset. Moreover, obtained error values were also less for ECMWF winds (considering NMRSE and NMAE). The different effect of JM on errors for each buoy can be explained in a more detailed way using RMSEs and RMSEu values from the Table 5.15.

Table 5.15 RMSE, RMSEs, RMSEu ,and BIAS values for JM in each buoy

		RMSE	RMSEs	RMSEu	BIAS
Gelendzhik	CJM	0.97	0.74	0.60	-0.65
	EJM	0.47	0.21	0.39	-0.01
Sinop	CJM	0.41	0.21	0.34	-0.12
	EJM	0.39	0.34	0.19	0.26
Hopa	CJM	0.59	0.37	0.43	-0.31
	EJM	0.56	0.45	0.30	0.23

As it is seen in Table 5.15, effects of JM on statistical parameters have also varied depending on the location. RMSEs values were adversely effected when CFSR winds were used with JM combination in Hopa and Gelendzhik. Highest RMSE values were observed in Gelendzhik where the systematic overestimation was also the highest, among other buoys. On the other hand, in Sinop, JM had a positive impact on RMSE and BIAS when it was used with CFSR winds. Such impact was similar to effect of JM combined with ECMWF winds. The reason behind this similarity was stronger underestimation observed in Sinop with both wind fields so that increased in wave height in Sinop with CJM was not resulted in overestimation like it happened in Gelendzhik or Hopa.

5.2.5 General Discussion on the Selected Source Terms in SWAN Model

In this part, the effects caused by the change of source term methodologies were discussed. This discussion was handled in two parts; differences of wind-wave interaction and dissipation terms and differences of non-linear interaction terms. In conclusion, best alternative couple was chosen according to their performance.

5.2.5.1 Discussion on the Discrepancies Observed Between the Wind-Wave Interaction and Dissipation Terms

Wind wave interaction and dissipation term is crucial for the realistic representation of the sea states in wave modelling, since those terms directly deal with the main input data of source term which is the wind speeds. In SWAN model two options were consider which are based on Komen et al., 1984 formulation and Janssen 1991 formulations. The preliminary comparisons showed that the total energy of the system tended to be higher when Janssen method was chosen over Komen method.

A comparison of performance of the Janssen and DIA combination to Komen and DIA combination using default coefficient values for Black Sea Basin is presented in statistical terms in Table 5.16.

Table 5.16 Statistical Analysis of the Komen and Janssen method using DIA for both wind fields

	RMSE	**RMSEs**	**RMSEu**	**NMAE**	**NBIAS**	**SI**	**R**
SCKD	0.45	0.31	0.29	0.43	0.15	0.31	0.88
SCJD	0.50	0.28	0.39	0.47	0.07	0.36	0.86
SEKD	0.72	0.68	0.22	0.77	0.43	0.44	0.76
SEJD	0.69	0.65	0.23	0.75	0.41	0.44	0.76

The obtained results showed that Janssen configuration generated higher wave height values than Komen configuration. This change is based on the change of wind-wave interaction term rather than change in dissipation. As it can be seen from the Figure 5.6, when KD method was replaced by JD, the increase in the wave heights were stronger for CFSR than ECMWF operational winds since CFSR wind fields have higher wind speed than ECMWF operational. Thus, JD method performed better with ECMWF as KD significantly underestimated the wave heights while increase in wave heights decreased the performance of JD method with CFSR winds especially for peak values as underestimation for KD method with CFSR were already low.

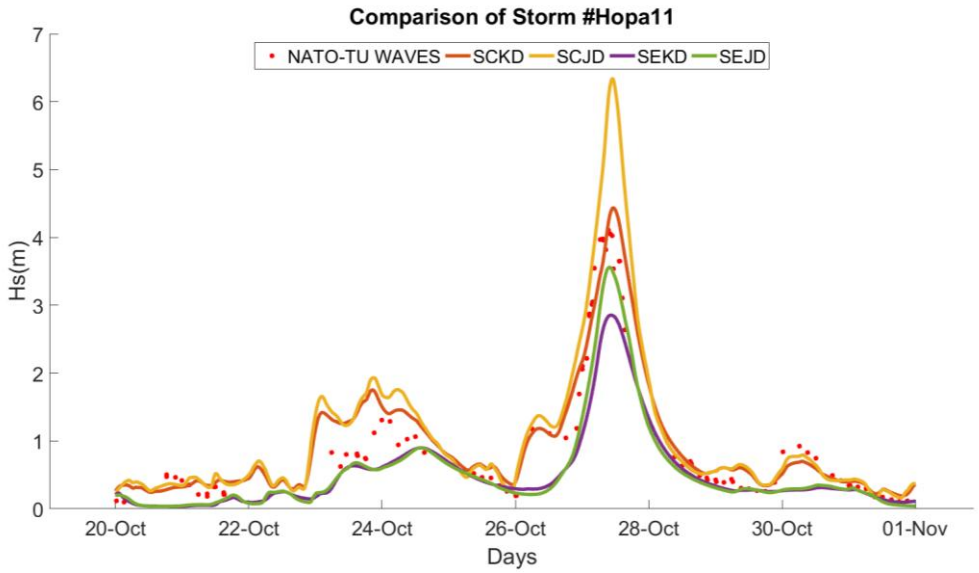

Figure 5.6 Comparison of the SEKD, SEJD, SCKD and SCJD methods for Hopa11 storm

Even though NBIAS value of 0.07 is a good result, increases in unsystematic error (increases in RMSEu and SI) were significant for JD with CFSR. Moreover, increase in scatter index values were also proof of increased random error, which was observed in CFSR coupled SWAN runs, and had a negative impact on the correlation coefficient for JD combination. Also, higher wave heights due to JD combination did not provide any remarkable improvement for ECMWF data as well.

In general, statistical results were in the favor of CFSR winds since the underestimation was less. However, if only individual storms are considered, it has seen that, for numerous storms ECMWF winds provided better correlation with JD than CFSR winds. Hopa 11 is also a good example in order to explain this situation (Figure 5.6). In Hopa 11, EJD shows better correlation than CJD since overestimation in CJD was very strong. This situation shows that same combinations and calibration might not be applicable to all events.

In an extreme event study, guessing the peak wave heights has significant importance since the most devastating effect is caused by the highest waves. Here, another discussion arises between the choices of the selected wind-wave interaction and white capping methods. Despite better statistical values of CKD over CJD when all storms are considered, CJD has shown better performance in terms of guessing the peak wave heights when the wave heights are higher than 3 m. This situation is demonstrated in Figure 5.7 in Gelendzhik4 storm.

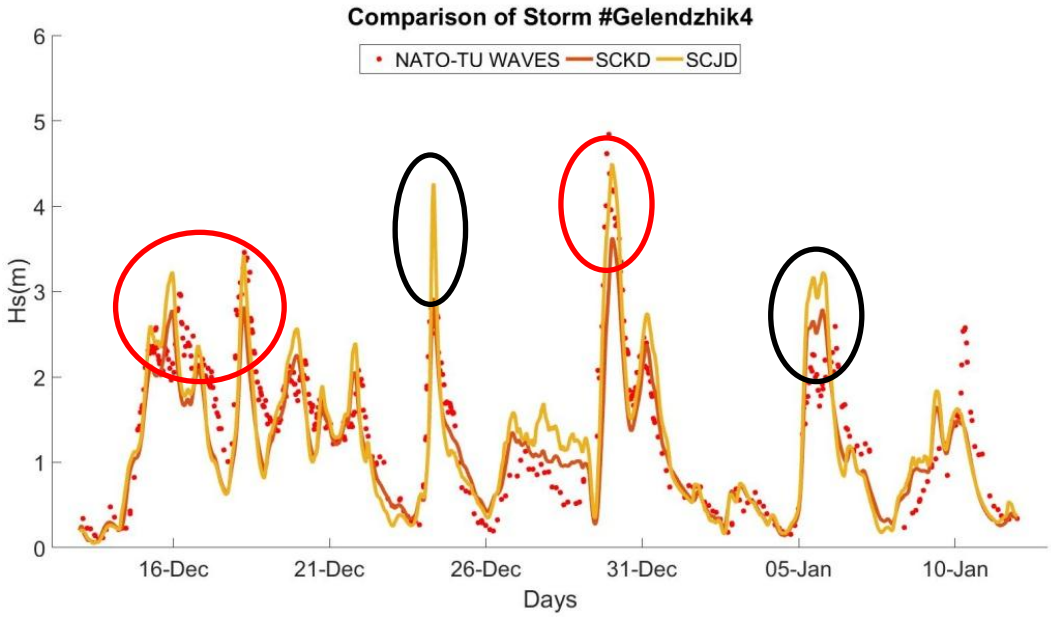

Figure 5.7 JD & KD Graph with CFSR winds for Storm Gelendzhik 4

In Figure 5.7, Janssen approach modeled the peak wave heights in red circles better, however overestimated the other lower peaks which are in black circles. Although the overall correlation and RMSE values of JD were affected negatively because of the increased unsystematic error and overestimated values through the storm, the most energetic parts of the storm (higher peaks) were modeled with a smaller error margin.

Additionally, another comparison between the Janssen and Komen approach was performed considering the wave period. Janssen approach underestimated the mean wave period compared to Komen approach (Figure 5.8). It is even stated in SWAN technical document that, "SWAN underestimates structurally the mean (or peak) wave periods by 10 to 20%." However, formulation selection of white capping dissipation could also cause up to %20 percent differences in wave period. Moreover, it is observed that Komen approach showed better correlation with the observed mean period. The reason behind this could be the difference of value δ which is taken as 1 in Komen and 0.5 in Janssen. The recommendation of Roger et al. (2003) for δ is 1 for Komen so that prediction of wave energy at low frequencies is improved. (SWANTeam, 2015).

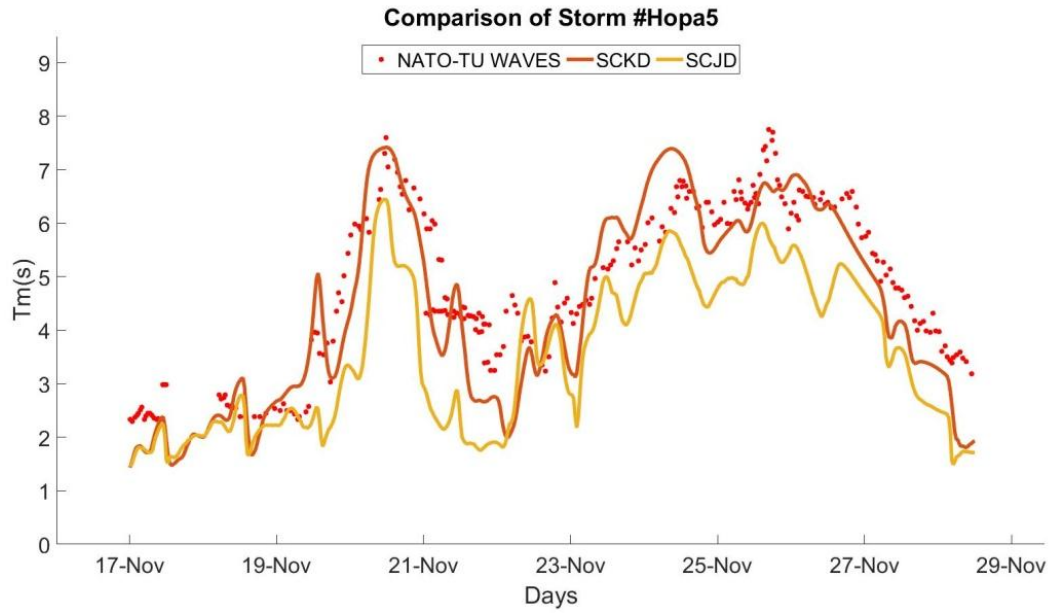

Figure 5.8 Comparison of Mean Wave Periods according to JD & KD for Hopa 11 Storm

5.2.5.2 Discussion on the Discrepancies Observed Between The Nonlinear Wave-Wave Interactions

According to Cavaleri,L. (2009) nonlinear interactions are probably the best-known subject in the physics of wave modeling since the exact solution of the equations are possible using the original six-dimensional Boltzmann integral formulation of Hasselmann(1962,1963). Nevertheless, exact solution requires too much computational effort (10^3 to 10^4 times more than the regular DIA). So, approximate methods are developed in order overcome the computational cost drawback of the solution of nonlinear wave-wave interactions. One of those methods is the Discrete Interaction Approximation (DIA) which is the most widely used method in wave modelling for the nonlinear interaction source term. Even though DIA is a successful method it has uncertainties as well. In this study 2 method were used for nonlinear interaction, first one is DIA, and the second one is the multiple DIA which is the improved version of DIA that uses 6 wave configurations instead of 4. The preliminary analysis showed that, MDIA method has resulted in higher wave heights than DIA.

Statistical analysis results of KD and KM combinations are presented in Table 5.17

Table 5.17 Statistical Analysis Results of KD and KM

	RMSE	**RMSEs**	**RMSEu**	**NMAE**	**NBIAS**	**SI**	**R**
SCKD	0.45	0.31	0.29	0.43	0.15	0.31	0.88
SCKM	0.43	0.29	0.29	0.41	0.13	0.30	0.89
SEKD	0.72	0.68	0.22	0.77	0.43	0.44	0.76
SEKM	0.71	0.67	0.22	0.76	0.43	0.44	0.76

The obtained results had shown that, using more nonlinear wave-wave interactions terms in solution did not change the results significantly when they were coupled

with Komen dissipation terms. A subtle increase was observed in wave heights in KM compared to KD. Mean wave periods also showed similar behavior as wave heights. The effect of change of nonlinear interaction terms cannot be traced by eye from the time series graphs most of time especially for Gelendzhik buoy (Figure 5.9).

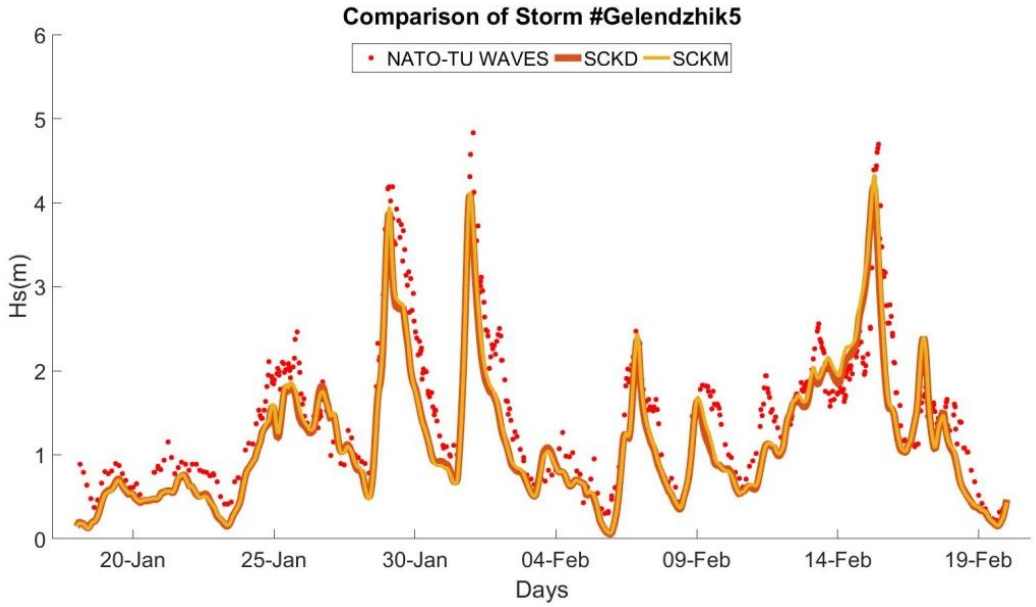

Figure 5.9 Comparisons of Significant Wave Heights According to KD & KM for Gelendzhik 5 Storm

However, the effect of MDIA was significantly different for Janssen formulations. On the contrary of almost no change in KM with respect to KD, the change in the results for JM and JD, strongly depended on the wind data source. The changes of the statistical parameters can be seen from Table 5.18

Table 5.18 Statistical Analysis Results for JD and JM with CFSR and ECMWF Operational Winds

	RMSE	**RMSEs**	**RMSEu**	**NMAE**	**NBIAS**	**SI**	**R**
SCJD	0.50	0.28	0.39	0.47	0.07	0.36	0.86
SCJM	0.73	0.50	0.49	0.64	-0.32	0.45	0.87
SEJD	0.69	0.65	0.23	0.75	0.41	0.44	0.76
SEJM	0.51	0.33	0.33	0.58	0.14	0.44	0.76

Switching from JD to JM increased the modeled wave heights significantly therefore CFSR data set performed worse with very high overestimation while ECMWF data set performed much better although the overall correlation coefficients did not change for this dataset. Thus, it can be concluded that underestimation of ECMWF dataset especially for higher wind speeds were compensated by the Janssen combinations. Use of MDIA had enhanced this effect. This effect also can be understood more clearly when statistical parameters of KM and JM change is compared with the KD and JD change (Table 5.19 and Table 5.20) for every location.

Table 5.19 Statistical Analysis Results of KM and JM for each buoy

		CFSR		ECMWF Opr.	
		KM	JM	KM	JM
BIAS	Gelendzhik	0.10	-0.65	0.53	-0.01
	Sinop	0.20	-0.12	0.49	0.26
	Hopa	0.16	-0.31	0.51	0.23
RMSE	Gelendzhik	0.46	0.97	0.71	0.47
	Sinop	0.43	0.41	0.59	0.39
	Hopa	0.41	0.59	0.76	0.56
RMSEs	Gelendzhik	0.24	0.74	0.66	0.21
	Sinop	0.37	0.21	0.58	0.34
	Hopa	0.31	0.37	0.71	0.45
RMSEu	Gelendzhik	0.38	0.6	0.25	0.39
	Sinop	0.21	0.34	0.12	0.19
	Hopa	0.24	0.43	0.21	0.30

Table 5.20 Statistical Analysis Results of KD and JM for each buoy

		CFSR		ECMWF Opr.	
		KD	JD	KD	JD
BIAS	Gelendzhik	0.13	-0.05	0.54	0.49
	Sinop	0.29	0.27	0.49	0.48
	Hopa	0.18	0.12	0.52	0.54
RMSE	Gelendzhik	0.47	0.56	0.72	0.67
	Sinop	0.45	0.42	0.61	0.60
	Hopa	0.43	0.47	0.76	0.75
RMSEs	Gelendzhik	0.26	0.22	0.67	0.61
	Sinop	0.39	0.33	0.58	0.56
	Hopa	0.33	0.32	0.72	0.71
RMSEu	Gelendzhik	0.38	0.50	0.24	0.26
	Sinop	0.22	0.24	0.18	0.19
	Hopa	0.24	0.33	0.21	0.20

The different effects of MDIA on Komen and Janssen in terms of wave heights changes can be better visualized from the scatter plots that are drawn for Gelendzhik in Figure 5.10.

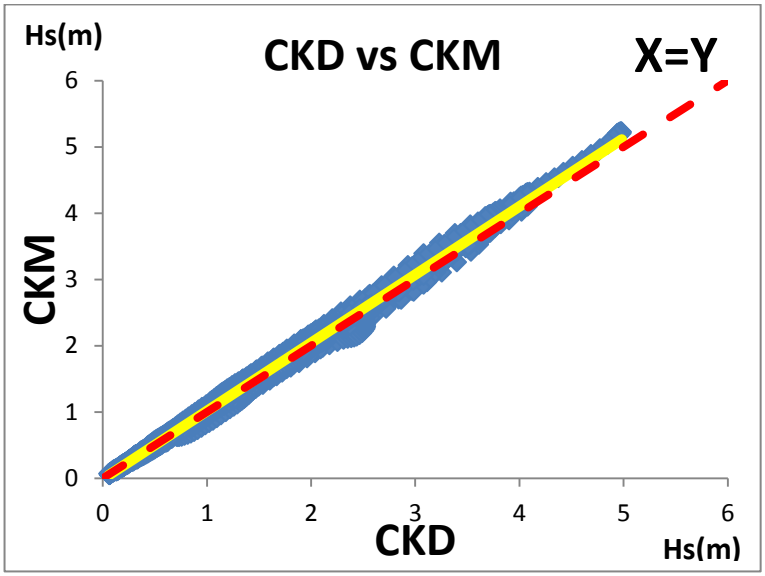

(I)

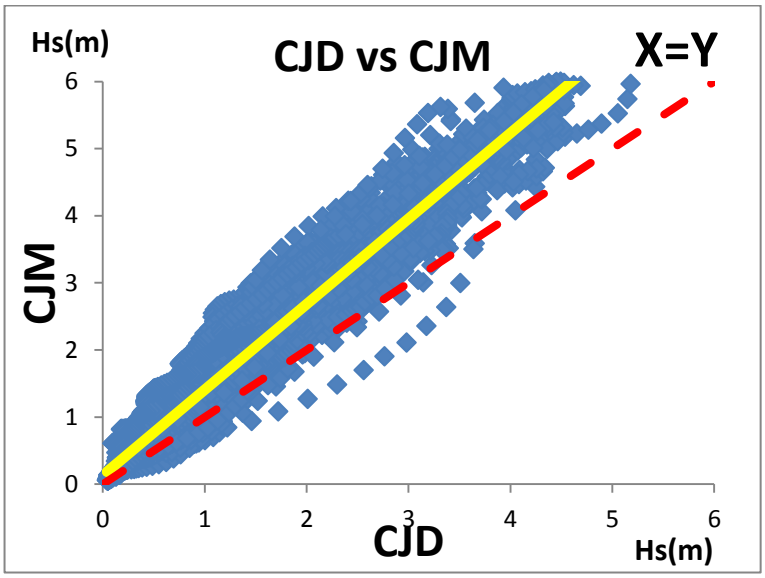

(II)

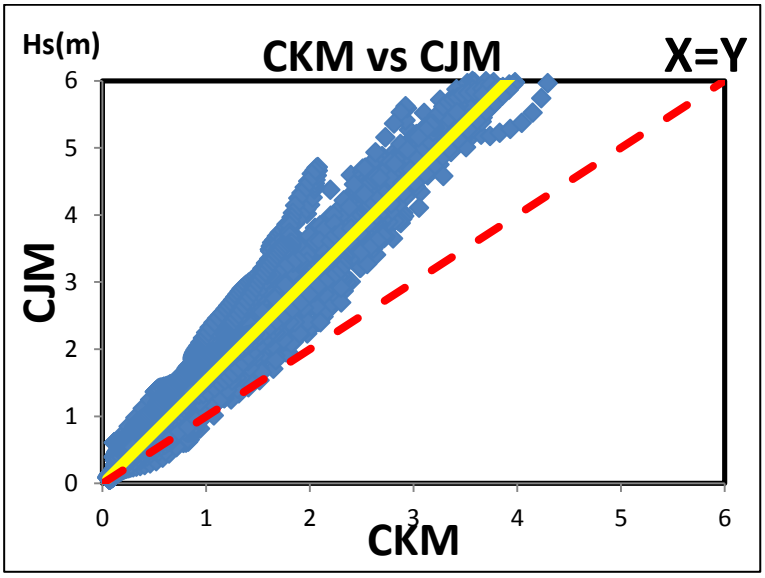

(III)

Hs(m)

Figure 5.10 Scatter plot of (I) CKD vs CKM, (II) CJD vs CJM, (III) CKM vs CJM

As it can be seen from Figure 5.10, the unsystematic errors had increased when JM was used for all cases. Moreover this over estimation was increased towards the peak points of the storms as in Figure 5.11.

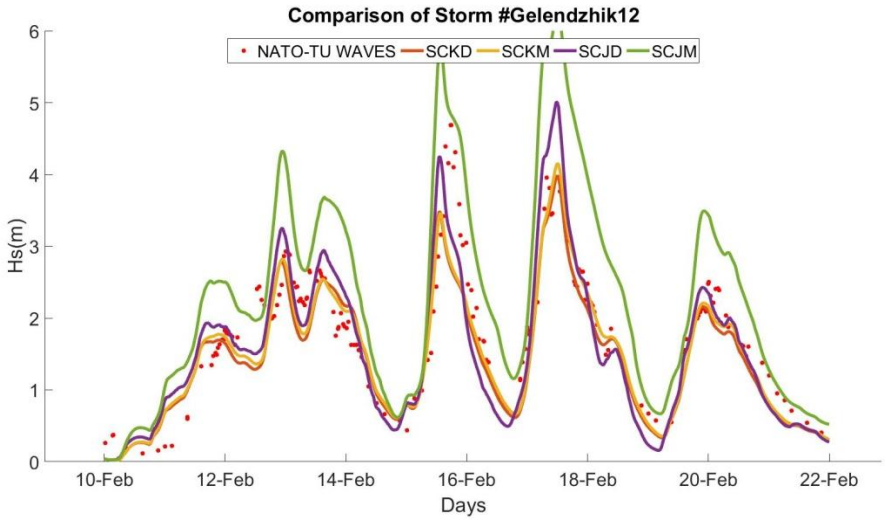

Figure 5.11 Comparison of Significant Wave Heights according to KD, KM, JM, JD for Gelendzhik 12 Storm.

JM combinations with EMCWF wind fields have shown a significant decrease in systematic underestimation and correspondingly strong decrease in RMSEs which represses the increase in RMSEu. So that, overall RMSE values were improved for ECMWF winds.

Only improvement for CFSR winds in terms of RMSE were observed in Sinop. The systematic error in Sinop was decreased since systematic underestimation has evolved in to weaker overestimation. However, the unsystematic error increased so that overall improvement is not significant.

JM approach is not as stable as other methods, so that it can be assumed that it is more beneficial to use in matter of short term individual cases. Nevertheless, JM can be shown as the appropriate methodology for ECMWF winds as in Figure 5.12.

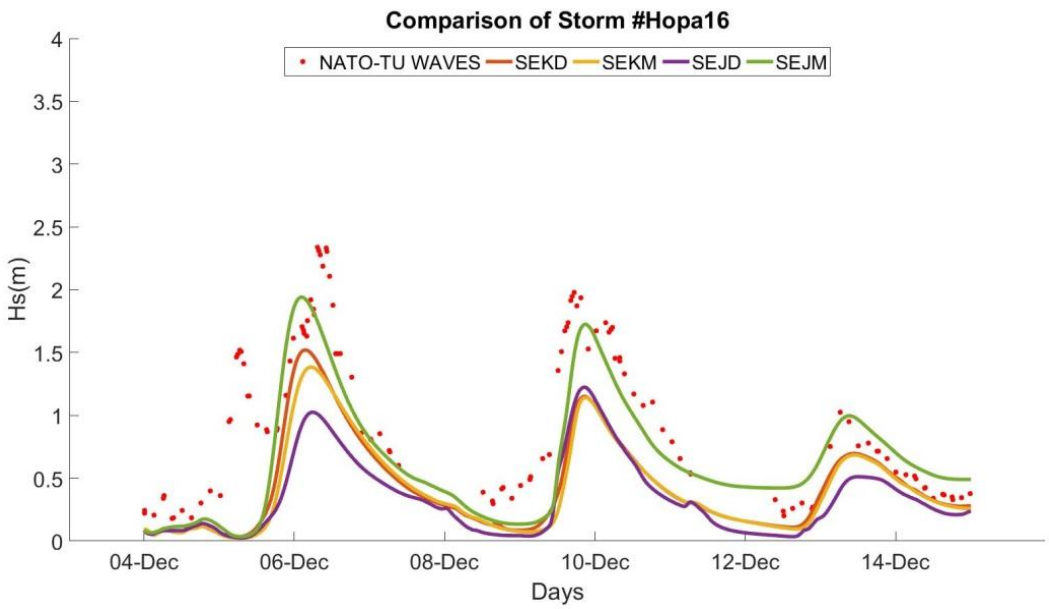

Figure 5.12 Comparison of Significant Wave Heights according to KD, KM, JM, JD for Hopa16 Storm.

According to the SWAN runs with recommended parameters, CKD was chosen as the best alternative couple according to its performance in Black Sea. Janssen method was not chosen because of the obtained high random error. CFSR winds were also chosen since they have shown better correlation with Komen and DIA approach than any other wind- dissipation- nonlinear interaction combinations.

Even though all the statistical methods are in the favor of using MDIA methods when Komen formulations were used, the improvements were not significant. Moreover, computational cost of the model has increased 3 or 4 time with respect to DIA. When the increase in the computational cost and the unavailability of tuning parameters of MDIA are considered, DIA methodology is selected for the calibration part of this study.

The final statistical parameters are given in Table 5.21 for CKD before calibration.

Table 5.21 Statistical Analysis Results of SCKD before calibration

CKD	RMSE	RMSEs	RMSEu	NMAE	NBIAS	SI	R
Black Sea	0.45	0.31	0.29	0.43	0.15	0.31	0.88
Gelendzhik	0.47	0.26	0.38	0.39	0.09	0.29	0.88
Sinop	0.45	0.39	0.22	0.54	0.26	0.30	0.87
Hopa	0.43	0.33	0.24	0.43	0.16	0.33	0.89

5.3 Calibration of SWAN Model for Extreme Events for Black Sea Basin

The initial assessment on performance of different combinations of parameters in SWAN determined that the combination of SCKM provided the best fit. However, SCKD configuration was selected to be calibrated although MDIA performed better, as SWAN does not permit external changes to MDIA algorithm. Depending on the

calibrated parameter, the number of storms modeled changed between 3 sets of storms. Small set(ss) was consisted of 3 representative storms (one from each buoy), which was mainly used for the runs that have been carried out in order to understand the general behavior of model with respect to the change of tunable parameters. Medium set(ms)was consisted of 8 storms which was used for more sensitive calibration of parameter and in some sensitivity tests. Final set is the large set(ls) which consist of all (54) storms. The large set was only used for the limited number of configuration which were chosen to be the best representative among other trial configurations. The used set in calibration and sensitivity analysis are specified in parenthesis in tables. The details of the selected representative storms are given in Table 5.22.

Table 5.22 Chosen storms for calibration

		Storm #	Start Date	End Date	Duration(days)	Max. Hs	# of Peaks
Medium Set	Small Set	Gelendzhik_1	1996.09.02	1996.10.02	30	3.50	10
		Sinop_2	1994.11.19	1994.12.22	33	3.50	10
		Hopa_12	1996.12.22	1997.01.01	10	2.77	3
		Gelendzhik_6	1997.03.14	1997.04.22	39	5.61	11
		Gelendzhik_9	1997.11.30	1997.12.23	23	4.89	4
		Sinop_7	1996.05.28	1996.06.09	12	2.10	2
		Hopa_16	1997.12.04	1997.12.15	11	2.30	2
		Hopa_19	1998.05.27	1998.06.01	5	2.30	1

Selected storms have long durations and multiple numbers of peaks since it is observed that hind casting problems are related with peak wave heights, in general. Additionally, results of initial model runs of these storms included most of the

observed problems regarding the wave modeling in Black Sea. These problems can be listed as;

- Missing the peak wave heights
- Systematic underestimation of wave parameters
- Discrepancy between the trends of model output and observed data. (Eg. wave heights increases in model while decreases in buoy data)
- Deterioration in model output after strong overestimation or underestimation

  (For instance, if 50 cm discrepancy is observed at the peak wave height, similar discrepancy continues after that peak, even if wave heights of both model and buoy data decreases at the same rate thorough the storm.)
- Low sensitivity of model against quick changes in storm characteristics such as sharp peaks.

Some of these problems are related to the quality of the wind input such as its resolution on spatial and temporal space. Peak wind speeds might not be reflected correctly in the wind input because of either low temporal resolution (ECMWF winds) or the low spatial resolution (NCEP winds). Nevertheless, some of the problems such as problems related to trends in wave parameters can be mostly caused by the parameterizations of the physical processes in SWAN. The errors related to the latter problems were tried to be minimized by the calibration process.

5.3.1 Calibration of Whitecapping Parameters

It has been observed in the previous parts of this study that whitecapping dissipation is the governing physical process in deep water for Black Sea. "There is much uncertainty concerning the physical mechanism of whitecapping in deep and shallow water and hence the appropriate form for its source term" (Westhuysen et. al, 2007). In SWAN, whitecapping term is controlled by $\tilde{\sigma}$ (mean frequency), $\tilde{k}$ (mean wave

number), $\tilde{s}_{PM}$ (wave steepness of Pierson-Moskowitz spectrum) (Eq.3.11). However, the calibration was achieved using the following coefficients; C_{ds}(coefficient for determining the rate of whitecapping dissipation) , δ (coefficient that determines the dependency of the whitecapping on wave number) and p (power of steepness normalized with the wave steepness of a Pierson-Moskowitz spectrum).

The main aim for calibration of whitecapping was to decrease the systematic underestimation of the model by reducing the effect of white capping dissipation. Therefore, C_{ds} coefficient was chosen to be modified which is a common approach in wave modeling. According to Akpinar and Leon (2015), best performance of SWAN in Black sea with CFSR winds was achieved when C_{ds} is set to 1.82e-5 for Komen approach. However, calibration in that study considered only one extreme storm which is the storm named as Gelendzhik 22 in this study. On the other hand, in this study, all 54 storms were analyzed for the calibration of C_{ds} coefficient.

The calibration started with setting $C_{ds} = 1.82e-5$. Compared to default case (SCKD), wave heights increased around the peak wave heights (Figure 5.13) and R values of mean wave periods improved slightly (Table 5.23).

Table 5.23 Comparison of C_{ds}=1.82 e-5 (Akpınar and Leon, 2015) and C_{ds}=2.36e-5(recommended by SWAN model)

	RMSE	**RMSEs**	**RMSEu**	**NMAE**	**NBIAS**	**SI**	**R**
C_{ds}=2.36e-5	0.43	0.30	0.30	0.47	0.17	0.31	0.87
C_{ds}=1.82e-5	0.42	0.30	0.27	0.43	0.15	0.30	0.88

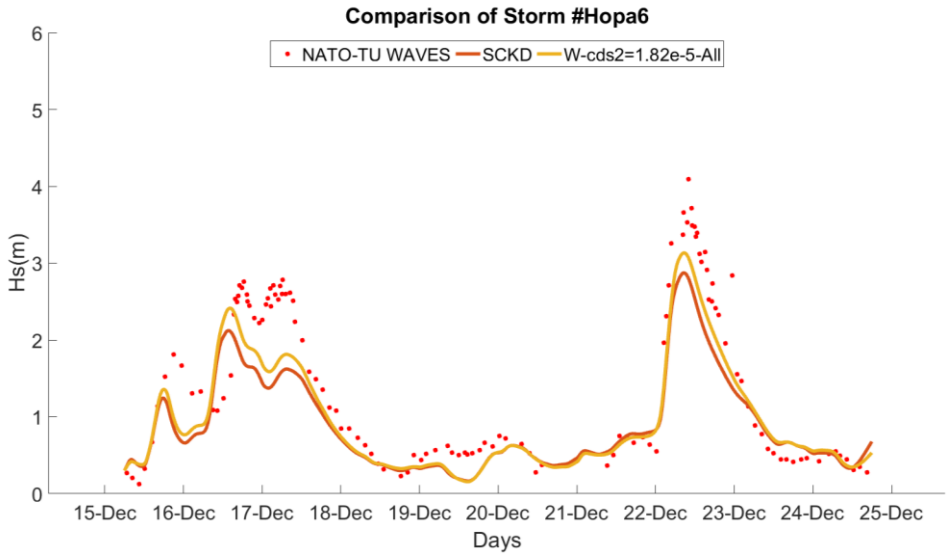

Figure 5.13 Effect of change of C_{ds} in Hopa6

Despite the improvement in NBIAS, NRMSE and R values, underestimation problem still existed. So C_{ds} value was decreased incrementally. The effect of changing C_{ds} can be observed in Figure 5.14.

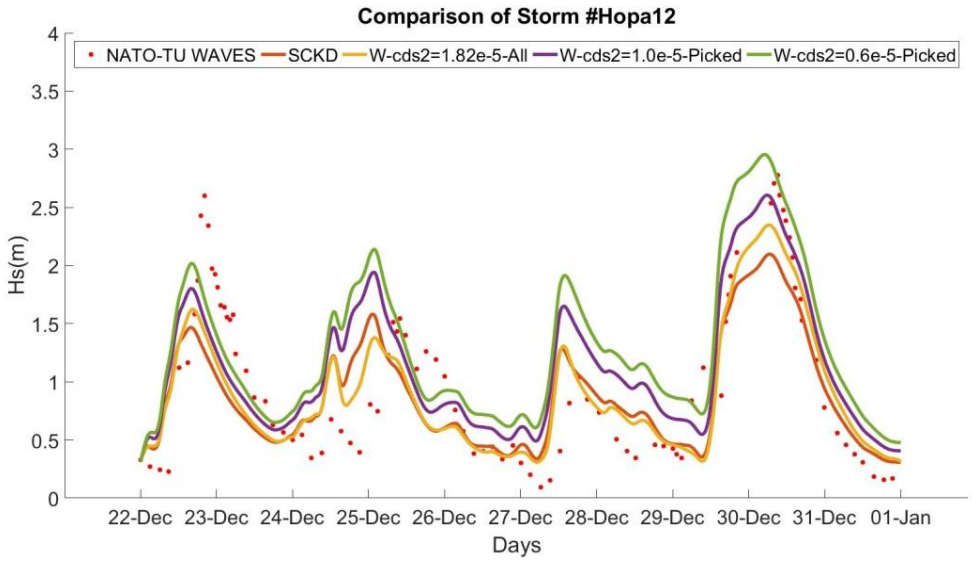

Figure 5.14 Effect of C_{ds} on wave height

Corresponding C_{ds} values in above figure are red line C_{ds} =2.36e-5, yellow line C_{ds} =1.82e-5, purple line C_{ds} =1.0e-5 and green line C_{ds} =0.6e-5. Higher energy in system was restored with decreasing the rate of white capping dissipation which resulted in higher wave height values.

The trial values of C_{ds} and corresponding RMSE are presented in Table 5.24 for all buoys and Sinop case.

Table 5.24 Effect of change of C_{ds} on RMSE for all buoys (right) and Sinop (left) corresponding wave height values (ms)

	RMSE	**RMSE s**	**RMSE u**	**BIAS**		**RMSE**	**RMSE s**	**RMSE u**	**BIAS**
C_{ds}=2.36e-5	0.41	0.35	0.20	0.29		0.43	0.30	0.30	0.20
C_{ds}=1.82e-5	0.39	0.34	0.19	0.25		0.42	0.30	0.27	0.18
C_{ds}=1.50e-5	0.37	0.31	0.20	0.23		0.40	0.28	0.28	0.14
C_{ds}=1.20e-5	0.35	0.28	0.20	0.20		0.39	0.25	0.29	0.10
C_{ds}=1.00e-5	0.29	0.21	0.21	0.02		0.38	0.23	0.30	-0.09
C_{ds}=0.8e-5	0.29	0.20	0.22	-0.02		0.39	0.24	0.31	-0.14

Table 5.24 shows that systematic error (RMSEs) and bias values improved with decreasing C_{ds} since increased wave heights compensated the systematic underestimation of the default model. Improvement of RMSEs stopped once bias values reached to 0. However, lower values C_{ds} increased the unsystematic errors thus increasing the overall RMSE. Therefore, it was concluded that an optimum value of C_{ds} was needed for the best model performance. Finally, C_{ds} = 1.0E-5 is proposed for wave modeling in Black Sea basin for SWAN.

On the other hand, in Sinop, improvement of RMSEs and bias continued up to C_{ds}= 0.8E-5 with slight increase in RMSEu as the systematic underestimation was significantly stronger than other locations. This result indicated that for the best performance of SWAN, buoys should be considered individually for better calibration.

Dependency of the whitecapping on wave number is investigated by setting up δ parameter (Eq.3.11). The recommended value of δ is 1 in Komen which corresponds to full dependency to wave number. Two different values of δ were tested. First one was $\delta = 0$ which corresponds to no relation with wave number and second one is δ=0.5 for Komen which was the default value of δ in WAM Cycle 4 model (SWANTeam, 2015). The obtained results of dependency of whitecapping on wave number are given in Table 5.25.

Table 5.25 Statistical Analysis for different values of $\boldsymbol{\delta}$ (ss)

	RMSE	RMSEs	RMSEu	NMAE	NBIAS	SI	R
$\delta = 1$	0.51	0.40	0.30	0.54	0.19	0.33	0.83
$\delta = 0.5$	0.51	0.40	0.31	0.53	0.19	0.33	0.83
$\delta = 0$	0.63	0.56	0.29	0.68	0.33	0.36	0.81

The statistical parameters showed when there was no dependency to wave number, increase on the systematic error was observed , which has been resulted in worsened NBIAS values as well. Nevertheless, there was no significant difference between setting δ to 0.5 and 1. Since small deterioration has been observed in RMSEu, full dependency to wave number was chosen.

5.3.2 Calibration of Quadruplets Parameters

The nonlinear wave-wave interaction term is another deep water process that represents the exchange of energy between spectral components as the wave field evolves in time. This process cannot be exactly explained by linear wave components for long time evaluations therefore, nonlinear terms are introduced in formulation.

Today, there are still shortcomings to explain the nonlinear wave-wave interaction. Moreover, "these shortcomings are commonly compensated by tuning of other source terms "(Ardhuin et al.,2006; Van Vledder,2006). There are different methods available to represent the nonlinear interactions, and accuracy of the chosen model has significant importance. "Spectral shapes are more peaked when an accurate method for computing non-linear four-wave interactions is used. (Van der Westhuysen et al, 2004 cited in Van Vledder, 2006)" DIA method is known as an accurate method, however it has shortcomings especially in short term computing. (Van Vledder. 2006). Also DIA approach is a poor approximation for long crested waves. (SWAN Team, 2015) Nevertheless, considering the computational cost and preference of use in the literature, DIA method was selected as most appropriate solution for nonlinear wave interaction in this study.

The calibration of DIA method can be done by tuning of the parameters Cnl4, (C in E.q.3.15) which is a proportionality coefficient for quadruplet interactions, and λ, the coefficient for quadruplet configurations (E.q 3.14). DIA method is also sensitive to frequency resolution which was discussed in Section 5.2.1.

Proportionality coefficient affects the rate of change of energy densities of wave numbers. To illustrate this effect, three cases with $Cnl_{low}=1x10^7$, $Cnl4_{mid}=3x10^7$ and $Cnl4_{high}=20x10^7$ were compared and the results are given in Figure 5.15. It was observed that when the sea state was dissipating energy (wave heights were decreasing), higher Cnl4 coefficients decelerated the energy loss of the system, so that the wave heights decreased slowly and could not reflect the lower boundary of the data accurately.

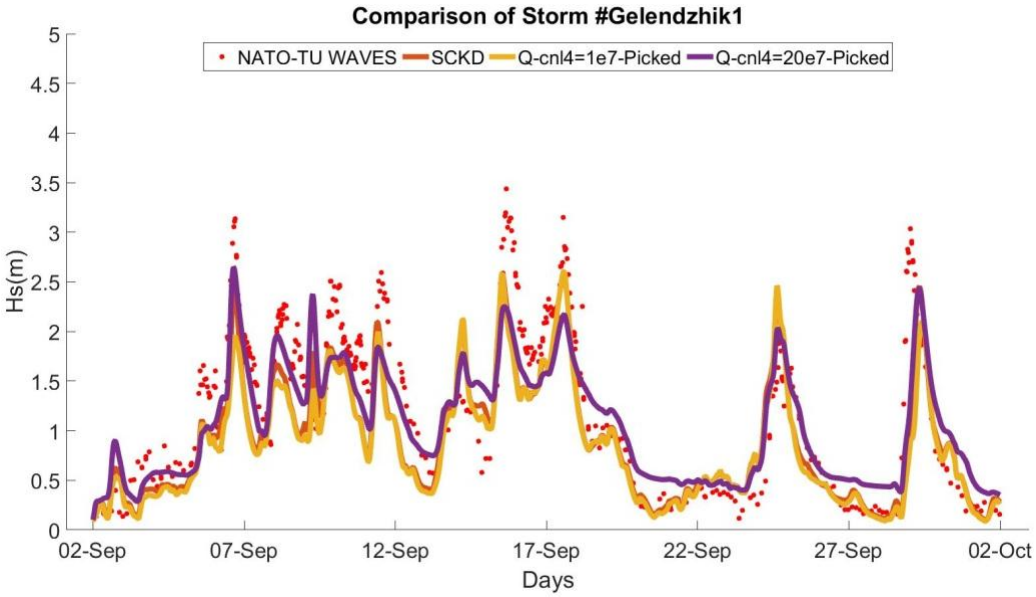

Figure 5.15 Comparison of effect of Cnl4 coefficient

A sensitivity analysis for Cnl4 coefficients were performed up to the value of 4 x10^8. The effect on the performance of the model is provided in Figure 5.16 and Figure 5.17 for RMSE and R, respectively. Although higher Cnl4 values increased the model performance statistically, very high values of Cnl4 could not model the observed dissipation as the energy was distributed equally across the waves restraining generation of waves across the sea state. This situation was illustrated in Figure 5.16.

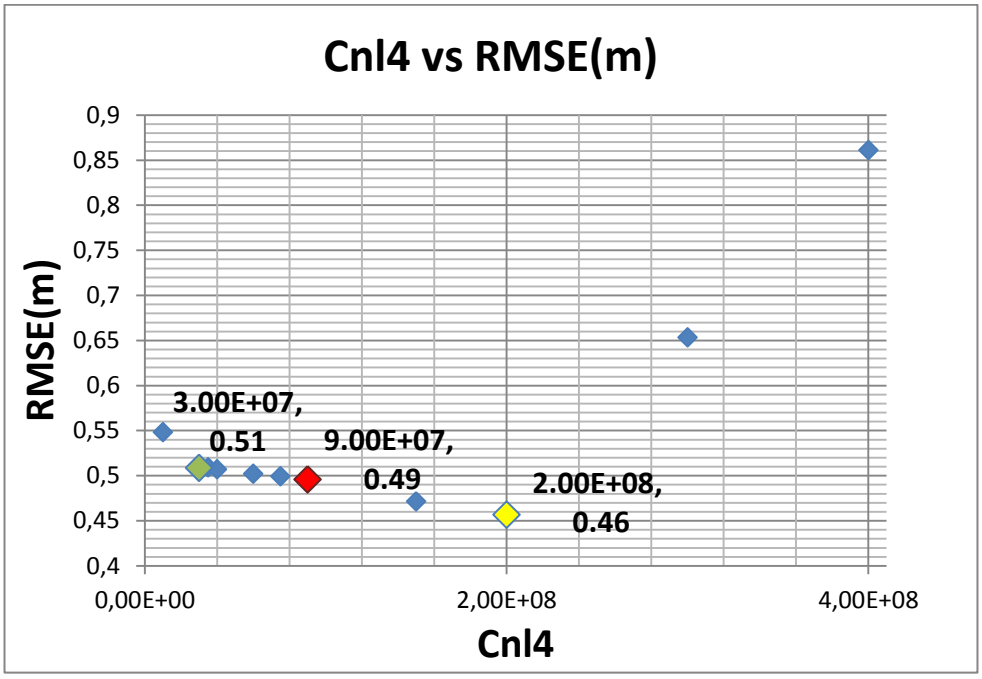

Figure 5.16 Cnl4 and RMSE correlation

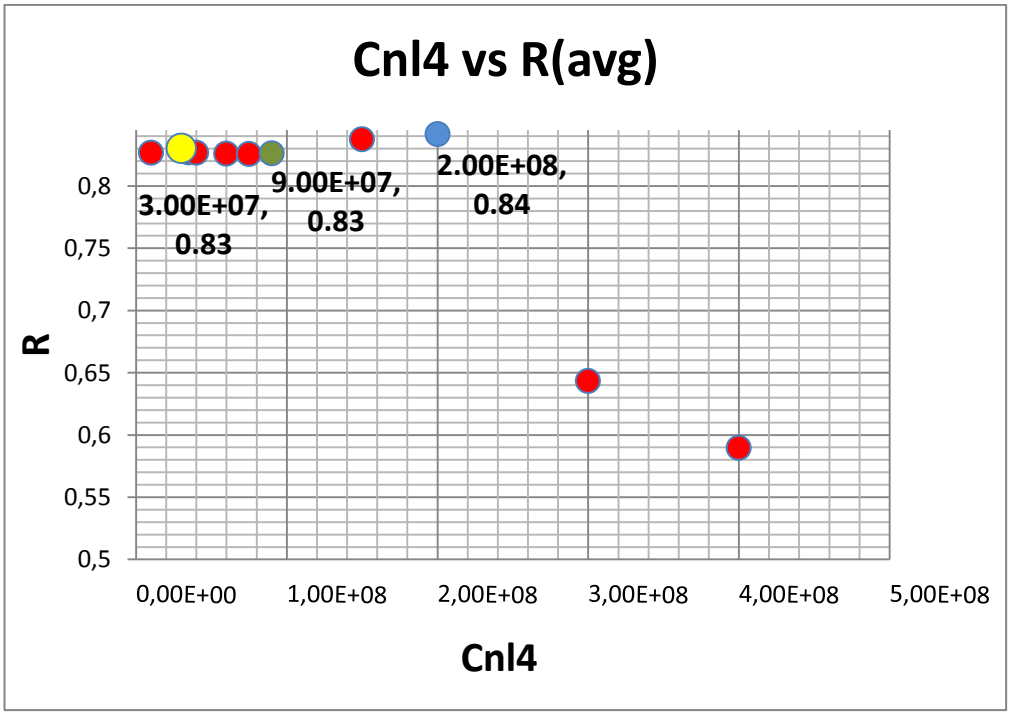

Figure 5.17 Cnl4 and RMSE correlation

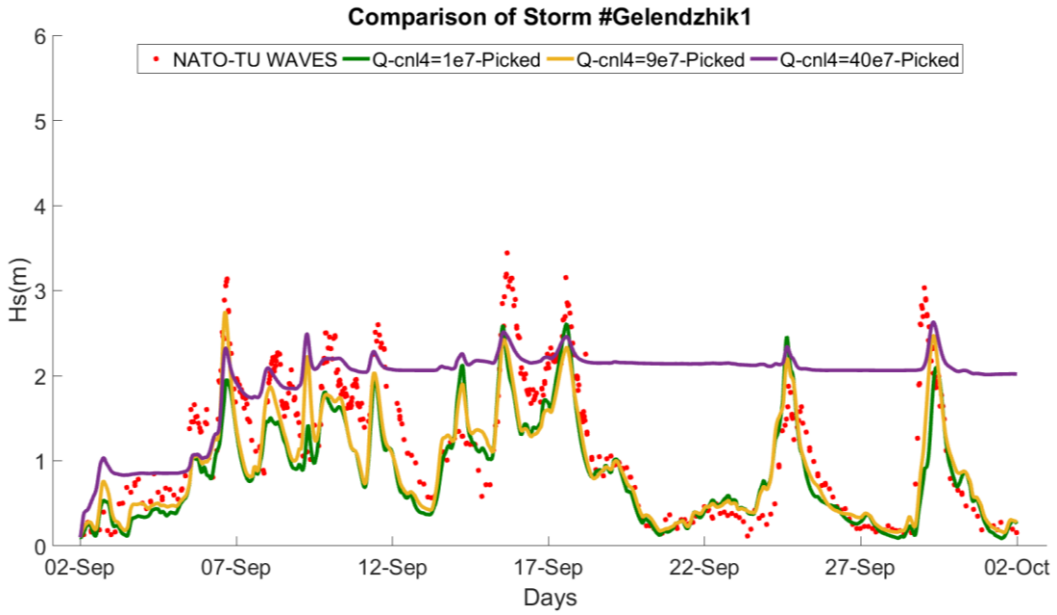

Figure 5.18 Behavior of Cnl4 for very high Cnl4 values (Cnl4=4e8 for purple line)

All of the Cnl4 values used in Figure 5.18 were not realistic; some were only implemented in order to show the effect of proportionality coefficients. Even though, nonlinear interaction was important for the modeling of the peak wave heights, DIA method was not the most appropriate method to achieve high accuracy between the model data and observed values at peak points.

The exponential growth part of the source input cannot be calibrated in SWAN model, so that energy input was limited with the default parameters. In order to solve the systematic underestimation of the system, only dissipation and nonlinear interaction parameters can be calibrated to decelerate the energy dissipation. Therefore, higher wave heights can be observed with respect to more energy conservation in the system. In order words decreasing the energy dissipation was the only way that system can be manipulated in order solve systematic underestimation. Although the recommended value of Cnl4 is $3x10^7$ by SWAN model, higher Cnl4 was chosen for Black Sea.

The other tunable parameter in quadruplet interactions is λ. λ is a shape parameter (Van Vledder et al.,2003) which arranges the shape of the interaction of wave number configurations. If λ changes, the angles of wave numbers also change in order to satisfy the resonance conditions. λ could change on the interval of 0 to 0.45 and DIA is set using standard value $\lambda = 0.25$. The applied values and the statistical analysis were given in Table 5.26 for different λ values.

Table 5.26 Comparison of the effect of $\boldsymbol{\lambda}$ values (ss)

	RMSE	**RMSEs**	**RMSEu**	**NMAE**	**NBIAS**	**SI**	**R**
$\lambda = 0.10$	0.68	0.63	0.26	0.73	0.39	0.35	0.82
$\lambda = 0.19$	0.57	0.49	0.28	0.60	0.29	0.33	0.84
$\lambda = 0.25$	0.51	0.40	0.30	0.54	0.19	0.33	0.83
$\lambda = 0.30$	0.53	0.41	0.32	0.57	0.16	0.36	0.80
$\lambda = 0.35$	0.56	0.45	0.33	0.62	0.16	0.38	0.77

According to obtained results higher energy in the system was observed when higher λ values are used (Figure 5.19) which results in as higher periods and higher wave heights. Figure 5.20 and Figure 5.21 shows results of model runs with λ=0.10, λ=0.35 and the default value for a storm#1 in Gelendzhik. The model behaved as predicted with significantly higher peak values generated when λ=0.35 was used. However, λ=0.25 generated the best statistical correlation between model and observed values. Even though higher λ values were better in guessing the peak wave parameters, they had low accuracy when entire storm was considered with calculated errors higher than the default value of λ=0.25.

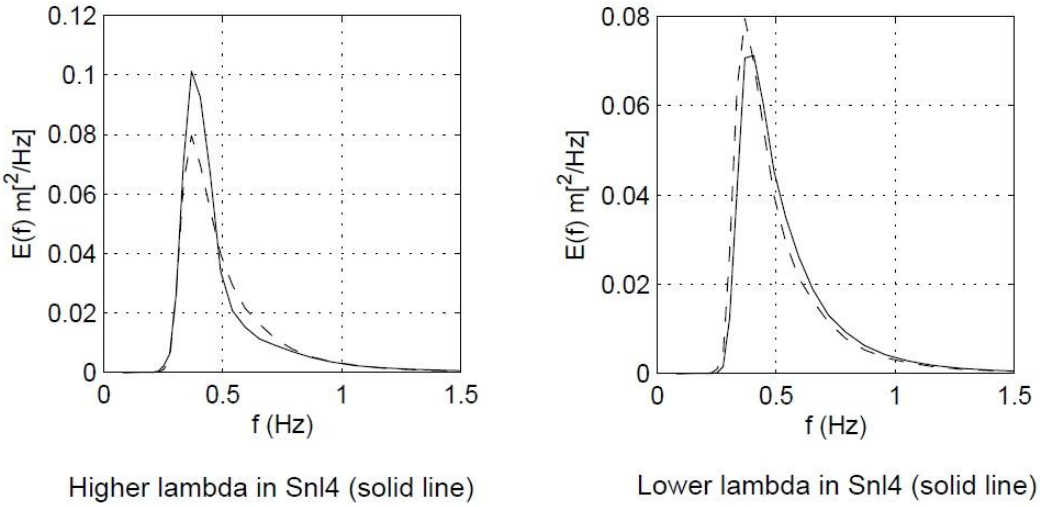

Figure 5.19 Spectrum distribution when different $\boldsymbol{\lambda}$ values are used (Van Vledder, 2003)

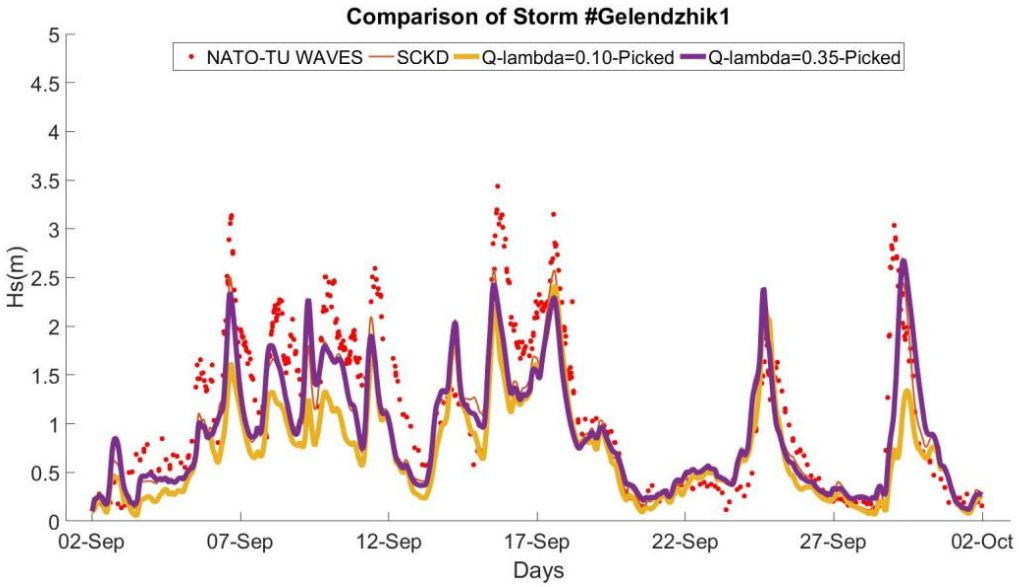

Figure 5.20 Comparison of Wave Heights for $\boldsymbol{\lambda = 0.10}$ and $\boldsymbol{\lambda = 0.35}$

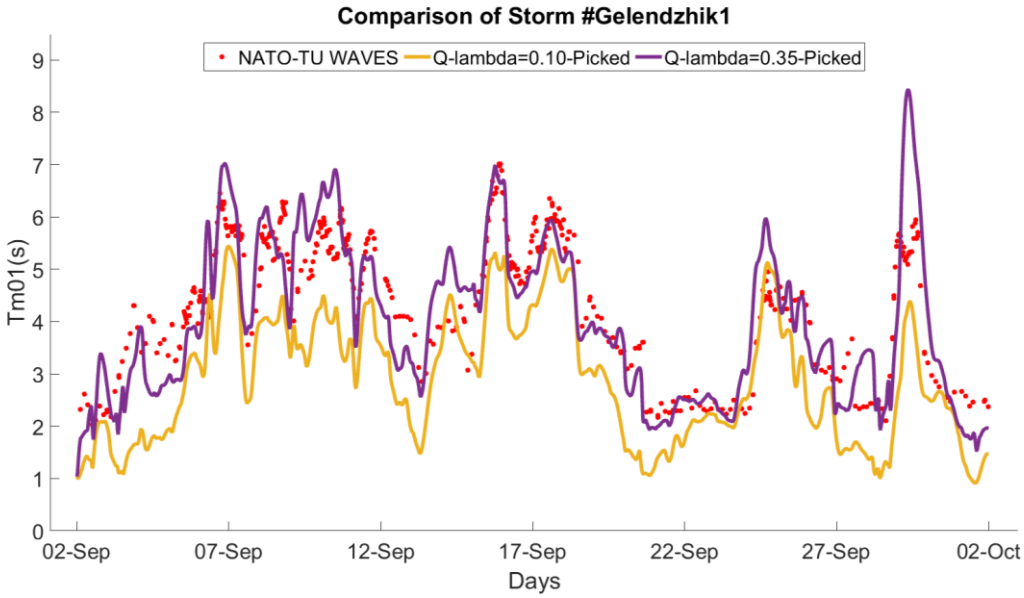

Figure 5.21 Comparison of Mean Wave Periods for $\boldsymbol{\lambda = 0.10}$ and $\boldsymbol{\lambda = 0.35}$

5.4 Sensitivity Analysis of SWAN Model: Spatial and Temporal Resolutions

In this part, the effects of using different bathymetries, time steps, propagation schemes, spatial and frequency resolutions on the performance of the SWAN model are discussed.

5.4.1 Sensitivity to Frequency Resolution

It is known that 3rd generation wave models are sensitive to frequency resolution since both general propagation and nonlinear interaction solution are affected. To understand the effect of this resolution on wave parameters, three frequency resolutions were compared. The lowest and the highest frequencies were chosen as 1 and 0.05, respectively.

In SWAN model, frequency resolution has a logarithmic distribution. The number of bins that covers the frequency interval which is represented with γ in Eq.4.1 defines the frequency resolution. In this study, frequency interval was divided into 40 parts that corresponds to $\gamma = 0.0778$. Other trial frequencies were 32 parts with $\gamma = 0.1$ (FI32) and 50 parts with $\gamma = 0.0630$ (FI50). The obtained results are presented in the Table 5.27

Table 5.27 Sensitivity of model according to frequency resolution (ss)

	RMSE	**RMSEs**	**RMSEu**	**NMAE**	**NBIAS**	**SI**	**R**
FI50	0.509	0.406	0.304	0.538	0.194	0.331	0.831
FI40	0.509	0.405	0.305	0.538	0.192	0.332	0.830
FI32	0.512	0.408	0.306	0.541	0.192	0.335	0.827

DIA method has been formed using frequency resolutions of 10% with 30 frequencies in the range of 0.03 Hz and 0.8 Hz (Van Vledder et al.,2000). Usually, higher resolutions tend to be more accurate in numerical models but DIA is an exception. Although Van Vledder et al.,2000 stated that for resolutions over and under 10%, DIA solutions are not as successful as 10% which is equal to $\gamma = 0.1$ .The difference between the obtained results for three frequency resolution were insignificant. The greatest difference between the R values of worst and best case observed in Hopa was only 1.4%. So it has been decided that, frequency resolution remain as 40 intervals with $\gamma = 0.0778$.

5.4.2 Sensitivity to Spatial Resolution

Computational mesh for model was set to 301x141 squared meshes with 0.05˚ x 0.05˚ spatial resolution. In order to understand the effect of spatial resolution, coarser

bathymetry was prepared with 0.1˚ x 0.1˚ (151x71in mesh size) using the same 1 minute gridded bathymetric data **r**etrieved from dataset of the study of "Global Bathymetric Prediction for Ocean Modeling and Marine Geophysics" by Sandwell and Smith (1996).

Table 5.28 Effects of Spatial Resolution (ss)

	RMSE	**RMSEs**	**RMSEu**	**NMAE**	**NBIAS**	**SI**	**R**
Fine	0.51	0.40	0.30	0.54	0.19	0.33	0.83
Coarse	0.50	0.38	0.33	0.51	0.17	0.34	0.82

The obtained results (Table 5.28) show that, there was no significant change when the grid sizes were doubled. Moreover, SWAN run with coarser grid has shown better performance considering RMSEs and BIAS values.

5.4.3 Sensitivity to Temporal Resolution

3 different time steps were chosen to present the effects of temporal resolution. General time step used throughout the study was set to 15 minutes. Shorter time steps often minutes, TS10, and longer time steps of thirty minutes, TS30, were applied with the calibrated model. The obtained results were given in Table 5.29

Table 5.29 Effects of Time Step (ms)

	RMSE	**RMSEs**	**RMSEu**	**NMAE**	**NBIAS**	**SI**	**R**
TS10	0.43	0.29	0.32	0.45	-0.07	0.32	0.85
TS15	0.44	0.30	0.32	0.46	-0.10	0.31	0.85
TS30	0.44	0.31	0.32	0.47	-0.12	0.32	0.85

The obtained result shows that, when the temporal resolution was increased, better performance of the model has been observed. Even though the improvement was not remarkable other than NBIAS value, differences were traceable on the time series graphs (Figure 5.22).

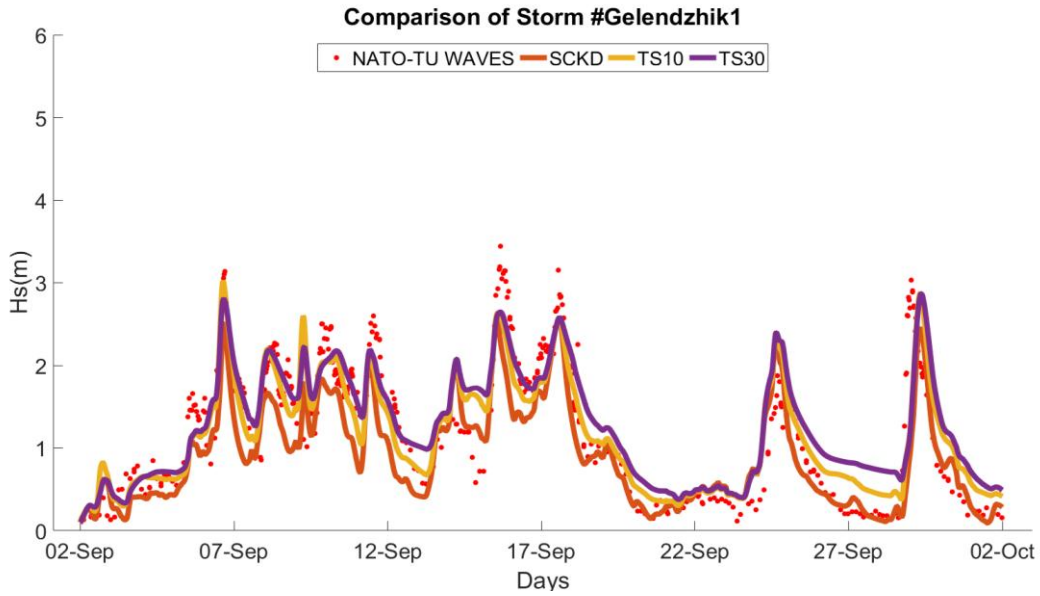

Figure 5.22 Effect of different time steps

TS15 was an appropriate time step; however TS10 or finer resolution could be beneficial in order to obtain more accurate results if the increased computational cost is compensable.

5.4.4 Sensitivity to Spectral Directional Resolution

In the initial runs of the model where default values were used, analysis was selected to cover the full 360˚ degrees. The full circle was divided to 36 intervals during with 10˚ of resolution (D36). Sensitivity analysis for directional resolution was carried

out using 16 intervals with 22.5˚ (D16) and 8 intervals with 45˚ (D8) of coarser resolutions. Finer resolution was not implemented because of high computational time. The obtained results are given in Table 5.30

Table 5.30 Sensitivity to Spectral Directional Resolution (ss)

	RMSE	**RMSEs**	**RMSEu**	**NMAE**	**NBIAS**	**SI**	**R**
D36	0.51	0.40	0.30	0.54	0.19	0.33	0.83
D16	0.52	0.43	0.29	0.55	0.20	0.33	0.83
D8	0.55	0.46	0.30	0.59	0.23	0.34	0.83

According to above table, 10˚ resolution showed better agreement with the observed buoy data than 22.5˚ and 45 ˚ resolutions. SWAN model was sensitive to spectral directional resolution. However, the improvements with the increased resolution were not significant when the D36 and D16 were considered. The difference between values could not be clearly observed on time series graph. Moreover, the computational cost has been significantly increasing with the increased directional resolution. In conclusion, directional resolutions in the interval of 10 ˚and 22.5˚ can be considered as appropriate for SWAN model considering both the computational cost and the accuracy of the model.

5.4.5 Sensitivity to Propagation Scheme

There are two propagation schemes available for nonstationary runs in SWAN as discussed in section 3.2.3.1. First order backward space, backward time (BSBT) scheme was used for this study. However, the other available option which is second order Stelling/Leendertse scheme was applied for all 54 storms using the calibrated model with CFSR wind fields to analyze influence of the propagation scheme.

The small differences observed in timeline graphs of storms (yellow and purple lines for Gelendzhik 16 storm in Figure 5.23) did not affect the overall statistical analysis results for 54 storms (Table 5.31).

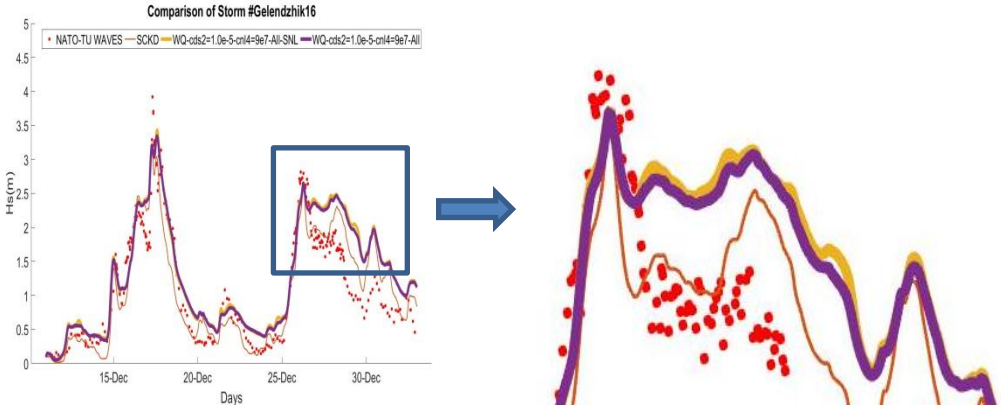

Figure 5.23 Differences of Stelling/Leendertse (yellow) and BSBT (purple) propagation schemes for #Gelendzhik16

Table 5.31 Statistical Analysis of Stelling/Leendertse and BSBT schemes for 54 storms (ls)

	NRMSE	NMAE	NBIAS	SI	R
SnL	0.2799	0.4187	-0.0808	0.3035	0.8766
BSBT	0.2789	0.4181	-0.0773	0.3024	0.8787

5.5 SWAN Model Discussions and Final Parameterization

The chosen methods (CKD), which was obtained from the runs with recommended values, were calibrated using the chosen parameters in Table 5.32 below.

Table 5.32 After Calibration and Default Values of the Selected Parameters

Source Term	Parameter	Variable Name in SWAN	KD (recommended values)	KD (S3) (values used in calibration set)	KD (S1) (values used in calibration set)
Dissipation	Cds	Cds2	-2.36E-05	-1.2E-05	-1.0E-05
	$\check{S}_{PM}$	stpm	3.02E-03	3.02E-03	3.02E-03
	p	powst	4	4	4
	δ	delta	1	1	1
Non-linear İnteractions	λ	lambda	0.25	0.25	0.25
(DIA)	C_{nl}	Cnl4	3.00E+07	4.50E+07	9.0E+07

Many different calibration sets were tried especially with different combinations of parameters Cds2 and Cnl4 since they were found to be the most effective parameters on the results. The improvements of the statistical analysis with respect to different Cds2 Cnl4 couples are presented in the table below (Table 5.33) The SCKD method and the final parameterization given in Table 5.32 were highlighted in Table 5.33

Table 5.33 Statistical Analysis for the calibration of SWAN model in Black Sea (ls)

		RMSE	**RMSEs**	**RMSEu**	**NMAE**	**NBIAS**	**SI**	**R**
s	**SCKD**	**0.449**	**0.311**	**0.295**	**0.432**	**0.146**	**0.313**	**0.884**
s1	Cds=1.00e-5 & Cnl4=9e+7	0.408	0.272	0.292	0.413	-0.097	0.296	0.888
s2	Cds=1.60e-5 & Cnl4=6e+7	0.384	0.254	0.281	0.407	0.056	0.296	0.878
s3	**Cds=1.20e-5 & Cnl4=4.5e+7**	0.392	0.258	0.278	0.373	0.039	0.294	0.873
s4	Cds=1.50e-5 & Cnl4=9e+7	0.375	0.246	0.278	0.399	0.027	0.297	0.877

After the calibration runs were carried out for all 54 storms, it was observed that similar results could be obtained using different configurations. S3 was selected as the best method even though S2 and S3 had better results in some of the statistical analysis . The main reason of this selection was based on the lower Cnl4 coefficient with respect to other couples since there is not any reliable information on the upper limits of proportionality coefficient of quadruplets.

Nonlinear interaction was important in order to achieve better representation of the real sea states since nonlinear processes have a crucial role in energy dissipation process during an extreme event as it is mentioned in the previous section 5.3.2. In this study, proportionality coefficient Cnl4 has been significantly increased in order to reduce the dissipation so that systematic error caused by the underestimation could be reduced as well. Even though higher values of Cnl4 such as 15e7 and 20e7 have shown better performance according to statistical analysis. They were not chosen since limits on those parameters is not available. Moreover, such applied values were not observed in literature as well. The highest applied value of Cnl4 was found to be 9.00E+7 which was used by RIKZ,(2003) in calibration of SWAN 40.20 for Slottermeer basin, which is a shallow lake in Netherlands. So the conditions were not similar for Black Sea. The chosen value of Cnl4 was still higher than the regular proportionality coefficients values in other wave model calculations. Nevertheless overall performance of the model was better compared to cases with recommended Cnl4 value (such as 3.00E+7).

Systematic underestimation and missing the peak wave heights were the most general problem. The default parametrization of SWAN was not applicable to Black Sea basin since parameterization are based on ocean conditions. This conclusion was also supported by Cherneva et al. (2008) and Akpınar and Leon (2015). Moreover, Akpınar and Leon have also calibrated Cds parameter for an extreme sea state in Gelendzhik.

According to Table 5 .33, 25% decrease in RMSEs and significant reduction in NBIAS values were obtained which was the proof that systematic underestimation was reduced. However, the problem was not completely solved. RMSEs error is still significant which means that still a systematic error between the predicted model data and observed data is present. The main reason of this situation is based on the drawbacks of the parametrization of wind-wave interaction which cannot be calibrated in SWAN model. This situation is discussed in Chapter 7.

The effect of calibration on wave height can be observed from the time series graph and scatter plots in Figure 5.24 and Figure 5.25.

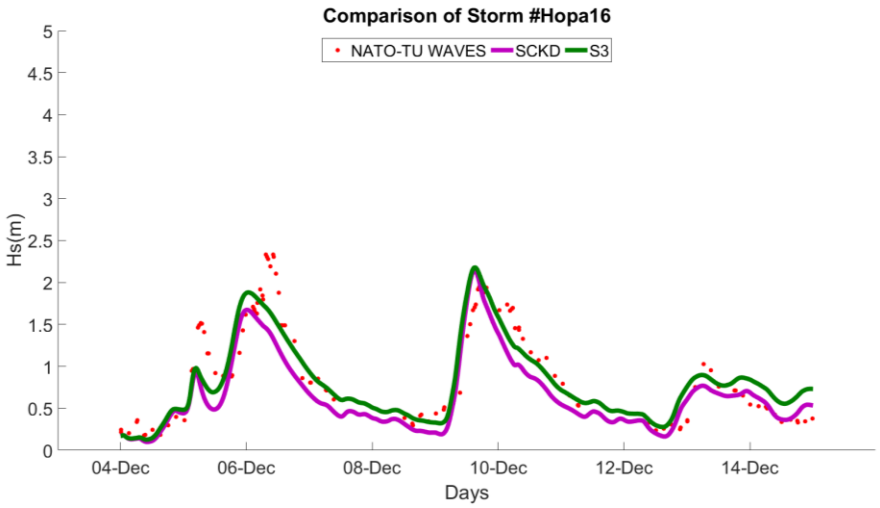

Figure 5.24 Time series graph of Hopa 16 storm for SCKD and S3 parametrization

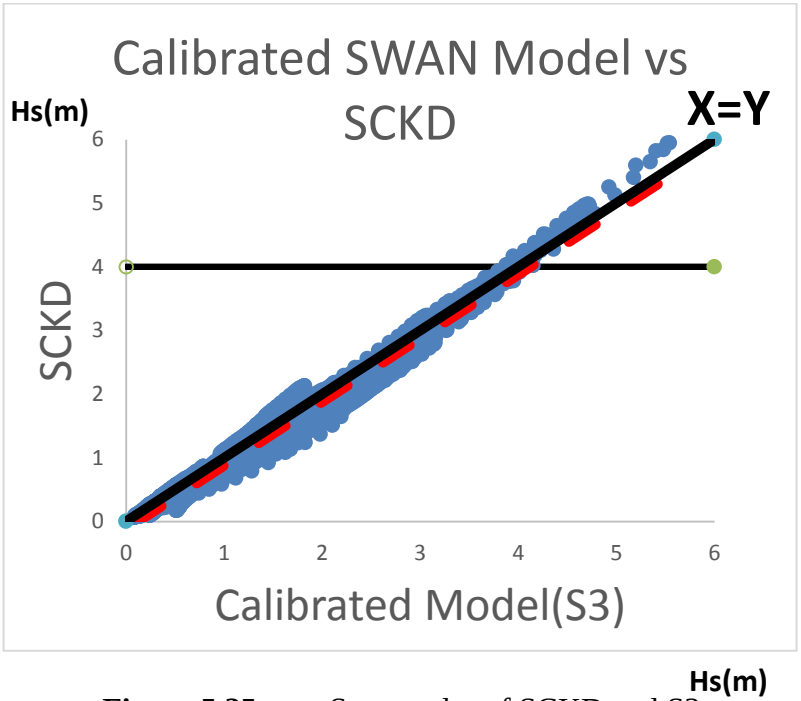

Figure 5.25 Scatter plot of SCKD and S3

In general the modeled wave heights increased with the calibrated model (S3). However Figure 5.25 showed that for the wave heights over 4 meters, SCKD method has estimated higher wave heights than the calibrated S3 parametrization. Therefore, another calibration option was considered which had better performance for the extreme wave heights. So S1 method was chosen for the modelling of extreme wave heights despite the high Cnl4 value and it is higher systematic error. The scatter plot of S1 and SCKD is given in Figure 5.26

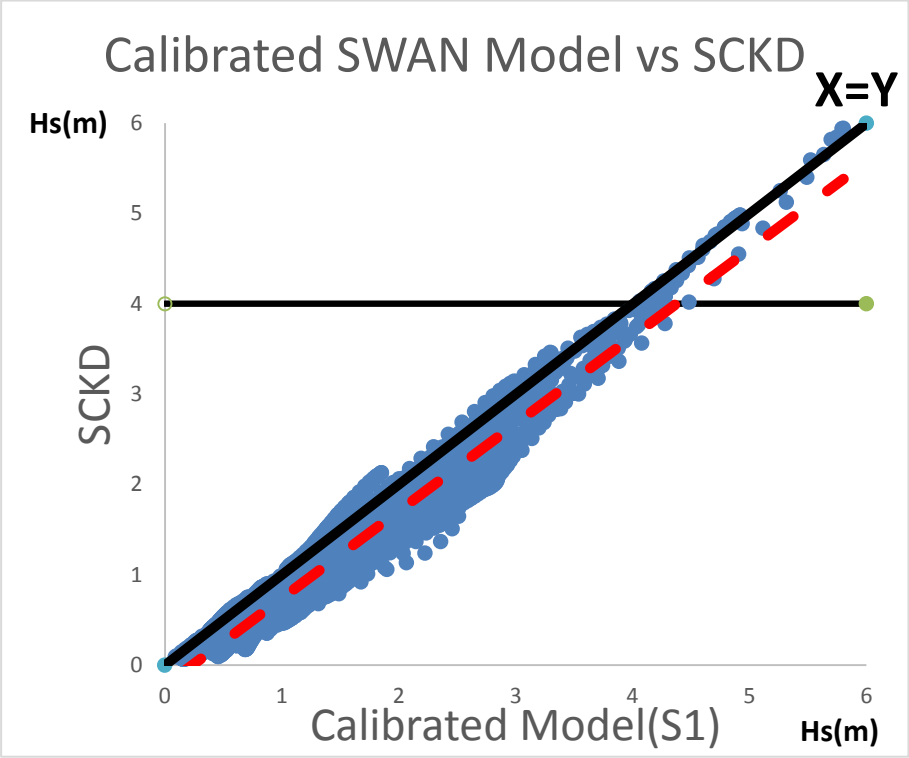

Figure 5.26 Scatter plot of SCKD and S1

Sensitivity of the SWAN model was also considered and it was observed that, selected resolutions of this study are appropriate considering the relationship between computational time and accuracy of the model with the increasing resolutions.

After the calibration of the SWAN model more applicable parameters of source terms were obtained for Black Sea region. However even with the calibrated parameters SWAN model still has drawbacks for Black Sea basin caused by the source terms which is discussed in Chapter 7 following comparison to WW3 results (given in Chapter 6).

CHAPTER 6

IMPLEMENTATION of WAVEWATCH III MODEL to BLACK SEA BASIN

In this chapter, implementation of 3rd generation wave model WAVEWACTH III in Black Sea basin is explained in details. Applied combination of numerical approaches of WW3 is given. Calibration and validation of model were performed. Improvements of the models are explained using different statistical methods. Effects of parameterization in models are discussed for all considered buoy locations and for overall study area.

6.1 WAVEWATCH III General Description

Implementation of WW3 model in Black sea basin was performed with a similar approach used in SWAN. Different aspects of WW3 were considered with suitable scheme in order to achieve the highest performance of the model in study basin which is explained in the course of implementation. Moreover, basic physical properties of the WW3 runs which are kept constant until the sensitivity analysis were given in section 6.1.2. Physical properties consist of mesh size, resolutions in frequency, directional and geological space, input and output details.

6.1.1 Flowchart of WW3 Model Implementation

In this study, WW3 version 4.18 is used. In this version, focused subjects are the deep water source terms which are wind-wave interaction, dissipation and nonlinear interactions. Same procedure is followed for WW3 as in implementation of SWAN(Chapter 5). Different switches are chosen and coupled, concerning the deep water physical processes, for application of model in Black Sea. First model runs carried out in order to determine the time steps which are discussed in the sensitivity section of this chapter. Then WW3 runs are completed for switch couples using the recommended parameterization for 54 storms using two wind sources. Best couple is chosen for calibration of the total source terms in order to obtain higher accuracy in wave parameters for Black Sea region.

In calibration part, 9 representative storms are used (3 storms from each buoy) to calibrate model. Representative storms are selected according to their statistical analysis results conformity to the averaged statistical analysis results of 3 buoys. Also, storm characteristics (observed wave height and period, number of peaks, wind speed) are taken into consideration. After the tuning of parameters, selected parameterizations based on performance are applied for all 54 storms. The results are discussed in calibration section (section 6.3).

In final step, sensitivity analyses are carried out with the calibration tests. Those analyses are completed in order to explain the effect of temporal, spatial, directional resolution changes and changes in propagation schemes (section 6.4).

In section 6.5 all obtained results are discussed for WW3 model.

6.1.2 Physical Dimensions and Other Properties of the WW3 Runs

WAVEWATCH III model solves the random phase spectral action density balance equation for wavenumber-direction spectra (Tolman, 2014) on directional, frequency and geographical space. In order to carry on such approach, WW3 model need the pre-defined boundary conditions for those spaces.

In geographical space, Black Sea region is divided into 151x71 square meshes with 0.1˚ x 0.1˚ spatial resolution. Coordinate system is set to spherical. In WW3 model, grid points are defined under 4 four groups;

- land points (defined with 0) where no wave action is allowed
- regular sea points (1), where wave action is allowed
- active boundary points(2) which are assigned to separate sea points from land points (Tolman, 2014)
- Points excluded from grid (3) where there is no action.

In WW3 mode outer grid cannot be defined as sea points. Selected basin for Black Sea satisfies this condition since bathymetry data is prepared including the surrounding land around entire Black Sea.

4 different time steps are available in WW3 model as mentioned in chapter 3.2.3. The first determined time step should be spatial time step (Δt_{xy}) since it must satisfy the Courant Friedrichs-Levy (CFL) criterion: the speed of fastest waves in the model must be less than or equal to the grid spacing divided by the time step (Spindler and Tolman, 2008). The governing parameters in determining spatial time steps are maximum latitude in grid (maxlat), first frequency (f), and grid resolution (Δx) in degrees. The formulation of the spatial time step is given in Spindler and Tolman (2008) as in Eq. 6.1

$$\Delta t_{xy} \leq 123766 * \Delta x * cosd(maxlat) * f \quad (6.1)$$

For this study Δt_{xy} is calculated that it should be smaller than 414 .1 seconds. So that Δt_{xy} is chosen as 100 seconds. The global time step, Δt_g, by which the entire solution is propagated in time, can be set to approximately 2 or 3 times the Δt_{xy} (Spindler and Tolman, 2008). $\Delta t_g$is chosen as 300 seconds. The others time steps which are directional time step(Δt_k) and source time stepsΔt_s, are chosen as 150 seconds and 10 seconds, respectively.

Spectral direction is chosen to cover full circle, and 360˚ is divided into 16 which corresponds the mesh size 22.5˚ on direction space. First (lowest) frequency is selected as 0.05 Hz with a frequency increment factor of 1.1 (=0.1). Numbers of frequencies are selected as 30.

A propagation scheme is selected as third order scheme (UQ) explained in chapter 3.2.3.1 with "Garden Sprinkler Effect" alleviation method of spatial averaging (PR3).

Field and point outputs are taken from the runs. Parameters obtained in field outputs are;

- Significant wave height (Hs)
- Wind speed
- Wave direction

Parameters obtained in point outputs are;

- Significant wave height (H_s),
- Representative Mean wave periods (T_r)
- Mean Wave direction
- Wind speed,

- Mean Directional Spread
- Coordinates and depth information
- Wave spectra

Outputs are drawn, compared and evaluated using graphical user interface on MATLAB software which is prepared for this thesis. Sample ww3 input files can be found in appendix.

6.2 WAVEWATCH III Runs with Recommended Values

In this section, different approaches of deep water source terms are considered in WAVEWATCH III (WW3) using recommended parameterizations. The governing whitecapping and wind wave interaction terms are considered together since they are defined within same switch in WW3. One of the key advantages of WW3 is that nonlinear part of wind –wave interaction is also tunable. Model runs here carried out in 12 groups which consist of combination of 4 different wind-wave interaction and whitecapping dissipation switches, and 3 nonlinear wave-wave interaction switches for both CFSR and ECMWF operational wind fields. Below abbreviation will be used throughout the section to define the run groups.

Table 6.1 Abbreviations of WW3

Used Method, Model & Data	Abbreviation
WAVEWATCH III	W
CFSR	C
ECMWF Opr.	E
WAM Cycle 3	ST1
Tolman and Chalikov 1996	ST2
WAM Cycle 4	ST3
Ardhuin et al. 2010	ST4
DIA	NL1
MDIA	NL3
Nonlinear Filter of DIA	NLS

6.2.1 WAM Cycle 3 & DIA (WCST1NL1 & WEST1NL1)

Both whitecapping configuration are based on the work of Komen(1984) and nonlinear interactions are solved by DIA. In ST1, proportionality constant (C_{in}) of exponential term of wind input can be defined by user. Recommended value of C_{in} is defined as 0.25. The other used parameter and their values can be seen in Table 6.2 below.

Table 6.2 ST1 & NL1 Parameters

Wind Input & Whitecapping ST1		
Cin	Cds	αpm
0.25	2.36e-5	3.02e-3
Quadruplets- NL1		
λ	Cnl	
0.25	2.78e7	

Performance of ST1 and NL1 combination for Black Sea Basin is presented in statistical terms in Table 6.3.

Table 6.3 Statistical Analysis results for ST1 and NL1 couple

ST1NL1	RMSE	RMSEs	RMSEu	NMAE	NBIAS	SI	R
Black Sea	0.49	0.37	0.29	0.47	0.21	0.32	0.88
Gelendzhik	0.51	0.31	0.37	0.43	0.14	0.30	0.88
Sinop	0.45	0.39	0.20	0.55	0.29	0.28	0.90
Hopa	0.48	0.40	0.24	0.47	0.25	0.34	0.88

ST1 and DIA method has shown a good conformity with the buoy data according to correlation coefficient values. However, high RMSE and NBIAS were also observed in Black Sea.

Effect ST1NL1 has changed depending on the buoy location. In Hopa and Sinop main part of the RMSE was caused due to systematic errors while in Gelendzhik dominant part of error was unsystematic. In Sinop and Hopa this systematic error was reflected on NBIAS values, so that it can be explained as systematic underestimation of wave height values for those locations. ST1NL1 method has shown its best performance in Sinop buoy where lowest RMSE, SI and highest R values were obtained.

6.2.2 Tolman and Chalikov 1996 & DIA (WCST2NL1 & WEST2NL1)

ST2 method uses input source term defined by Chalikov and Belevihc (1993) and Chalikov (1995) (Tolman, et al.,2014). Source term is defined in Eq.3.32 which consist of non-dimensional wind-wave interaction parameter, β. “β is a nondimensional wind–wave interaction parameter approximated by 12 empirical parameters that are functions of the nondimensional frequency of a spectral

component and depend on the drag coefficient at a specific height, through a series of empirical relationships" (Kalantzi et al.,2009). The dissipation term in ST2 consist of two part, energy dissipation due turbulence for low frequency energy level and empirical high frequency dissipation part (for details see chapter 3.3.2.2). So that used parameters are given as high frequency constant and low frequency constant for dissipation term (Table 6.4). Tolman and Chalikov also resets the Cnl coefficient of DIA for ST2 & DIA coupling (Table 6.4) .

Table 6.4 ST2 & NL1 Parameters

Wind Input - ST2		
Zwnd	Swellf	
10	0.1	
Dissipation - ST2		
High Frequency Constants		
a_0	a_1	a_2
4.8	1.7e-4	2.0
Low Frequency Constants		
b_0	b_1	$\emptyset_{min}$
0.3e-3	0.47	0.003
Quadruplets- NL1		
λ	Cnl	
0.25	1.00e7	

In above table Zwnd refers to height of wind and Swellf is the factor for negative swell.

Performance of ST2NL1 can be seen in Table 6.5

Table 6.5 Performance of ST2NL1

ST2NL1	RMSE	RMSEs	RMSEu	NMAE	NBIAS	SI	R
Black Sea	0.61	0.54	0.25	0.57	0.33	0.35	0.87
Gelendzhik	0.62	0.54	0.30	0.52	0.27	0.31	0.88
Sinop	0.60	0.58	0.16	0.77	0.44	0.31	0.90
Hopa	0.59	0.54	0.23	0.56	0.35	0.40	0.85

Significant deterioration is observed for the ST2 methodology for all buoys caused by the strong underestimation tendency of ST2 method (Figure 6.1). High NBIAS values for all buoys supports this conclusion. In below figure RMSE is around 1 meter where maximum wave height observed is 3.5 meters.

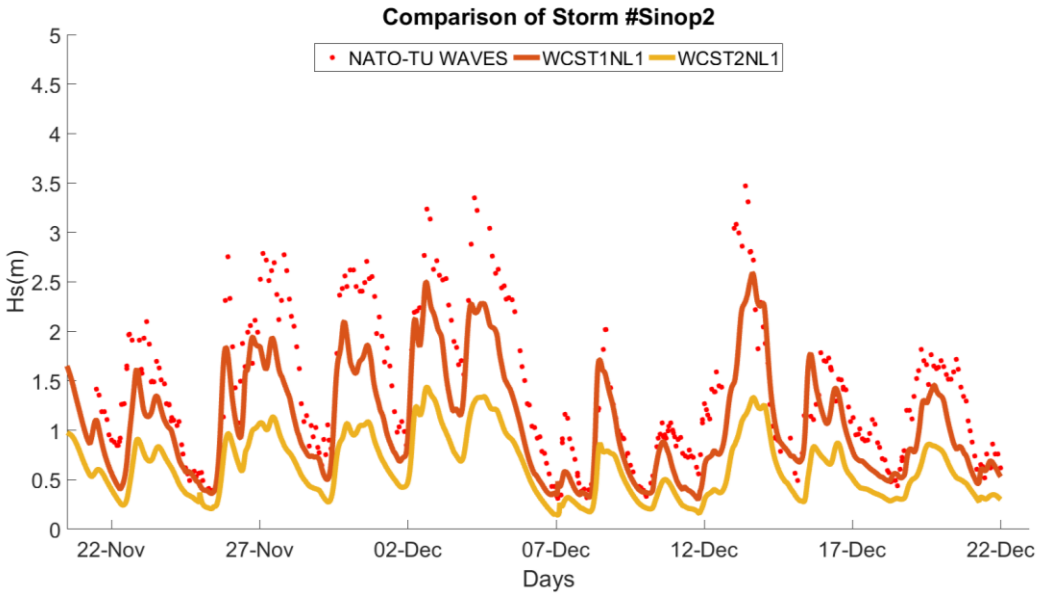

Figure 6.1 WCST2NL1 vs WCST1NL1 for the storm Sinop 2

The worst effected buoy from the change of ST1 to ST2 was Sinop where already systematic underestimation was more significant compared to Hopa and Gelendzhik. Despite the good correlation of 90% in Sinop for ST2NL1, highest NMAE value was

observed (30% higher) compared to other buoys. Moreover, the average NBIAS error in Sinop has increased 0.29 to 0.44. Nevertheless, the high NMAE and high NBIAS values of Sinop buoys were not strongly affected the overall parameters in Black Sea, since the number of considered storms was significantly less than other buoys.

Effect of recommended value lower Cnl coefficient with ST2 is also significant in results. However, the problem is mainly caused by the wind-wave interaction term rather than dissipation and nonlinear interactions according to obtained results and time series. To concludem the combination ST2NL1 does not perform well for Black Sea region. This method would be applicable to other region where underestimation of data is not a problem.

6.2.3 WAM Cycle 4 & DIA (WCST3NL1 & WEST3NL1)

ST3 input and dissipation term is based on WAM Cycle 4 which consist of Jannsen(1982) formulations. Later on dissipation term is adapted by Janssen (1994) and rehshaped by Bidlot et al. (2005) (Tolman, 2014). The recommended parameters used in ST3 (Table 6.6) is adjusted by Bidlot, Janssen and Abdallah and called as "BJA" parameterization which is a well-known combination in wave modeling based on paper Bidlot et al. (2005). Cnl4 for DIA is reshaped again and recommended value is adjusted as 2.78E7.

Table 6.6 ST3 & NL1 Parameters

Wind Input - ST3						
α_0 (Charnoch Coeff.)	Zwnd	Z0max	β_{max}	p_{in}	z_α	s_1
0.0095	10	0	1.2	2	0.011	0
Dissipation -ST3						
C_{ds}		δ_1 (coeff of k)		δ_2 (coeff of k2)		
-2.1		0.4		0.6		
Quadruplets- NL1						
λ			Cnl			
0.25			2.78e7			

s_1 in wind input part in above table is set to 0, so that linear damping of swell in not included in calculations according to BJA settings(Eq. 3.32 and Eq.3.47)

The performance analysis for BJA setting are presented in Table 6.7

Table 6.7 Statistical Analysis Parameters for ST3NL1

ST3NL1	RMSE	RMSEs	RMSEu	NMAE	NBIAS	SI	R
Black Sea	0.44	0.31	0.29	0.42	0.16	0.30	0.89
Gelendzhik	0.46	0.26	0.36	0.39	0.11	0.28	0.89
Sinop	0.42	0.36	0.20	0.51	0.26	0.27	0.90
Hopa	0.43	0.34	0.25	0.42	0.19	0.33	0.89

The statistical analysis parameters have shown that, ST3NL1 coupled method was an appropriate choice for Black Sea. First of all, around 90% correlation was achieved for all buoys. Moreover, RMSE values were consistent compared to each other for all buoys. This situation was also true for systematic and unsystematic part of RMSE

that, RMSEs and RMSEu values have fallen within 10 cm and 16 cm intervals, respectively. Stronger underestimation of wave heights in Sinop can be also observed in ST3NL1 combinations as well.

In Gelendzhik low NBIAS values were obtained compared to two other buoys.

6.2.4 Ardhuin et al. 2010 & DIA (WCST4NL1 & WEST4NL1)

ST4 model is actually a modified version of ST3 in terms of swell dissipation and a reduction in U_* in order to allow a balance with saturation based dissipation (Tolman, 2014) (See Chapter 3.3.2.2). The general wind input term (positive part) is kept same with ST3. The recommended parameterization of ST4 (Table 6.8) is based on Saha et al. (2010) for CFSR winds in global scale. Cnl4 of DIA has adjusted for ST4. For more detailed information see study of Ardhuin et, al 2010.

Table 6.8 ST4 and NL1 Parameters

Wind Input - ST3						
α0 (Charnoch Coeff.)	Zwnd	Z0max	β_{max}	p_{in}	z_α	s_1
0.0095	10	0	1.52	2	0.006	1
Swell Parameters- ST4						
s	s2	s3	s4	s5	s6	s7
0.8	-0.018	0.015	100000	1.2	0	230000
Dissipation - ST4						
C_1	C_2	C_{cum}	C_4	C_5	C_6	
0	-2.2.e-5	-0.403	1	0	0.3	
Quadruplets- NL1						
λ			Cnl			
0.25			2.5e7			

Performance analysis of ST4NL1 can be seen from the Table 6.9

Table 6.9 Statistical Analysis Parameters for ST4NL1

ST4NL1	RMSE	RMSEs	RMSEu	NMAE	NBIAS	SI	R
Black Sea	0.42	0.28	0.29	0.39	0.13	0.30	0.89
Gelendzhik	0.45	0.24	0.36	0.37	0.08	0.28	0.89
Sinop	0.37	0.28	0.22	0.45	0.19	0.27	0.90
Hopa	0.42	0.31	0.26	0.40	0.16	0.33	0.89

Applied ST4 and DIA configuration shows good conformity with the buoy data. Considering all storms, systematic and unsystematic parts of RMSE were almost equal. The effect of systematic underestimation was not significant in ST4NL1, which can be also obtained from the NBIAS and RMSEs values and the time series graphs. In Gelendzhik the dominant part of RMSE was caused due to unsystematic errors of the model and input values. Moreover NBIAS value has reached to an acceptable range.

In wave modeling, effect of systematic error which is represented by bias and RMSEs can be easily observed from the time series graphs. If unsystematic error was not significantly high and correlation coefficient is also in an acceptable range (over 90%). NBIAS, RMSEs values around zero would show great resemblance with the observed data. Improvements for such events shows high convergence after the mentioned level have reached. In order words, the model has been reached its optimum level for that specific event, no further calibration needed. Even with the default values of ST4NL1 such situation was observed for in a few storms in Gelendzhik. In Figure 6.2, an example for such situation is given for Gelendzhik 18 storm with ST4NL1 combination.

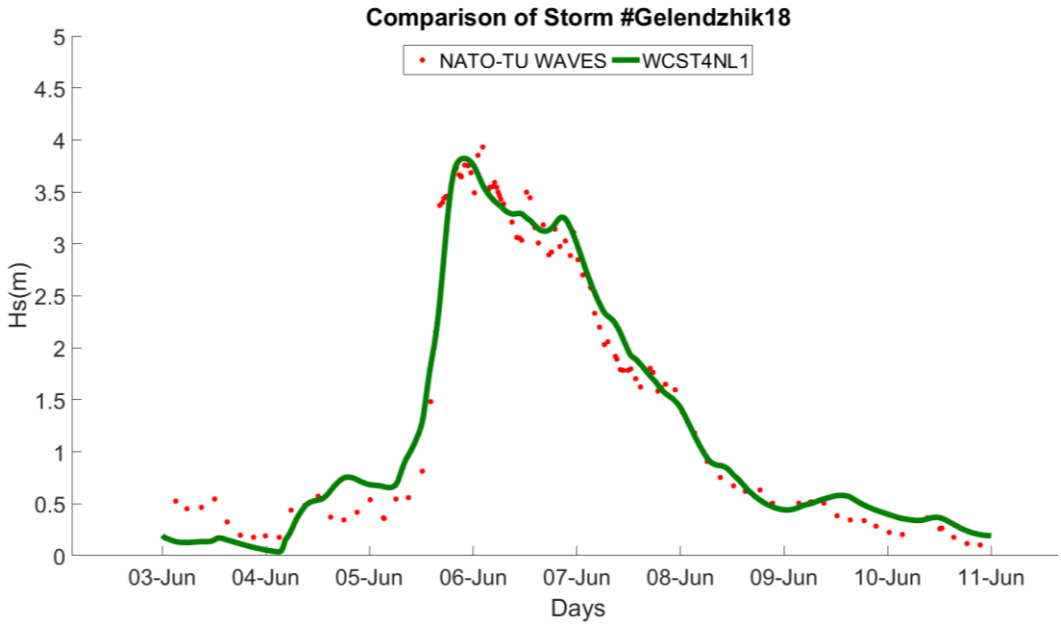

Figure 6.2 ST4NL1 coupled model for Gelendzhik 18

The bias and RMSEs of the above storm is -3.6 cm and 0.05 respectively and R is 0.99.

In addition to successful examples in Gelendzhik, the significant improvements for ST4 method has taken place in Sinop. Remarkable reduction in RMSE , NMAE and NBIAS values were observed for Sinop buoy. The effect of ST4 can be understood from the time series figure of Sinop2 storm (Figure 6.3), which actually consist of many storms through November-December 1994 period.

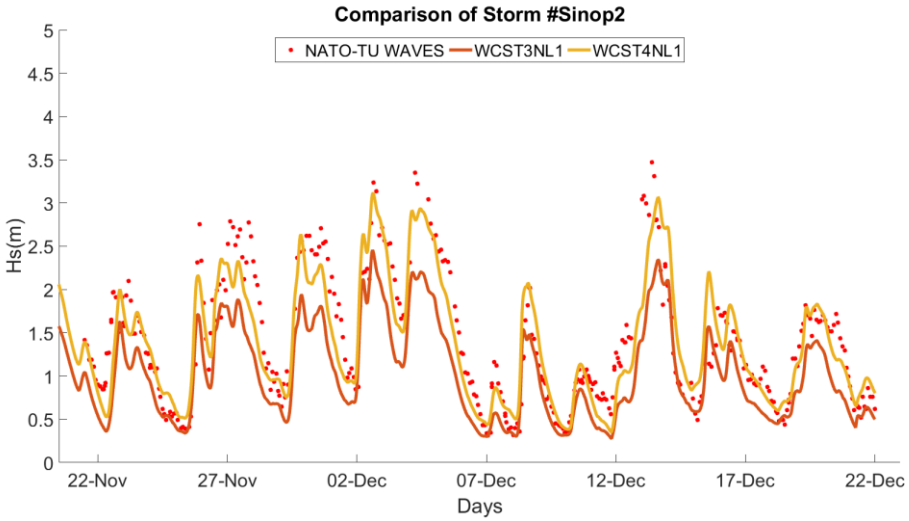

Figure 6.3 WCST3NL1 vs. WCST4NL1 for the storm Sinop 2

This change is based on the formulation of ST4 method. In ST4 newly introduced in dissipation term such as swell dissipation is available. Moreover, implementations made to wind-wave interaction parameters are another reason behind the good values obtained. The more details of this improvement is discussed in the calibration of dissipation term part of this chapter.

6.2.5 WAM Cycle 3 & GMD (WCST1NL3 & WEST1NL3)

Wam Cycle 3 (ST1) & GMD formulations are applied for dissipation and quadruplets respectively source term in WW3 runs.

NL3 represents the Generalized Multiple DIA (GMD) method for nonlinear wave-wave interaction term. GMD is a developed version of DIA in sense of expanded quadruplet definitions (see chapter 3.2.2.3). Multiple DIA configurations (two or more configurations) can be defined using GMD approach, however the default parameterization here is given for classical DIA approach with λ=0.25 and

Cdeep=1.00e7 which corresponds to Cnl=3.00e7 as in traditional WAM setting(WAMDIG,1988;Tolman, 20142010). Nevertheless, preliminary runs showed that there is a slight difference even though GMD is set as classical DIA approach. Therefore, GMD with classical DIA approach is coupled with all dissipation source method to see the overall effect of GMD. At this part of study, sensitivity analysis of nonlinear interaction term calibrations are not carried out for WW3 model so that other GMD configurations are not applied here. Other GMD configurations with the calibrated parameters will be mentioned in calibration and sensitivity analysis part of this chapter. The following parameterization is used for ST1NL3 methodology (Table 6.10). NQDEF stands for the number of quadruplets chosen in GMD and KDFD is the deep water scaling parameter mention in Eq.3.66 in Chapter 3.2.2.3.

Table 6.10 ST1 and NL3 Parameters

Wind Input & Whitecapping ST1			
Cin	Cds		αpm
0.25	2.36e-5		3.02e-3
Quadruplets GMD - NL3			
NQDEF	KDFS	λ	Cdeep
1	0.2	0.25	1.00e7

The statistical analysis results are presented in Table 6.11

Table 6.11 The statistical analysis of ST1NL3

ST1NL3	RMSE	RMSEs	RMSEu	NMAE	NBIAS	SI	R
Black Sea	0.68	0.62	0.25	0.67	0.39	0.37	0.85
Gelendzhik	0.72	0.61	0.34	0.62	0.32	0.34	0.85
Sinop	0.63	0.60	0.17	0.82	0.47	0.31	0.89
Hopa	0.67	0.63	0.21	0.68	0.44	0.42	0.85

When the GMD configurations are used for nonlinear interaction term and coupled with ST1, stronger dissipation of energy was observed. In Figure 6.4 effect of dissipation especially at the peak wave heights can be observed for Hopa 18 storm with ST1NL3 configurations.

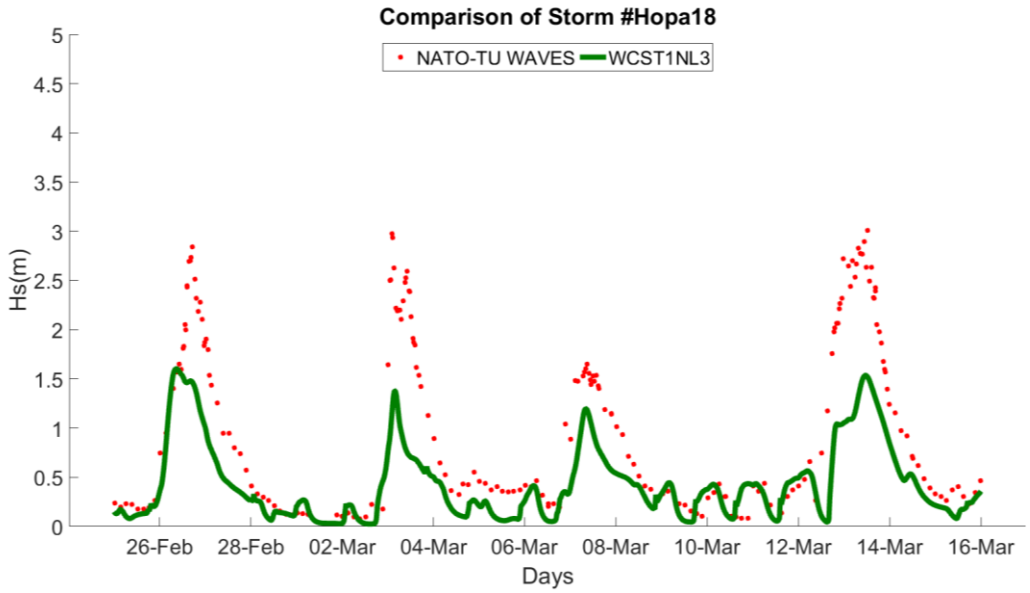

Figure 6.4 Effect of dissipation NL3 compared to NL1 in Hopa 18 storm

This strong dissipation has resulted in low wave height guesses which reflected to statistical analysis as high bias and RMSEs. Systematic error for ST1NL3 was very strong such that RMSE values were reached almost 70 cm.

Significant changes occurred for Gelendzhik buoy where correlations coefficient dropped to its lowest value of 85%. In Gelendzhik, unsystematic part of RMSE was also greater than other buoys.

The error in nonlinear interactions usually decreases when GMD method is used according to Tolman (2010) when DIA, GMD and exact solution are compared. GMD results are more consistent with the exact solution (Tolman, 2010). According to this information and knowing that the dissipation is increased in ST3 so that, nonlinear interaction terms or the parameters used in quadruplet calculations in Black Sea is not sufficient enough to solve real case interactions. As it has been mentioned before, nonlinear interaction solutions in 3rd generation models has numerous shortcoming comings (Van Vledder et al, 2000). In practice these shortcomings are commonly compensated by tuning of other source terms (Van Vledder ,2006:Ardhuin et al., 2006). This tuning is performed in the calibration section.

6.2.6 Tolman and Chalikov 1996 & GMD (WCST2NL3& WEST2NL3)

Tolman and Chalikov 1996 & GMD formulations are applied for dissipation and quadruplets respectively source term in WW3 runs. Following parameterization is used (Table 6.12).

Table 6.12 ST2 and NL3 Parameters

Wind Input - ST2			
Zwnd	Swellf		
10	0.1		
Dissipation - ST2			
High Frequency Constants			
a_0	a_1	a_2	
4.8	1.7e-4	2.0	
Quadruplets GMD - NL3			
NQDEF	KDFS	λ	Cdeep
1	0.2	0.25	1.00e7

The statistical analysis were given in Table 6.13

Table 6.13 The statistical analysis of ST2NL3

ST2NL3	RMSE	RMSEs	RMSEu	NMAE	NBIAS	SI	R
Black Sea	0.61	0.54	0.25	0.57	0.33	0.35	0.87
Gelendzhik	0.63	0.54	0.30	0.52	0.27	0.31	0.88
Sinop	0.57	0.54	0.17	0.72	0.41	0.30	0.90
Hopa	0.60	0.55	0.23	0.57	0.36	0.40	0.85

Strong systematic errors were also observed here for all buoys. Although Sinop has the highest correlation coefficient, the systematic underestimation was strongest in Sinop which can be observed via highest NBIAS values among other buoys. An example of such underestimation is given in Figure 6.5

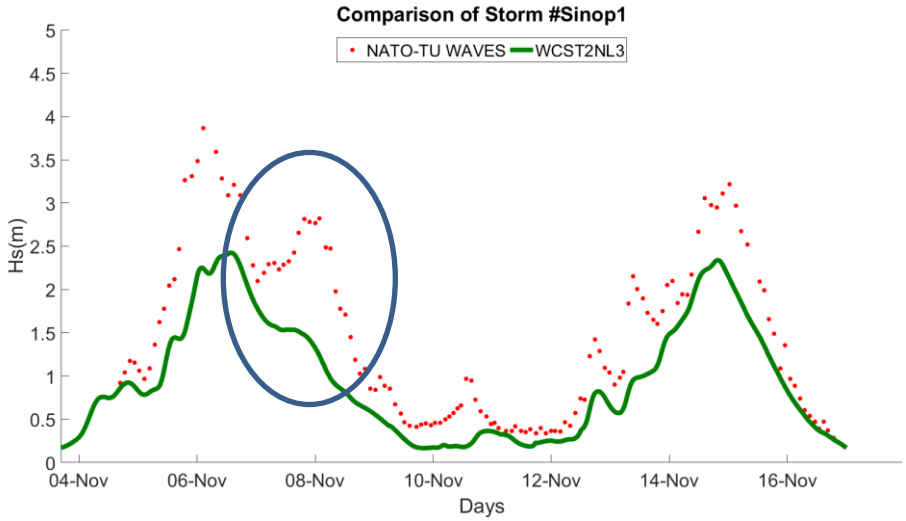

Figure 6.5 ST2NL3 method for Sinop1 storm.

As seen from the Figure 6.5 almost every modeled data was under the observed value. The errors were increased at peaks points. However, the main problem behind this situation is not high dissipation rates. The reason is the weak input term caused by application of not fully appropriate wind-wave interaction terms. Such conclusion is supported by Figure 6.5. At the second peak for the NATO-Tu waves data (area in circle), model did not even showed a developing sea state. General energy level was continued its decreasing trend since input source term was weak. This situation was either caused by deficiencies in wind input or drawbacks in wind-wave interaction method.

6.2.7 WAM Cycle 4 & GMD (WCST3NL3& WEST3NL3)

Wam Cycle 4 (ST3) & GMD formulations are applied for dissipation and quadruplets respectively source term in WW3 runs. Following parameterization is shown in Table 6.14.

Table 6.14 ST3 & NL3 Parameters

Wind Input - ST3						
α_0 (Charnoch Coeff.)	Zwnd	Z0max	β_{max}	p_{in}	z_α	s_1
0.0095	10	0	1.2	2	0.011	0
Dissipation -ST3						
C_{ds}		δ_1 (coeff of k)		δ_2 (coeff of k2)		
-2.1		0.4		0.6		
Quadruplets GMD - NL3						
NQDEF	KDFS	λ	Cdeep			
1	0.2	0.25	1.00e7			

Performance of ST3NL3 model is presented with statistical analysis in Table 6.15.

Table 6.15 The statistical analysis of ST3NL3

ST3NL3	RMSE	RMSEs	RMSEu	NMAE	NBIAS	SI	R
Black Sea	0.47	0.33	0.30	0.44	0.19	0.31	0.89
Gelendzhik	0.49	0.28	0.38	0.41	0.12	0.29	0.88
Sinop	0.44	0.38	0.20	0.54	0.29	0.26	0.90
Hopa	0.46	0.37	0.25	0.44	0.22	0.34	0.88

According the statistical analysis results, two different behaviors were observed with respect to RMSE in ST3NL3. In Sinop and Hopa the dominant part of this error was caused by the RMSEs. On the other hand, in Gelendzhik unsystematic error was greatest among other buoys and dominant than systematic error which was specific to Gelendzhik buoy. However, all of the correlation coefficients were varied in small range of 88% to 90%. Also, improvements in scattered data were observed in Sinop compared to other methods (SI=0.26)

6.2.8 Ardhuin et al. 2010 & GMD (WCST4NL3 & WEST4NL3)

Ardhuin et al. 2010 (ST4) & GMD formulations are applied for dissipation and quadruplets (respectively) source term in WW3 runs. Following parameterization is used (Table 6.16).

Table 6.16 ST4 & NL3 Parameters

Wind Input - ST3						
α0 (Charnoch Coeff.)	Zwnd	Z0max	β_{max}	p_{in}	z_α	s_1
0.0095	10	0	1.52	2	0.006	1
Swell Parameters- ST4						
s	s2	s3	s4	s5	s6	s7
0.8	-0.018	0.015	100000	1.2	0	230000
Dissipation - ST4						
C_1	C_2	C_{cum}	C_{br}	C_5	sdsth	
0	-2.2.e-5	-0.403	0.9e-3	0	70	
Quadruplets GMD - NL3						
NQDEF	KDFS	λ	Cdeep			
1	0.2	0.25	1.00e7			

Performance of ST4NL3 model is presented with statistical analysis in Table 6.17.

Table 6.17 The statistical analysis of ST4NL3

ST4NL3	RMSE	RMSEs	RMSEu	NMAE	NBIAS	SI	R
Black Sea	0.45	0.30	0.31	0.43	0.17	0.30	0.89
Gelendzhik	0.47	0.26	0.37	0.40	0.12	0.27	0.90
Sinop	0.43	0.35	0.21	0.55	0.28	0.27	0.90
Hopa	0.43	0.32	0.28	0.43	0.19	0.33	0.88

ST4NL3 model shows a good performance in Black Sea. Despite the different characteristics were observed for each location (dominant part of RMSE as in ST3NL3), many statistical analysis results have fallen within a small range except NBIAS. Thus, the effect of ST4NL3 was similar in each buoy.

6.2.9 WAVEWATCH III with ECMWF Operational Wind Fields

WW3 model has also tested for ECMWF operational wind fields for all 12 combinations of source terms for 6 storms (2 from each buoy). ECMWF winds have showed lower correlation and have included significantly higher errors compared to CFSR winds as in SWAN model. The average of statistical parameters combining all CFSR and all ECMWF results for 12 combinations, and results of best methods for each wind field (ST4NLS for both models) are presented in Table 6.18. Lower wind speeds of ECMWF winds have resulted in more systematic underestimation (Figure 6.6). Therefore, bulk of runs were carried out only using CFSR wind fields.

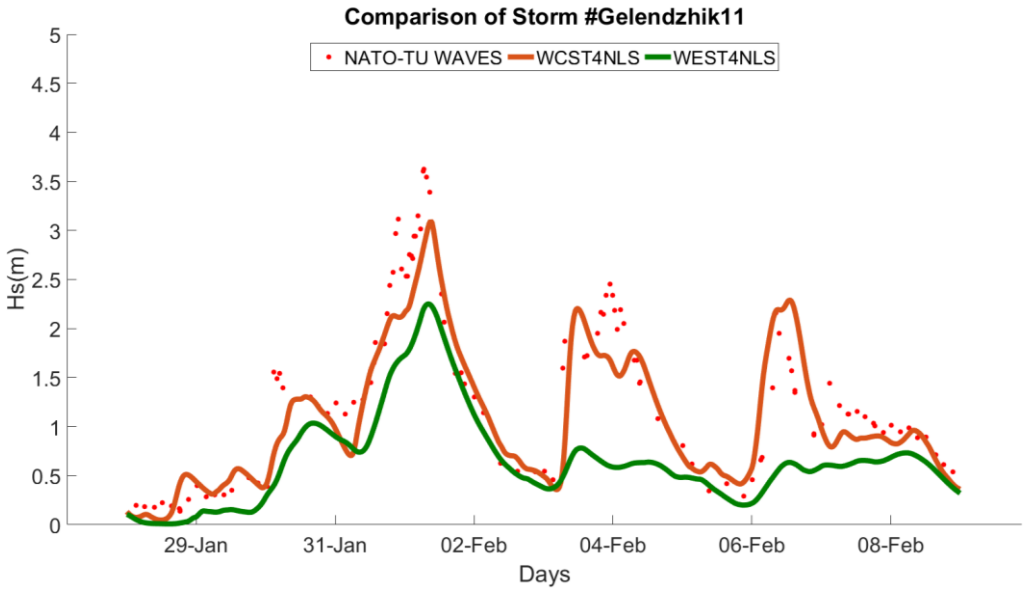

Figure 6.6 Comparison of ECMWF (green line) and CFSR (red line) for Gelendzhik 11 Storm using ST4NLS

Table 6.18 Comparison of CFSR and ECMWF wind fields in WW3 Model

	RMSE	RMSEs	RMSEu	NMAE	NBIAS	SI	R
CFSR average	0.49	0.38	0.28	0.49	0.25	0.31	0.88
ECMWF average	0.76	0.72	0.23	0.80	0.49	0.38	0.85
CFSR (ST4NLS)	0.29	0.29	0.17	0.39	0.15	0.28	0.89
ECMWF(ST4NLS)	0.24	0.52	0.51	0.71	0.43	0.35	0.86

6.2.10 General Discussion on the Selected Source Terms in WAVEWATCH III Model

In this part, the effects caused by the change of source term methodologies were discussed. This discussion was handled in two part, differences of wind-wave interaction and dissipation terms (ST1, ST2, ST3, ST4) and differences of non-linear interaction terms (NL1, NL3, NLS). In conclusion, best alternative couple was chosen according to their performance.

6.2.10.1 Discussion on the Discrepancies Observed Between the Wind-Wave Interaction and Dissipation Terms

The wind-wave interaction and dissipation terms are dominated by the exponential growth term $S_{in}(k,\theta)$. Thus, different methods of $S_{in}(k,\theta)$ or small changes in parameters in this term could cause significant differences in the outputs which reflects on the statistical parameters as well. The mentioned differences can be seen from the Table 6.19 which features the statistical analysis of ST1, ST2, ST3, ST4 methods with the constant nonlinear interaction term DIA.

Table 6.19 Statistical Analysis for ST1 ,ST2,ST3,ST4 coupled with NL1

	RMSE	RMSEs	RMSEu	NMAE	NBIAS	SI	R
ST1NL1	0.49	0.37	0.29	0.47	0.21	0.32	0.88
ST2NL1	0.61	0.54	0.25	0.57	0.33	0.35	0.87
ST3NL1	0.44	0.31	0.29	0.42	0.16	0.30	0.89
ST4NL1	0.42	0.28	0.29	0.39	0.13	0.30	0.89

Even though all methods have shown an acceptable performance with respect to correlations coefficient, the error differences are significant. The most systematic error was obtained in the ST2 method which was caused due to underestimation. Representative Figure 6.7 also supports this conclusion.

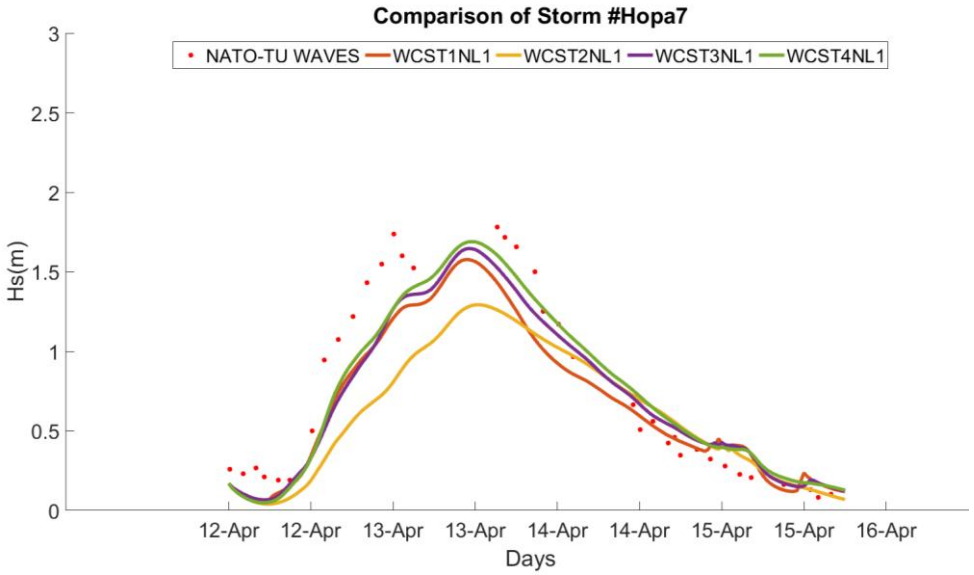

Figure 6.7 Effect of change of dissipation source term method

In above figure, ST2 (yellow line) was significantly underestimating with respect to other methods in the developing stage of the storm. This figure explains the

drawbacks of the exponential growth term in ST2 in Black Sea. This situation can be better explained with Figure 6.8, the scatter plot of all storms in Sinop using ST2LN1 and ST1NL1.

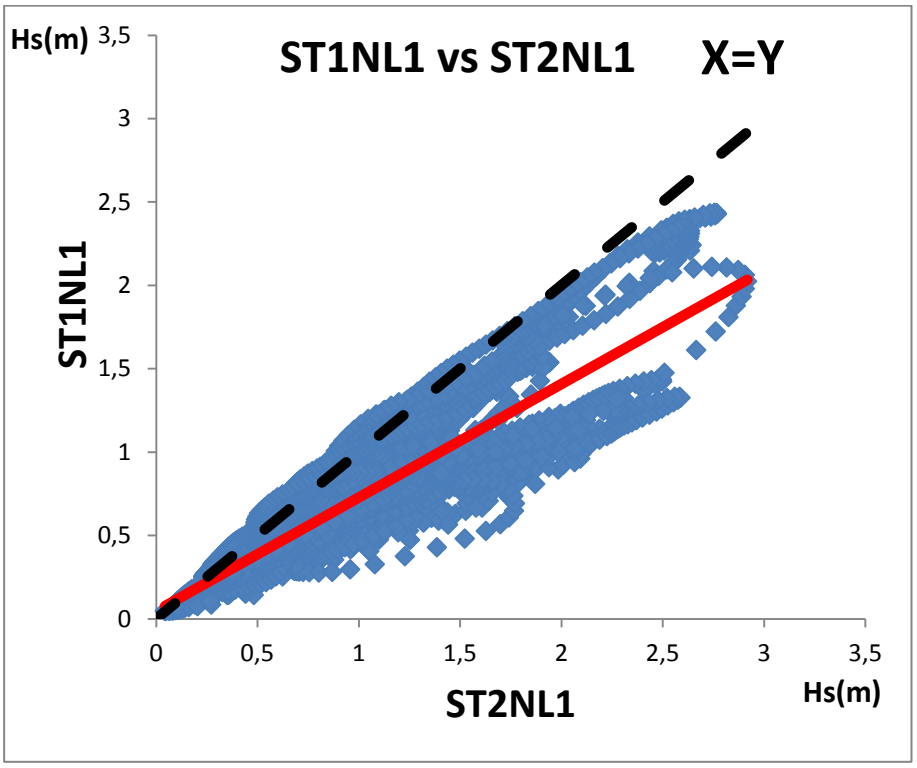

Figure 6.8 Scatter plot of significant wave height of ST1Nl1 and ST2NL1 for Sinop Storms.

The underestimation of ST2 compared to ST1 was clear, almost all values were under x=y and the data is highly scattered.

Other three terms have resulted in better correlation both with respect to observed parameters and with respect to buoy data. This was an expected outcome for ST3 and ST4 since ST4 uses the modified version of ST3 for the exponential growth term. However, ST1 has also showed similar correspondence.

In Figure 6.8 scatter plots of the first 10 storms in Gelendzhik are given for comparison between the guessed wave heights using ST1 and ST3.

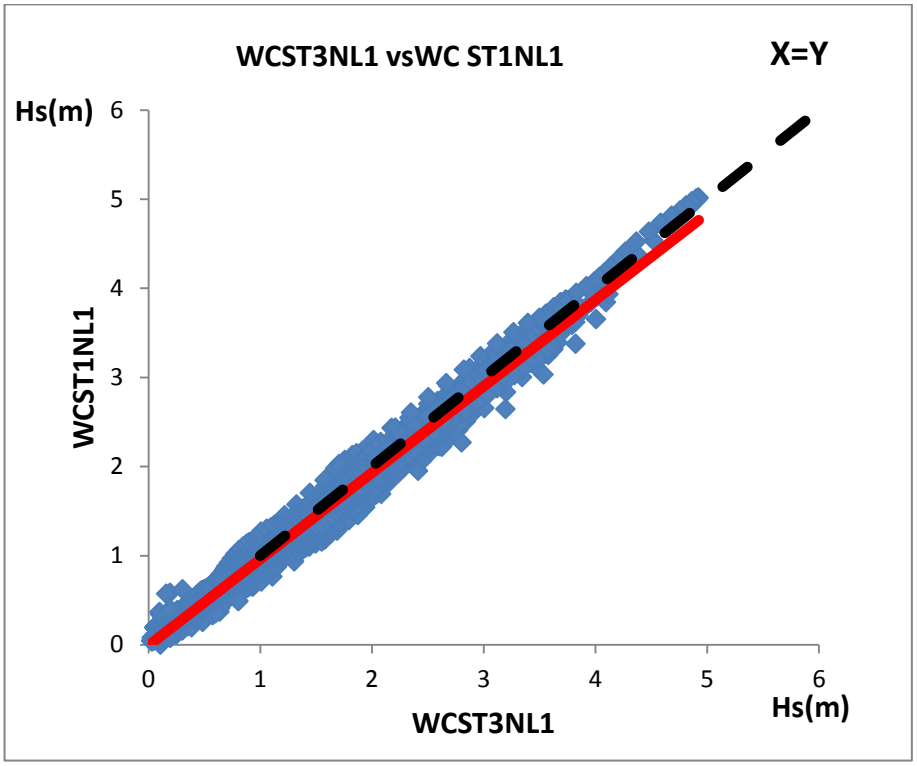

Figure 6.9 Scatter plots of significant wave height of WCST1NL1 and WCST3NL1 for first 10 storms in Gelendzhik.

The model guesses of wave parameters were increased with respect to ST1 in ST3 configuration which also has reduced the error caused by underestimation. Moreover, statistical improvement in the range of 10% to 15% is obtained with ST3NL1 combination compared to ST1NL1.

ST4 model has shown the best performance among other method. The most improved statistical term is the NBIAS value in ST4 with respect to ST3. Slight improvements were also observed for the remaining statistical parameters (up to 5%). The improvement in wave height can also be seen by looking at the systematic

part of RMSE. In Sinop, systematic RMSE is decreased from 0.36 to 0.28 while unsystematic deterioration in RMSEs was not significant (Table 6.20).

Table 6.20 Comparsion of ST3 and ST4 in Sinop buoy

	RMSE	RMSEs	RMSEu	NMAE	NBIAS	SI	R
ST3NL1	0.42	0.36	0.20	0.51	0.26	0.27	0.90
ST4NL1	0.37	0.28	0.22	0.45	0.19	0.27	0.90

Another difference between ST3 and ST4 was observed when the individual storms were investigated. Usually the effects caused by the change of methods are highly similar when individual storms were considered (such as similar increases in the wave heights for all storms). However, in ST3-ST4 comparison, it was seen that, the effects were variable according to storms. This variance was not dependent on wave height. In the following figures (Figure 6.10 and 6.11) time series graphs of wave heights and wave periods are given for Sinop 1 and Sinop 2 storms. Also, occurrence dates of the storms were following each other with two days (Sinop2 started after two days Sinop1 had ended) using ST3NL1 and ST4NL1.

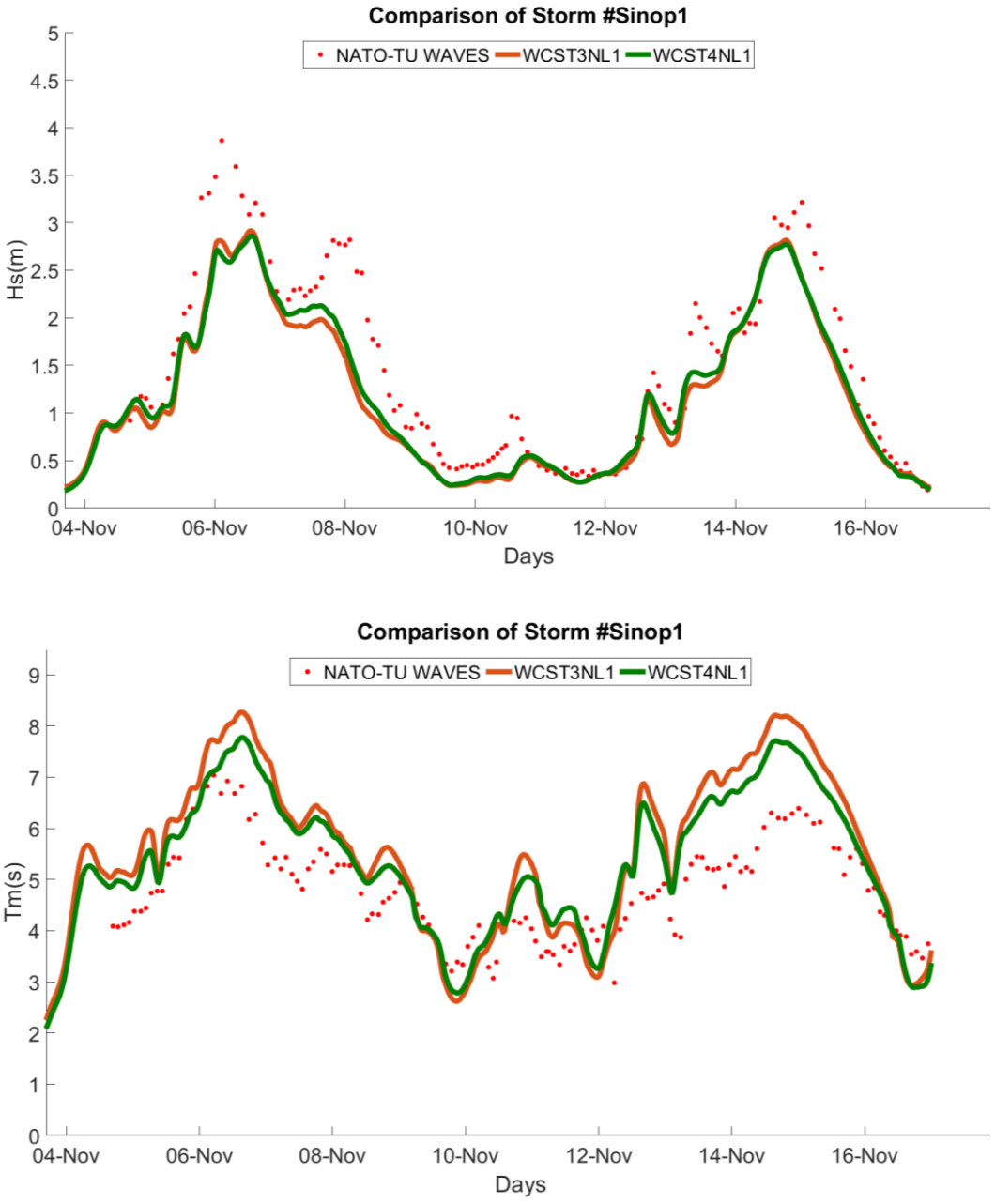

Figure 6.10 WCST3NL1 vs. WCST4NL1 for the storm Sinop 1 (Wave height on top, mean wave period (Tm01) is on bottom)

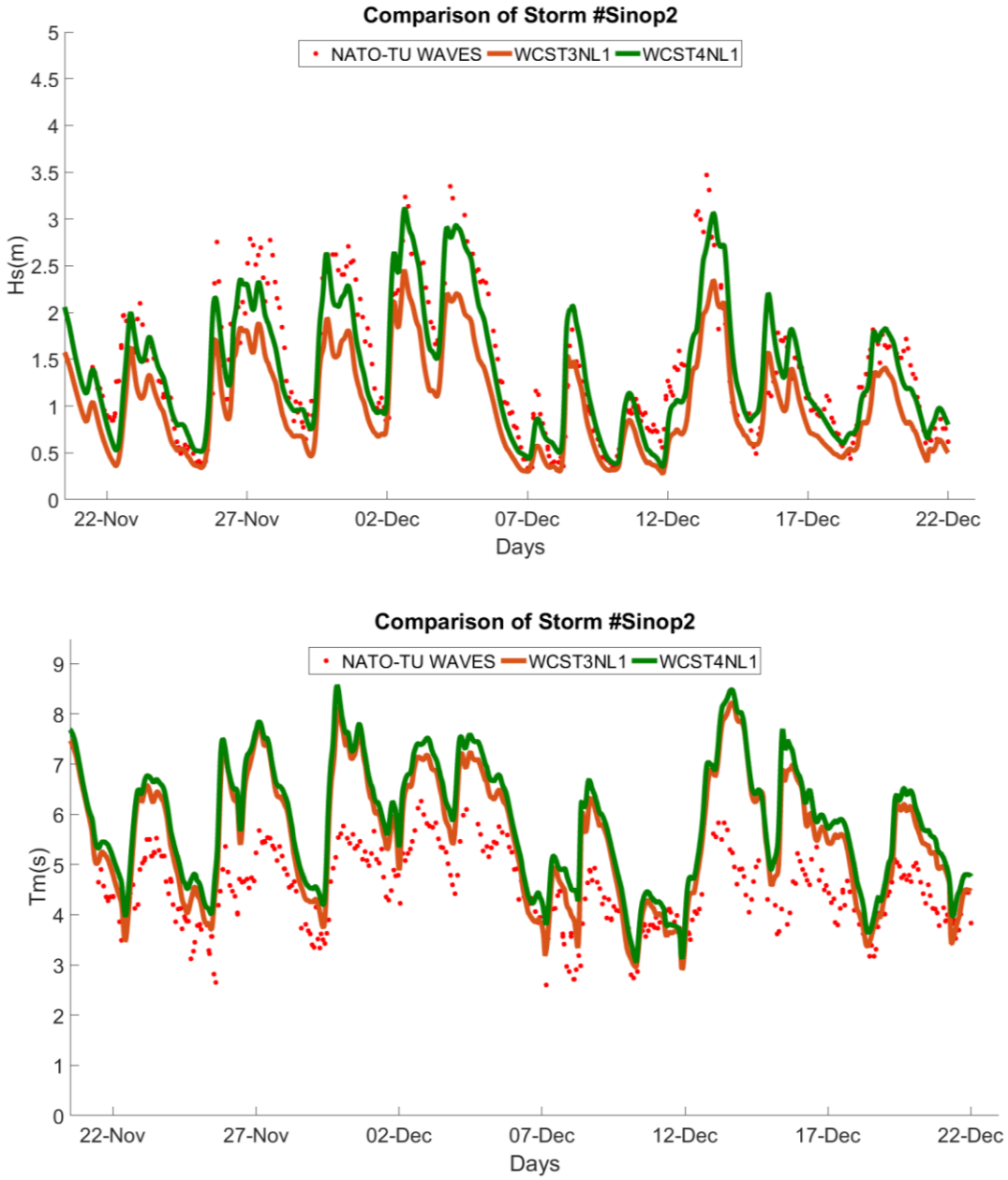

Figure 6.11 WCST3NL1 vs. WCST4NL1 for the storm Sinop 21 (Wave height on top, mean wave period (Tm01) is on bottom)

The different effect of ST4 can be easily observed from the above graphs. This difference can be explained with the wave steepness in deep water (H_0/L_0) and swell

waves in Black Sea. WW3 model has estimated wave heights similar to swell waves in Sinop2 where the wave steepness for those waves was changing between 0.015 and 0.02.

The similar behaviors were observed between ST3, ST4 when the nonlinear interaction term was set to NLS and NL3 which can be seen from the statistical analysis of those combinations in Table 6.21

Table 6.21 Statistical analysis results for ST3NL3, ST3NLS, ST4NL3, ST4NLS

	RMSE	RMSEs	RMSEu	NMAE	NBIAS	SI	R
ST3NL3	0.47	0.33	0.30	0.44	0.19	0.31	0.89
ST4NL3	0.45	0.30	0.31	0.43	0.17	0.30	0.89
ST3NLS	0.44	0.31	0.29	0.42	0.16	0.30	0.89
ST4NLS	0.42	0.28	0.29	0.39	0.13	0.30	0.89

Similar improvements were present when it has switched from ST3 to ST4. Same situation was also observed for combinations of ST1 –ST2 and NL1-NLS. On the other hand, different situation were observed in ST1-ST2 and NL1-NL3 combinations which was caused by changed of non-linear interaction term that is discussed in the following section.

According to all observed values and statistical analysis best method that has shown highest performance was selected as ST4 switch for the wind-wave interaction and dissipation method.

6.2.10.2 Discussion on the discrepancies observed between the nonlinear wave-wave interactions

The main difference of third generation wave models is that nonlinear wave-wave interactions are calculated explicitly. The DIA term is the base economic solutions of nonlinear interaction and used in this study with NL1 switch. Other options considered was the GMD (NL3) develop by Tolman, H..(2010) and NLS developed by Tolman, H.(2011).

The performance of NL1 has shown a good conformity with all $S_{in}(k,\theta)$ and $S_{ds}(k,\theta)$ terms (Table 6.19). However different effects were observed when NL1 was replaced with NL3 for different dissipation and wind-wave interaction terms.

When the GMD configurations are used for nonlinear interaction term and coupled with ST1, stronger dissipation of energy was observed compared to NL1 even though GMD default parameterization of Cdeep =1.00e7 corresponds to Cnl4=3.00e7 in regular DIA. The performances of the two methods are presented in Table 6.22.

Table 6.22 Comparison of ST1NL1 and ST1NL3

	RMSE	RMSEs	RMSEu	NMAE	NBIAS	SI	R
ST1NL1	0.49	0.37	0.29	0.47	0.21	0.32	0.88
ST1NL3	0.68	0.62	0.25	0.67	0.39	0.37	0.85

Significant increase in the systematic RMSE was observed which was also reflected as increase in NBIAS values. SI index and R values were also worse than ST1NL1.

In Figure 6.11 effect of dissipation especially at the peak wave heights can be observed for Hopa 18 storm with configurations ST1NL3 and ST1NL1.

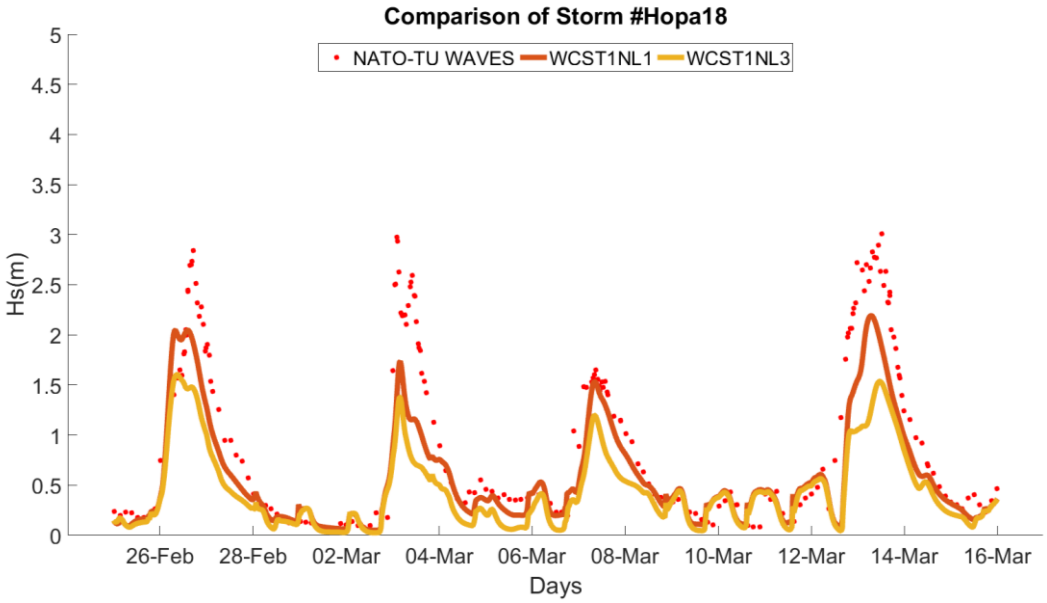

Figure 6.12 Effect of dissipation NL3 compared to NL1 in Hopa 18 storm

However, different situation occurs when NL1 and NL3 was coupled with ST2. The obtained values were very similar for these cases. Statistical analysis values are given in Table 6.23

Table 6.23 Comparison of ST2NL1 and ST2NL3

	RMSE	RMSEs	RMSEu	NMAE	NBIAS	SI	R
ST2NL1	0.61	0.54	0.25	0.57	0.33	0.35	0.87
ST2NL3	0.61	0.54	0.25	0.57	0.33	0.35	0.87

The main reason of this situation is that, in ST2 recommended version of Cnl4 coefficient was set to 1.00e7 while it was 2.78e7 in ST1 for NL1. So that, the recommended configurations of GMD with Cdeep =1.00e7 have shown good

correspondence to recommended DIA configuration of Tolman and Chalikov (1996) (ST2) method.

The results show that there is no significant difference between NL1 and NL3 when ST2 is used. The differences in individual runs cannot be observed visiually on the time series graph. Also the scatter plot of significant wave heights in Hopa buoy shows the great resemblance between two methods (Figure 6.13)

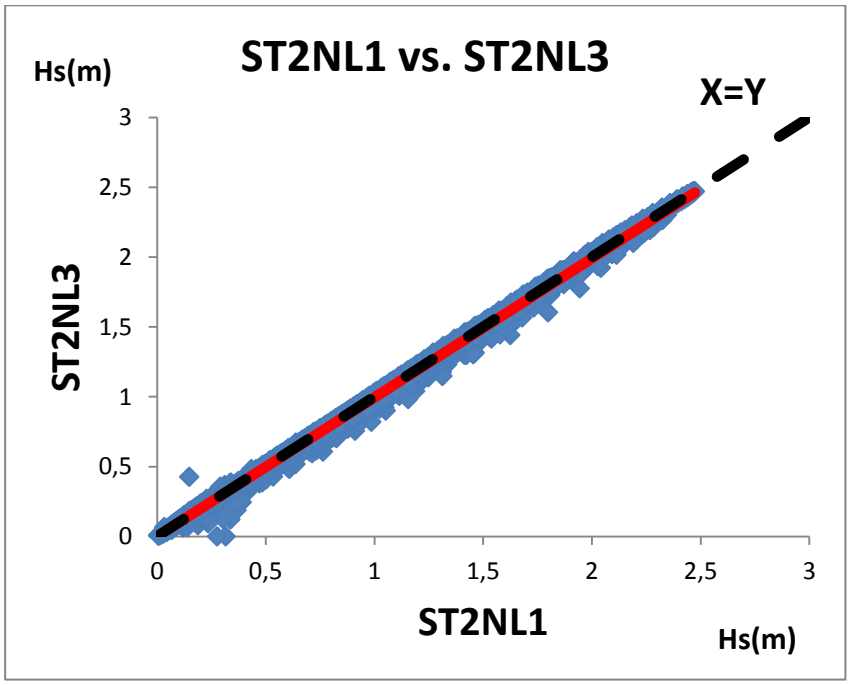

Figure 6.13 Scatter Plot of significant wave heights in Hopa buoy

The result for ST3NL3 and ST4NL3 also showed that behavior of the NL3 changes according to selected input and dissipation term. The statistical analysis are given in Table 6.24

Table 6.24 Statistical Analysis for ST3NL1, ST4NL1, ST3NL3, ST4NL3

	RMSE	RMSEs	RMSEu	NMAE	NBIAS	SI	R
ST3NL1	0.44	0.31	0.29	0.42	0.16	0.30	0.89
ST3NL3	0.47	0.33	0.30	0.44	0.19	0.31	0.89
ST4NL1	0.42	0.28	0.29	0.39	0.13	0.30	0.89
ST4NL3	0.45	0.30	0.31	0.43	0.17	0.30	0.89

The statistical analysis parameters are worsened compared to ST3NL1 and ST4NL1. However, GMD configuration also shows good agreement with the ST3 and ST4 methods with predefined Cdeep value. Moreover, the mentioned deterioration was not as significant as the deterioration caused by changing to NL3 instead of NL1 using ST1 (Figure 6.14).

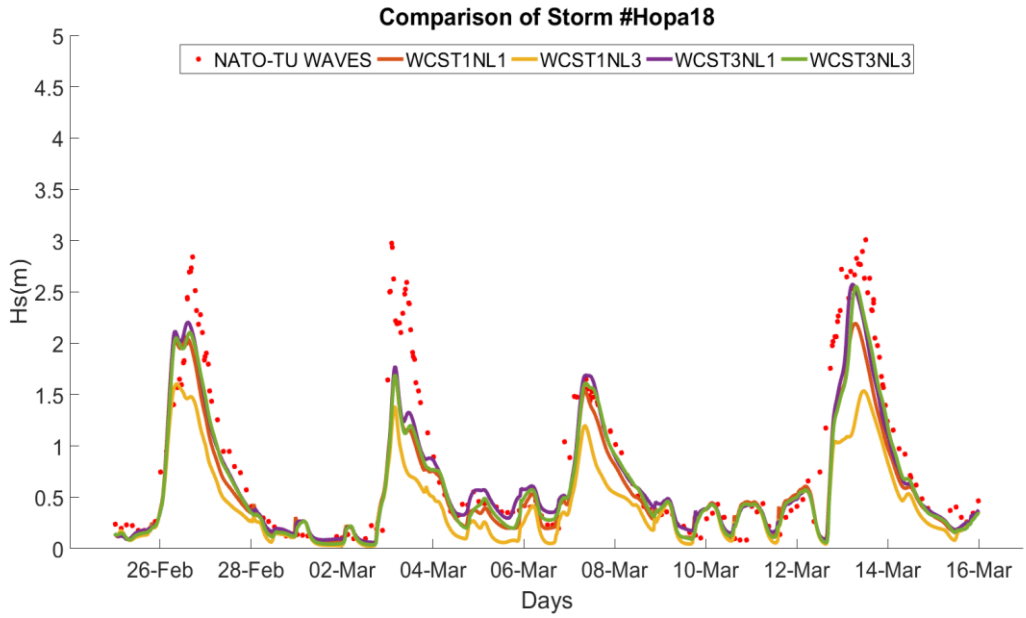

Figure 6.14 Effect of dissipation NL3 compared to NL1 in Hopa 18 storm with ST1 and ST3

In above figure, it is clearly seen that when ST3 is used the obtained values and followed trend are similar (green and purple lines), also ST1NL1 (red line) shows high resemblance with ST3 configurations. However, ST1NL3 (yellow line) significantly underestimates the wave heights compared to other coupled methods. Statistical representation of the Figure 6.14 is given in Table 6.25

Table 6.25 Statistical Analysis of Hopa 18 for ST1&ST3 and NL1&NL3

	RMSE	**RMSEs**	**RMSEu**	**MAE**	**BIAS**	**SI2**
ST1NL1	0.52	0.45	0.25	0.37	0.31	0.28
ST3NL1	0.45	0.35	0.28	0.30	0.22	0.26
ST1NL3	**0.75**	**0.72**	**0.21**	**0.55**	**0.53**	**0.36**
ST3NL3	0.47	0.38	0.28	0.31	0.25	0.27

Hopa18 is not an exceptional event, many storms in all three buoys follows similar trend. The deterioration is on the scale of 5% on average for all parameters in Black Sea.

In some individual storm, NL3 has closer guesses for the peak wave heights, however when the entire storm is examined, it is more biased than NL1. GMD formulations may result in sharper peaks than regular DIA method in ST4 and ST3 combinations. For many cases it is observed that, if the sea state development is fast, GMD method shows better representation when only peaks are considered (Figure 6.15).

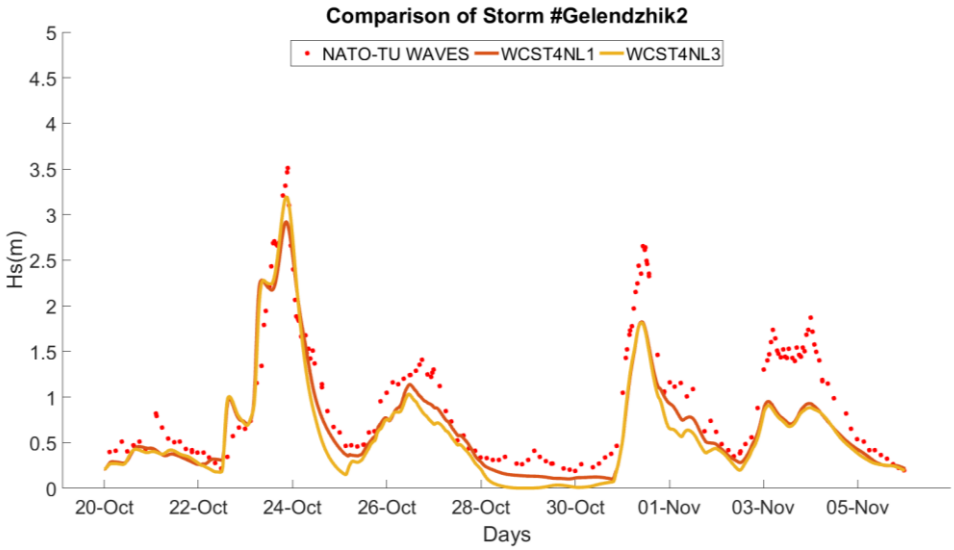

Figure 6.15 Comparisons of ST4NL3 and ST4NL1 in Gelendzhik2 Storm

On the other hand, for slowly developing sea states NL1 method is more advantageous with default parameterization in Black Sea (Figure 6.16) since development stage for GMD starts later than NL1.

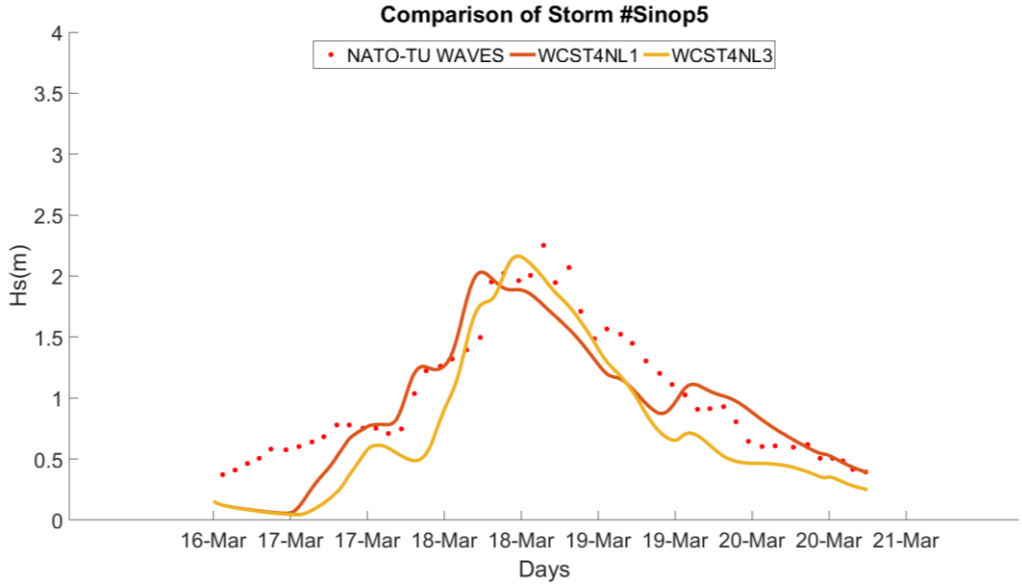

Figure 6.16 Comparisons of ST4NL3 and ST4NL1 in Sinop5 Storm

Finally, NLS formulations are applied for dissipation and quadruplets respectively. NLS is the DIA approach with an applied nonlinear filter. The main aim of the filter is the stabilization of DIA approach for the high frequency tail of the spectrum. Equations are given in chapter in Eq. 3.68 to Eq. 3.71 The used parameters are given in Table 6.26.

Table 6.26 NLS Parameters

Quadruplets- NL1					
λ			Cnl		
0.25			2.5e7		
Nonlinear Filter -NLS					
C_{nlf}	α_{34}	$\widetilde{S_{max}}$	c_1	c_2	c_3
1e10	0.05	0.25	1.25	1.5	1.6

The performance of the NLS combinations compared to NL1 combinations are given in Table 6.27.

Table 6.27 Statistical analysis results for ST1,ST2,ST3,ST4 coupled with NL1 and NLS.

	RMSE	RMSEs	RMSEu	NMAE	NBIAS	SI	R
ST1NL1	0.490	0.365	0.288	0.468	0.212	0.315	0.882
ST1NLS	0.489	0.364	0.288	0.467	0.211	0.315	0.882
ST2NL1	0.607	0.544	0.250	0.572	0.329	0.349	0.867
ST2NLS	0.602	0.538	0.251	0.567	0.325	0.348	0.868
ST3NL1	0.443	0.307	0.288	0.418	0.165	0.298	0.891
ST3NLS	0.442	0.306	0.288	0.418	0.163	0.298	0.891
ST4NL1	0.423	0.277	0.293	0.395	0.130	0.297	0.890
ST4NLS	0.422	0.276	0.294	0.395	0.129	0.297	0.891

The results of the combination of NLS show that application of nonlinear filter to the high frequency end of spectrum has no significant effect in statistical analysis. Moreover, No difference were observed on time series graphs of wave heights and wave periods. Nevertheless, when the statistical parameters were investigated, it has been observed that parameters were improved in scale of 0.1% compared to NL1 for all buoys. Since ranking between methods are done automatically in MATLAB code. NLS results seems to be the best option for nonlinear interactions. Moreover, NLS consist of NL1 parameters as well, only an additional filter was applied in NLS. Therefore, NL1 can be controlled via NLS as well. So that it is chosen as best method since more calibration parameters are available also for the nonlinear filter.

According to the WW3 runs with recommended parameters, ST4NLS was chosen as the best alternative couple that has shown the best performance in Black Sea among 12 methods. The final statistical parameters are given in Table 6.28 for ST4NLS before calibration.

Table 6.28 Statistical analysis results for ST4NLS in Black Sea

ST4NLS	RMSE	RMSEs	RMSEu	NMAE	NBIAS	SI	R
Black Sea	0.42	0.28	0.29	0.39	0.13	0.30	0.89
Gelendzhik	0.45	0.24	0.36	0.37	0.08	0.28	0.89
Sinop	0.37	0.28	0.22	0.40	0.16	0.33	0.89
Hopa	0.42	0.31	0.26	0.39	0.13	0.30	0.89

6.3 Calibration of WAVEWATCH III Model for Extreme Events for Black Sea Basin

ST4NLS couple is chosen as the best switch combination after analysis of WW3 run completed for 54 events in Black Sea. Calibration of the chosen method is carried out using the defined parameters of switches given in tables above. Calibration is carried out using 9 representative storms given in Table 6.29. After a certain validation is reached, tuned parameters are applied to the remaining storms in order see the overall performance of the parameters.

Table 6.29 Chosen storms for calibration in WW3

Storm #	Start Date	End Date	Duration (days)	Max. Hs	# of Peaks
Gelendzhik_7	1997.10.01	1997.10.10	9	3.87	2
Gelendzhik_11	1998.01.28	1998.02.09	12	3.70	3
Gelendzhik_17	2001.01.08	2001.01.16	8	3.88	2
Sinop_3	1995.12.14	1996.01.01	18	4.36	3
Sinop_6	1996.03.31	1996.04.15	15	2.28	2
Sinop_7	1996.05.28	1996.06.09	12	2.10	2
Hopa_4	1995.11.05	1995.11.15	10	3.99	3
Hopa_5	1995.11.17	1995.11.28	11	4.26	2
Hopa_18	1998.02.25	1998.03.16	19	3.00	4

The selected storms are also including the main problems that have been seen in WW3 runs with recommended parameters.

In WW3 runs, observed problem can be listed as follows (similar to SWAN model);

- Missing the peak wave heights

- Systematic underestimation of wave parameters
- Mismatch between the trends of model output and observed data.
- Deterioration in model output after strong overestimation or underestimation
- Low sensitivity of model against quick changes in storm characteristics.
- Error on the guesses of sharp peaks

Some of the observed errors are related with the source data while others are due to the model itself. The calibration part of study is analyzed using same statistical analysis methods as in other WW3 runs.

6.3.1 Calibration of Wind Wave Interaction Parameters

Wind wave interaction term in ST4 of WW3 is a detailed process which is controlled by many parameters. Moreover, almost all of those related parameters are user tunable unlike SWAN model.

The most effective parameters in modified version of the Janssen equation for wind wave interaction (Eq.3.32) are found to be β_{max} (maximum value of the wind wave coupling) and z_α (wave age shift to account for gustiness). In BJA parameterization (Bidlot et al.,2008) β_{max} and z_α are given as 1.2 and 0.011 respectively(as in ST3) According to Ardhuin et al. (2010) β_{max} is adjusted as 1.52 so that higher wind wave coupling value produces high wind stress value which results in strong high-frequency input. Ardhuin et al. (2010) also adjusted z_α by reducing to 0.06 which reduces the effect of wind input for frequencies between 0.15-0.2 Hz. Such adjustment also affects the wave parameters in Black Sea (ST3 –ST4 difference in chapter 6.2.4). Moreover, in study of Mentashi et al. (2015) which investigates the model performance of WW3 for Mediterranean Sea, β_{max} and z_α parameters are adjusted as 1.68 and 0.04 in order to suppress the systematic underestimation of wave height. The obtained results in Mentashi et al. (2015) have been found to be

improved compared to BJA configuration. Since Mediterranean region is also a closed basin, similar effect could also occur in Black Sea. In consideration of these studies, the best fitting β_{max} and z_α values are searched by trial runs. Effect of β_{max} and z_α can be visualized in Figure 6.17 where β_{max} and z_α for red line (ST4NLS) are 1.52 and 0.06, for purple line (ck4) 2.00 and 0.04 and for green line(c) 1.75 and 0.04 respectively.

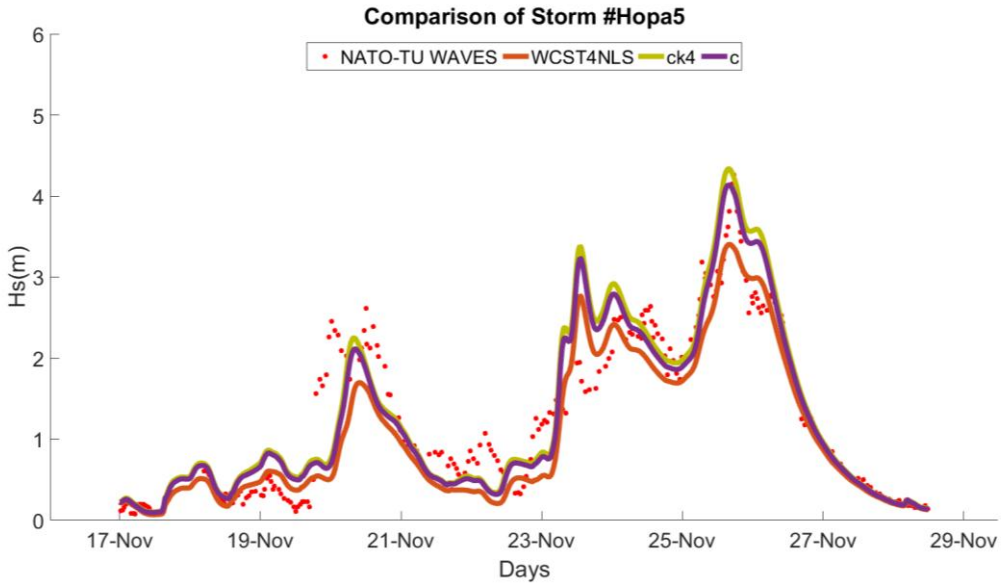

Figure 6.17 Comparisons of effects of $\boldsymbol{\beta_{max}}$ and $\boldsymbol{z_\alpha}$ in Hopa5 Storm

The more detailed effect can be observed from the scatter plots given in Figure 6.18

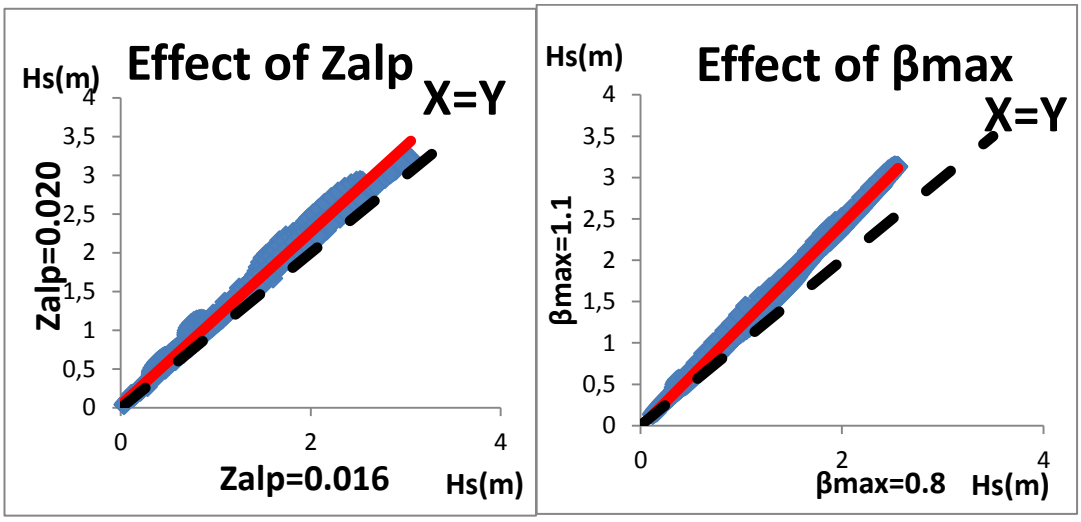

Figure 6.18 Scatter plots of effects of z_α (left) and β_{max} (right) in Gelendzhik1 Storm

Higher increases in those parameters cause negative biased data (overestimation) of wave height in model output. Moreover, unsystematic error starts to increase for respectively higher values such as $\beta_{max} = 2.00$ and $z_\alpha = 0.016$.

Over 20 different configurations are tried in order to improve the correlation of model with respect to two parameters. The best statistical analysis results are obtained for values of β_{max} and z_α are 1.75 and 0.04 respectively (will be called "c" configuration hereafter). (Table 6.30) The RMSE values are improved by 10% with "c" configuration with respect to ST4NL3 which is significant in wave modeling. The reduction in systematic part of RMSE for the selected storms shows that most of the error caused by the model itself was limited with these new values of parameters. Accordingly, NBIAS values strongly decreased.. Despite the improvements, missing the peak values still remains. The "c" configuration was accepted as the base configuration for the following calibration process.

Table 6.30 Statistical analysis for before and after tuning of $\boldsymbol{\beta_{max}}$ and $\boldsymbol{z_\alpha}$ values for ST4NLS (WCST4NLS vs c)

	RMSE	RMSEs	RMSEu	NMAE	NBIAS	SI	R
WCST4NLS	0.40	0.28	0.28	0.40	0.16	0.29	0.89
c	0.36	0.12	0.33	0.36	0.00	0.29	0.89

The effect of new calibrated parameters on time series can be illustrated with the Figure 6.19 for Sinop6 storm.

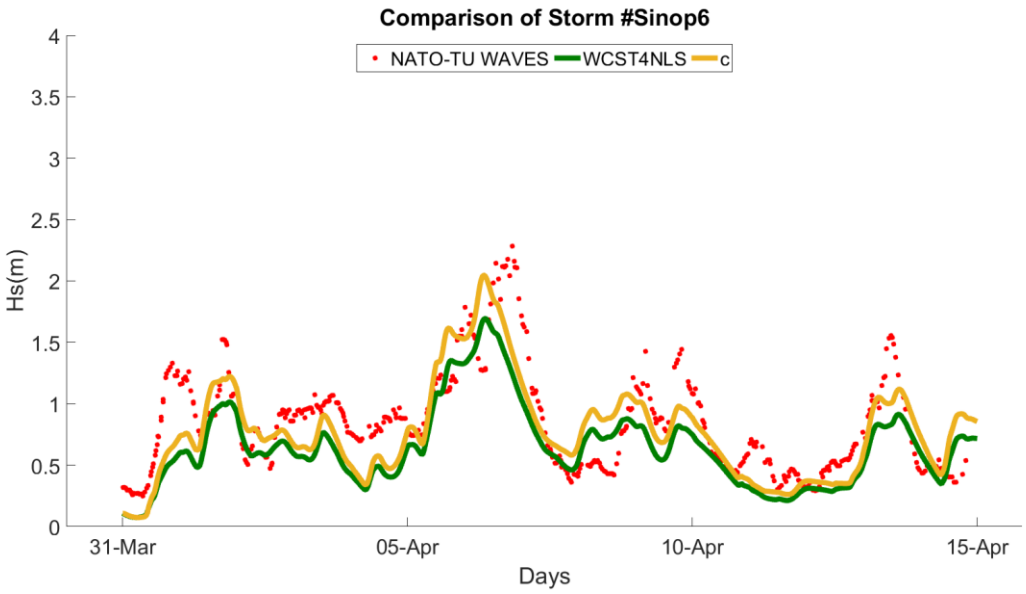

Figure 6.19 Difference between WCST4NLS and c for Sinop6 storm

Wind-wave interaction is also sensitive to the directional spreading (term $\cos^{p_{in}}(\theta - \theta_w)$ in Eq.3.32. Effect of directional changes can be controlled by p_{in} parameter which was selected as 2.0 in ST4NLS. Increase in p_{in} results in small decreases in wave heights. If the model results are overestimated, increase of power of cosine term has a positive effect on correlation, in terms of underestimation reverse situation

can be observed. p_{in} was changed to 2.0 and used with the new β_{max} and z_α values. The obtained results have shown that change in p_{in} did not significantly affect the results. So p_{in}has remained 1.7 since it has shown better correlation with the real data
(Table 6.31).

Table 6.31 Comparison of $\mathbf{p_{in} = 1.7}$ and $\mathbf{p_{in} = 2.0}$

	NRMSE	NMAE	NBIAS	SI	R
$p_{in} = 1.7$	0.250	0.358	0.002	0.293	0.888
$p_{in} = 2.0$	0.249	0.357	0.011	0.292	0.889

6.3.2 Calibration of Dissipation Parameters

In ST4 approach dissipation of energy is controlled by two main source terms which are $S_{out}(k,\theta)$(defines the swell dissipation process in Eq.3.32), and $S_{ds}(k,\theta)$ (defines the remaining total dissipation such as whitecapping dissipation process in Eq. 3.60).

In ST4, dissipation rather than swell (only$S_{ds}(k,\theta)$) consist of saturation based term ($B(k)$, direction-integrated spectral saturation), cumulative breaking term ($S_{bk,cu}(k,\theta)$), which represents the smoothing of the surface, and wave –turbulence interaction terms (see chapter 3.2.2.2) (Tolman, 2014).

Saturation based term is controlled by the saturation dissipation coefficient (C_{ds}^{sat}) and threshold value of Br. If C_{ds}^{sat} (C_2 in sections 6.2.4 and 6.2.8) is increased the dissipation also increases. Two different values were chosen in addition to recommended value for C_{ds}^{sat} (-2.2 e-5) in ST4. Other values are $C_{ds}^{sat}low$ and $C_{ds}^{sat}high$ as -2.6 e-5 and -1.6 e-5 respectively. As expected, lower coefficients have

resulted in increased wave height values. However, the change with respect to C_{ds}^{sat} was not significant so that statistical analysis were not strongly affected (Table 6.32)

Table 6.32 Comparisons of the effect of different $\boldsymbol{C_{ds}^{sat}}$ values

	NRMSE	NMAE	NBIAS	SI	R
$C_{ds}^{sat} low$	0.249	0.356	0.027	0.290	0.889
$C_{ds}^{sat} recommended$	0.250	0.358	0.002	0.293	0.888
$C_{ds}^{sat} high$	0.256	0.366	-0.033	0.298	0.888

Most effected term among all statistical analysis was NBIAS. Although the optimum value for NBIAS has reached for the recommended value of C_{ds}^{sat}, considering the slight improvements in terms of SI and NRMSE $C_{ds}^{sat} low$ has shown a good performance also.

For the effect of Br in equation 3.60, if the threshold value is exceeded by the directional integrated spectral saturation first term equals to 0. So that setting a higher value for Br increases the exceedance of B and decrease the dissipation. The default value for Br is 9e-4. As in C_{ds}^{sat}, one lower and one higher parameters were tried for Br in WW3 model. Br_{low} is set to 8.5e-4 while Br_{high} is 1.2e-3. Br_{low} low value has chosen from the Test405 of Ardhuin et al (2010), which is suggested as slightly superior for short fetches. On the other hand, Br_{high} value has selected according to Babanin and Young (2005) which has found to be realistic threshold for wave breaking (Ardhuin et al., 2010). The statistical analyses and figure representing general behavior of model for different Br values are given in Table 6.33.

Table 6.33 Comparisons of the effect of different ***Br*** values

	NRMSE	NMAE	NBIAS	SI	R
Br_{high}	0.25	0.36	0.05	0.28	0.90
$Br_{recommended}$	0.28	0.40	0.16	0.28	0.90
Br_{low}	0.29	0.42	0.20	0.28	0.90

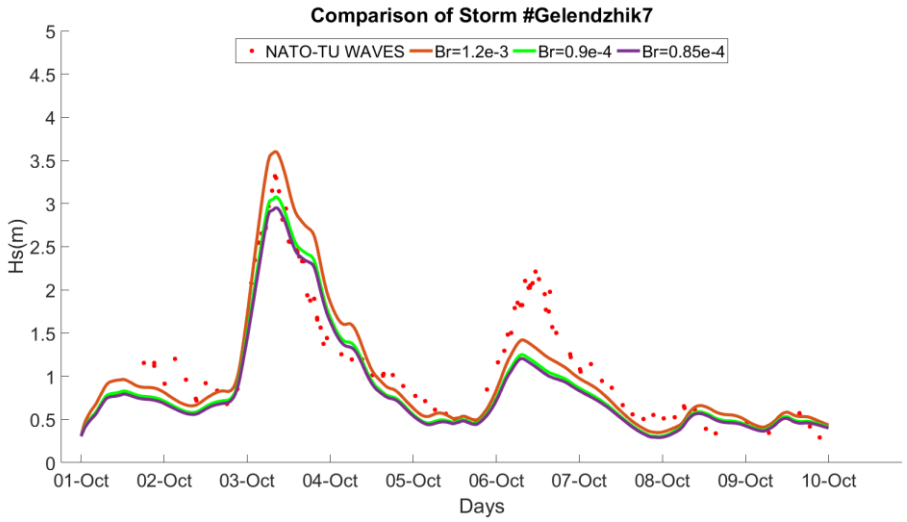

Figure 6.20 Effect of different ***Br*** values for Gelendzhik 7 storm

It has been observed that, ST4 runs are highly sensitive to changes of Br. Increased Br values have resulted in more energy preservation which corresponds to higher wave height values (Figure 6.20). In other words, because of the higher threshold value, the numbers of broken waves were reduced. This situation directly affects the bias values and the systematic error, while unsystematic parameters and correlation coefficients were not changed. After the analysis Br value was set to Br_{high}, 1.2e-3.

Final considered parameter in saturation-based term is $\Delta_\theta$which is the directional restriction for B. Since the directional spectra were too narrow when spectrum integrated over full circle, integration is restricted byΔ_θ (Ardhuin and Boyer, 2006;Tolman, 20142014). The recommended value of Δ_θ is 80 degrees, however study of Mentashi et al. 2015) shows that, wider range around 100 degrees is more

appropriate for closed basin. In that study, also narrower 40 degrees were considered as well. However, the performance of such narrow band was not found to be successful. According to this information two different ranges were chosen in this study, different than recommended value, which are Δ_θ is equal to 90 and 100.

The observed difference caused by the change of $\Delta_\theta$was so small that, effect cannot be traced from the time series graph. The statistical analysis also shows no difference between 90 degree and 100 degree. An improvement of 0.25% is observed (Table 6.34) when Δ_θ is set to 90 instead 80 which shows that Δ_θ is not a governing parameter. After this point, Δ_θ is set to 100˚ for the consistency of study.

Table 6.34 Change of statistical analysis results according to Δ_θ.

	NRMSE	NMAE	NBIAS	SI	R
$\Delta_\theta = 80^\circ$	0.2501	0.3579	0.0016	0.2928	0.8885
$\Delta_\theta = 90^\circ$	0.2498	0.3573	0.0050	0.2925	0.8884
$\Delta_\theta = 100^\circ$	0.2498	0.3573	0.0050	0.2925	0.8884

On the other hand $S_{bk,cu}(k,\theta)$ term is controlled by the C_{cu} coefficient which is inversely proportional to the dissipation. The recommended value of C_{cu} is -0.4034. First trial value of C_{cu} was set to -1 which was suggested for ocean scale simulations in order to reduces the energy level in the tail below observed levels. (Ardhuin et al.,2010) . However C_{cu} was also set to 0 by Ardhuin et al 2010 for Test 405 which parameterization is applicable to short fetches. Setting C_{cu} to 0 cancels effect smoothing term, $S_{bk,cu}(k,\theta)$.

Table 6.35 Effect of change of C_{cu} coefficient

	NRMSE	NMAE	NBIAS	SI	R
$C_{cu} = 0$	0.254	0.363	-0.024	0.296	0.888
$C_{cu} = -0.403$	0.250	0.358	0.002	0.293	0.888
$C_{cu} = -1$	0.249	0.356	0.031	0.290	0.889

Results obtained in Table 6.35 shows that, change of C_{cu} most significantly has affected the NBIAS values. Since NBIAS values were already calibrated to be around 0, no calibration is needed for the C_{cu} parameter. However, in case of underestimation C_{cu} values could set to 0 in order reduce the energy loss of the system.

Finally, C_{turb} controls the wave –turbulence interaction terms which adjusts wave groupiness. C_{turb} is taken as 0 in default runs so that wave –turbulence is not considered in dissipation process. It is mentioned by Tolman et al. (2014) that C_{turb} could be in the order of 1. So that C_{turb} was set to 1 in order compare with default parameterization (Table 6.36)

Table 6.36 Effect of change of C_{turb} coefficient

	NRMSE	NMAE	NBIAS	SI	R
$C_{turb} = 0$	0.25	0.36	0.02	0.30	0.88
$C_{turb} = 1$	0.26	0.36	0.06	0.30	0.88

The obtained results shows that wave –turbulence interaction terms was not significant in Black Sea, so C_{turb} was set to 0.

In calibration of swell parameter different procedure was followed. First of all, different 9 storms (3 from each buoys) were chosen for calibration (Table 6.37). The selection of storms was based on their performance with ST3NLS and ST4NLS since

one of the differences between the ST3 and ST4 were activation of swell dissipation terms. The selected storms were the most effected events from the change of dissipation method. After the selection, ST3NLS combination using s1=1 (swell dissipation term activated for ST3) has applied to the new calibration group of storms since swell parameters were not the only difference between ST3 and ST4. This process is followed by calibration of swell parameters for ST4 method using the new group of storms.

Table 6.37 New set of calibration storms for Swell Dissipation Analysis

Storm #	Start Date	End Date	Duration (days)	Max. Hs	# of Peaks
Gelendzhik_1	1996.09.02	1996.10.02	30	3.50	10
Gelendzhik_10	1998.01.04	1998.01.18	14	3.40	4
Gelendzhik_17	2001.01.08	2001.01.16	8	3.88	2
Sinop_2	1994.11.19	1994.12.22	33	3.50	10
Sinop_6	1996.03.31	1996.04.15	15	2.28	2
Sinop_7	1996.05.28	1996.06.09	12	2.10	2
Hopa_5	1995.11.17	1995.11.28	11	4.26	2
Hopa_14	1997.08.31	1997.09.07	7	2.10	3
Hopa_20	1998.06.20	1998.06.25	5	3.50	1

The comparison between ST4, and active and not active ST3 swell dissipation cases shows that (Table 6.38), the effect of swell dissipation term was not dominant. So that the main reason of difference between ST4 and ST3 was occurred because of the other dissipation parameters.

Table 6.38 Effect of swell dissipation for ST3 and ST4

	NRMSE	NMAE	NBIAS	SI	R
ST3 s=0	0.33	0.53	0.24	0.29	0.86
ST3 s=1	0.33	0.54	0.25	0.29	0.86
ST4 s=1	0.29	0.46	0.17	0.28	0.86

Above table indicates that, ST4 shows better correlation with the observed values especially low bias of ST4 was remarkable.

In swell dissipation part of ST4 which is explained Chapter 3.2.2.2 and using Eq. 3.52 to Eq. 3.59. 4 parameters were considered for tuning which are swell attenuation factor of s_1, s_2 , and s_3 . The coefficients s_1, s_2 , s_3 are used to determine the friction factor (f_e) (Eq.3.59) which is used in turbulent boundary layer expression (Eq.3.58) of the $S_{out}(k,\theta)$. According to Ardhuin et al. (2010), adequate swell dissipation is obtained when f_e is in the range of 0.04 to 0.07. So that, s_1, s_2 , s_3 parameters are to 0.8, -0.018 and 0.015 respectively. Moreover when s_3 is set to greater value $S_{out}(k,\theta)$ term is applied to entire spectrum which is the recommended case since in Eq.3.59 absolute value of s_3 is used. s_1 and s_3 are directly proportional with f_e . So that, an increase in those coefficients causes increase in friction factor which results in more energy dissipation. On the other hand s_2 is given a negative value in order to obtain stronger dissipation for swells opposed to winds (Ardhuin et al, 2010).

First of all, s_1 was set to 1.1 and compared to recommended value of 0.8. The obtained results shows that recommended value of s_1 has shown better correlation with the buoy data. Moreover s_1 is taken as 0.8 for Test405 of Ardhuin et al. (2010) for short fetches, which has shown a good conformity in terms of parameterization for Black Sea region. Effect of s_1 parameter is presented in Table 6.38

Table 6.39 Effect of Change of s_1 in swell term

	NRMSE	NMAE	NBIAS	SI	R
$s_1 = 0.8$	0.24	0.37	0.06	0.27	0.88
$s_1 = 1.1$	0.25	0.39	0.09	0.27	0.88

One higher and one lower value were applied to WW3 model in order to understand the sensitivity of s_2 and s_3. The selected values and the effects of change for swell parameters were shown in Table 6.40 and Table 6.41

Table 6.40 Effect of Change of s_2 in swell term

	NRMSE	NMAE	NBIAS	SI	R
$s_{2\_high} = -0.012$	0.24	0.37	0.04	0.27	0.88
$s_{2\_def} = -0.018$	0.24	0.37	0.06	0.27	0.88
$s_{2\_low} = -0.024$	0.24	0.38	0.08	0.27	0.88

Table 6.41 Effect of Change of s_3 in swell term

	NRMSE	NMAE	NBIAS	SI	R
$s_{3\_low} = 0.010$	0.24	0.37	0.04	0.27	0.89
$s_{3\_def} = 0.015$	0.24	0.37	0.06	0.27	0.88
$s_{3\_high} = 0.020$	0.24	0.38	0.08	0.27	0.88

The effects of changes in swell parameters were not significant as seen in Table 6.40 and Table 6.41 above. Only bias values have changed since lower s_1, higher s_2 and lower s_3 values have resulted in slightly higher wave heights. Since the tuning of parameter were carried out for the other calibration set which NBIAS were already set to 0 with default swell parameters, no change for swell parameters were considered at this point. It can be concluded from the obtained results from both the

sensitivity of swell parameters and activation or deactivation of the swell term that, swell mechanism exists in Black sea, however it is not effective.

6.3.3 Calibration of Nonlinear Interaction Parameters

Calibration process of nonlinear interaction parameters were carried out in two separate parts. In first part, calibration of DIA coefficients, which are quadruplet configurations coefficient (λ) and proportionality coefficient for quadruplet interactions (Cnl4), were taken into consideration. The effects of both parameters were discussed in previous sections. The smaller and larger values of those parameters were applied beside the already used recommended values of Cnl4 and λ in WW3 model. The obtained results were analyzed in order to understand the sensitivity of model to these parameters. The applied values and corresponding results were given below in Table 6.42 and Table 6.43

Table 6.42 Used values and corresponding statistical analysis results of Cnl4

	NRMSE	NMAE	NBIAS	SI	R
Cnl4=5.0e7	0.258	0.369	-0.030	0.300	0.882
Cnl4=2.5e7	0.257	0.363	-0.016	0.300	0.885
Cnl4=1.0e7	0.263	0.366	0.082	0.296	0.888

Table 6.43 Used values and corresponding statistical analysis results of $\boldsymbol{\lambda}$

	NRMSE	NMAE	NBIAS	SI	R
$\lambda = 0.30$	0.255	0.374	-0.019	0.298	0.880
$\lambda = 0.25$	0.250	0.358	0.002	0.293	0.888
$\lambda = 0.20$	0.258	0.363	0.042	0.296	0.891

Obtained results in Table 6.42 shows that, recommended value of Cnl4=2.5e7 has shown the best performance among others. Also, it was observed that WW3 was more sensitive to decrease than increase of Cnl4 in term of NBIAS. So that Cnl4 was set to 2.5e7. Similar situation was also obtained for the λ values. Since DIA was calibrated with $\lambda = 0.25$, changing that value did not result in better performance. As Cnl4, λ value was not changed for WW3.

In second part, effects of application of nonlinear filter on DIA were investigated using the tunable parameters of NLS. The preliminary results showed that application nonlinear filter was not effective in Black Sea as the improvements were small. However, NLS was chosen as best method for nonlinear interactions since among the other methods, only NLS was tunable. There are 6 parameters which are related with the nonlinear filter; C_{nlf} , α_{34},$\widetilde{S_{max}}$,c_1,c_2,c_3.

First considered term was C_{nlf} which is the proportionally coefficient (Eq.3.69) of DIA in filter. The recommended value of C_{nlf} is 1e10. Higher value of C_{nlf} was selected in order to amplify the effect of nonlinear filter. So that C_{nlf} was set to 2e10. The results (Table 6.44) have shown that no effect was observed from this change.

Table 6.44 Sensitive of Model to $\mathbf{C_{nlf}}$

	NRMSE	NMAE	NBIAS	SI	R
C_{nlf}= 1e10	0.244	0.349	0.031	0.284	0.898
C_{nlf}= 2e10	0.244	0.350	0.031	0.284	0.898

The second considered term was the α_{34}(Eq.3.72) ,which is the offset of quadruplets 3 and 4. The recommended value of α_{34} is 0.05 and it is tunable in the interval of 0 to 1. α_{34} was set to 0.04 however no change was observed again. Similar, approach was applied to $\widetilde{S_{max}}$ and the value of $\widetilde{S_{max}}$ has changed from 0.25 to 0.3. The exact same results in Table 6.44 were obtained.

In order to increase the effect of nonlinear filter combined values of $C_{nlf} = 2e11$, $\alpha_{34} = 0.02$ and $\widetilde{S_{max}} = 0.15$ were considered. These combined parameters has shown no effect and the results in Table 6.45 is obtained.

Table 6.45 Effect of Nonlinear filter (NLS)

	NRMSE	NMAE	NBIAS	SI	R
NLS recommended	0.244	0.349	0.031	0.284	0.898
NLS trial	0.244	0.349	0.033	0.284	0.898

The nonlinear filter was designed to be applied only to high frequency end of the spectrum. Therefore actual filter $\Phi(f)$,which is tunable by parameters c_1,c_2,c_3, is calibrated such that $\Phi(f_p)$ would be approximately 0 and $\Phi(f > f_p)$ would be approximately 1. In order the apply this filter to wider range of frequency, values of c_1,c_2,c_3 are calibrated. c_1,c_2,c_3 were changed from 1.25 to 1.50 , 1.5 to 1 and 6.0 to 4.0, respectively. These new values of parameters result in at most $\Phi(f_p)$=0.66 and $\Phi(f > f_p) = 1$. However these changes have not resulted in any significant improvement (Table 6.46) . In conclusion, application of nonlinear filter was not effective on wave parameters for Black Sea region.

Table 6.46 Effects of parameters $\mathbf{c_1}$,$\mathbf{c_2}$,$\mathbf{c_3}$ in NLS

	NRMSE	NMAE	NBIAS	SI	R
Recommended c_1,c_2,c_3	0.244	0.349	0.031	0.284	0.898
$c_1 = 1.25 \rightarrow 1.5$	0.244	0.349	0.032	0.284	0.898
$c_2 = 1.5 \rightarrow 1.0$	0.244	0.349	0.031	0.284	0.898
$c_3 = 6 \rightarrow 4$	0.244	0.350	0.030	0.284	0.898

In order to increase the completeness of the investigation of most appropriate nonlinear interaction methods, different GMD (NL3) configurations were also considered. Two of the different configurations of GMD method were also applied and compared with the default GMD configuration which corresponds to regular DIA method. The used configurations of GMD were (based on Tolman H., 2010) GMD3 (G13d) and G35d(GMD5) where the number stands for the number of quadruplet configurations (regular DIA is GMD1) used in calculation.

The results (Table 6.47) show that significant improvements were observed when higher numbers of quadruplets were present instead of only regular DIA approach.

Table 6.47 Comparison of Higher Number of Quadruplet Configurations using GMD

	NRMSE	NMAE	NBIAS	SI	R
GMD	0.32	0.46	0.22	0.30	0.89
GMD3	0.29	0.42	0.16	0.30	0.89
GMD5	0.31	0.44	0.19	0.31	0.88

The improvements were much stronger for the GMD3 configuration which also requires less computational time with respect to GMD5 but still has taken 4 or 5 times longer durations compared to DIA. The decrease in NBIAS values were

significant when GMD3 was chosen instead of GMD. This situation is also mentioned by Tolman (2010) in a way that, "adding quadruplets (going from GMD to GMD3) systematically reduces the errors for the deep water tests." The improvement on the systematic error was more significant for Gelendzhik buoy (Table 6.48) so that RMSEs was reduced by almost 40%.

Table 6.48 Comparison of RMSE for GMD , GMD3 and GMD5 for Gelendzhik Buoy

	RMSE	RMSEs	RMSEu	BIAS
GMD	0.45	0.29	0.34	0.26
GMD3	0.41	0.18	0.37	0.16
GMD5	0.42	0.22	0.36	0.20

If the systematic underestimation is present and this problem was tried to solve by tuning of parameters, such as in tuning of β_{max} or Cds coefficients, generally overall increase in the wave height values through the storm are observed (Figure 6.21).

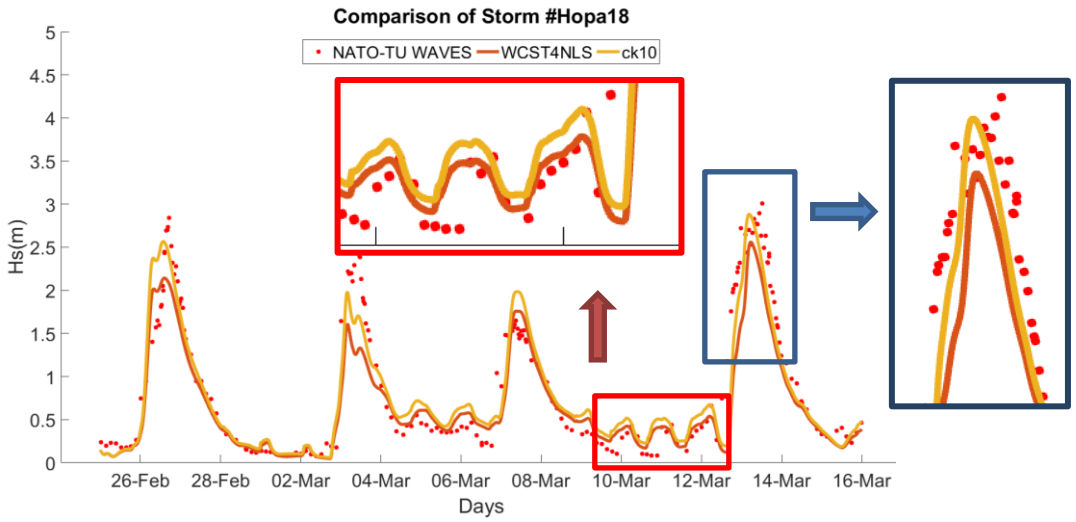

Figure 6.21 Comparison of Hopa 18 storm before and after tuning of $\boldsymbol{\beta_{max}}$

However, in the case of GMD to GMD3, increase of wave heights was focused at the peaks points which are the main source of the error (blue box in Figure 6.22). On the

other hand, for lower sea states the estimated wave heights were almost same for all GMD configurations (red box in Figure 6.22). Effects of such behavior can be also explained using scatter index values. Differences between the SI were not significant, which has proven that almost no unsystematic error was added to system while systematic error was decreasing.

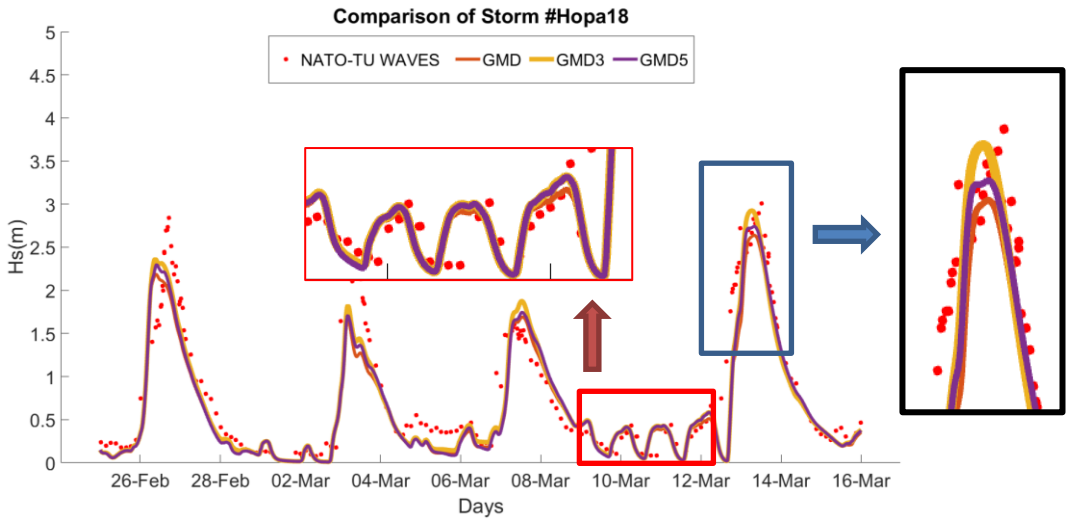

Figure 6.22 GMD,GMD3 and GMD5 comparison for Hopa 18 storm

The obtained GMD3 values are also compared to ST4NLS values for the same storms (Table 6.49). Even though GMD3 has showed better performance over DIA and GMD5, the statistical analysis results were slightly worse than DIA with nonlinear filter.

Table 6.49 ST4NLS and ST4GMD3 comparisons for the calibration storms

	NRMSE	NMAE	NBIAS	SI	R
ST4NLS	0.28	0.39	0.16	0.29	0.90
ST4GMD3	0.29	0.42	0.16	0.30	0.89

6.4 Sensitivity Analysis for WAVEWATCH III Model Regarding Physical Dimension

In this part, effects of using different bathymetries, time steps, propagation schemes, spatial and frequency resolutions are discussed.

6.4.1 Sensitivity to Frequency Resolution

Sensitivity to frequency resolution is mostly related with nonlinear wave-wave interactions. In WW3 model, quadruplet term is based on DIA approach which is originally calibrated with a resolution of γ =0.1. In most of the WW3 runs, γ was taken as 0.1 so that frequency resolution is in sync with DIA method. However, experience from the SWAN model predicted that higher frequency resolution might show better correlation with observed data in terms of statistical analysis. So, same trial of resolutions in SWAN model were also applied to WW3 model which are 40 frequency values with γ =0.0778 in and 50 frequency values with γ =0.0630. The obtained results can be seen in the Table 6.50.

Table 6.50 Sensitivity of model according to frequency resolution

	NRMSE	NMAE	NBIAS	SI	R
FI30	0.24	0.35	0.03	0.28	0.90
FI40	0.24	0.35	0.03	0.28	0.90
FI50	0.24	0.35	0.02	0.28	0.90

Change in frequency resolution has no significant effect on results. An improvement exists with increasing frequency resolution; however it is only 0.2% for γ =0.0778 and 0.4% for γ =0.0630 in terms of RMSE. Greatest change is observed in bias however it is in range of 1cm on average where wave height of selected storms

average is 1.09 m. γ =0.1 is an acceptable frequency resolution in WW3 application in Black Sea considering the increased computational cost.

6.4.2 Sensitivity to Spatial Resolution

WW3 model grid size is interrelated with time steps also. If finer spatial resolution is used, limit of the available time step also should be lowered in order to avoid instability conditions. However, this situation also increases the computational cost. In WW3 runs, coarser grid size are used with respect to 0.05˚ x 0.05˚ in SWAN model, in order to decrease the cost of the model.

In this section, finer SWAN resolution is applied to WW3 model with the same bathymetry as well. Time steps remain the same since Δt_{xy} is applicable to this bathymetry as well. It is also known that, the resolution of wind forcing is the main source of error in the wave models, especially in small and enclosed basins. (Menthashi et al.,2015).

Table 6.51 Effects of Spatial Resolution

	NRMSE	NMAE	NBIAS	SI	R
Coarse	0.24	0.35	0.03	0.28	0.90
Fine	0.25	0.35	0.02	0.29	0.89

Obtained results in Table 6.51 shows that, even though there are small changes in statistical values, spatial resolution have not provided significant effect on model output. The difference was observed in bias values which indicate the slight increase in wave heights when finer resolution was used (Figure 6.23).

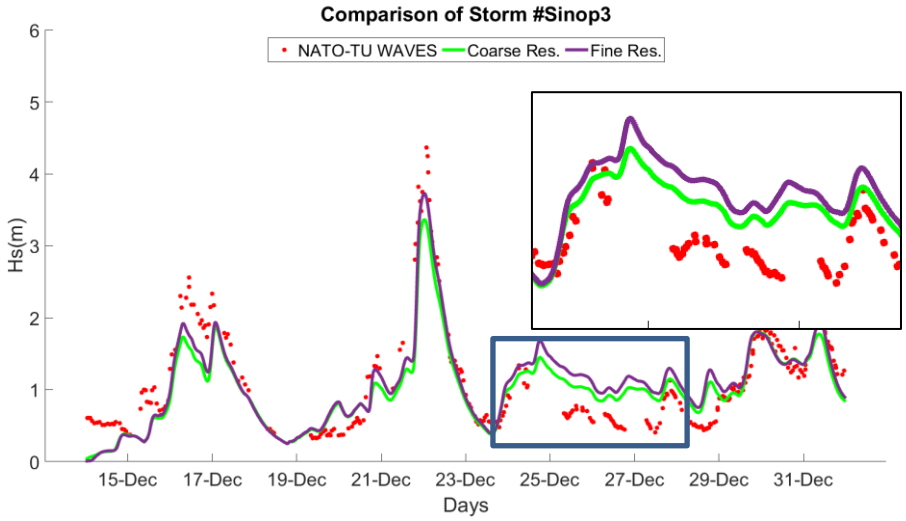

Figure 6.23 Effect Spatial Resolution (Coarse –Green line , Fine Purple line)

One of the reasons of change in wave height is based on the relationship of the usage of new wind-wave interactions parameters on a finer grid. Even though, both wind speeds are based on same wind field, WW3 model interpolates the wind data in order to obtain wind source for every grid, so the wind forcing resolution is increased. Since calibration of model was based on coarse grid size and the effect of wind-wave interaction term was increased (section 6.3.1), usage of this new parameter in finer resolution might have enhanced the effect on wave heights.

The spatial resolution used in WW3 runs was appropriate for Black Sea Region.

6.4.3 Sensitivity to Temporal Resolution

In this part, effects of changes of 4 time steps are considered. The considered time step combinations are given in Table 6.52 below.

Time stepping decision starts with calculation of the highest available Δt_{xy} given in Eq.6.1. After this criteria is ensured, other time steps are chosen according to

suggested ratios with respect to each other such as "$\Delta t_g$is usually two times or three times Δt_{xy} and two times Δt_k but Δt_k can be taken as equal to Δt_g in deep water". Similar general suggestions are applied in all time steps.

Table 6.52 Considered Time Step for Sensitive

	$\Delta t_g(s)$	$\Delta t_{xy}(s)$	$\Delta t_k(s)$	$\Delta t_s(s)$
Main TS	300	100	150	10
TS1	**150**	100	150	10
TS2	300	**200**	150	10
TS3	300	100	150	**30**
TS4	300	100	**300**	10
TS5	600	300	300	30

No significant change was observed when different time steps are used (Table 6.53). The best time step configurations for each individual storm also have varied according to statistical results. Moreover, the greatest improvement observed in analysis results was in NBIAS parameter which was in the order of 1cm observed for the coarse time step (TS5).

Table 6.53 Statistical Analysis for different time steps

	NRMSE	NMAE	NBIAS	SI	R
Main TS	0.247	0.352	0.035	0.288	0.897
TS1	0.248	0.353	0.038	0.289	0.896
TS2	0.247	0.352	0.035	0.288	0.897
TS3	0.247	0.352	0.035	0.288	0.897
TS4	0.248	0.353	0.035	0.289	0.896
TS5	0.247	0.352	0.027	0.288	0.897

According to these observations, the durations of time steps were not very effective in WW3 for Black Sea. However, in this study extreme time steps were not applied to WW3 such as Δt_s equals to Δt_g. In the presence of such cases, time stepping could have serious effects on model results.

6.4.4 Sensitivity to Spectral Directional Resolution

In order to understand the sensitivity of WW3 model to directional resolution, 10˚ directional resolution is applied to representative storms and compared to original 22.5˚ resolution.

The statistical analysis results indicate no significant change when the increased resolution of 10 ˚ was used. (Table 6.54)

Table 6.54 Sensitivity to Spectral Directional Resolution

	NRMSE	NMAE	NBIAS	SI	R
DIR16	0.244	0.349	0.031	0.284	0.898
DIR36	0.246	0.354	0.031	0.286	0.898

In the scope of this study only storm conditions are considered, which are specified as short term simulation. Effect of this directional resolution could be significant when the long terms simulations are considered as more change in directions of wind velocities are present.

6.4.5 Sensitivity to Propagation Scheme

In WW3 model four options are available for propagation which are no propagation (PR0), first order scheme (PR1), second order scheme (UNO), and third order scheme (UQ) (chapter 3.2.3.1). Users are also obliged to choose one of the

appropriate Garden Sprinkler Effect (GSE) alleviation switch. There is no alleviation option available for PR0 and PR1. Other GSE alleviation methods PR2 and PR3 can be used in combination with UNO and UQ.

In order to understand the effect of both propagation scheme and GSE alleviation methods, different combinations are applied which are given in Table 6.55 Options that are not available are shown with "-" in the Table 6.55 below.

Table 6.55 Available Propagation Schemes and GSE Alleviation Methods.

Prop Scheme\GSE Alleviation	PR2	PR3	No GSE A.
PR0	-	-	Not Applied
PR1	-	-	Applied
UNO	Not Applied	Applied	-
UQ	Applied	Applied	-

No changes were observed in wave parameters for the different propagation schemes except for PR1. However, the change related to first order scheme was not significant either (Table 6.56)

Table 6.56 Statistical Analysis for first order and third order propagation scheme

	NRMSE	NMAE	NBIAS	SI	R
UQ&PR3	0.244	0.349	0.031	0.284	0.898
PR1	0.240	0.347	0.034	0.280	0.899

In this study, it is concluded that propagation schemes are not an effective factor for Black Sea simulations.

6.4.6 Sensitivity to Wind Speed Interpolation in Temporal and Spatial Space

The spatial and temporal resolution of the defined WW3 model is finer than wind field resolutions of CFSR. So that, interpolation of wind data is needed to obtain wind speeds at each grid and each global time step. There are two methods available for interpolation on both temporal and spatial space which are linear interpolation (WNT1, WNX1) and quadratic interpolation (WNT2, WNX2). No interpolation option is also available but not used in this study. In regular WW3 runs linear interpolation option is considered (WNT1, WNX1). In order to investigate the sensitivity, 2 sets are also applied in WW3 which are quadratic interpolation in time and linear interpolation in space (WNT2, WNX1) and linear interpolation in time and quadratic interpolation in space (WNT1, WNX2). The statistical analysis are given in the Table 6.57 below.

Table 6.57 Sensitivity to Wind Speed Interpolation Methods

	NRMSE	NMAE	NBIAS	SI	R
WNT1 WNX1	0.244	0.349	0.031	0.284	0.898
WNT2 WNX1	0.243	0.349	0.025	0.284	0.899
WNX2 WNT1	0.244	0.349	0.031	0.284	0.898

The obtained results show of no change between the different spatial interpolations techniques. On the other hand, small improvement was observed when the quadratic interpolation was selected instead of linear interpolation method. However, this improvement was only %0.3 from NRMSE and R values. In conclusion, interpolation technique of wind speed is not a governing process that affects the error of WW3 in Black Sea.

6.5 WAVEWATCH III Model Discussions and Final Parameterization

The best couple of methods (ST4NLS) with CFSR data, obtained from the runs with recommended values, were calibrated using the chosen parameters in Table 6.58 below.

Table 6.58 After Calibration and Default Values of the Selected Parameters

Source Term	Parameter	Variable Name in WW3	ST4NLS (recommended values)	ST4NLS (values used in calibration set)
Wind- Wave Interaction	Z_{wnd}	ZWIND	10	10
	β_{max}	BETAMAX	1.52	1.75
	z_{α}	ZALP	0.06	0.04
	p_{in}	SINHTP	2	1.7
Swell	s	SWELLFPAR	1	1
	s1	SWELLF	0.8	0.8
	s2	SWELLF2	-0.018	-0.018
	s3	SWELLF3	0.015	0.015
Dissipation	C_{ds}^{sat}	SDSC2	-2.20E-05	-2.60E-05
	C_{cu}	SDSCUM	-0.4034	0
	Br	SDSBR	9.00E-04	1.20E-03
	C_{turb}	SDSC5	0	0
	Δ_{θ}	SDSDTH	80	100
Non-linear İnteractions (DIA)	λ	LAMBDA	0.25	0.25
	Cnl4	NLPROP	2.50E+07	2.50E+07
NLS Filter	α_{34}	A34	0.05	0.05
	C_{nlf}	FHFC	1.00E+10	1.00E+10
	S_{max}	DNM	0.25	0.25
	c_1	FC1	1.25	1.25
	c_2	FC2	1.5	1.5
	c_3	FC3	6	6

Many different calibration sets were tried and the analysis results of those calibrations showed that improvement after a certain point had shown a high convergence. The changes in the statistical analysis were almost reached to 0 as seen many times in the calibration process. The improvements of the statistical analysis

with respect to recommended parameterization are presented in the table below (Table 6.59) for the final parameterization given in Table (6.58)

Table 6.59 Statistical Analysis before and after calibration of WW3 model in Black Sea

	RMSE	RMSEs	RMSEu	NMAE	NBIAS	SI	R
ST4NLS	0.423	0.276	0.294	0.395	0.130	0.297	0.890
Calibrated	0.378	0.199	0.322	0.382	-0.028	0.308	0.890

The most observed problem in Black Sea basin was the systematic underestimation of the wave heights. The default parameters were not accurate enough for Black Sea basin because calibrations of those parameters were done according to global scale and for ocean waves. According to Table 6.59, % decrease in RMSEs and NBIAS values were obtained which was the proof that systematic underestimation problem was solved. In the solution of this problem, governing term was the wind-wave interaction term ($S_{in}(k,\theta)$) and the two dominant parameters in this term was found to be β_{max} (maximum value of the wind wave coupling) and z_α (wave age shift to account for gustiness). The wind speeds in closed basins were not as high as in ocean scale so that a small amplification in wind-wave interaction term is needed in order to represent the local effect of the growth term due to wind forcing. Such conclusion was also achieved by Mentashi et al.(2015) in another closed basin, Mediterranean sea.

The increase in the wave heights can be observed from the scatter plot of the wave heights before and after calibration (Figure 6.24).

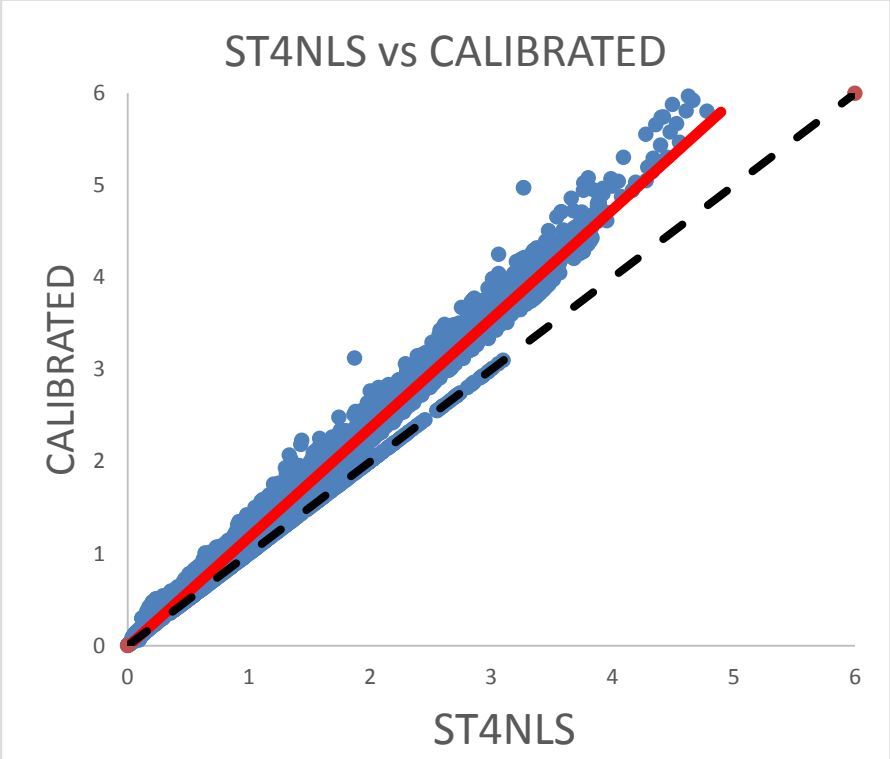

Figure 6.24 Scatter plot of ST4NLS before and after calibration

Calibrations of dissipation parameters and nonlinear interaction parameters have importance for the accuracy of the model and the reduction of the remaining error for the Black Sea.

Dissipation parameters have to be in sync with the wind-wave interaction term so that, accurate wave heights could be obtained throughout events. These interactions between terms are also important in order to solve the problems such as missing the general trend of the model, decreasing the deterioration in model output after strong overestimation or underestimation and increasing the sensitivity of model against quick changes in storm characteristics. White capping dissipation parameters also have crucial importance in the better performance of the guesses at the peak wave heights. Because one reason of behind missing the peak wave heights is that whitecapping formulations are based on the bulk of the data, their performance have

not been considered for the peak wave heights (Cavaleri, L., 2009) Thus, error at peak points cannot be solved fully with the present method however calibration of the parameters could result in better approximations.

Nonlinear interaction term has also a significant effect on the guesses at peak points. According to Cavaleri, 2009 DIA approximation leads to too-wide energy distribution both in frequency and direction spaces which results in as decreases in the wind and reflects on the wave heights as well. This is one of the many reasons behind the missing the peak wave heights in extreme condition. So that, better approximations are needed in order reflect the real world conditions in numerical models. Until better solutions are going to be implemented, the errors in DIA method could be tried to be compensated by calibration of the parameters for the study basin

After calibration, better approximate results were obtained for the peak wave heights as well which can be seen from Figure 6.25

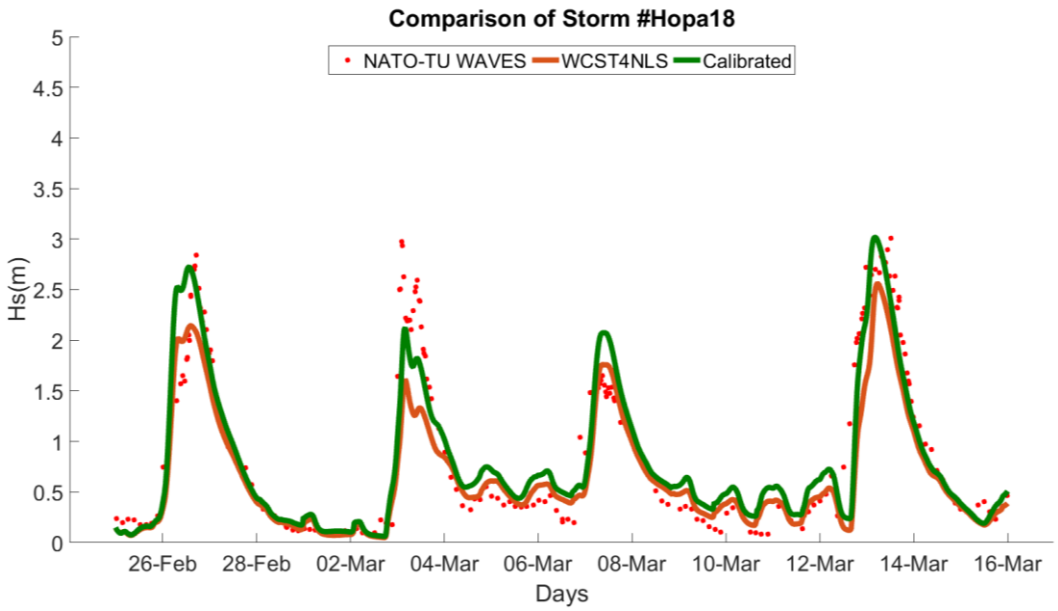

Figure 6.25 Times series graph before and after calibration

Swell dissipation term was only effective in small number storms, however in general this effect was not reflected on the overall results for 54 events. This shows that swells of Black Sea was not significantly effective in the modeled storms of this study.

Applications of nonlinear filter to the high frequency end of the spectrum in WW3 also was not effective on the results.

Sensitivity of the WW3 model was also considered and it was observed that, selected resolutions have shown enough accuracy. Moreover, model is not highly sensitive to frequency, directions, spatial and temporal resolution as mentioned in previous sections.

Calibrated WW3 model is highly applicable for the extreme conditions in Black Sea basin, considering the obtained statistical results and capabilities of the model.

CHAPTER 7

CONCLUSION AND FUTURE RECOMMENDATIONS

The main aim of this study was to evaluate the performance of the third generation wave models in Black Sea basin and to calibrate both models for extreme conditions.

The results from Chapter 5 and Chapter 6 has shown that, both models have performed considerably well in Black Sea basin. The best available combination of each model (CKD in SWAN, CST4NLS in WW3) have obtained over 88% of correlation between the buoy data even before the calibration process. Other statistical results are presented in the Table 7.1 for best cases before calibration.

Table 7.1 CFSR winds with KD and ST4NLS

	RMSE	**RMSEs**	**RMSEu**	**NMAE**	**NBIAS**	**SI**	**R**
SCKD	0.45	0.31	0.29	0.43	0.15	0.31	0.88
ST4NLS	0.42	0.28	0.29	0.39	0.13	0.30	0.89

The first conclusion of the study is on the selection of wind field data since both models performed significantly better using CFSR wind data as evident in the best alternatives. Even though CFSR wind data has lower spatial resolution, it represents

the wind climate of the extreme events significantly better compared to ECMWF data set. The coarser temporal resolution and the lower wind speeds of ECMWF has resulted in lower correlation with buoy data and high systematic error.

Table 7.1 has shown that preliminary performance of WW3 is better in every statistical analysis, however the differences are not very significant. The difference is in general due to different formulations that are used for wind-wave interaction term and dissipation term. Selected method in SWAN is based on WAM Cycle 3 formulations, while ST4 in WW3 uses the modified version of WAM Cycle 4.ST1 & DIA approach of WW3 can be directly compared to KD of SWAN since mostly same formulations (based on Komen et al.,1984) are used in both models. As expected, obtained results are quite similar (Table 7.2). However, BIAS values of SWAN model is less than WW3. One reason for this result is that Cnl coefficients were set to 3e7 in SWAN and 2.78e7 in WW3 According to table below, SWAN has shown better performance with WAM Cycle 3 physics compared to WW3.

Table 7.2 WAM Cycle 3 based Physics for Both Model

	RMSE	**RMSEs**	**RMSEu**	**NMAE**	**NBIAS**	**SI**	**R**
SCKD	0.45	0.31	0.29	0.43	0.15	0.31	0.88
WCST1NL1	0.49	0.37	0.29	0.47	0.21	0.32	0.88

On the other hand, significantly different performance was observed when both model have used WAM Cycle 4 physics (Table 7.3). Comparison between WCST3NL1 and SCJD shows that, WW3 has shown a significantly better performance compared to SWAN when Janssen (1989,1991) wind wave interaction terms were used.

Table 7.3 WAM Cycle 4 based Physics for Both Model

	RMSE	**RMSEs**	**RMSEu**	**NMAE**	**NBIAS**	**SI**	**R**
WCST3NL1	0.44	0.31	0.29	0.42	0.16	0.30	0.89
SCJD	0.50	0.28	0.39	0.47	0.07	0.36	0.86

However, when Table 7.2 and Table 7.3 were considered together it was seen that, this change of performance was not because of the ST3 method used in WW3 application. While WW3 results of both applications were consistent, strong deterioration was observed between JD and KD in SWAN model. This conclusion is also supported by Lalbeharry (2002) who states that SWAN using WAM3 physics performs better than SWAN using WAM4 physics for extreme storm conditions. This difference between models can be better shown by the scatter plots (Figure 7.1) given for first 10 storm in Gelendzhik (when the major extreme storms were observed). On figure 7.1(I) the slight increased wave height in ST3 can be observed compared to ST1. The scatter index is very low between two methods of same model. On the other hand, more scatter is observed in SWAN implementation as shown in figure 7.1(II). Especially, for the wave heights smaller than 2 meters, the difference between in SCKD and SCJD were much higher.

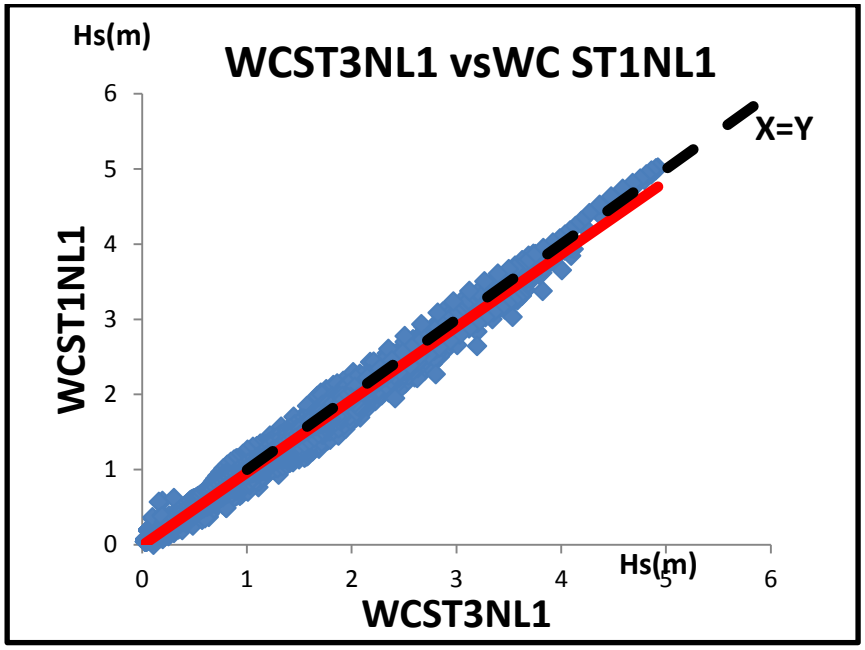
Hs(m)
WCST3NL1 vsWC ST1NL1
X=Y
WCST1NL1
0
1
2
3
4
5
6
Hs(m)
WCST3NL1

(I)

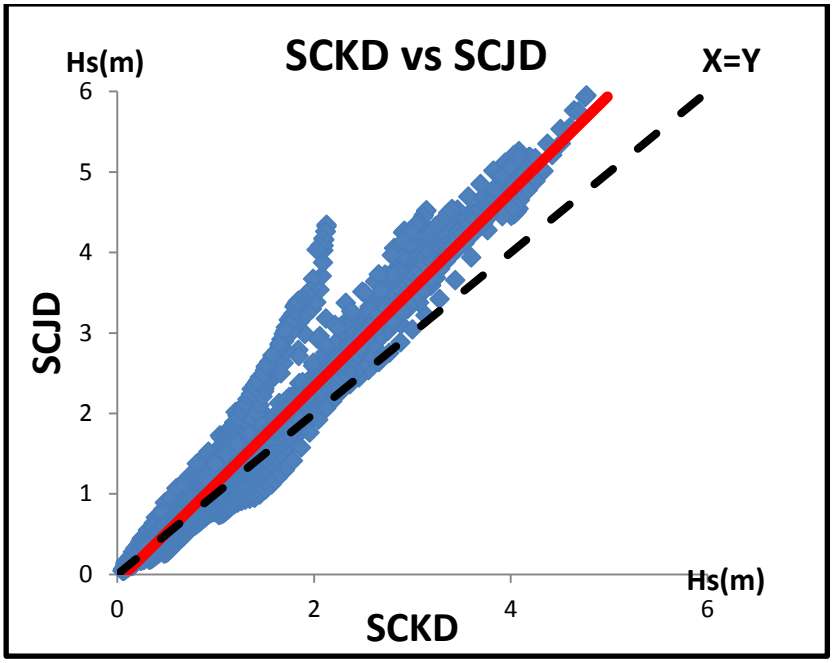
Hs(m)
SCKD vs SCJD
X=Y
SCJD
0
1
2
3
4
5
6
Hs(m)
SCKD

(II)

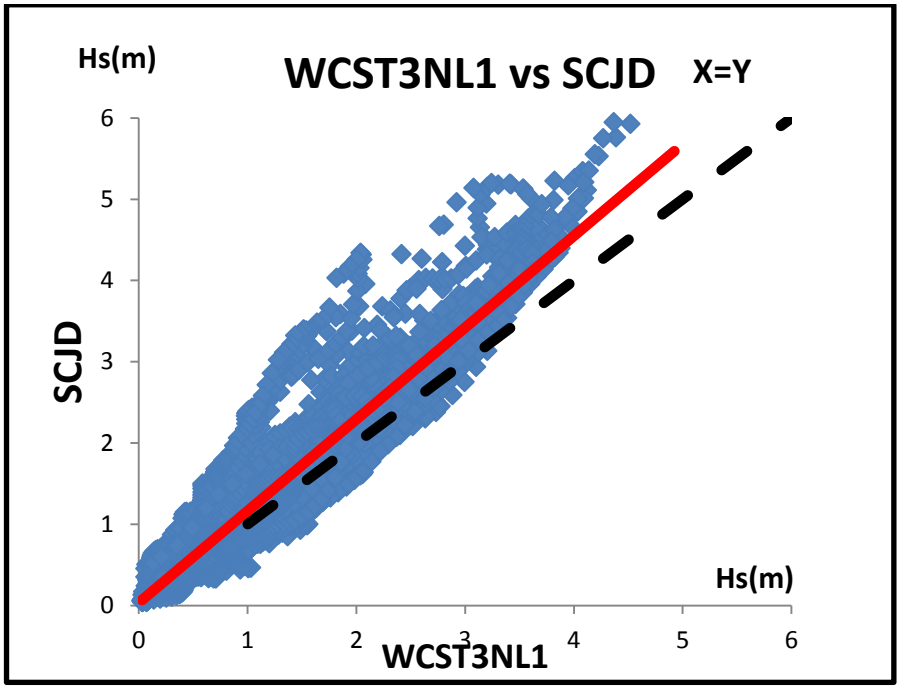

(III)

Figure 7.1 Scatter plots of significant wave height of WCST1NL1 and WCST3NL1 (I), SCJD and SCKD (II), and SCJD and WCST3NL1 (III), for first 10 storms in Gelendzhik

Scatter plots in Figure 7.1 (II) and (III) show the increased inconsistency of SWAN model using WAM Cycle 4 physics. It can be concluded that the SWAN implementation of WAM4 is not consistent with the actual implementation of WAM4 as also stated by Lalbeharry et al.(2009). One of the key reasons of this problem was z_α parameters, which was found to be one of the governing parameters in WW3 for ST3 and ST4 models. However, these approaches are not available in SWAN model. Moreover, the non-dimensional growth term (β_{max}) in Janssen(1991) approach was fixed to 1.2 in SWAN model which was found to be inadequate for the wind fields in Black Sea basin as shown in Chapter 6. Moreover, β_{max}=1.2 was also found to be inadequate by Rascle and Ardhuin (2013) and they calibrated this parameter as β_{max}=1.33 for CFSR winds and β_{max}=1.52 for ECMWF

winds on global scale. As the value of β_{max} cannot be changed in SWAN model, significant lack of performance exist and this appears to be the biggest drawback of SWAN model for extreme cases in Black Sea basin .

The direct comparison of SWAN and WW3 models considering the source terms was possible up to this point. Even though the physics applied in ST4 method was based on WAM Cycle 4, the direct comparison was not possible since the modifications in ST4 did not have equivalence in SWAN model.

Overall, similar problems were observed in both models even if the best available approaches for Black Sea were used to model extreme events. The most significant problem was the systematic underestimation of wave parameters and missing the peak wave heights. Calibrations of the model were carried out in order to overcome these problem. The results of SWAN and WW3 after calibration are presented in Table 7.4

Table 7.4 Statistical Analysis of SWAN and WW3 before and after calibration

	RMSE	**RMSEs**	**RMSEu**	**NMAE**	**NBIAS**	**SI**	**R**
SWAN Bef. Calib.	0.45	0.31	0.29	0.43	0.15	0.31	0.88
SWAN Calibrated	0.39	0.26	0.28	0.37	0.04	0.29	0.87
WW3 Bef. Calib.	0.42	0.28	0.29	0.39	0.13	0.30	0.89
WW3 Calibrated	0.38	0.20	0.32	0.38	-0.03	0.31	0.89

It has been observed that, the improvement made on wind-wave interaction term in WW3 had a stronger positive impact on reduction of systematic error caused by underestimation. Since there are more tunable parameters in wind wave interaction term in WW3, the calibration has become more effective in WW3 model compared to SWAN model. This is also a fundamental issue with the SWAN model that effect the total energy of the system. This difference can be observed from 1-D spectra of

calibrated models (Figure 7.5) which are obtained for Hopa12 storm in 22.12.1994 at 18:00:00 when observed Hs was around 2.5 meters

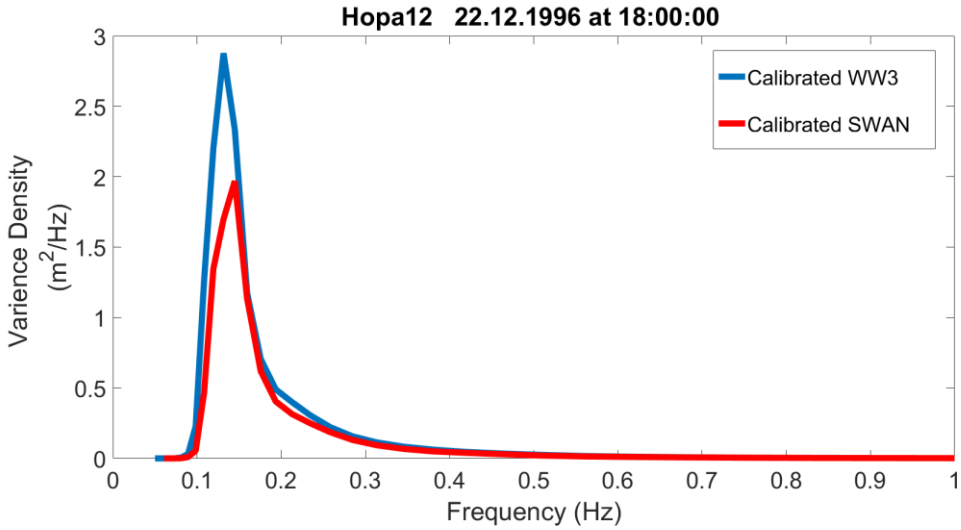

Figure 7.2 1-D spectra taken from Sinop2 03.12.1994 06:00:00.

Missing the peak wave heights was the second major problem in implementation of wave models in Black Sea. BIAS values of calibrated SWAN and WW3 considering over 10000 data can be seen separately in Figure 7.6 and 7.7

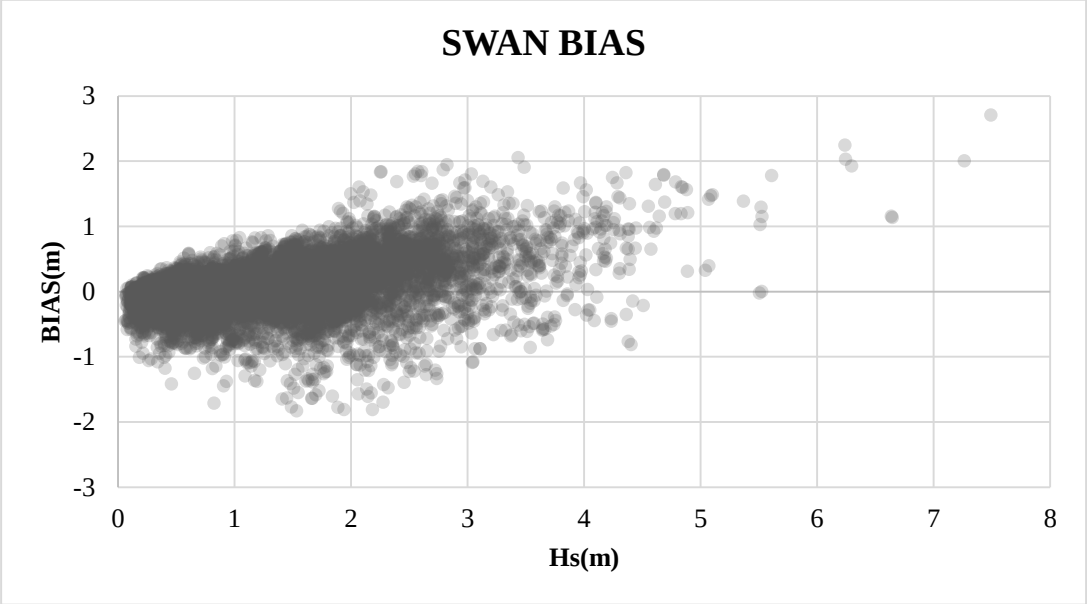

Figure 7.3 Bias distribution of SWAN model

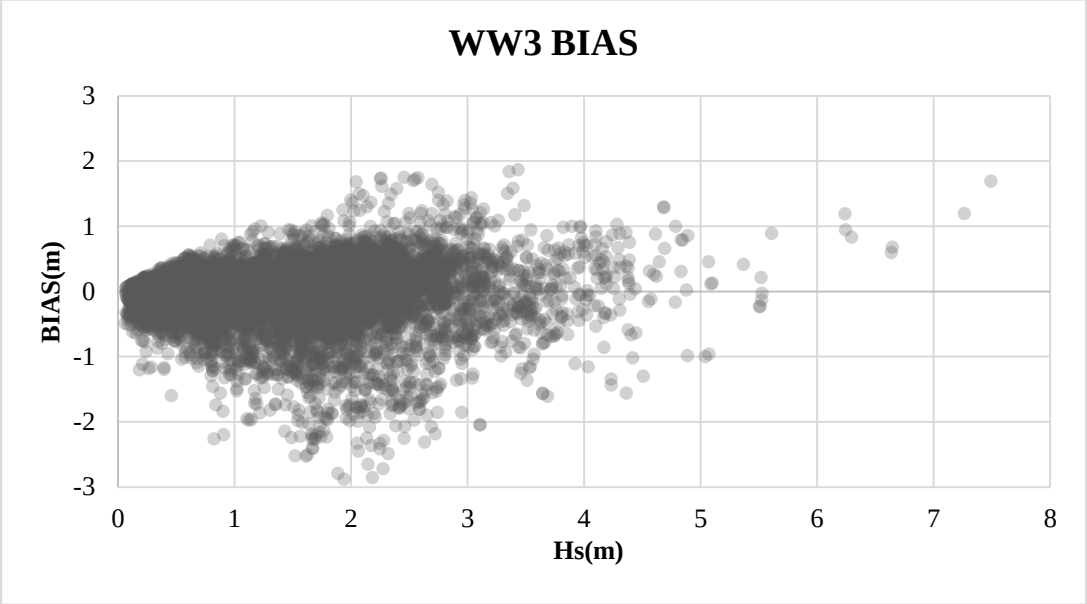

Figure 7.4 Bias distribution of WW3 model

According to Figures 7.3 and 7.4 above, WW3 has modeled peak wave heights significantly better, while SWAN has almost 3 meter bias in the most extreme conditions. It is also seen that, BIAS values do not significantly change according to wave heights in WW3, while BIAS in SWAN model increases with increasing wave

heights. Moreover, effect of calibration on peak wave heights can be observed from Figure 7.5 and Figure 7.6

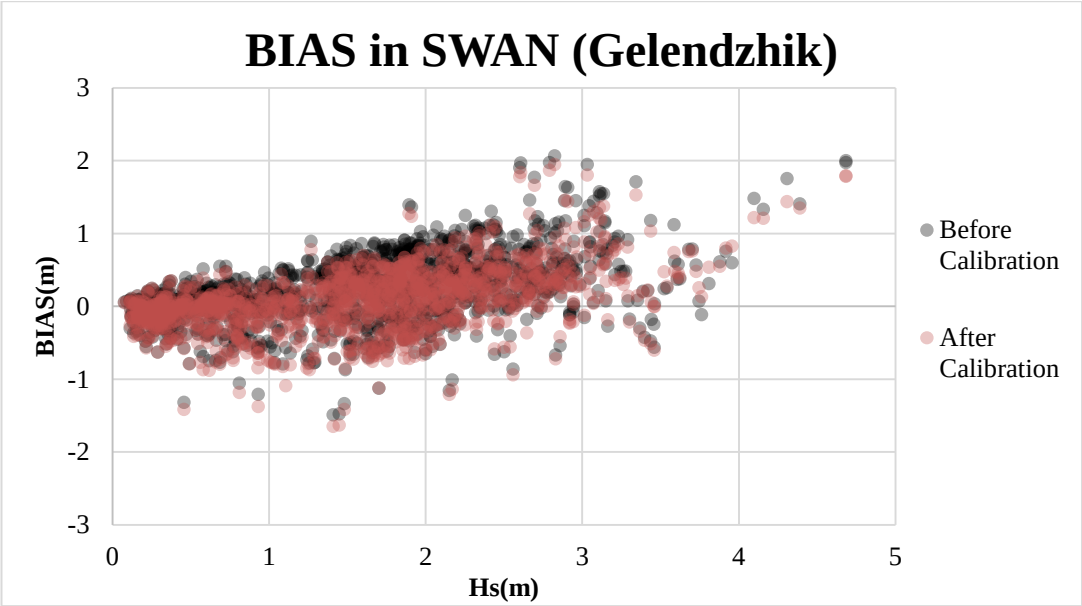

Figure 7.5 Effect of Calibration in BIAS considering Gelendzhik Buoy in SWAN

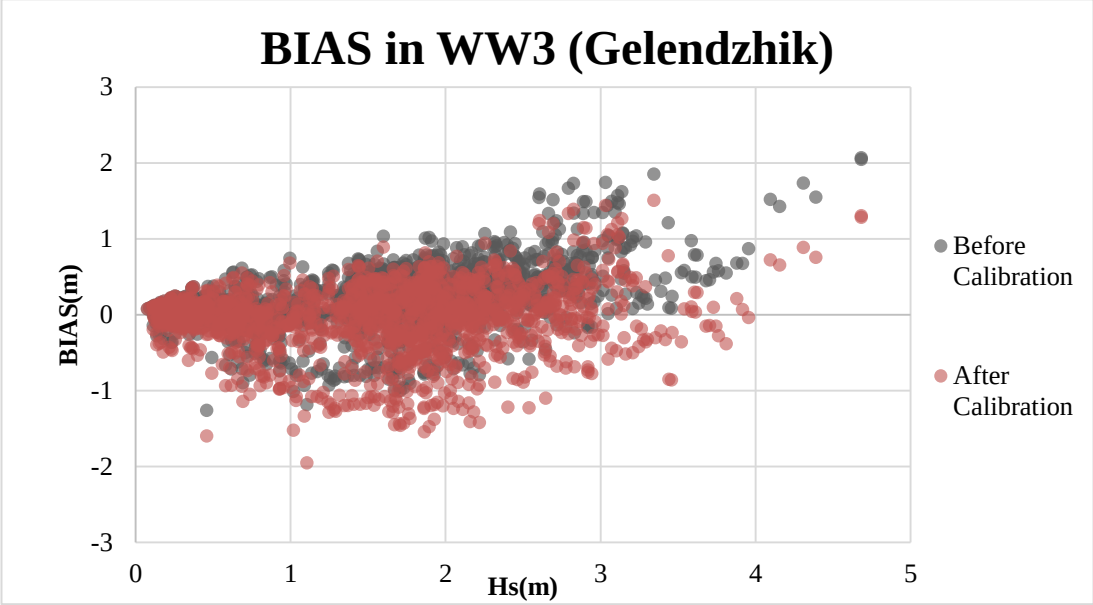

Figure 7.6 Effect of Calibration in BIAS considering Gelendzhik Buoy in WW3

Improvement in peak guesses was more significant in WW3 compared to improvement of SWAN model. The positive impact the results were also based on better representation of the wind-wave interactions term by WW3.

Although improvements were observed, the problem of missing the peak wave heights was still significantly present even after the calibration. There can be other possible reasons as it cannot be solved the calibration effort. The first reason is the available wind field data. The wind fields are also model outputs of atmospheric models which are usually applied with data assimilations such as smoothing of data. This processlower the peak wind speeds that results in lower estimations of wave heights (Cavaleri, 2009). It is also stated by Cavaleri and Sclova(2006) that one of the reason of the underestimation of the wave parameters could be the lower wind speed estimated by atmospheric models in closed basins. Another reason stated by Cavaleri(2009) is that, energy transfer from the atmosphere to waves depends directly on the air density ρ_a (Eq.3.6) nevertheless variability of ρ_a is not considered in the wave models. Moreover, most of the generated empirical coefficients are based on field tests which are usually carried out on lower wind speeds, thus in general the extreme wind conditions are not considered in wave models (Cavaleri, 2009).

Another main source of uncertainity in wave models has been caused by the nonlinear wave wave interaction terms. However, “the current state of the art in wave modeling via third-generation models can be significantly impaired by the lack of fidelity in the DIA”. (Young and Van Vledder, 1993;Resio and Perrie,2008). DIA is the most preferred nonlinear interaction term physics even though it has some significant deficiencies. (Van Vledder, 2000). The main reason of the popularity of DIA is the low computational cost of application compared to exact solution. However DIA is not able to provide a consistent representation for Snl when compared to the full integral solution. (Resio and Perrie, 2008). The main reason of deficiencies in DIA method is because the calibration of DIA was only based on the JONSWAP spectrum and field observation carried out by Hasselmann et al. (1985).

Moreover, according to Resio and Perrie (2008), these errors cannot be tuned out since DIA is based on a reduced form of the Boltzmann integral that does not include the majority of the actual interactions within a spectrum. It was observed that higher proportionality coefficients have resulted in lower dissipation of energy which was reflected as better accuracy in statistical analysis in SWAN. However, application of the exact solution to the selected events in Black Sea should be completed in order to determine the best performance on nonlinear interactions.

In conclusion, it was found that modeled wave heights were highly sensitive to wind forcing fields which was one of main sources of the unsystematic error. Therefore, calibration of the wind-wave interaction term had the most crucial effect on results using the available wind sources in this study. Depending on the experience gained on from this study, starting point of wind wave modelling should be wind-wave interaction term. The implicit scheme of SWAN models on geographical space has shown a faster convergence, however explicit scheme of WW3 was found to be more accurate for the solution of deep water wave terms. The obtained results were also location dependent, wave models have shown different behavior for different buoys. For instance, more significant underestimation of wave height in Sinop gauge was observed for the same model configurations.

In this study, general aim was to show to performance of the third generation wave models in Black Sea basin and obtain a set of parameters that can be applicable for the majority of the extreme events while quantifying the observed errors in models. In accordance with this aim, it has been found that best representation of the actual cases based on the measured wave heights are obtained using WAVEWATCH III model with CFSR wind fields. The selected source terms are based on the ST4 physics and DIA approach developed by Ardhuin et al. (2010) and Hasselmann et al. (1985), respectively.

For the future of the study, obtained spectra can be investigated in a detailed way for better understanding of the physical process rather than analysis based on basic wave parameters. Directional distributions can be analyzed considering 2-d spectra.

The effect of short fetches especially on the wave growth and the boundary conditions of closed basins can be implemented in a more effective way. This conclusion is also supported by Akpınar and Leon(2015) who proposed that spatial resolutions in the order of 4 or 5 minutes may be too coarse to accurately predict the wave growth at short fetches such as in Black Sea and has suggested application using unstructured meshes for those basins. Also regional conditions should be considered for more accurate results since the results were location dependent.

Moreover, performance of calibrated models can be considered for long term hind cast studies. Satellite altimeter data can be included in the validation process.

Additional sensitivity analysis for every considered space using various resolutions should be carried out for better understanding of the model behavior. Also, additional time stepping combinations can be considered for WW3 model. Moreover, uncertainty analysis should be carried out in order to reduce the both systematic and unsystematic errors.

REFERENCES

Akpinar, A., & Kömürcü, M. Ihsan. (2013). Assessment of wave energy resource of the Black Sea based on 15-year numerical hindcast data. *Applied Energy*, *101*, 502–512. http://doi.org/10.1016/j.apenergy.2012.06.005

Akpinar, A., & Ponce de León, S. (2016). An assessment of the wind re-analyses in the modelling of an extreme sea state in the Black Sea. *Dynamics of Atmospheres and Oceans*, *73*, 61–75. http://doi.org/10.1016/j.dynatmoce.2015.12.002

Akpinar, A., Özger, M., Bekiroglu, S., & Komurcu, M. I. (2014). Performance evaluation of parametric models in the hindcasting of wave parameters along the south coast of Black Sea. *Indian Journal of Geo-Marine Science*, *43*(6), 899–914. http://doi.org/10.1007/s00773-013-0226-1

Akpinar, A., van Vledder, G. P., Kömürcü, M. I., & Özger, M. (2012). Evaluation of the numerical wave model (SWAN) for wave simulation in the Black Sea. *Continental Shelf Research*, *50–51*, 80–99. http://doi.org/10.1016/j.csr.2012.09.012

Alves, J. H. G. M., & Banner, M. L. (2003). Performance of a Saturation-Based Dissipation-Rate Source Term in Modeling the Fetch-Limited Evolution of Wind Waves. *Journal of Physical Oceanography*, *33*, 1274–1298. http://doi.org/10.1175/1520-0485(2003)033<1274:POASDS>2.0.CO;2

Ardhuin, F., Bertotti, L., Bidlot, J.-R., Cavaleri, L., Filipetto, V., Lefevre, J.-M., & Wittmann, P. (2007). Comparison of wind and wave measurements and models in the Western Mediterranean Sea. *Ocean Engineering*, *34*(3–4), 526–541. http://doi.org/10.1016/j.oceaneng.2006.02.008

Ardhuin, F., Rogers, E., Babanin, A. V., Filipot, J.-F., Magne, R., Roland, A., … Collard, F. (2010). Semiempirical Dissipation Source Functions for Ocean Waves. Part I: Definition, Calibration, and Validation. *Journal of Physical Oceanography*, *40*(9), 1917–1941. http://doi.org/10.1175/2010JPO4324.1

Arinaga, R. A., & Cheung, K. F. (2012). Atlas of global wave energy from 10 years of reanalysis and hindcast data. *Renewable Energy*, *39*(1), 49–64. http://doi.org/10.1016/j.renene.2011.06.039

Arkhipkin, V. S., Gippius, F. N., Koltermann, K. P., & Surkova, G. V. (2014). Wind waves in the Black Sea: Results of a hindcast study. *Natural Hazards and Earth System Sciences*, *14*(11), 2883–2897. http://doi.org/10.5194/nhess-14-2883-2014

Aydoĝan, B., Ayat, B., & Yüksel, Y. (2013). Black Sea wave energy atlas from 13 years hindcasted wave data. *Renewable Energy*, *57*, 436–447. http://doi.org/10.1016/j.renene.2013.01.047

Banner, M. L. (2010). Refined Source Terms in WAVEWATCH III with Wave Breaking and Sea Spray Forecasts, (2003), 1–6.

Barnett, T. P. (1968). On the generation, dissipation, and prediction of ocean wind waves. Journal of Geophysical Research, 73(2), 513-529.

Battjes, J. A., & Janssen, J. P. F. M. (1978). Energy loss and set-up due to breaking of random waves. *Coastal Engineering Proceedings*, *1*(16)

Bernardino, M., Salvação, N., & Rusu, L. (2012). Assessment of wind and wave simulations for an enclosed sea using satellite data. Maritime Engineering and Technology, 467.

Bidlot, J., Janssen, P., Abdalla, S., & Hersbach, H. (2007). A revised formulation of ocean wave dissipation and its model impact.

Bolaños-Sanchez, R., Sanchez-Arcilla, A., & Cateura, J. (2007). Evaluation of two atmospheric models for wind-wave modelling in the NW Mediterranean. *Journal of Marine Systems*, *65*(1–4 SPEC. ISS.), 336–353. http://doi.org/10.1016/j.jmarsys.2005.09.014

Booij, N., Ris, R. C., & Holthuijsen, L. H. (1999). A third-generation wave model for coastal regions: 1. Model description and validation. *Journal of geophysical research: Oceans*, *104*(C4), 7649-7666.

Bouws, E., & Komen, G. J. (1983). On the balance between growth and dissipation in an extreme depth-limited wind-sea in the southern North Sea.Journal of Physical Oceanography, 13(9), 1653-1658.

Cavaleri, L., & Rizzoli, P. M. (1981). Steadily during the last years stimulating the development approach was not of many different methods for the evaluation of the wind In addition to the reasons specified above , upon the continuous

Cavaleri, L. , Bertotti, L., Bidlot, J., Sclavo, M., Mork, G., Barstow, S., & Athanassoulis, G. (1999). Hindcast and calibration of the wave conditions in the Black Sea Proc. of Int. Conf. on Wind and Wave Climate of the Mediterranean and the Black Sea, Proc. Int. Conf. M., MEDCOAST 99, Antalya, Turkey (1999), pp. 139–151

Cavaleri, L., & Bertotti, L. (2006). The improvement of modelled wind and wave fields with increasing resolution. *Ocean Engineering*, *33*(5–6), 553–565. http://doi.org/10.1016/j.oceaneng.2005.07.004

Cavaleri, L., & Sclavo, M. (2006). The calibration of wind and wave model data in the Mediterranean Sea. *Coastal Engineering*, *53*(7), 613–627. http://doi.org/10.1016/j.coastaleng.2005.12.006

Cavaleri, L., Alves, J. H. G. M., Ardhuin, F., Babanin, A., Banner, M., Belibassakis, K., … Young, I. (2007). Wave modelling - The state of the art. *Progress in Oceanography*, *75*(4), 603–674. http://doi.org/10.1016/j.pocean.2007.05.005

Cavaleri, L. (2009). Wave Modeling—Missing the Peaks. *Journal of Physical Oceanography*, *39*(11), 2757–2778. http://doi.org/10.1175/2009JPO4067.1

Chai, T., & Draxler, R. R. (2014). Root mean square error (RMSE) or mean absolute error (MAE)?–Arguments against avoiding RMSE in the literature. Geoscientific Model Development, 7(3), 1247-1250.

Chawla, A., Spindler, D. M., & Tolman, H. L. (2013). Validation of a thirty year wave hindcast using the Climate Forecast System Reanalysis winds. *Ocean Modelling*, *70*, 189–206. http://doi.org/10.1016/j.ocemod.2012.07.005

Chelton, D. B., & Freilich, M. H. (2005). Scatterometer-Based Assessment of 10-m Wind Analyses from the Operational {ECMWF} and {NCEP} Numerical Weather Prediction Models. *Monthly Weather Review*, *133*(2), 409–429. http://doi.org/10.1175/MWR-2861.1

Cherneva, Z., Andreeva, N., Pilar, P., Valchev, N., Petrova, P., & Guedes Soares, C. (2008). Validation of the WAMC4 wave model for the Black Sea. *Coastal Engineering*, *55*(11), 881–893. http://doi.org/10.1016/j.coastaleng.2008.02.028

Chiara, G. De, & Abdalla, S. (2014). Active Techniques for Wind and Wave Observations :

Chiara, G. De, Janssen, P., Hersbach, H., & Bormann, N. (2012). Assimilation of scatterometer winds at ECMWF Scatterometer data at ECMWF, (November), 1–14.

Demirbilek, Z., & Linwood Vincent, C. (2006). Water wave mechanics. *Coastal Engineering Manual*, *1100*(June), 1–121. http://doi.org/10.1080/01634372.2013.794031

Ergin, A. (2009). *Coastal Engineering*. METU Press

European Centre for Medium-Range Weather Forecasts. (2008). ECMWF Wave Model. *IFS Documentation - Cy33e1*, (June), 1–65. Retrieved from http://www.ecmwf.int/research/ifsdocs/CY33r1/WAVES/IFSPart7.pdf

Ewing, J. A. (1971). A numerical wave prediction method for the North Atlantic Ocean. Deutsche Hydrografische Zeitschrift, 24(6), 241-261.

Fallis, A. . (2013). Swan Scientific and Technical Documentation. *Journal of Chemical Information and Modeling*, *53*(9), 1689–1699. http://doi.org/10.1017/CBO9781107415324.004

Galabov, V. (2013). on the Wave Energy Potential of the Bulgarian Black Sea Coast. *Sgem.Org*. Retrieved from http://sgem.org/sgemlib/spip.php?article3104

Gōda, Y. (2000). *Random seas and design of maritime structures*. World scientific.

Gramstad, O., & Babanin, A. (2016). **The g**eneralized kinetic equation as a model for the nonlinear transfer in third-generation wave models. *Ocean Dynamics*, *66*(4), 509–526. http://doi.org/10.1007/s10236-016-0940-4

Hanson, J. L., & Phillips, O. M. (2001). Automated Analysis of Ocean Surface Directional Wave Spectra. *Journal of Atmospheric and Oceanic Technology*, *18*(2), 277-293. http://doi.org/10.1175/15200426(2001)018<0277:AAOOSD>2.0.CO;2

Hasselmann, D., Bösenberg, J., Dunckel, M., Richter, K., Grünewald, M., & Carlson, H. (1986). Measurements of wave-induced pressure over surface gravity waves. In Wave *Dynamics and Radio Probing of the Ocean Surface*(pp. 353-368). Springer US.

Hasselmann, K. (1962). On the non-linear energy transfer in a gravity wave spectrum., (1960).

Hasselmann, K., Barnett, T. P., Bouws, E., Carlson, H., Cartwright, D. E., Enke, K., ... & Meerburg, A. (1973). Measurements of wind-wave growth and swell decay during the Joint North Sea Wave Project (JONSWAP). Deutches Hydrographisches Institut.

Hasselmann, K., Sell, W., Ross, D. B., & Müller, P. (1976). A parametric wave prediction model. Journal of Physical Oceanography, 6(2), 200-228.

Hersbach, H. (n.d.). The Usage of Scatterometer Data at ECMWF Assessment of EARS ASCAT data, 1–19.

Hogrefe, C., Hao, W., Civerolo, K., Ku, J. Y., & Sistla, G. (2006). Exploring approaches to integrate observations and CMAQ simulations for improved air quality forecasts. CMAS Conference, October 16 – 18, 2006

Janssen, P. (2004). The interaction of ocean waves and wind. Cambridge University Press.

Janssen, P., & Bidlot, J. R. (2003). Part VII: ECMWF wave-model documentation. IFS documentation cycle CY23r4, 48.

Kalantzi, G. D., Gommenginger, C., Srokosz, M., Centre, N. O., & Kingdom, U. (2009). Assessing the Performance of the Dissipation Parameterizations in WAVEWATCH III Using Collocated Altimetry Data. *Journal of Physical Oceanography*, *39*(11), 2800–2819. http://doi.org/10.1175/2009JPO4182.1

Kanbua, W. (n.d) Third Generation Ocean Wave Model. Retrieved August 29, 2016, from http://www.marine.tmd.go.th/wamdoc/thirdwave.html

Korres, G., Papadopoulos, A., Katsafados, P., Ballas, D., Perivoliotis, L., & Nittis, K. (2011). A 2-year intercomparison of the WAM-Cycle4 and the WAVEWATCH-III wave models implemented within the Mediterranean Sea. *Mediterranean Marine Science*, *12*(1), 129–152. http://doi.org/10.12681/mms.57

Kortcheva, A., Dimitrova**, M., &** Galabov, V. (2009). A wave prediction system for real time sea state forecasting in Black Sea, *1*, 1–16.

Kowalewski, M. J. (1994, October). Quality and statistics: total quality management. Astm.

L. Mentaschi, Besio, G., Cassola, F., & Mazzino, A. (2013). Improving wave model validation based on {RMSE}. *13th International Workshop on Wave Hindcasting and Forecasting and Coastal Hazards*.

Lalbeharry, R. (2002). Comparison of the performances of three state-of-the-art ocean wave models in extreme storm cases. *Int. Workshop on Wave Hindcasting and Forecasting*, (1). Retrieved from http://scholar.google.com/scholar?hl=en&btnG=Search&q=intitle:COMPARISON+OF+THE+PERFORMANCES+OF+THREE+STATE-OF-THE-ART+OCEAN+WAVE+MODELS+IN+EXTREME+STORM+CASES#0

Lalbeharry, R., Bigio, R., Thomas, B. R., & Wilson, L. (2009). Numerical Simulation of Extreme Waves During the Storm of 20-22 January 2000 Using Winds Generated by the CMC Weather Prediction Model. *Atmosphere-Ocean*, *47*(1), 99–122. http://doi.org/10.3137/OC292.2009

Leckler, F., Ardhuin, F., Filipot, J. F., & Mironov, A. (2013). Dissipation source terms and whitecap statistics. *Ocean Modelling*, *70*, 62–74. http://doi.org/10.1016/j.ocemod.2013.03.007

Lefevre, J.-M., Stefanescu, S. E., & Makin, V. (2004). Implementation of New Source Terms in a Third Generation Wave Model. *3rd WWH*, (Patente de EE.UU. WO2002089373A1). Retrieved from ftp://www.wmo.ch/Documents/PublicWeb/amp/mmop/documents/JCOMM-TR/J-TR-29-WH8/Papers/E4.pdf\npapers2://publication/uuid/370D82E5-7A5B-423F-A5F6-B6B0137C1EFD

Melorose, J., Perroy, R., & Careas, S. (2015). No Title No Title. *Statewide Agricultural Land Use Baseline 2015*, *1*(July). http://doi.org/10.1017/CBO9781107415324.004

Mentaschi, L., Besio, G., Cassola, F., & Mazzino, A. (2015). Performance evaluation of Wavewatch III in the Mediterranean Sea. *Ocean Modelling*, *90*, 82–94. http://doi.org/10.1016/j.ocemod.2015.04.003

Miles, J. W. (1957). On the generation of surface waves by shear flows.*Journal of Fluid Mechanics*, *3*(02), 185-204.

Mitsuyasu, H. (1968). On the growth of the spectrum of wind-generated waves. 1. Rep. Res. Inst. Appl. Mech., Kyushu Univ, 16, 251-264.

Mitsuyasu, H. (1969). On the growth of the spectrum of wind-generated waves. 2. Rep. Res. Inst. Appl. Mech., Kyushu Univ, 16(55), 459-482.

Özhan, E., & Abdalla, S. (1999). Turkish Coast Wind and Deep Water Wave Atlas. Applied Project Report, Middle East Technical University, Civil Engineering Dept., Ocean Eng. Research Center., Ankara.

Padilla-Hernandez, R., Perrie, W., & Toulany, B. (2004). An intercomparison of modern operational wave models. *Workshop on Wave*, *2*(3), 2–6. Retrieved from http://scholar.google.com/scholar?hl=en&btnG=Search&q=intitle:INTERCOMPARISON+OF+MODERN+OPERATIONAL+WAVE+MODELS#1

Pallares, E., Sánchez-Arcilla, A., & Espino, M. (2014). Wave energy balance in wave models (SWAN) for semi-enclosed domains-Application to the Catalan coast. *Continental Shelf Research*, *87*, 41–53. http://doi.org/10.1016/j.csr.2014.03.008

Pe, S. (2006). Palladium (Ii) Complexes With Bidentate (N , S) or Terdentate (C , N , S) - Ferrocenyl Ligands in Allylic Alkylation of Cinnamyl Acetate, (Ii), 6.

Perrie, W., & Resio, D. T. (2009). A Two-Scale Approximation for Efficient Representation of Nonlinear Energy Transfers in a Wind Wave Spectrum. Part II: Application to Observed Wave Spectra. *Journal of Physical Oceanography*, 39(10), 2451–2476. http://doi.org/10.1175/2009JPO3947.1

Phillips, O. M. (1957). On the generation of waves by turbulent wind. J. Fluid Mech, 2(5), 417-445.

Pierson, W. J. (1955). Wind generated gravity waves. Advances in geophysics,2, 93-178.

Ponce de León, S., & Guedes Soares, C. (2008). Sensitivity of wave model predictions to wind fields in the Western Mediterranean sea. *Coastal Engineering*, *55*(11), 920–929. http://doi.org/10.1016/j.coastaleng.2008.02.023

Rascle, N., & Ardhuin, F. (2013). A global wave parameter database for geophysical applications. Part 2: Model validation with improved source term parameterization. *Ocean Modelling*, *70*, 174–188. http://doi.org/10.1016/j.ocemod.2012.12.001

Rascle, N., & Ardhuin, F. (2013). A global wave parameter database for geophysical applications. Part 2: Model validation with improved source term parameterization. *Ocean Modelling*, *70*, 174–188. http://doi.org/10.1016/j.ocemod.2012.12.001

Rogers, W. E., Hwang, P. A., & Wang, D. W. (2003). Investigation of wave growth and decay in the SWAN Model: three regional-scale applications*.*Journal of Physical Oceanography*, *33*(2), 366-389.

Rusu, E., Rusu, L., & Soares, C. G. (2006). Prediction of Extreme Wave Conditions in the Black Sea With Numerical Models. *9th International Workshop on Wave Hindcasting and Forecasting*.

Rusu, E. (2009). Wave energy assessments in the Black Sea. Journal of marine science and technology, 14(3), 359-372.

Rusu, L., Bernardino, M., & Soares, C. G. (2014). Wind and wave modelling in the Black Sea. *Journal of Operational Oceanography*, *7*(1), 5–20. http://doi.org/10.1080/1755876X.2014.11020149

Saha, S., Moorthi, S., Pan, H. L., Wu, X., Wang, J., Nadiga, S., … Goldberg, M. (2010). The NCEP climate forecast system reanalysis. *Bulletin of the American Meteorological Society*, *91*(8), 1015–1057. http://doi.org/10.1175/2010BAMS3001.1

Sandwell, D. T., Smith, W. H., Sichoix, L., & Frey, H. V. (2001). Global bathymetric prediction for ocean modeling and marine geophysics.

Schwartz, M. (Ed.). (2006). Encyclopedia of coastal science. Springer Science & Business Media.

Signell, R. P., Carniel, S., Cavaleri, L., Chiggiato, J., Doyle, J. D., Pullen, J., & Sclavo, M. (2005). Assessment of wind quality for oceanographic modelling in semi-enclosed basins. *Journal of Marine Systems*, *53*(1–4), 217–233. http://doi.org/10.1016/j.jmarsys.2004.03.006

Snyder, R. L., Dobson, F. W., Elliott, J. A., & Long, R. B. (1981). Array measurements of atmospheric pressure fluctuations above surface gravity waves. Journal of Fluid Mechanics, 102, 1-59.

Spatiale, O. (2012). Dissipation parameterizations in spectral wave models and general suggestions for improving on today ' s wave models Fabrice Ardhuin e, (June), 25–27.

Swan Team. (2009). USER MANUAL SWAN - Cycle III version 41.01A. *Cycle*, 126.

Taylor, K. E. (2001). in a Single Diagram. *Journal of Geophysical Research*, *106*(D7), 7183–7192. http://doi.org/10.1029/2000JD900719

Thomas, T. J., & Dwarakish, G. S. (2015). Numerical wave modelling – A review. *Aquatic Procedia*, *4*(Icwrcoe), 443–448. http://doi.org/10.1016/j.aqpro.2015.02.059

Tolman, H. L. (2008). Optimum discrete interaction approximations for wind waves. Part 3: Generalized multiple DIAs, (269).

Tolman, H. L. (2014). User manual and system documentation of WAVEWATCH III version 4.18. *NOAA / NWS / NCEP / MMAB Technical Note*, *151*(316), 97. http://doi.org/10.3390/ijerph2006030011

Tolman, H., & Krasnopolsky, V. (2004). Nonlinear interactions in practical wind wave models. *... of 8Th International Workshop on Wave ...*. Retrieved from ftp://www.wmo.int/Documents/PublicWeb/amp/mmop/documents/JCOMM-TR/J-TR-29-WH8/Papers/E1.pdf

Ueno, K., & Kohno, N. (2004). The development of the third generation wave model MRI-III for operational use. *... Int. Workshop on Wave Hindcasting and ForecastingG*. Retrieved from ftp://ftp.wmo.int/Documents/PublicWeb/amp/mmop/documents/JCOMM-TR/J-TR-29-WH8/Papers/G2.pdf

Van Vledder, G. P., & Akpınar, A. (2015). Wave model predictions in the Black Sea: Sensitivity to wind fields. *Applied Ocean Research*, *53*, 161–178. http://doi.org/10.1016/j.apor.2015.08.006

Wu, J. (1982). Wind-stress coefficients over sea surface from breeze to hurricane. *Journal of Geophysical Research: Oceans*, *87*(C12), 9704-9706

Zheng, K., Sun, J., Guan, C., & Shao, W. (2016). Analysis of the global swell and wind sea energy distribution using WAVEWATCH III. *Advances in Meteorology*, *2016*(1996). http://doi.org/10.1155/2016/8419580

APPENDICES

A. EXAMPLE WAVE MODEL INPUT DETAIL FILES

A1. SWAN Model Input

```
                    Execution started at 20160119.180953
                    ------------------------------------

                                  SWAN
                    SIMULATION OF WAVES IN NEAR SHORE AREAS
                             VERSION NUMBER 41.01A
                    ------------------------------------


 $*************HEADING*************************************
PROJECT 'Blacksea' 'G6'
$ PURPOSE OF TEST: the wind generation on Black Sea
$   --|-------------------------------------------------------------
|--
     $    | This SWAN input file is for the test run of swan with
wind  |
$   | generation on Black Sea.                                     |
$***********MODEL INPUT*************************************
MODE NONSTATIONARY TWODimensional
COORDinates SPHErical
CGRID REGular 27. 40.5 0. 15. 7. 300 140 CIRcle 36 0.05 1. 40
 Resolution in sigma-space: df/f =  0.0778


INPgrid BOTtom REGular 27. 40.5 0. 300 140 0.05 0.05
```

```
READinp BOTtom -1. '3min_topex_blacksea.bot' 3 0 FREE

INPgrid WInd REGular 26.875 39.809 0. 48 26 0.312 0.313 &

                NONSTATionary 19970314:000000 1. hr 19970422:000000

READinp WInd 1. 'gelen_6_cfsr.wnd' 2 2 FREE

 **  Heading lines file gelen_6_cfsr.wnd **

 -> 19970314 0

 -> 1

    GEN3 KOMEN cds2=2.36e-5 stpm=3.02e-3 AGROW a=0.0015

  WCAPping KOM cds2=2.36e-5 stpm=3.02e-3 powst=2 delta=1

QUADrupl iquad=2 lambda=0.25

BREaking CON alpha=1.0 gamma=0.73

FRICTION JONSWAP cfjon=0.038

PROP BSBT

$************ OUTPUT REQUESTS *************************

$***buoy locations***

POINT 'Sinop' 35.0867, 42.1233

POINT 'Hopa' 41.3833, 41.4233

POINT 'Gelen' 37.978333, 44.5075

TABLE 'Hopa' HEADER 'W_Hopa6.dat' Time XP YP DEPTH HS TM01 DIR WIND
OUTPUT 19970314:000000 30 MI

TABLE 'Gelen' HEADER 'W_Gelendzhik6.dat' Time XP YP DEPTH HS TM01
DIR WIND  OUTPUT 19970314:000000 30 MI


 TABLE 'Sinop' HEADER 'W_Sinop6.dat' Time XP YP DEPTH HS TM01 DIR
WIND  OUTPUT 19970314:000000 30 MI

TABLE 'Hopa' HEADER 'E_Hopa6.dat' Time XP YP PROPAGAT GENWIND DISSIP
DISWCAP  OUTPUT 19970314:000000 30 MI

TABLE 'Gelen' HEADER 'E_Gelendzhik6.dat' Time XP YP PROPAGAT GENWIND
DISSIP DISWCAP  OUTPUT 19970314:000000 30 MI

TABLE  'Sinop'  HEADER  'E_Sinop6.dat'  Time  XP  YP  PROPAGAT  GENWIND
DISSIP DISWCAP  OUTPUT 19970314:000000 30 MI

GROUP 'blacksea' SUBG 1 300 1 140

BLOCK 'blacksea' NOHEAD 'HS6.mat' LAY 4 HS  OUTPUT 19970314:000000 3
HR

BLOCK   'blacksea'   NOHEAD   'WIND6.mat'   LAY   4   WIND     OUTPUT
19970314:000000 3 HR
```

```
BLOCK 'blacksea' NOHEAD 'DIR6.mat' LAY 4 DIR  OUTPUT 19970314:000000
3 HR

TEST 1,0

COMPUTE NONSTat 19970314:000000 15 MI 19970422:000000

 Time of computation ->  19970314.001500      in sec:        900.

------------------------------------------------------------------

                  COMPUTATIONAL PART OF SWAN

------------------------------------------------------------------


 Gridresolution       : MXC              301 MYC             141
                      : MCGRD          42442
                      : MSC               41 MDC              36
                      : MTC             3744
                      : NSTATC             1 ITERMX            1
 Propagation flags    : ITFRE              1 IREFR             1
 Source term flags    : IBOT               1 ISURF             1
                      : IWCAP              1 IWIND             3
                      : ITRIAD             0 IQUAD             2
                      : IVEG               0 ITURBV            0
                      : IMUD               0
 Spatial step         : DX       0.5000E-01 DY      0.5000E-01
 Spectral bin         : df/f     0.7777E-01 DDIR    0.1000E+02
 Physical constants   : GRAV     0.9810E+01 RHO     0.1025E+04
 Wind input           : WSPEED   0.0000E+00 DIR     0.0000E+00
 Tail parameters      : E(f)     0.4000E+01 E(k)    0.2500E+01
                      : A(f)     0.5000E+01 A(k)    0.3000E+01
 Accuracy parameters  : DREL     0.1000E-01 NPNTS   0.9950E+02
                      : DHABS    0.5000E-02 CURVAT  0.5000E-02
                      : GRWMX    0.1000E+00
 Drying/flooding      : LEVEL    0.0000E+00 DEPMIN  0.5000E-01
 The Cartesian convention for wind and wave directions is used
 Scheme for geographic propagation is BSBT
 Scheme geogr. space  : PROPSC             1 ICMAX             3
```

```
 Scheme spectral space: CSS      0.5000E+00 CDD     0.5000E+00
 Current is off
 Quadruplets          : IQUAD             2
                      : LAMBDA   0.2500E+00 CNL4    0.3000E+08
                      : CSH1     0.5500E+01 CSH2    0.8330E+00
                      : CSH3    -0.1250E+01
 Maximum Ursell nr for Snl4 :    0.1000E+02
 Triads is off
 JONSWAP (`73)        : GAMMA    0.3800E-01
 Vegetation is off
 Turbulence is off
 Fluid mud is off
 W-cap Komen (`84)    : EMPCOF (CDS2):   0.2360E-04
 W-cap Komen (`84)    : APM (STPM)   :   0.3020E-02
 W-cap Komen (`84)    : POWST        :   0.2000E+01
 W-cap Komen (`84)    : DELTA        :   0.1000E+01
 W-cap Komen (`84)    : POWK         :   0.1000E+01
 Snyder/Komen wind input
 Battjes&Janssen (`78): ALPHA    0.1000E+01 GAMMA   0.7300E+00
 Set-up is off
 Diffraction is off
 Janssen (`89,`90)    : ALPHA    0.1000E-01 KAPPA   0.4100E+00
 Janssen (`89,`90)    : RHOA     0.1280E+01 RHOW    0.1025E+04

 1st and 2nd gen. wind: CF10     0.1880E+03 CF20    0.5900E+00
                      : CF30     0.1200E+00 CF40    0.2500E+03
                      : CF50     0.2300E-02 CF60   -0.2230E+00
                      : CF70     0.0000E+00 CF80   -0.5600E+00
                      : RHOAW    0.1249E-02 EDMLPM  0.3600E-02
                      : CDRAG    0.1230E-02 UMIN    0.1000E+01
                      : LIM_PM   0.1300E+00
Time of computation ->  19970314.003000      in sec:       1800.
```

A2. WAVEWATCH III Model Input

```
                  *** WAVEWATCH III Grid preprocessor ***

             ==============================================

 Comment character is '$'

 Grid name : BLACK SEA

 Spectral discretization :

-------------------------------------------------

      Number of directions        :  16

      Directional increment (deg.):  22.5

      First direction       (deg.):   0.0

      Number of frequencies       :  30

      Frequency range        (Hz) :   0.0500-0.7932

      Increment factor            :   1.100

 Model definition :

-------------------------------------------------

      Dry run (no calculations)   :  ---/NO

      Propagation in X-direction  :  YES/--

      Propagation in Y-direction  :  YES/--

      Refraction                  :  YES/--

      Current-induced k-shift     :  ---/NO

      Source term calc. and int.  :  YES/--

 Time steps :

-------------------------------------------------

      Maximum global time step      (s) :  300.00

      Maximum CFL time step X-Y     (s) :  100.00

      Maximum CFL time step k-theta (s) :  150.00

      Minimum source term time step (s) :   10.00

 Preprocessing namelists ...

 Preprocessing namelists finished.

 Linear input (C&M-R 82) (default values) :

-------------------------------------------------
```

```
      CLIN                          :   80.00
      Factor for fPM in filter      :    1.00
      Factor for fh in filter       :    0.50
 Wind input (WAM 4+) (default values) :
-------------------------------------------------
      minimum Charnock coeff.       :    0.0095
      betamax                       :    1.520
      power of cos. in wind input   :    2.000
      z0max                         :    0.000
      zalp                          :    0.006
      Height of input wind (m)      :   10.00
      wind stress sheltering        :    1.000
      swell attenuation param.      :    1
      swell attenuation factor      :    0.800
      swell attenuation factor2     :   -0.018
      swell attenuation factor3     :    0.015
      critical Reynolds number      : 100000.0
      swell attenuation factor5     :    1.200
      swell attenuation factor6     :    0.000
      swell attenuation factor7     :    230000.000
      ratio of z0 for orb. & mean   :    0.040
 Nonlinear interactions (DIA) (default values) :
-------------------------------------------------
      Lambda                        :    0.25
      Prop. constant                : 0.250E+08
      kd conversion factor          :    0.75
      minimum kd                    :    0.50
      shallow water constants       :    5.50  0.83 -1.25
 HF filter based on Snl (default values) :
-------------------------------------------------
      a34 (lambda)                  :    0.050   0.0050
      Prop. constant                : 0.100E+11
      maximum relative change       :    0.250
```

```
      filter constants            :    1.25  1.50  6.00
 Dissipation (Ardhuin et al. 2010) (default values) :
 -------------------------------------------------
      SDSC2, SDSBCK, SDSCUM           : -0.220E-04    0.000E+00  -
0.403E+00
      Power of k in mean k        :    0.50
  Bottom friction (JONSWAP) (default values) :
 -------------------------------------------------
      gamma                       : -0.0670
  Surf breaking (B&J 1978) (default values) :
 -------------------------------------------------
      alpha                       :   1.000
      gamma                       :   0.730
      Using Hmax/d ratio only.
  Triad interactions not defined.
  Bottom scattering not defined.
  Propagation scheme :
 -------------------------------------------------
      Type of scheme (structured) : 3rd order UQ + GSE averaging
                                    (default values)
      CFLmax depth refraction     :    0.700
      Averaging area factor Cg    :    1.50
      Averaging area factor theta :    1.50
  Miscellaneous (user def. values) :
 -------------------------------------------------
  Spectral output on full grid (default values) :
 -------------------------------------------------
      Second order pressure at K=0:   0   1  15
      Spectrum of Uss             :   0   1  30
      Frequency spectrum          :   0   1  30
  Miscellaneous (user def. values) :
 -------------------------------------------------
      Ice concentration cut-offs  :    0.50  0.50
```

```
    Dynamic source term integration scheme :
       Xp                       (-) :    0.150
       Xr                       (-) :    0.100
       Xfilt                    (-) :    0.050
    Wave field partitioning :
       Levels                   (-) :  100
       Minimum wave height      (m) :    0.050
       Wind area multiplier     (-) :    1.700
       Cut-off wind sea fract.  (-) :    0.333
       Combine wind seas             :  YES/--
       Number of swells in fld out :    5
    Miche-style limiting wave height :
       Hs,max/d factor          (-) :    1.600
       Hrms,max/d factor        (-) :    1.131
       Limiter activated             :  YES/--



  Equivalent namelists ...
  &SLN1 CLIN =  80.0, RFPM =  1.00, RFHF =  0.50 /
  &SIN4 ZWND = 10.0, ALPHA0 = 0.00950, Z0MAX = 0.00000, BETAMAX =
1.52000,
        SINTHP = 2.00000, ZALP = 0.00600, TAUWSHELTER = 1.00000,
SWELLFPAR = 1,
        SWELLF = 0.80000, SWELLF2 =-0.01800, SWELLF3 = 0.01500,
SWELLF4 = 100000.0,
        SWELLF5 = 1.20000, SWELLF6 = 0.00000, SWELLF7 =   230000.00,
Z0RAT = 0.04000 /
  &SIN4 ZWND =  0.0, ALPHA0 =
  &SNL1 LAMBDA =  0.250, NLPROP = 0.250E+08, KDCONV =  0.750, KDMIN
=  0.500,
        SNLCS1 =  5.500, SNLCS2 =  0.833, SNLCS3 =  -1.250 /
  &SNLS A34 = 0.050, FHFC = 0.1000E+11,  DNM = 0.250,
        FC1 = 1.250,  FC2 = 1.500,  FC3 = 6.000 /
```

```
  &SDS4  SDSC1  =    0.0000E+00,  SDSC2  =  -0.2200E-04,  SDSCUM  =  -
0.4034E+00,
        SDSC4  =     0.1000E+01,  SDSC5  =     0.0000E+00,  SDSC6  =
0.3000E+00,
        WNMEANP =0.50, FXPM3 =4.00,FXFM3 =9.90,
        SDSBINT =  0.3000E+00, SDSBCK =  0.0000E+00, SDSABK = 1.500,
SDSPBK = 4.000,
        SDSHCK = 1.50, SDSBR =   0.9000E-03, SDSSTRAIN = 0.000,
        SDSBR2 = 0.80, SDSP = 2.00, SDSISO = 2, SDSCOS =2.0, SDSDTH
= 80.0,
        SDSBRF1 =  0.50, SDSBRFDF = 0,
        SDSBM0 =  1.00, SDSBM1 = 0.00, SDSBM2 = 0.00, SDSBM3 = 0.00,
SDSBM4 = 0.00,
,       WHITECAPWIDTH = 0.30, SDSLFGEN =  0.00, SDSHFGEN =  0.00 /
  &SBT1 GAMMA = -0.6700E-01 /
  &SDB1 BJALFA =  1.000, BJGAM =  0.730, BJFLAG = .TRUE. /
  &PRO3 CFLTM = 0.70, WDTHCG = 1.50, WDTHTH = 1.50 /
  &UNST UGOBCAUTO =  T, UGOBCDEPTH = -10.000
,       EXPFSN =  T,EXPFSPSI =  F,EXPFSFCT =  F,IMPFSN =  F
  &OUTS P2SF  = 0, I1P2SF = 1, I2P2SF = 15,
        US3D  = 0, I1US3D =  1, I2US3D = 30,
        E3D   = 0, I1E3D  =  1, I2E3D  = 30,
        TH1MF = 0, I1TH1M =  1, I2TH1M = 30,
        STH1MF= 0, I1STH1M=  1, I2STH1M= 30,
        TH2MF = 0, I1TH2M =  1, I2TH2M = 30,
        STH2MF= 0, I1STH2M=  1, I2STH2M= 30 /
  &MISC  CICE0  =  0.500,  CICEN  =  0.500,  LICE  =         0.0,  PMOVE  =
0.500,
        XSEED = 1.000, FLAGTR = 0, XP = 0.150, XR = 0.100, XFILT =
0.050
        IHM =   100, HSPM = 0.050, WSM = 1.700, WSC = 0.333, FLC =
.TRUE.
        NOSW =  5, FMICHE = 1.600, RWNDC = 1.000,
        FACBERG = 1.0, GSHIFT =   0.000E+00 /
  Equivalent namelists finished.
  The spatial grid:
```

```
------------------------------------------------
      Grid type                    : rectilinear
      Coordinate system            : spherical
      Index closure type           : none
      Dimensions                   :    151      71
      Increments           (deg.)  :    0.1000    0.1000
      Longitude range      (deg.)  :   27.0000   42.0000
      Latitude range       (deg.)  :   40.5000   47.5000

      Bottom level unit            :    20
      Limiting depth           (m) :    0.10
      Minimum depth            (m) :    0.20
      Scale factor                 :    1.00
      Layout indicator             :     1
      Format indicator             :     1
      File name                    : blacksea_coarse.bot
      Sub-grid information         : Not available.
      Mask information             : From file.
      Mask unit                    :    30
      Layout indicator             :     1
      Format indicator             :     1
      File name                    : blacksea_coarse.mask
 Input boundary points :
------------------------------------------------
      No boundary points.
 Excluded points :
------------------------------------------------
      Number of excluded points    :    14
 Legend :
------------------------------
   0 : Land point
   1 : Sea point
   2 : Active boundary point
```

```
   3 : Excluded point
 Output boundary points :
-------------------------------------------------
      No boundary points.
 Writing model definition file ...
Filling 3D look-up table for SIN4. please wait
 Summary grid statistics :
-------------------------------------------------
      Number of longitudes      :       151
      Number of latitides       :        71
      Number of grid points     :     10721
      Number of sea points      :      5440 (50.7%)
      Number of input b. points :         0
      Number of land points     :      5267
      Number of excluded points :        14
 End of program
=========================================
        WAVEWATCH III Grid preprocessor
```

B. USER INTERFACE SCREENSHOTS

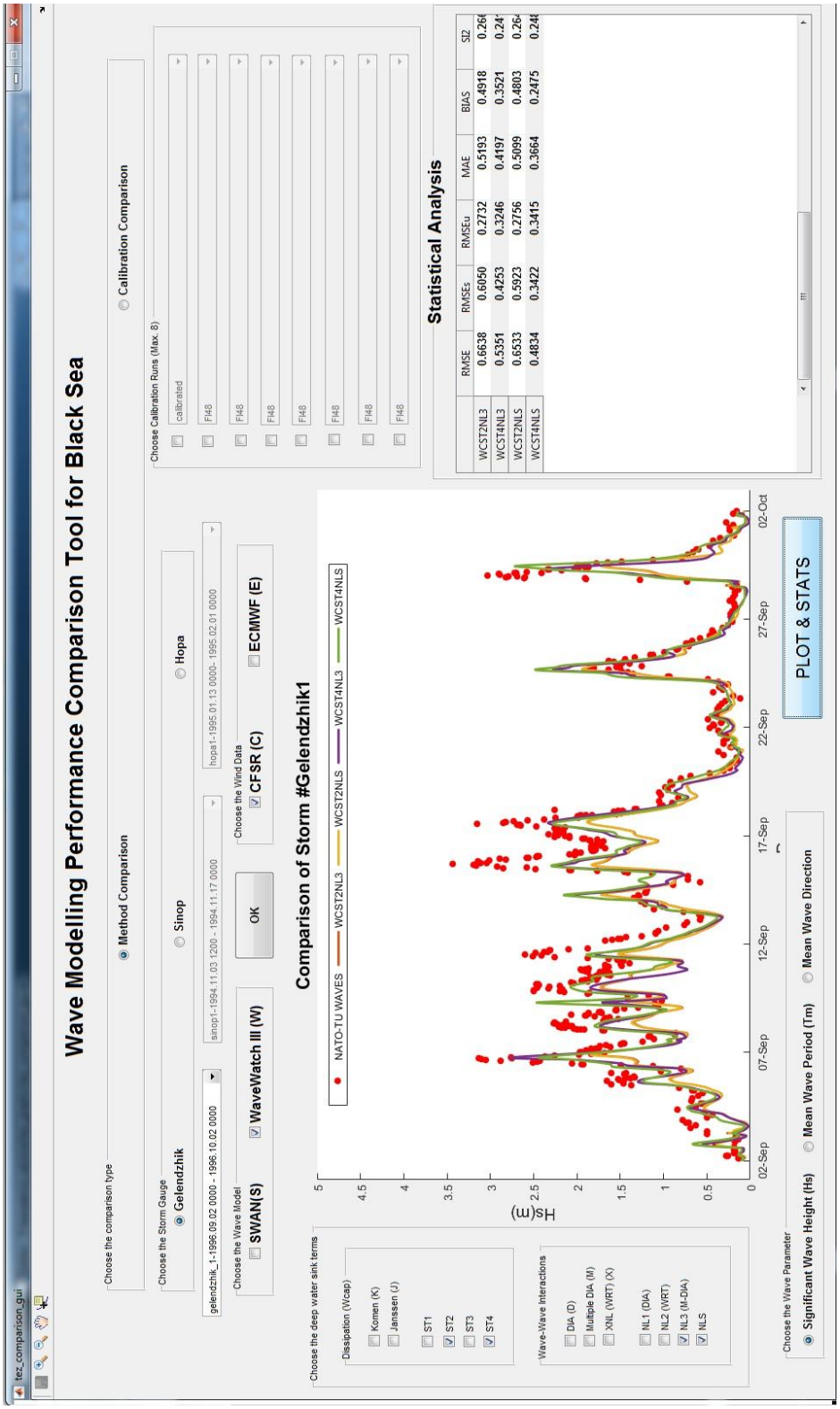

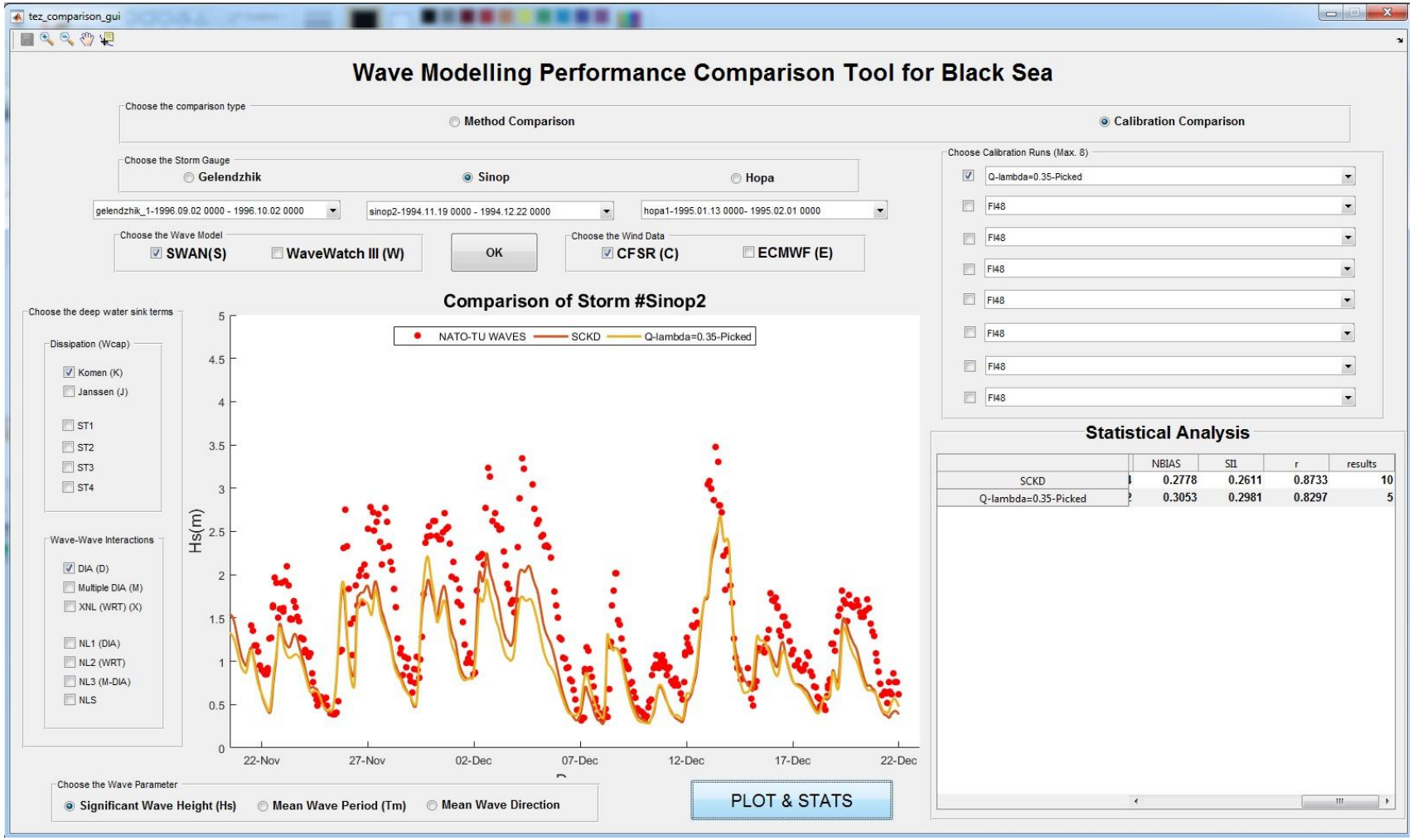
tez_comparison_gui
Wave Modelling Performance Comparison Tool for Black Sea
Choose the comparison type
Method Comparison
Calibration Comparison
Choose the Storm Gauge
Gelendzhik
Sinop
Hopa
gelendzhik_1-1996.09.02 0000 - 1996.10.02 0000
sinop2-1994.11.19 0000 - 1994.12.22 0000
hopa1-1995.01.13 0000- 1995.02.01 0000
Choose the Wave Model
SWAN(S)
WaveWatch III (W)
OK
Choose the Wind Data
CFSR (C)
ECMWF (E)
Choose Calibration Runs (Max. 8)
Q-lambda=0.35-Picked
FI48
Comparison of Storm #Sinop2
NATO-TU WAVES
SCKD
Q-lambda=0.35-Picked
Hs(m)
22-Nov
27-Nov
02-Dec
07-Dec
12-Dec
17-Dec
22-Dec
Choose the deep water sink terms
Dissipation (Wcap)
Komen (K)
Janssen (J)
ST1
ST2
ST3
ST4
Wave-Wave Interactions
DIA (D)
Multiple DIA (M)
XNL (WRT) (X)
NL1 (DIA)
NL2 (WRT)
NL3 (M-DIA)
NLS
Statistical Analysis
NBIAS
SI1
r
results
SCKD
0.2778
0.2611
0.8733
10
Q-lambda=0.35-Picked
0.3053
0.2981
0.8297
5
Choose the Wave Parameter
Significant Wave Height (Hs)
Mean Wave Period (Tm)
Mean Wave Direction
PLOT & STATS